

SERI/TR-635-1166  
UC Category: 60  
DE85002947

# **Acoustic Noise Associated with the MOD-1 Wind Turbine: Its Source, Impact, and Control**

N. D. Kelley  
H. E. McKenna  
R. R. Hemphill  
C. L. Etter  
R. L. Garrelts  
N. C. Linn

**February 1985**

Prepared under Task Nos. 1066.70 and 4803.10  
WPA No. 171A

## **Solar Energy Research Institute**

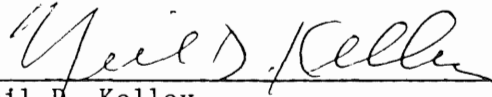
A Division of Midwest Research Institute

1617 Cole Boulevard  
Golden, Colorado 80401

Prepared for the  
**U.S. Department of Energy**  
Contract No. DE-AC02-83CH-10093

**PREFACE**

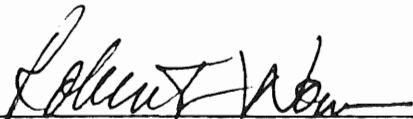
This report summarizes extensive research by staff of the Solar Energy Research Institute and its subcontractors conducted to establish the origin and possible amelioration of acoustic disturbances associated with the operation of the DOE/NASA MOD-1 wind turbine installed near Boone, North Carolina. Results have shown that the most probable source of this acoustic annoyance was the transient, unsteady aerodynamic lift imparted to the turbine blades as they passed through the lee wakes of the large, cylindrical tower supports. Nearby residents were annoyed by the low-frequency, acoustic impulses propagated into the structures in which the complainants lived. The situation was aggravated further by a complex sound propagation process controlled by terrain and atmospheric focusing. Several techniques for reducing the abrupt, unsteady blade load transients were researched and are discussed.



Neil D. Kelley,  
Principal Scientist  
Wind Energy Section

Approved for

SOLAR ENERGY RESEARCH INSTITUTE



Robert J. Noun, Manager  
Wind Energy Section



Donald Ritchie, Director  
Solar Electric Research Division

## ACKNOWLEDGMENTS

The authors wish to acknowledge the support and assistance of the following organizations in SERI's MOD-1 research:

- Appalachian State University
- The Blue Ridge Electric Membership Corporation
- Engineering Dynamics, Inc.
- Fairchild-Weston
- Cornell University, Sibley School of Mechanical and Aerospace Engineering
- The General Electric Company
- Massachusetts Institute of Technology, Department of Aeronautics and Astronautics
- NASA Langley Research Center, Structural Acoustics Branch
- NASA Lewis Research Center, Wind Energy Program Office
- Pacific Northwest Laboratories, Atmospheric Physics Department
- Pennsylvania State University, Departments of Meteorology and Mechanical Engineering
- The Portland General Electric Company
- Rocky Flats Wind Energy Research Center
- University of Colorado-Boulder, Departments of Mechanical and Aerospace Engineering
- University of Virginia, Department of Environmental Sciences

Special thanks are extended to the residents of Boone, North Carolina, particularly those near the MOD-1 site who aided us in this investigation. Some parts of the program could not have been accomplished without the help of SERI staff members Stan Thues, Bob McConnell, and Jane Ullman. Benjamin Bell was responsible for developing much of the computerized, time-domain analysis technique. University of Colorado-Boulder (UCB) engineering undergraduates Robert Wooten, David Dill, and Daniel Schell were responsible for supporting the testing at the Rocky Flats Research Center and provided the bulk of the support and planning for the testing in the UCB wind tunnel. This work was supported by the DOE Wind Energy Technology Division under contracts EG-77-C-01-4042 and DE-AC02-83CH10093.

## SUMMARY

This document summarizes the results of an extensive investigation into the physical factors surrounding noise complaints related to the DOE/NASA MOD-1 wind turbine operating near Boone, North Carolina. The work reported here presents the results of investigative efforts of staff members of the Solar Energy Research Institute (SERI) and its subcontractors: the Fluid Dynamics Research Laboratory of the Massachusetts Institute of Technology (MIT), the Departments of Meteorology and Mechanical Engineering of Pennsylvania State University, and the Departments of Mechanical and Aerospace Engineering of the University of Colorado-Boulder.

Complaints of noise emanating from the operating MOD-1 were confined to about a dozen families living within a 3-km radius of the turbine, about half of whom were annoyed frequently. These families represented a very small fraction of the total households within this radial distance, a number exceeding 1000 homes, including most of the town of Boone itself. In summary, the complaints centered on the following perceptions:

- The annoyance was described as an intermittent "thumping" sound accompanied by vibrations.
- A "feeling" or "presence" was described, felt rather than heard, accompanied by sensations of uneasiness and personal disturbance.
- The "sounds" were louder and more annoying inside the affected homes.
- Some rattling of loose objects occurred.
- In one or two instances, structural vibrations were great enough to cause loose dust to fall from high ceilings and create an additional nuisance.

The primary objectives of SERI's investigation have been (1) to identify the physical mechanisms responsible for the generation, propagation, and human response (impact) of the annoying "sounds" related to the operation of the MOD-1 turbine and (2) to develop suggestions for its amelioration.

A definitive set of physical measurements that document the characteristics of the MOD-1 acoustic emissions, the vertical structure of the atmospheric velocity and thermal fields controlling the sound propagation, and the internal acoustic pressure variations and structural vibrations of two of the affected homes has been obtained through a series of field surveys. In addition, a number of supporting wind tunnel and full-scale tests using a small, downwind turbine have been conducted to enhance our basic understanding of the suspected physical processes involved. To aid in the investigation, a numerical model of the noise generation process has also been developed. These field measurements and model results allowed us to conclude the following:

- The annoyance was real and not imagined.

- The source of the annoyance was aerodynamic and involved the passage of the turbine blades through the lee wakes of the large, 0.5-m cylindrical tower legs.
- The coherent characteristics of the radiated acoustic impulses (produced by the leg wake-blade interaction) were responsible for the annoyance of the complaining residents.
- The responsible acoustic impulses were being propagated through the air and, in some instances, being focused on the complainants' homes as a consequence of ground reflection and refraction by the atmosphere.

Using a SERI-developed impulse waveform/energy analysis technique, we tested significant differences in the generation processes associated with the wakes from two of the support legs in the data taken during the June 1980 field survey. The impulses produced during this period were far more intense than those observed during our earlier survey in March-April 1980. The impulse analysis demonstrated that the severity of the intermittent impulses was not a unique function of the leg wake momentum deficit and that other factors were also involved. The analysis further demonstrated that slowing the rotor rotational speed from 35 to 23 rpm would reduce but not eliminate the annoyance.

Our analysis of field studies conducted at the MOD-1 strongly suggests that the leg wake-blade interaction was the ultimate source of the annoying acoustic impulses and that the physical process responsible was aerodynamic in origin. Through both controlled wind tunnel testing and experiments performed using a small, downwind turbine in the natural airflow, we determined that vortex-dominated circulations in the cylinder wakes can cause transient lift fluctuations and therefore be a source of acoustic impulses. In particular, the leg wake influences the severity of the impulses generated by

- providing a spatial coherency parallel to the cylinder's major axis and the spanwise direction of the rotor blade;
- its lateral dimensions;
- its turbulence characteristics (whether broadband chaotic or narrowband discrete);
- its time-varying (dynamic) properties as opposed to mean quantities.

The wake characteristics are externally influenced by conditions in the free-stream that reach the cylindrical tower legs, including embedded perturbations containing turbulent length scales equivalent to the Strouhal shedding frequency. Other important variables are the freestream velocity, the vertical wind shear and hydrodynamic stability of the layer between the surface and hub height, the upwind fetch characteristics, and the wind direction controlling the orientation of the rotor plane with respect to the tower structure.

We have found that a number of turbine design parameters influence the severity of the acoustic impulses, including the rotor airfoil shape (close to

stall), the operating angle of attack, and the leg-to-blade distance downwind of the tower. The airfoil shape may be a primary contributor to the impulse generation, particularly when the incidence approaches the stall angle. Factors in the impulse generation at the intersection of the blade and wake are spatially organized turbulent perturbations that simultaneously affect the lift generating portion of the blade span and incorporate length scales ranging from less than a chordwidth to several chords.

Perturbation pressure distributions, resulting from vortex core pressure deficits in the leg wakes, have been shown to adversely influence the blade leading edge pressure gradient, resulting in a transient separation of the blade boundary layer as it passes through the wakes. This is a consequence of the characteristic chordwise pressure distribution of the 44xx-series airfoil shape. Because of a forward shift (towards the stagnation point) in the peak negative pressure with an increasing quasi-steady incidence angle, transient leading edge separation and reattachment, as well as airfoil hysteresis, apparently become more severe when the upwash circulation and core pressure deficits created by the embedded vortices in the leg wakes are encountered. Wind tunnel tests have shown, and comparisons of full-scale field data have confirmed, the existence of a critical turbulent scale defined by the reduced frequency parameter  $k$  and covering the range  $0.5 < k < \pi$  or, expressed in terms of a perturbation length scale,  $2\pi c > \lambda_p' > c$  (where  $c$  is the chord dimension at 80% span). Turbulent structures in these ranges that are spatially coherent in a direction parallel to the span impart the most severe lift fluctuations through an interaction with the blade and account for not only the intense, impulsive acoustic radiation but the generation of strong aeroelastic stresses in the blade structure as well. Critical, unsteady aerodynamic parameters, which have been identified as exerting control over these unsteady processes, include the reduced frequency  $k$  (or, equivalently, the perturbation wavelength  $\lambda_p'$ ), the quasi-steady incidence angle  $\bar{\alpha}$ , the perturbation spanwise coherence (with respect to the blade span), and possibly the vortex core pressure deficit  $\Delta p_v$ , all of which are stochastic with narrowband (critical) sensitivities.

An investigation into the role atmospheric propagation plays in the MOD-1 annoyance has shown that surface and ground propagation are negligible in comparison with a combination of terrain reflection and atmospheric refraction. Strong focusing (25 dB or more) of the emitted MOD-1 acoustic impulses as a result of these processes can account for local, far-field enhancements (caustics).

Acoustic and seismic (vibration) measurements taken in two of the affected homes near the MOD-1 site revealed that the structures had been undergoing transient elastic deformation under the periodic acoustic loadings from the turbine's operation. The excitation of lightly damped structural modes has also been responsible for summarily exciting cavity (Helmholtz) and air volume resonances within the rooms of the homes and producing secondary acoustic emissions from loose objects. Possibly very important, however, are the strongly oscillatory (harmonic), low-frequency pressure fields created within the smaller rooms and their relation to annoyance of the residents. A measurement of the indoor threshold perception (audible stimuli but no sensation of vibration) at one of the homes undergoing excitation by the MOD-1 impulsive noise led us to suggest the design goal of limiting peak coherent

emission in the 8, 16, 31.5, and 63 Hz standard octave frequency bands (measured on-axis 1.5 rotor diameters upwind or downwind of the subject turbine) to band intensity levels of 60, 50, 40, and 40 dB (re  $1 \text{ pW m}^{-2}$ ), respectively, under all atmospheric and operating conditions. The sensitivity of these threshold levels measured in a Boone home compares favorably with documented cases of human annoyance known to be associated with industrial sources of low-frequency noise.

A number of ways to ameliorate the MOD-1 impulsive noise were investigated. Because the leg wakes were found to be ultimately responsible, the abatement of coherent noise emissions has been targeted towards techniques that convert the offending 2-D, discrete wakes to 3-D chaotic by minimizing the spatially organized wake energy in the critical turbulent length scales. Three aerodynamic spoiling devices designed to be placed around the large, cylindrical tower legs were investigated in terms of their ability to achieve the desired transformation of the wake characteristics. We found that installing a helical strake or fence or covering the leg's cylindrical surface with square vortex generator elements or turbulators, placed over most of the leg's surface extending above and below the rotor disk, provided the necessary wake modification. Tests of a perforated shroud-type spoiler indicated it is unusable when the blade plane is less than three cylinder diameters downstream, but it may be adequate at distances beyond that (cylinder far wake). Additional analysis and testing of this type of spoiling device will be necessary before it can be considered as a solution to the problem.

## TABLE OF CONTENTS

	<u>Page</u>
1.0 Introduction.....	1
1.1 Characteristics of the MOD-1 Wind Turbine.....	1
1.2 Background.....	1
1.2.1 The Nature of the Complaints.....	4
1.2.2 The SERI Program.....	5
1.3 Related Studies.....	6
1.4 SERI Program Investigation Objectives.....	6
2.0 The Investigative Procedure.....	8
2.1 MOD-1 Field Studies.....	8
2.1.1 October 1979 Study.....	8
2.1.2 February 1980 Study.....	9
2.1.3 March/April 1980 Study.....	9
2.1.4 June 1980 Study.....	9
2.1.5 January 1981.....	9
2.2 Instrumentation.....	10
2.2.1 Acoustic.....	10
2.2.2 Seismic.....	10
2.2.3 Atmospheric.....	10
2.2.4 Turbine Operational Information.....	11
2.2.5 Data Recording.....	11
2.3 Data Reduction.....	11
2.4 Analytical Modeling.....	11
3.0 MOD-1 Field Investigation Results.....	12
3.1 Identification of Source of Acoustic Annoyance.....	12
3.1.1 Annoyance-Related Acoustic Emission Characteristics of the Wind Turbine.....	12
3.1.2 Annoyance and Acoustic-Structural Interaction.....	21
3.1.2.1 External/Internal Acoustic Fields Under Turbine-Induced Impulsive Excitation.....	21
3.1.2.2 Structural Response in Houses #7 and #8 under Turbine-Induced Impulsive Excitation.....	26
3.1.2.3 Groundborne (Seismic) Propagation/ Excitation by Turbine.....	30
3.2 Factors Affecting Noise Generation.....	31
3.3 Factors Affecting the Propagation of Turbine Noise.....	33
3.4 Initial Conclusions Based on Field Measurements.....	34
4.0 Analysis and Interpretation.....	35
4.1 Aeroacoustic Noise Generation Mechanisms.....	35
4.1.1 Aeroacoustic Mechanism for Impulse Noise Generation....	35
4.1.1.1 Rotor Noise Characteristics.....	35



## TABLE OF CONTENTS (Continued)

	<u>Page</u>
4.1.1.2 Physical Basis for Impulsive Noise Generation.....	36
4.1.1.3 Impulse Waveform Analysis and Interpretation.....	39
4.2 Multivariate Statistical Analysis of Parameter Impulsive Noise Generation.....	40
4.2.1 Impulse and Operational Data Reduction.....	40
4.2.1.1 Impulse Data Reduction.....	40
4.2.1.2 Operational Data Reduction.....	40
4.2.2 Analysis Results.....	40
4.2.3 Multivariate Statistical Analysis.....	51
4.2.3.1 Methodology.....	51
4.2.3.2 Analysis Results.....	52
4.2.3.3 Impulse Analysis Interpretation and Conclusions.....	77
5.0 Aerodynamic Noise-Generating Mechanisms.....	81
5.1 Wakes from Cylindrical Bluff Bodies.....	81
5.1.1 Effect of Reynolds Number on Wake Characteristics.....	85
5.1.2 Three-Dimensional Aspects of Cylinder Vortex Shedding..	87
5.1.3 Cylinder Far Wake Characteristics.....	87
5.1.4 Field Verification of Vertical Coherency of Cylinder Wake Structures in Natural Flow.....	89
5.2 Impulsive Noise Generation Mechanism(s).....	89
5.2.1 Wind Tunnel Verification of Tower Leg Wakes as the Principal Cause of Impulse Generation.....	94
5.2.1.1 Acoustic Results.....	94
5.2.1.2 Aerodynamic Results.....	99
5.2.1.3 Conclusions from Anechoic Wind Tunnel Experiment.....	103
5.2.2 The Role of Freestream Turbulence in Influencing Severity of Impulse Generation.....	103
5.2.2.1 Field Experimentation.....	104
5.2.2.2 Results.....	104
5.2.2.3 Interpretation and Conclusions.....	107
5.2.3 Role of Blade Unsteady Aerodynamic Response in Impulsive Noise Generation.....	114
5.2.3.1 A Physical Description of the Turbine- Radiated Acoustic Impulse.....	114
5.2.3.2 Proposed Unsteady Aerodynamic Mechanism Responsible for Impulse Generation.....	121
5.2.4 Airfoil Unsteady Boundary Layer Dynamics Applicable to the MOD-1 Situation.....	121
5.2.4.1 Factors Influencing the Magnitude of Blade Airload Fluctuations.....	122
5.2.4.2 Role of Blade-Vortex Interaction in Impulse Generation.....	129

TABLE OF CONTENTS (Continued)

	<u>Page</u>
5.2.4.3 Wind Tunnel Verification.....	140
5.3 Summary and Confirmation of Causal Factors Responsible For Aerodynamic Generation of MOD-1 Acoustic Impulses.....	149
5.3.1 Summary of Physical Parameters Responsible for Mod-1 Acoustic Impulse Generation.....	149
5.3.1.1 Operational Parameters.....	150
5.3.1.2 Cylinder Wake Parameters.....	151
5.3.1.3 Cylinder Wake Parameters.....	151
5.3.2 Comparison of Supportive Research Effort Results with Analysis of Physical Parameters Related to MOD-1 Noise Situation.....	152
5.3.3 Interpretation of the MOD-1 Impulsive Noise in Terms of the Unsteady, Fluid Dynamic Parameters.....	152
5.3.3.1 Confirmation of Influence of Reduced Frequency Parameter on MOD-1 Impulse Noise Generation.....	153
5.3.3.2 Comparison of MOD-1 Results with Other "Receptor" Variables.....	154
5.3.3.3 Comparison of MOD-1 Results with Available "Excitor" Information.....	154
6.0 The Role of Atmospheric Propagation in the MOD-1 Situation.....	157
6.1 Atmospheric and Terrain Structural Features Controlling MOD-1 Noise Propagation to Affected Homes.....	157
6.2 Results of the Propagation Investigation.....	160
6.3 Influence of Site Wind Direction on Propagation and Frequency of Annoyance.....	168
6.4 Conclusions Regarding the Effects of Propagation on the MOD-1 Noise Situation.....	168
7.0 A Proposed Physical Mechanism Deemed Responsible for Annoyance from MOD-1 Impulsive Noise.....	172
7.1 Characteristics of Large Wind Turbine Noise.....	172
7.2 A Proposed Physical Mechanism Responsible for MOD-1 Annoyance.....	173
7.2.1 Factors Controlling the Internal Dynamic Pressure Fields of Subject Rooms.....	173
7.2.2 Human Perception of Internal Pressure Field.....	178
7.3 Comparison of Annoyance Related to MOD-1 with Similar Situations.....	179
7.3.1 Low-Frequency Resonant Properties of Residential Structures.....	179
7.3.2 Low-Frequency Excitation by a Nonimpulsive Source.....	182
7.3.3 Comparison of the Severity of the MOD-1 Situation with other Low-Frequency Noise Situations.....	187

## TABLE OF CONTENTS (Concluded)

	<u>Page</u>
7.4 An Annoyance Potential Assessment Method.....	189
7.4.1 A Synopsis of the Technique.....	189
7.4.2 Analysis Results.....	192
7.4.3 Comparison of Proposed Low-Frequency Coherent Emission Guidelines with Available Data.....	197
8.0 Procedures for Mitigating MOD-1 Impulsive Noise Radiation.....	199
8.1 Possible Ways to Ameliorate the MOD-1 Impulsive Noise.....	199
8.2 Decreasing Impulsive Noise Intensity by Reducing Rotor Rotational Speed.....	199
8.3 Aerodynamic Modification of Tower Legs to Control Impulsive Noise Generation.....	200
8.3.1 The Perforated Shroud Spoiler.....	201
8.3.1.1 Acoustic Results.....	203
8.3.1.2 Wake Characteristics.....	203
8.3.1.3 Interpretation.....	203
8.3.2 The Vortex Generator Spoiler.....	203
8.3.2.1 Acoustic Results.....	211
8.3.2.2 Wake Characteristics.....	211
8.3.2.3 Interpretation.....	211
8.3.3 The Helical Strake Spoiler.....	216
8.3.3.1 Acoustic Results.....	216
8.3.3.2 Wake Characteristics.....	216
8.3.3.3 Interpretation.....	218
8.4 Concluding Remarks.....	218
9.0 Conclusions.....	224
9.1 A Proposed Physical Mechanism Responsible for Human Annoyance.....	224
9.2 Aerodynamics Generating Mechanism Responsible For MOD-1 Impulsive Noise.....	225
9.3 Role of Atmospheric Propagation in the Severity of the MOD-1 Annoyance.....	225
9.4 Answers to Questions Posed in Section 1.5.....	226
10.0 References.....	228

LIST OF FIGURES

	<u>Page</u>
1-1 DOE/NASA MOD-1 Wind Turbine Installed Atop Howard's Knob near Boone, North Carolina, in 1979.....	2
1-2 Schematic Map Showing MOD-1 Site and Relationship of Complainants' Homes.....	5
3-1 Averaged MOD-1 Sound Pressure Spectrum with No Periodic Impulses Present.....	13
3-2 Typical Pressure-Time Plot of MOD-1 Acoustic Emissions with No Periodic Impulses Present.....	14
3-3 Typical Pressure-Time Plot of MOD-1 Acoustic Emissions Containing Strong Period Impulses.....	15
3-4 Averaged Sound Pressure Spectrum of MOD-1 Acoustic Emissions Containing Strong Periodic Impulses.....	16
3-5 Detail of Typical Pressure-Time Plot of MOD-1 Acoustic Emissions with No Periodic Impulse Present.....	17
3-6 Detail of Typical Pressure-Time Plot of MOD-1 Acoustic Emissions Containing Strong Periodic Impulses.....	18
3-7 MOD-1 Tower Base Layout and Relationships to Rotor Plane, Prevalent Operating Wind Direction, and Orientations of Complainants' Homes.....	19
3-8 Pressure Time Plot of Moderate-to-Severe MOD-1 Acoustic Impulse Measured Outside House #8.....	20
3-9 Schematic Example of the Transformation of a Time Domain Acoustic Impulse into the Frequency Domain as a $(\sin x)/x$ Function.....	21
3-10 Acoustic Energy Level Distribution of the Single Impulse Shown in Figure 3-8 Received at House #8.....	22
3-11 Plot Showing Time Delay between Arrival of Outdoor MOD-1 Impulse and Onset of 31.5-Hz Octave Band Acoustic Pressure Level.....	23
3-12 External-Internal Acoustic Coupling Modes of House #7 under MOD-1 Impulsive Excitation.....	24

## LIST OF FIGURES (Continued)

	<u>Page</u>
3-13 External-Internal Acoustic Coupling Modes of House #8 under MOD-1 Impulsive Excitation.....	25
3-14 Peak Interior Sound Pressure Levels Observed in Houses #7 and #8 during Threshold Perception and Moderate Impulsive Annoyance Conditions, Respectively.....	26
3-15 Peak Internal-External Sound Pressure Level Differences for Moderate Annoyance and Threshold Perception in Houses #7 and #8.....	27
3-16 Peak Sound Pressure Levels Above Ground for Moderate Impulsive Excitation (Outdoors and Indoors, House #8) and Threshold Perception (Indoors, House #7).....	28
3-17 External Acoustic Energy Density Level Narrowband Spectrum For Single Impulse Corresponding to Threshold Perception in House #7.....	29
3-18 Background and Peak Horizontal Floor Acceleration Levels in House #7 during Perception-Level Mod-1 Impulsive Excitation.....	29
3-19 Peak, Average, and Background Horizontal Floor Acceleration Levels in House #8 during Moderate Annoyance MOD-1 Impulsive Excitation.....	30
3-20 Horizontal and Vertical Plane Acceleration (Deformation)-Forced Internal Acoustic Pressure Transmissibility for House #8 under Moderate Impulsive Excitation.....	31
3-21 Elastic (Deformation) Response of Floor Vertical Plane in House #8 under Moderate, External Impulsive Acoustic (Pressure) Loading.....	32
3-22 Ground Motion Velocity Spectra Measured near House #8 when Undergoing Moderate Impulsive Annoyance.....	33
4-1 Scatter Diagram of Impulse Energy Intensity vs. Hub-Height Wind Direction for March and June 1980 Field Surveys.....	42
4-2 Scatter Diagram of Impulse Overpressures vs. Hub-Height Wind Direction for March and June 1980 Field Surveys.....	42
4-3 Scatter Diagram of Impulse Overpressures vs. Blade Rotational Speed.....	43

**LIST OF FIGURES (Continued)**

	<u>Page</u>
4-4 Scatter Diagram of Impulse Overpressure vs. Minimum Tower Leg-to-Rotor Blade Distance (in Tower Leg Diameters) as a Function of rpm and Survey Period.....	43
4-5 Scatter Diagram of Impulse Rise Rate vs. Rotor Blade Pitch Angle as a Function of Blade rpm for June 1980 Survey.....	44
4-6 Scatter Diagram of Impulse Overpressure vs. Rotor Blade Pitch Angle as a Function of Blade rpm for June 1980 Survey.....	44
4-7 Scatter Diagram of Impulse Overpressure vs. Generator Output Power for 35 rpm Operation during June 1980 Survey.....	45
4-8 Scatter Diagram of Impulse Overpressure vs. Generator Output Power for 35 rpm Operation during March 1980 Survey.....	45
4-9 Summary Scatter Diagram of Impulse Overpressure vs. Generator Output Power under 35 rpm Operation for both March and June 1980 Surveys.....	46
4-10 Scatter Diagram with Linear Regression Line of Reference Sound Pressure Level as a Function of Hub-Height Wind Speed.....	46
4-11 Scatter Diagram with Linear Regression Lines for Impulse Overpressure vs. Hub-Height Mean Wind Speed for March and June 1980 Survey Periods.....	47
4-12 Scatter Diagram with Linear Regression Line of Impulse Overpressure vs. Hub-height Wind Speed for 35 rpm Operation during March 1980 Surveys.....	48
4-13 "Power" Wind Rose--Directional Probability of Receiving Hub-Height Speeds between Turbine Cut-In and Cut-Out Values--for MOD-1 Site.....	49
4-14 Scatter Plot of Impulse Peak Overpressure vs. Hub-Height Wind Speed as a Function of Rotor rpm. (Solid lines represent best fits for upper and lower groups of points and the dashed line was chosen as an approximate divider in between.).....	50
4-15 Cumulative Probability Plot of Impulse Energy Intensity as a Function of Rotor rpm.....	53
4-16 Cumulative Probability Plot of Impulse Overpressure as a Function of Rotor rpm.....	54

## LIST OF FIGURES (Continued)

	<u>Page</u>
4-17 Cumulative Probability Plot of Impulse Rise Rate as a Function of Rotor rpm.....	55
4-18 Cumulative Probability Plot of Impulse Energy Intensity as a Function of Survey Period and Specific Tower Leg Wake.....	64
4-19 Cumulative Probability Plot of Impulse Peak Overpressure as a Function of Survey Period and Specific Tower Leg Wake.....	65
4-20 Cumulative Probability Plot of Impulse Rise Rate as a Function of Survey Period and Specific Tower Leg Wake.....	66
4-21 Impulse Energy Intensity as a Function of Tower Leg-to-Blade Distance (in leg diameters) and Hub-Height Wind Speed for June 1980 Survey Period.....	68
4-22 Impulse Peak Overpressure as a Function of Tower Leg-to-Blade Distance and Hub-Height Wind Speed for June 1980 Survey Period....	69
4-23 Impulse Rise Rate as a Function of Tower Leg-to-Blade Distance and Hub-Height Wind Speed for June 1980 Survey Period.....	70
4-24 Impulse Energy Intensity as a Function of Rotor Distance and Hub-Height Wind Speed for March 1980 Survey Period.....	71
4-25 Impulse Peak Overpressure as a Function of Rotor Distance from Tower Leg and Hub-Height Wind Speed for March 1980 Survey Period.....	72
4-26 Impulse Rise Rate as a Function of Rotor Distance from Tower Leg Distance and Hub-Height Wind Speed for March 1980 Survey Period.....	73
4-27 Comparison of Energy Intensity of Impulses Associated with the East Tower Leg as Function of the Rotor rpm and Tower Leg-to-Blade Distance.....	74
4-28 Comparison of Peak Overpressures of Impulses Associated with the East Tower Leg as Function of the Rotor rpm and Tower Leg-to-Blade Distance.....	75

LIST OF FIGURES (Continued)

	<u>Page</u>
4-29 Comparison of Rise Rate of Impulses Associated with the East Tower Leg as Function of the Rotor rpm and Tower Leg-to-Blade Distance.....	76
4-30a Schematic of MOD-1 Tower and Rotor Structure Showing Small Tower Leg-to-Blade Clearances and 9° Coning Angle.....	79
4-30b Tower Leg-to-Blade Clearance with Rotor Nominally Parallel to Southeast Flat.....	80
4-30c Vertically Oriented View, Similar to Figure 4-30b.....	80
5-1 Physical Mechanisms Responsible for Noise Generation by Wind Energy Conversion Systems (WECS).....	82
5-2 Schematics of Cylinder Wake Flows in the Subcritical and Supercritical Regimes.....	84
5-3 Example of the Vertical Windshear Variability Immediately Upwind of the MOD-1 Turbine.....	86
5-4 Sketch of cylinder Vortex Shedding from a Vertical Separation Line Parallel to Major Axis and when this Line is Distorted.....	88
5-5 Vertically-Separated, Dual Hot-Film Anemometer Configuration for Measuring Cylinder Wake Characteristics in Natural Turbulent Flow.....	90
5-6 Cross-Spectral Estimate of the Upper and Lower Bare Cylinder Wake Velocities as Measured by the Technique Shown in Figure 5-5.....	91
5-7 Vertical Coherence of Bare Cylinder Wake as Determined by Measurements of Figure 5-5.....	92
5-8 Comparisons of Cylinder Base Pressure and Wake Velocity RMS Spectra for Bare Cylinder Tower Element.....	93
5-9 Experimental Configuration Used in the MIT Anechoic Wind Tunnel Testing.....	95
5-10 On-Axis Peak Impulse Pressure as a Function of Cylinder-to-Rotor Distance and Upstream Cylinder Diameter.....	96
5-11 Acoustic Pressure-Time Plot of Impulses Emitted from Cylinder Wake-Blade Interaction with a Single Upstream Cylinder and with a Second Augmenting Cylinder Present.....	97



## LIST OF FIGURES (Continued)

	<u>Page</u>
5-12 On-Axis Acoustic Pressure-Time Plot of Impulses Generated by Three Passages through Wakes Produced by Single and Dual Upstream Cylinders.....	98
5-13 Power Spectral Density of Wake Velocities Associated with Single and Dual Upstream Cylinders.....	100
5-14 Wake Velocity Probability Densities for Both Single and Dual Upstream Cylinders.....	101
5-15 Statistical Ensemble Averages of a Single-Cylinder Wake and a Wake Augmented by a Second Cylinder Installed 17D Upstream.....	102
5-16 Sketch Experimental Setup Used for Acoustic/Aerodynamic Studies Small Wind Turbine and Various Test Section Configurations.....	105
5-17 Averaged Acoustic Spectrum as Measured by a VLF Microphone Mounted at the Base of the Cylindrical Test Section.....	106
5-18 Scatter Plot and Indicated Linear Regression for the Mean-Square Velocity in the 2.5-8.0 Hz (Strouhal Excitation) Band vs. the Mean Freestream Velocity.....	108
5-19 Scatter Plot of the 35.25 $\pm$ 0.125 Hz Tone Band Pressure vs. the Strouhal Excitation Band Mean-Square Inflow Velocity.....	108
5-20 Same as Figure 5-19, but for the 23.5-43.0 Hz Root-Sum-Square Tone Pressure Sum vs. the Inflow Strouhal Excitation Band Mean-Square Velocity.....	109
5-21 Results of Trivariate Linear Regression Model Relating the Mean 23.5-43.0 Hz Total RSS Acoustic Band Pressure to the Inflow Strouhal Excitation Band Turbulence Level and Velocity.....	111
5-22 Scatter Diagrams for Inflow Strouhal Excitation Band Turbulence Levels vs. Freestream Velocity for August 24, 1981, and August 20, 1981.....	113
5-23 On-Axis Acoustic Pressure-Time Plot of Impulse Generated by 1.6-cm Cylinder Wake at a Freestream Velocity of 13.4 $\text{ms}^{-1}$ in MIT Anechoic Tunnel.....	115
5-24 Acoustic Pressure-Time Plots Made on Both the Pressure (Upwind) and Suction (Downwind) Sides of a WECS Rotor Periodic Unsteady Lift in the Wake of a Cylindrical Tower Element.....	116

## LIST OF FIGURES (Continued)

	<u>Page</u>
5-25 Acoustic Pressure Time Signature of a Single Blade Passage and Impulse Generation.....	118
5-26 Acoustic Pressure-Time Trace Showing Variability from Blade Passage to Blade Passage through Tower Wake.....	119
5-27 Acoustic Pressure Signature Showing No Evidence of Transient Lift Behavior and Impulse Generation.....	120
5-28 Effect of $\alpha_{max}$ on Dynamic Airloads.....	124
5-29 Effect of Mach Number on Dynamic Normal Force and Moment Coefficients.....	125
5-30 Chordwise Pressure Distribution as a Function of the Incidence Angle for a NACA 0012 Airfoil.....	126
5-31 Effect of Reduced Frequency on the NACA 0012 Airfoil.....	127
5-32 A Comparison of Dynamic Stall Regimes.....	128
5-33 Example of $CL_{max}$ Overshoot for NACA 2301x Airfoil.....	130
5-34 Typical Vortex Radial Velocity and Pressure Distributions.....	132
5-35 Schematic of Airfoil Boundary Layer and Chordwise Pressure Distribution Properties.....	134
5-36 Comparison of Wake Velocity and Dynamic Pressure Spectra 1.5D Downstream of a Cylindrical Tower Element.....	135
5-37 Comparison of Wake Velocity and Dynamic Pressure Spectra Taken 1.5D Downstream of a Perforated Shroud-Covered Cylinder.....	136
5-38 Mean Chordwise Pressure Distribution for a NACA 4412 Airfoil Section as a Function of Incidence Angle.....	138
5-39 Vortex Core Pressure Gradient vs. Core Diameter in Percent of Leg Wake Width at 7.5D Downstream for Both Subcritical and Supercritical Regimes.....	139
5-40 Sketch of Experimental Configuration for Unsteady Flow Testing of Rigid Airfoil Sections.....	141

## LIST OF FIGURES (Continued)

	<u>Page</u>
5-41 Probability Density of Leading Edge-to-0.15 Chord Pressure Gradient for the 63(2)-015 Airfoil with Two-Chord-Diameter Upstream Cylinder Excitation.....	143
5-42 Probability Density of Leading Edge-to-0.25 Chord Pressure Gradient for 63(2)-015 Airfoil with Two-Chord-Diameter Upstream Cylinder Excitation.....	144
5-43 Relative Aeroacoustic Transfer Function for the 63(2)-015 Airfoil Section as a Function of Cylinder Wake Perturbations.....	145
5-44a Measured Turbulent Acoustic Transfer Function Modulus for 63(2)-015 Test Section at Incidence Angles of 4, 8, and 12 Degrees.....	146
5-44b Measured Turbulence Normal Force ( $C_n$ ) Transfer Function Modulus at 15%-Chord for 63(2)-015 Test Section at Incidence Angles of 4, 8, and 12 Degrees.....	147
5-44c Comparison of Acoustic Emissions and Normal Force ( $C_n$ ) at 15%-Chord Transfer Function Moduli for 63(2)-015 Airfoil Section at an Incidence Angle of 4 Degrees.....	147
5-44d Comparison of Acoustic Emissions and Normal Force ( $C_n$ ) at 15%-Chord Transfer Function Moduli for 63(2)-015 Airfoil Section at an Incidence Angle of 8 Degrees.....	148
5-44c Comparison of Acoustic Emissions and Normal Force ( $C_n$ ) at 15%-Chord Transfer Function Moduli for 63(2)-015 Airfoil Section at an Incidence Angle of 12 Degrees.....	148
5-45 Single MOD-1 Impulse Energy Density Level Spectrum Reaching House #8 with Equivalent Critical Reduced Frequency Values Indicated.....	155
6-1 Area Surrounding MOD-1 Site Showing Terrain and Locations of Complainants' Homes.....	158
6-2 Three Consecutive Tethered Balloon Profiles of Wind Speed above the ASU Water Treatment Plant.....	159
6-3 Representative Vertical Profiles of Wind Speed and Air Temperature Taken above ASU Water Treatment Plant.....	161
6-4 SODAR Record of 7 February 1980 above ASU Water Treatment Plant...	162
6-5 Acoustic Ray Tracing for 1930 Hours, 18 March 1980, along 048° Radial from MOD-1 Site.....	163

**LIST OF FIGURES (Continued)**

	<u>Page</u>
6-6 Acoustic Ray Tracing along 048° Radial for 2032 Hours, 18 March 1980.....	164
6-7 Representative Acoustic Ray Tracing along 105° Radial from MOD-1 Site Passing near Houses #7 and #8.....	165
6-8 Representative Acoustic Ray Tracing along 277° Radial from MOD-1 Site Passing near House #2.....	166
6-9 Representative Acoustic Ray Tracing for 355° Radial from MOD-1 Site Passing near House #3.....	167
6-10 One Lobe of MOD-1 Impulsive Noise Dipole Directivity Pattern.....	169
6-11 MOD-1 "Power Wind Rose" with ±3db Impulse Noise Directivity Pattern Added for Mean Wind Direction of 290°.....	170
7-1 Schematic Representation of an Averaged Radiation Sound Pressure Spectrum from a Large Wind Turbine.....	173
7-2 Schematic Sound Spectrum of Figure 7-1 with Structural Modes and Applicative Damping Mechanisms Added.....	174
7-3 Diagram Showing Relationship of Fundamental Structural Resonances To Construction Details of Typical Homes.....	176
7-4 Peak Internal-External Sound Pressure Level Differences for Moderate Annoyance and Threshold Perception in Houses #7 and #8...	177
7-5 Peak Sound Pressure Levels Existing above Background for Moderate Impulsive Excitation (Outdoors and Indoors, House #8) and Threshold Perception (Indoors, House #7).....	180
7-6 Comparison of the External Averaged, Radiated Acoustic Spectral Characteristics of a 100-MW Gas Turbine Peaking Station and the 2-MW MOD-1 Turbine.....	183
7-7 Same as Figure 7-5, but Adding the Response of Oregon Home to 100-MW Gas Turbine.....	184
7-8 Comparison of Averaged External and Internal Acoustic Pressure Fields Associated with Low-Frequency Annoyance from 100-MW Gas Turbine at a Distance of 1 km.....	185
7-9 Comparison of Averaged, Interior 1/3-Octave Band Pressure Levels for Excitation by 100-MW Gas Turbine and Moderate Annoyance and Threshold Perception from MOD-1 Wind Turbine.....	186

## LIST OF FIGURES (Continued)

	<u>Page</u>
7-10 Comparison of Interior Overall Sound Pressure Levels (OASPL) for Common Low Frequency Sources and Moderate Annoyance from the MOD-1 Wind and 100 MW Gas Turbines.....	188
7-11 Comparison of Summary of Documented Low-Frequency Annoyance Cases with Observed Octave-Band Acoustic Levels Associated with Moderate Annoyance from MOD-1 Turbine in House #8.....	190
7-12 Comparison of Documented Low-Frequency Annoyance Cases with Threshold Perception of MOD-1 Impulsive Noise at House #7.....	191
7-13 Joint Probability Distributions of 8/16 Hz Octave Band Spectrum Levels for House #7 Background and Threshold Perception and Maximum Severity at 1.5D from MOD-1 Turbine.....	193
7-14 Same as Figure 7-13, but for 16/31.5 Hz Octave Band Spectrum Level.....	194
7-15 Same as Figure 7-14, but for 31.5/63 Hz Octave Band Spectrum Level.....	195
7-16 Triple Joint Probability of 8/16/31.5 Hz Octave Band Spectrum Levels with Conditional Probability of an 8 Hz Band Pressure Level > 70 dB.....	196
7-17 Comparison of Suggested Minimum Wind Turbine Radiated Joint Octave Band Pressure Levels at 1.5D with Low-Frequency Annoyance Summary.....	198
8-1 View of a Section of the Perforated Shroud Spoiler Installed on the 0.5-m Cylindrical Test Section at the Rocky Flats Wind Energy Research Center.....	202
8-2 Cylinder Base Acoustic Pressure Time Signature for Two Blade Passages by the Tower with the Perforated Shroud Installed.....	204
8-3 Upper (Cylinder Midpoint Height) and Lower (Cylinder Base) RMS Wake Velocity Spectra Measured 1.5D Downstream of Shrouded Test Section on Tower.....	205
8-4 Same as Figure 8-3, but Cross-Spectrum and Phase of Upper and Lower Wake Velocities.....	206
8-5 RMS Spectra of Wake Velocity and Dynamic Pressure for Shrouded Cylinder at 1.5D Downstream.....	207

**LIST OF FIGURES (Concluded)**

	<u>Page</u>
8-6 Cross-Spectral Magnitude of Wake Velocity and Dynamic Pressure of Figure 805.....	208
8-7 Peak South Level of On-Axis Microphone.....	209
8-8 View of Vortex Generator or Turbulator Spoiler Installed on 0.5-m Cylindrical Test Section. (Note microphone installed at cylinder base.).....	210
8-9 Coherent Power Analysis of Freestream Turbulence and Tower Base Dynamic Pressure.....	212
8-10 Upper (Cylinder Midpoint) and Lower (Cylinder Base) RMS Velocity Spectra at 1.5D Downstream of Vortex Generator-Modified Cylinder..	213
8-11 Coherent Power Analysis of Upper and Lower Wake Velocities of Figure 8-10.....	214
8-12 Coherent Power Analysis of Upper and Lower Wake Velocities and Dynamic Pressure at 1.5D Downstream of Vortex Generator-Treated Cylinder.....	215
8-13 View of Helical Strake (Spiral Fence) Spoiler with Vortex Generator Sections Installed Below on 0.5-m Test Cylinder.....	217
8-14 Upper and Lower RMS Wake Velocity Spectra Measured 1.5d <sub>r</sub> Downstream of Cylinder Treated with Helical Strake.....	219
8-15 Coherent Power Analysis of Upper and Lower Wake Velocities of Figure 8-14.....	220
8-16 Coherent Power Analysis of Midpoint Wake Velocity and Dynamic Pressure and Base Velocity and Wake Dynamic Pressure.....	221
8-17 Drag Coefficients vs. Reynolds Number for Smooth and Straked Cylinders.....	222
8-18 Suggested Helical Strake Treatment of MOD-1 Tower Legs.....	223

## LIST OF TABLES

	<u>Page</u>
1-1 Original Specifications for the MOD-1 Wind Turbine.....	3
4-1 Correlation Matrix of Mean Impulse Characteristics and Operational Parameters.....	52
4-2 Summary Statistics of Mean Impulse Characteristics and Operational Parameters for March 1980 Data.....	57
4-3 Summary Statistics of Mean Impulse Characteristics and Operational Parameters for March 1980 Data.....	58
4-4 Summary Statistics of Mean Impulse Characteristics and Operational Parameters for June 1980 Data.....	59
4-5 Correlation Matrix of Mean Impulse Characteristics and Operational Parameters for June 1980 Data.....	60
4-6 Correlation Matrix of Mean Impulse Characteristics and Operational Parameters for March 1980 Data.....	60
4-7 Summary Statistics for a Comparison of Leg Wake Mean Impulse Characteristics.....	61
4-8 Multiple Linear Regression Coefficients.....	63
5-1 Summary Statistics of Natural Strouhal Excitation of Acoustic Impulses for 0.5-m Cylinder.....	107
5-2 Impulse Generation Relationship with Natural Tower Strouhal Excitation: Correlation Analysis Results.....	110
5-3 Statistical Summary of Aerodynamic and Acoustic Impulse Parameters for Observations made on August 20 and 24, 1981.....	112
5-4 Relative Importance of Unsteady Fluid Dynamic Parameters in Leading Edge Stall Phenomena.....	123
5-5 Steady Leading Edge Chordwise Pressure (Suction) Gradients for a NACA 4412 Airfoil Section (95% MOD-1 Span) at Equivalent 35 rpm Rotational Speed.....	140
5-6 Measured Structural Resonant Modes of 63(2)-015 Airfoil Test Section.....	149
7-1 Resonant Modes of Rooms in Houses #7 and #8.....	175
7-2 Major Normal and Coupled Structural Modes of Houses #7 and #8.....	178

**LIST OF TABLES (Concluded)**

	<u>Page</u>
7-3 Preferred Acoustic Pressure Spectral Peaks for Typical MOD-1 Impulses.....	179
7-4 Average Residence Properties By Geographic Location.....	181



## NOMENCLATURE

## Abbreviations

A-weighting	referenced to frequency response characteristic defined by ANSI Standard S1.4-1971 for Sound Level Meters
ANSI	American National Standards Institute
B.G.	background reference
BPL	band pressure level
BREMC	Blue Ridge Electric Membership Corporation
BSL	band spectrum level
CHABA	National Academy of Science, National Research Council, Armed Forces Committee on Hearing, Bioacoustics and Biomechanics
COEF VAR	coefficient of variation
DOE	U.S. Department of Energy
FM	frequency modulation
IRIG-B	Inter-Range-Instrumentation-Group "B" Time Code Format
ISO	International Organization for Standardization
MAF	minimum audible field
MIT	Massachusetts Institute of Technology
MOD-0	DOE/NASA test bed wind turbine
MOD-OA	DOE/NASA 200-kW experimental wind turbine
MOD-1	DOE/NASA 200-MW experimental wind turbine model
MSL	mean sea level
NACA	National Advisory Committee for Aeronautics
NASA	National Aeronautics and Space Administration
OASPL	overall sound pressure level
PDF	probability density function
SERI	Solar Energy Research Institute

## NOMENCLATURE (Continued)

SI	International System of Units
SPL	sound pressure level
UCB	University of Colorado-Boulder
VLF	very low frequency
WTS-4	Hamilton-Standard wind turbine design
2-D	two-dimensional
3-D	three-dimensional

**Symbols**

$B_e$	effective bandwidth
$c$	local sound speed
$c_o$	undisturbed sound speed
$\bar{c}$	mean chord dimension
$c_s$	section chord dimension
$C_L$	section lift coefficient
$C_{Lmax}$	peak lift coefficient
$C_m$	section pitching-moment coefficient
$C_p$	section pressure coefficient
$d_s$	wake downstream distance in leg diameters
$d_w$	mean cylinder wake diameter
$D$	cylinder diameter
$D_r$	rotor diameter
$D_{n,e,s,w}$	rotor separation distance from N, E, S, W tower legs
$E_I$	acoustic energy intensity (energy per unit area)
$f$	frequency
$f_n$	natural frequency

## NOMENCLATURE (Continued)

$f_s$	Strouhal shedding frequency
F	force per unit volume
$G_a(f)$	floor/wall acceleration power spectrum
$G_p(f)$	interior acoustic pressure field power spectrum
k	reduced frequency parameter
K	vorticity rate parameter
$\lambda_s$	blade loading per unit span
L	total span lift
M, $M_\infty$	Mach number
O( )	order of
p	total pressure
$p_0$	barometric pressure
$\hat{p}$	acoustic (dynamic) pressure, $\hat{p} = p - p_0$
$P_0$	reference pressure, 100 kPa
$P(f)$	harmonic acoustic energy spectrum
Q	mass source strength
r	source to observer distance, vortex radius
R	turbine rotor radius
Re	Reynolds number
$Re_c$	Reynolds number referenced to chord dimension
$Re_d$	Reynolds number referenced to cylinder diameter
St	Strouhal number
t	time
T	period of time
$T_{ij}$	Lighthill stress tensor

## NOMENCLATURE (Continued)

$t-r/c_0$	retarded time
$U$	relative blade speed
$\ U_\infty$	freestream velocity magnitude
$U_\theta$	vortex tangential velocity
$x_i$	distance in $i$ direction
$X_n$	source dipole coordinates
$z$	vertical distance
$\alpha$	incidence angle
$\dot{\alpha}$	rate of change of incidence angle
$\alpha_o, \alpha_{ss}$	quasi-steady incidence angle
$\alpha_{max}$	peak incidence angle
$\alpha_s$	static stall incidence angle
$\Gamma$	vortex circulation parameter
$\delta_c$	effective correlated span length
$\delta_s$	blade airload per unit span
$\Delta\alpha_s$	incidence angle excess over static value
$\Delta p_v$	vortex core pressure deficit
$\zeta$	damping ratio
$\theta$	potential temperature
$\kappa$	fraction of wake containing vortex core
$\lambda$	perturbation wavelength
$\mu$	absolute viscosity
$\nu$	kinematic viscosity
$\rho$	density
$\sigma_{ij}$	viscous stress tensor

**NOMENCLATURE (Concluded)**

$\phi(f)$	phase spectrum
$\psi$	nacelle yaw angle
$\omega$	radian frequency
$\Omega$	rotor rotation rate

**Units**

dB	decibels
dB(A)	decibels referenced to A-weighted scale
Hz	hertz (frequency in cycles per second)
J	joules (SI unit for energy)
k	kilo ( $10^3$ multiplier)
K	kelvins (SI unit for absolute temperature)
m	milli ( $10^{-3}$ multiplier), meter
M	mega ( $10^6$ multiplier)
p	pico ( $10^{-12}$ multiplier)
Pa	pascals (SI unit for pressure)
rpm	revolutions per minute
s	seconds
W	watts (SI unit for power)

## SECTION 1.0

### INTRODUCTION

This document summarizes the results of an extensive investigation into the factors surrounding noise complaints related to the operation of the DOE/NASA 2-MW MOD-1 wind turbine installed atop Howard's Knob near Boone, North Carolina. The work reported here primarily represents the efforts of staff members of the Solar Energy Research Institute (SERI). Companion documents include results obtained by the Fluid Dynamics Research Laboratory of the Department of Aeronautics and Astronautics, Massachusetts Institute of Technology (MIT), in the analytical modeling aspects of the investigation (SERI Report No. TR-635-1247). The part of this work related to propagation effects has been excerpted from research performed by a team of staff members of the Departments of Meteorology and Mechanical Engineering and the Noise Control Laboratory of Pennsylvania State University (Penn State), which are summarized in SERI Report No. TR-635-1292.

#### 1.1 CHARACTERISTICS OF THE MOD-1 WIND TURBINE

The subject wind turbine of this study, referred to as the MOD-1, was the fifth DOE/NASA Lewis (U.S. Department of Energy/National Aeronautics and Space Administration, Lewis Research Center) operational wind turbine constructed as part of the Federal Wind Energy Program. It was located atop a small, somewhat isolated peak known as Howard's Knob [elevation: 1348 m (4420 ft) MSL] overlooking the town of Boone in the Blue Ridge Mountains of northwestern North Carolina. Figure 1-1 illustrates the turbine and its surroundings. At the time of its dedication in July 1979, the MOD-1 was the largest wind turbine so far constructed, surpassing the Smith-Putnam machine that operated in the Green Mountains of Vermont in the early 1940s. The MOD-1 had a rotor diameter of 61 m (200 ft) and, as originally installed, was capable of generating 2 MW of power at rated windspeed. The machine was designed and constructed by the General Electric Company under a contract managed by the NASA Lewis Research Center, Wind Energy Program Office. Power generated by the MOD-1 was fed to the local utility grid operated by the Blue Ridge Electric Membership Corporation (BREMCO), a nongenerating rural electric cooperative that delivers electrical service in seven northwestern North Carolina counties. The first rotation of the MOD-1 occurred in May 1979, and the first grid synchronization took place in September 1979. The turbine operated until early 1981, when a major mechanical failure occurred, effectively terminating the program. The turbine has since been decommissioned and removed. Table 1-1 summarizes the original design and mechanical specifications of the turbine.

#### 1.2 BACKGROUND

In the fall of 1979, as the MOD-1 turbine was undergoing a series of engineering shakedown tests, a number of sporadic and totally unexpected noise complaints were received from a few homeowners living within a 3-km radius of the installation atop Howard's Knob. These complaints came as a surprise, since a series of earlier sound measurements taken at the 100-kW MOD-0 wind

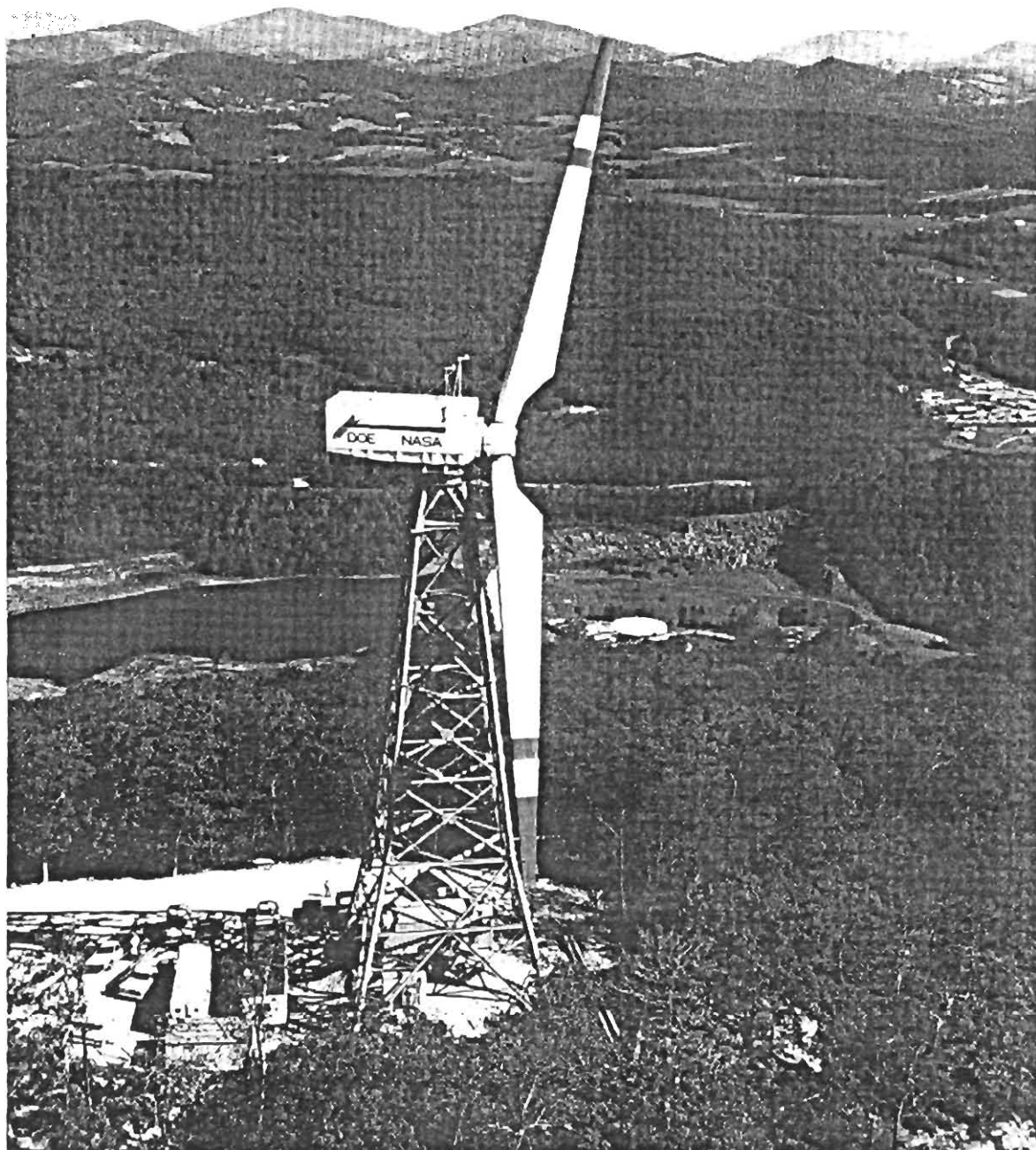


Figure 1-1. DOE/NASA Wind Turbine Installed Atop Howard's Knob near Boone, North Carolina, in 1979

**Table 1-1. Original Specifications for the MOD-1 Wind Turbine**

<b>Rotor</b>		<b>Generator</b>	
Number of blades . . . . .	2	Type . . . . .	Synchronous ac
Diameter [m (ft)] . . . . .	61 (200)	Rating (kVA) . . . . .	2225
Speed (rpm) . . . . .	35	Power factor . . . . .	0.8
Location relative		Voltage . . . . .	4160 (3-ph)
to tower . . . . .	Downwind	Speed (rpm) . . . . .	1800
Type of hub . . . . .	Rigid	Frequency (Hz) . . . . .	60
Method of power			
regulation . . . . .	Variable pitch		
Cone angle (degrees) . . . . .	9		
Tilt angle (degrees) . . . . .	0		
<b>Blade</b>		<b>Tower</b>	
Length [m (ft)] . . . . .	30 (97)	Type . . . . .	Pipe truss
Material . . . . .	Steel spar/foam tr. edge	Height [m (ft)] . . . . .	40 (131)
Airfoil shape . . . . .	NACA 44xx	Ground clearance [m (ft)] . . . . .	12 (40)
Twist (deg) . . . . .	11	Hub height [m (ft)] . . . . .	43 (140)
Tip chord [m (ft)] . . . . .	0.9 (2.8)	Access . . . . .	Hoist
Chord taper . . . . .	Linear		
<b>Performance</b>		<b>Control System</b>	
Rated Power (kW) . . . . .	2000	Supervisory . . . . .	Computer
Wind speed at 10 m (m/s):		Pitch actuator . . . . .	Hydraulic
Cut-in . . . . .	6		
Rated . . . . .	13		
Cut-out . . . . .	18		
Maximum design . . . . .	64		

turbine operating near Sandusky, Ohio, indicated that acoustic emissions associated with the machine's operation were indistinguishable from the wind-dominated background at distances greater than 200 m [1]. These early reports



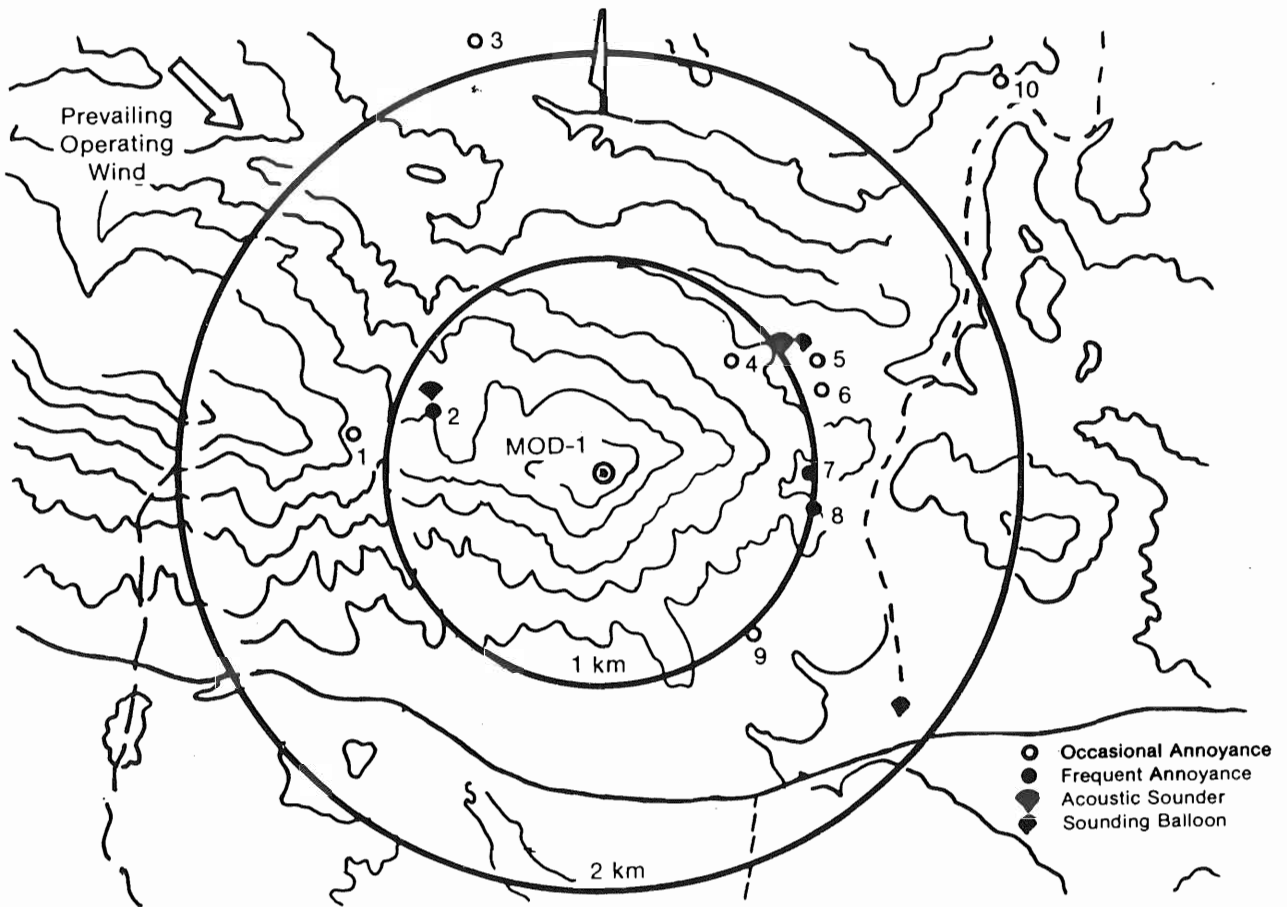
associated with the MOD-1 were also puzzling, because complaints were not received each time the turbine was operated, and attempts to correlate the type and location of the complaints with machine operating modes were inconclusive. So, the NASA Wind Energy Program Office and SERI entered into a cooperative effort to document and establish the source of the noise, ultimately to implement a suitable abatement procedure. Since that time, a number of organizations have made considerable efforts to study the situation in order to discover the exact nature of the noise responsible for annoying the neighbors, its origin and production mechanism, its propagation path, and what could be done to eliminate it or at least reduce it to below perceptible levels. This report summarizes a three-year SERI research effort to develop an understanding of the physical processes responsible for the MOD-1 noise annoyance.

### 1.2.1 The Nature of the Complaints

It is important, first, to place the MOD-1 noise situation in the proper perspective. The nature of the complaints generally did not change materially from the earliest to the latest reports received, and the total number of families known to be affected did not increase above the dozen identified within the first few months, even though more than 1000 families lived within a 3-km radius of the turbine installation. About a third of those dozen families were annoyed more frequently than the others. Figure 1-2 shows the location of the complainants' homes with respect to the wind turbine and also indicates those reporting a higher frequency of annoyance. Most homeowners described the annoyance as periodic "thumping sounds and vibrations," similar to the sensation of having someone walk heavily across a wooden porch or a heavy truck passing with a flat tire. During our investigation, we visited many of the complainants' households and received descriptions of the annoying sounds. The complaints can be summarized in the following perceptions:

- The annoyance was described as an intermittent "thumping" sound accompanied by the vibrations mentioned above.
- Many persons reported they could "feel" more than hear the "sounds," which created a sensation of uneasiness and personal disturbance.
- The "sounds" were louder and more annoying inside their homes than outside.
- Some people noticed loose glass rattling in picture frames mounted on outside walls, as well as small objects such as miniature perfume bottles on top of furniture in contact with an inside wall.
- In one or two severe situations, structural vibrations were sufficient to cause loose dust to fall from high ceilings, which created an additional nuisance.

The intermittence of the noise and disturbing feelings brought on by the noise were the most objectionable qualities of this annoyance. When visiting a complainants' home, we asked in which room did the residents believe the "sounds" were most noticeable. Without fail, we were shown rooms that had at least one window that faced the turbine. More often than not, the room was a relatively small one, usually a bedroom.



004685

**Figure 1-2. Schematic Map Showing MOD-1 Site and Relationship of Complainants' Homes**

**1.2.2 The SERI Program**

In cooperation with NASA, its contractor, the General Electric Company, and BREMC, SERI performed a series of field measurements at and near the MOD-1 installation during five separate sessions including October 1979 (within a week after the initial complaints were received), February 1980, March-April 1980, June 1980, and January 1981. The most comprehensive efforts in March-April and June 1980. The Pacific Northwest Laboratories and their subcontractor, the University of Virginia Department of Environmental Science, supported SERI field efforts at Boone during the March/April experiments. In addition

to the measurement programs at the MOD-1, SERI conducted ancillary experimental studies at the NASA Plumbrook Facility using the MOD-0 experimental turbine, the facilities of the DOE Rocky Flats Wind Energy Research Center, the anechoic wind tunnel of MIT's Department of Aeronautics and Astronautics, and the subsonic wind tunnel facilities of the Department of Aerospace Engineering of the University of Colorado-Boulder (UCB). Both analytical and field studies of low-frequency noise propagation in the vicinity of the MOD-1 turbine were conducted by a multidisciplinary group at Penn State and analytical studies of aerodynamic noise generation were performed by staff members of the Fluid Dynamics Research Laboratory of MIT's Department of Aeronautics and Astronautics, both under subcontract to SERI in support of the overall effort. The results of these studies are summarized in this document.

### 1.3 RELATED STUDIES

In addition to the SERI/MIT/Penn State effort, a number of other organizations have been active in the MOD-1 noise investigation:

- NASA Lewis Research Center--analytical modeling of noise generation by wind turbines [46]
- NASA Langley Research Center--aeroacoustical and psychophysical studies of wind turbine noise [45, 51, 32]
- General Electric Company Corporate Research Center--analytical and statistical studies of the MOD-1 noise situation and wind turbine noise in general [31,47]
- Boeing Vertol Division--wind turbine aeroacoustic studies [48]
- Hamilton-Standard Corporation--analytical studies of wind turbine aeroacoustics [49].

### 1.4 SERI PROGRAM INVESTIGATION OBJECTIVES

In cooperation with NASA, the SERI Program objectives were to (1) identify the physical mechanisms responsible for the generation of the MOD-1 noise, (2) determine the method of noise propagation to the homes below, (3) determine resulting subjective responses (impacts), and (4) develop suggestions for noise abatement techniques. In addition, the SERI studies attempted to answer the following questions:

1. Why did the noise not reach annoying levels each time the turbine was operated?
2. Why were some families annoyed more often than others, and why did the situation confine itself to such a small fraction of the total population living within 3 km of the machine?
3. Why was the noise more noticeable inside the affected homes and why did it become more persistent and louder during the evening and nighttime hours?

The SERI effort went beyond the specific noise situation associated with the MOD-1 so that the knowledge gained in this study can be applied to understand the acoustic performance and human annoyance potentials of a number of generic wind turbine designs.

## SECTION 2.0

### THE INVESTIGATIVE PROCEDURE

As a result of the initial assessment of the MOD-1 situation, made during preliminary on-site investigations in October 1979 and February 1980, we recognized the problem had three major components: (1) the actual noise generation process (which was suspected to be aeroacoustic in origin); (2) the propagation of the sound in the surrounding terrain; and (3) the mechanism responsible for producing the impact or annoyance in the affected homes. The Fluid Dynamics Research Laboratory of MIT's Department of Aeronautics and Astronautics and a multidisciplinary group comprising faculty and staff members from the Departments of Meteorology and Mechanical Engineering and the Noise Control Laboratory at Penn State were retained under SERI subcontracts to develop analytical techniques for evaluating the physics of the sound generation process and the propagation aspects of the problem, respectively.

A definitive set of physical measurements was needed that would document (1) the acoustic characteristics of the annoying sounds produced by the turbine, (2) the atmospheric motions and thermodynamic structure controlling the noise propagation, and (3) the structural and ground motions of the affected homes. In addition to the MOD-1 on-site studies, additional limited field experiments were performed using a small wind turbine at the Rocky Flats Wind Energy Research Center during spring and summer 1981. Supporting wind tunnel experiments were conducted in both the MIT anechoic wind tunnel and the UCB subsonic tunnel in May 1981 and February 1982, respectively.

#### 2.1 MOD-1 FIELD STUDIES

SERI performed five field measurements at the MOD-1 site in the course of its investigation. The first two were initial assessments to gather information for planning more extensive measurement efforts at a later date. The third was the first extensive study of many important parameters of the situation. The fourth was a comprehensive effort comprising acoustic measurements of the turbine under various operating conditions, including use with a resistive load bank instead of the utility grid. The last measurement involved evaluating the effectiveness of lowering the turbine rotational speed from 35 to 23 rpm to reduce the noise.

##### 2.1.1 October 1979 Study

The purpose of the study conducted in late October 1979 was to obtain an initial assessment of the noise that had recently been reported. The limited available acoustic data could not furnish any information about the severity of the reported noise problem, because it did not occur while SERI personnel were on site. BREMC personnel canvassed some of the complaining residents later, who indicated that they did not perceive the annoyance during the period of our data collection.

### 2.1.2 February 1980 Study

BREMC personnel received a number of complaints of a "thumping" noise during November and December 1979 and January 1981, after our initial visit. After our initial analysis of the first data set, we decided to return to Boone to try to obtain data during one of the complaint periods in order to (1) take a closer look at factors related to the annoyance, and (2) collect information needed to plan a larger field measurement effort later in the year. During this period the Penn State Group also installed the two acoustic sounders (SODARS) in the locations shown in Figure 1-2 (see Section 1.0). During the last evening of our visit we were able to obtain a data set representative of a typical annoyance episode.

### 2.1.3 March/April 1980 Study

This comprehensive study began during the third week of March. Its major objectives included detailed measurements of the vertical atmospheric structure using tethered balloons and SODARS to assess meteorological factors on sound propagation; seismic measurements of at least two homes experiencing actual annoyance episodes to varying degrees including measurements taken in the buildings and in the soil near the foundations; and, of course, detailed simultaneous acoustic data taken near the turbine and at the homes being monitored. The program was a reasonable success in that all three objectives were met. The findings are discussed in Section 4.0.

### 2.1.4 June 1980 Study

The June 1980 experiment was a combined effort of NASA, General Electric, and SERI to (1) collect more detailed acoustic data under a wide range of operating conditions; (2) evaluate the noise reduction achieved by reducing the rotor rotational speed from 35 to 23 rpm; and (3) assess the effects of treating two of the four major vertical support members of the tower with wire mesh on the severity of the noise measured. To place a load on the turbine at the lower rotational speed, a 1-MW (actual capacity, ~750 kW) resistive load bank was installed in place of the normal utility grid connection, and the operating sequences were altered accordingly to accommodate the maximum available load.

During this experimental series, SERI obtained its most comprehensive data set on the acoustic emissions from the turbine under a wide range of inflow wind speeds. Also during this series, on the evening of June 9th, the most severe instance of acoustic annoyance occurred that we were able to tape record. Unfortunately, during that episode we were not able to simultaneously collect acoustic and structural data at one of the affected homes.

### 2.1.5 January 1981

The objective of the January 1981 experiment was to evaluate the effectiveness of reducing the permanent rotor speed from 35 to 23 rpm under a full range of load conditions--which could not be accomplished in June because of the

capacity limits of the resistive load bank. Because the tests conditions required by the SERI test plan were not present, we supported NASA and General Electric in their specific efforts. Some data were obtained, but the critical turbine operating data were not yet available; therefore, the results have been of limited value. At the conclusion of this set of experiments, a failure occurred in the drive train that made the turbine inoperable.

## 2.2 INSTRUMENTATION

### 2.2.1 Acoustic

Special, very-low-frequency (VLF) microphone systems were employed. These instruments can measure acoustic pressures down to a frequency of 0.02 Hz (Bruel & Kjaer Model 2631 FM-carrier preamplifiers with Type 4147 microphones). The same preamplifier was also used with a back-sealed, Type 4144 microphone with a minimum frequency response of 0.1 Hz. Although the upper frequency limits of these combinations were 18 kHz and 8 kHz, respectively, in fact the upper frequency responses were limited by the FM tape recording used. In addition to the low-frequency systems, standard ANSI Type-1 Precision Sound Level Meters (Bruel & Kjaer Model 2209) also supplemented the acoustic measuring systems. All microphone calibrations were referenced to a standard piston-phone calibrator (Bruel & Kjaer Model 4220) corrected for the local barometric pressure. The VLF acoustic equipment allowed us to study accurately the time-pressure signatures of the acoustic field radiated from the turbine without the amplitude and phase distortion resulting from highpass characteristics of most microphones and their preamplifiers.

### 2.2.2 Seismic

Seismic range accelerometers (Bruel & Kjaer Type 8306) with a flat frequency response of 0.08 Hz to 1 kHz and a minimum sensitivity of more than -120 dB (referenced to 1  $g_{rms}$ ) measured the structural response of two of the affected homes. The Penn State investigators employed two Hall-Sears Model HS-10-1 seismometers (geophones) to measure any ground-borne component of the MOD-1 noise coupling to the foundations of the homes.

### 2.2.3 Atmospheric

The vertical wind and thermal structure of the atmosphere near the MOD-1 were measured directly by means of two tethered balloon systems which recorded windspeed and direction, temperature, humidity, and altitude during the March/April 1980 field study. In addition to the direct measurements, a pair of monostatic acoustic sounders (SODARs) were employed to qualitatively map the vertical thermal (and to some extent wind) structure during known annoyance episodes. One of these sounders was equipped with a telephone hookup that sent real-time data to the Penn State Meteorology Department computer at State College, Pennsylvania, for immediate analysis and interpretation. The map in Figure 2-1 shows the location of the tethered balloons and acoustic sounders.

#### **2.2.4 Turbine Operational Information**

Several turbine operating parameters that we believed were important were recorded for further analysis. These included the nacelle azimuth angle, Blade No. 1 position and pitch (blade) angles, hub-height wind direction and speed, generator output power, and the flat bending moment at the root of Blade No. 1. Because of the tape recorder's channel limitations, not all of the parameters listed were recorded during each field phase.

#### **2.2.5 Data Recording**

All acoustic, seismic, and supporting turbine operating data were recorded on multichannel, analog magnetic tape in FM format. Some of the acoustic data were also recorded in direct (amplitude-modulated) format to achieve a greater dynamic range and higher upper frequency limit. The recorders used in the field programs evolved from one portable, 4-channel machine employed during the initial assessments in October 1979 and February 1980 to three recorders used simultaneously (during the January 1981 experiment) consisting of 14-, 7-, and 4-channel units. In addition to the acoustic data (from as many as four microphone systems) and the turbine operating parameters, an IRIG-B digital time code signal was recorded during the June 1980 and January 1981 field programs to allow us to time-synchronize and reproduce certain time sequences more accurately than we could with footage counters alone. The time code was synchronized with the site data acquisition system for later comparisons with more of the turbine operational information.

### **2.3 DATA REDUCTION**

When they were available, the supporting turbine operating data (e.g., blade pitch and position angles, nacelle azimuth angle, generator output, and hub height wind speed) were digitized, scaled, and stratified into 2- to 3-minute record segments that exhibited relatively stationary statistics. The near- and far-field acoustic data and the structural seismic data taken at the affected homes were analyzed using both time and frequency domain methods through the facilities of a commercial, dual-channel narrowband Fast Fourier Transform (FFT) spectrum analyzer (Nicolet Model 660A). Much of the single parameter data were analyzed using the high resolution (800-line) mode of this instrument. Impulses found in the acoustic signal were analyzed in the single-channel, time domain mode under the control of an external computer to obtain statistical estimates of various waveform parameters. The dual-channel, 400-line mode was used to study the dynamic interaction between the acoustic and elastic, structural responses of the affected homes.

### **2.4 ANALYTICAL MODELING**

To better understand the physics of the noise generation process associated with the MOD-1, an analytical model was developed by MIT's Fluid Dynamics Research Laboratory. The physical basis of this model and the first set of results achieved with it are discussed in SERI report TR-635-1247 [2].



## SECTION 3.0

### MOD-1 FIELD INVESTIGATION RESULTS

#### 3.1 IDENTIFICATION OF SOURCE OF ACOUSTIC ANNOYANCE

The factors chiefly responsible for the annoyance reported by the dozen residents near the MOD-1 are discussed here in terms of both source and impact. The characteristics of the turbine acoustic emissions that occurred during the annoyance episodes are discussed first, and then the effects of these emissions on the residential structures.

##### 3.1.1 Annoyance-Related Acoustic Emission Characteristics of the Wind Turbine

Our analysis of the near-field acoustic data (measurements taken at 1.5 rotor diameters or 107 m upwind from the turbine rotor hub at ground level) has shown that the averaged frequency spectrum indicates three types of aerodynamic or aeroacoustic sources. The relative contribution of each of these sources, and the resulting distribution of acoustic energy across the frequency spectrum, occur in different proportions depending on the characteristics of the wind blowing through the turbine support tower and the rotor disk. Figure 3-1 illustrates an averaged sound pressure spectrum in which two of the three aeroacoustic sources identified are present. This spectrum is composed chiefly of broadband, incoherent rotor noise with a few discrete tones in evidence out to about 10 Hz. Two distinct tones at 60 and 79 Hz are related to mechanical and electrical equipment in the turbine. The low-frequency tones or rotational noise discretions are the reflection of unsteady aerodynamic loads on the blades as they move around the rotor disk and are brought about by such factors as wind shear, inflow turbulence, and the tower wake. Figure 3-2 depicts the corresponding pressure-time plot of a portion of the record used to obtain the average of Figure 3-1 but contains four blade passages by the tower or two complete rotor revolutions. The windspeed at the hub at that time averaged  $9 \text{ m s}^{-1}$  (20 mph), was rather steady, and apparently low in turbulence.

Figure 3-3 illustrates the strong, highly energetic impulses recorded during the evening of February 7, 1980, which are imbedded in the normal pressure-time signature similar to that of Figure 3-2. Compare the sharpness and higher peak overpressures of these impulses with those of Figure 3-2. Figure 3-4 plots the corresponding averaged, sound pressure spectrum for the two-minute period from which the time domain plot was taken. Note the many discrete tones extending all the way to 100 Hz. Compare this spectrum with that of Figure 3-3. Figures 3-5 and 3-6 increase the time resolution of the time-pressure plots to include only a single blade passage by the tower, allowing waveforms to be compared in much greater detail. The more gentle traces of Figures 3-2 and 3-5 were made when the rotor was parallel to the southeast-facing side of the tower (SE flat) and those of Figures 3-3 and 3-6 were made as the blade passed slightly closer while perpendicular to the tower north-south (N-S) diagonal. Figure 3-7 illustrates the tower construction arrangement and blade passage distance relationships. The blade came slightly closer to the tower leg (5 leg diameters downstream) near the N-S axis,

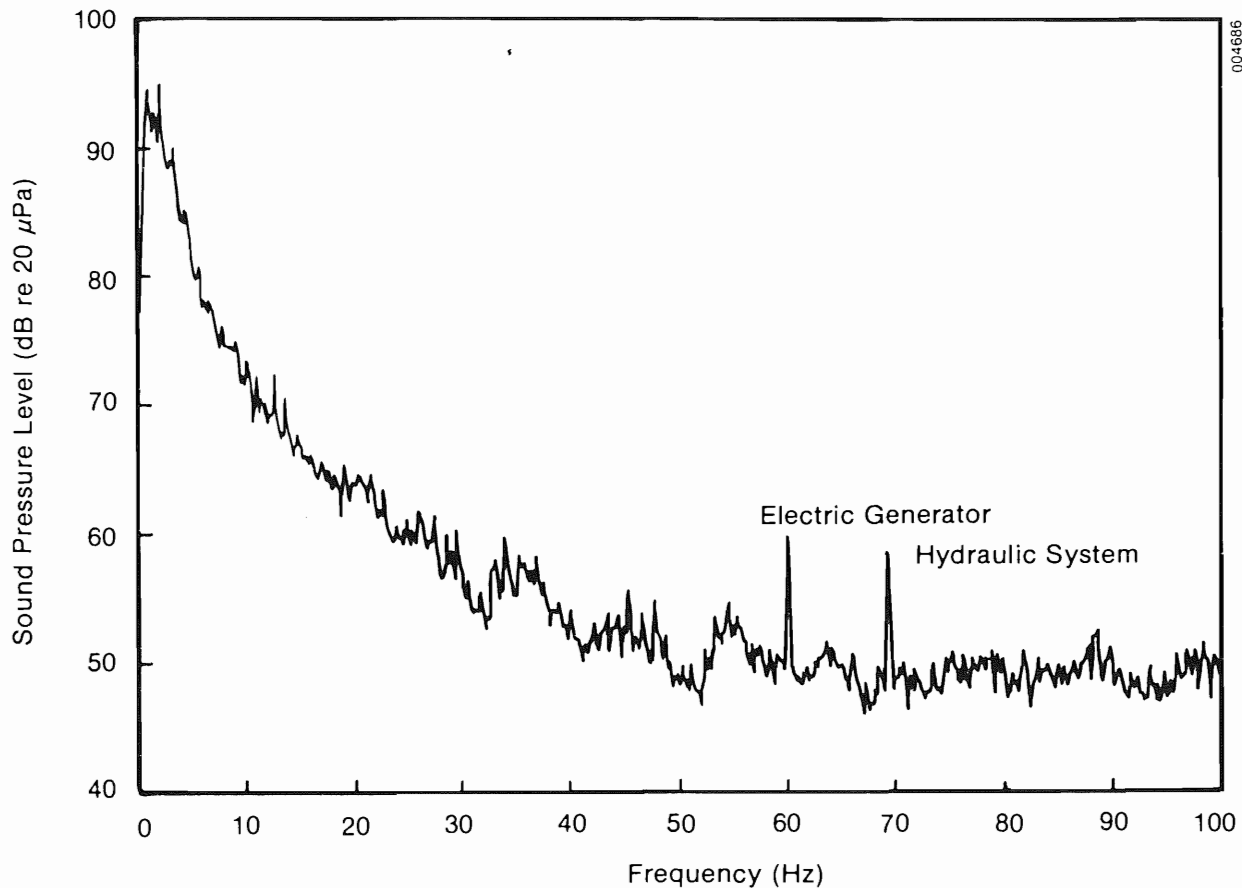


**Figure 3-1. Averaged MOD-1 Sound Pressure Spectrum with No Periodic Impulses Present ( $B_e = 0.25$  Hz)**

compared with the 7.5 leg diameter spacing while the blade was parallel to the SE flat. The wind speed during the period of intense impulses was  $11 \text{ m s}^{-1}$  (25 mph).

The pressure-time history of Figure 3-8 is similar to the intense impulse periods illustrated in Figures 3-3 and 3-6 but was recorded on March 31, 1980, in the far-field outside of House #8 shown in Figure 1-2. This 1-1/2 story, frame construction home is located about 1 km to the ESE and 300 m below the turbine. At the time of this recording, the home was experiencing what was described by the SERI personnel in the house as a "very heavy thumping" sensation. Confirmation was provided by two of the residents who were also

present. The turbine rotor was oriented at that time slightly closer to one leg but almost parallel to the SE flat of the tower. Examining Figure 3-8 more closely, the time delay between the two major negative-going pulses (81 ms) translates to an equivalent linear distance (for a MOD-1 blade tip velocity of  $111 \text{ ms}^{-1}$  at 35 rpm) of 9.3 m (30.5 ft). The horizontal spacing of the two vertical members of the tower at tip height on the SE flat is 9.5 m (31.2 ft). The wind at hub height was gusty and averaged  $11\text{-}13 \text{ ms}^{-1}$  (25-30 mph).

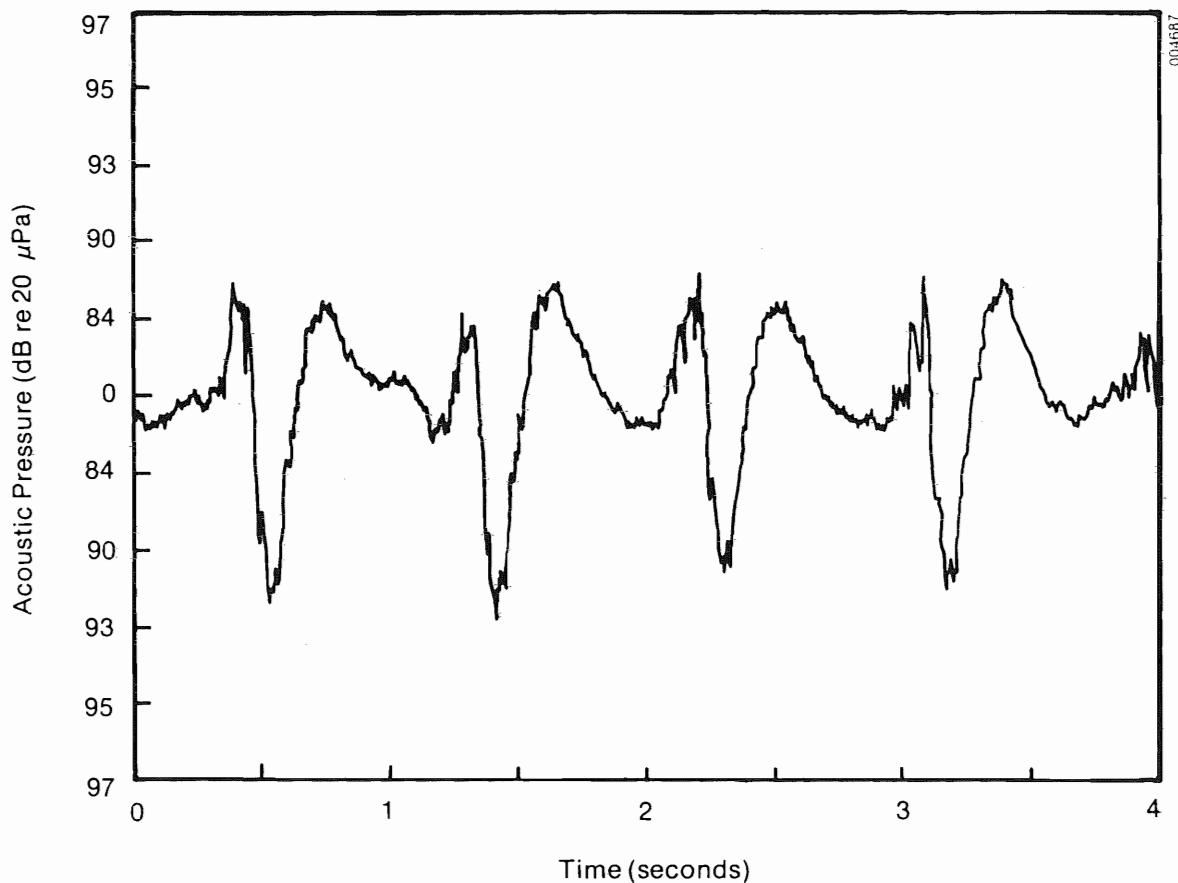


**Figure 3-2. Typical Pressure-Time Plot of MOD-1 Acoustic Emissions with No Periodic Impulses Present.** (Two complete rotor revolutions and four blade passages)<sub>14</sub>

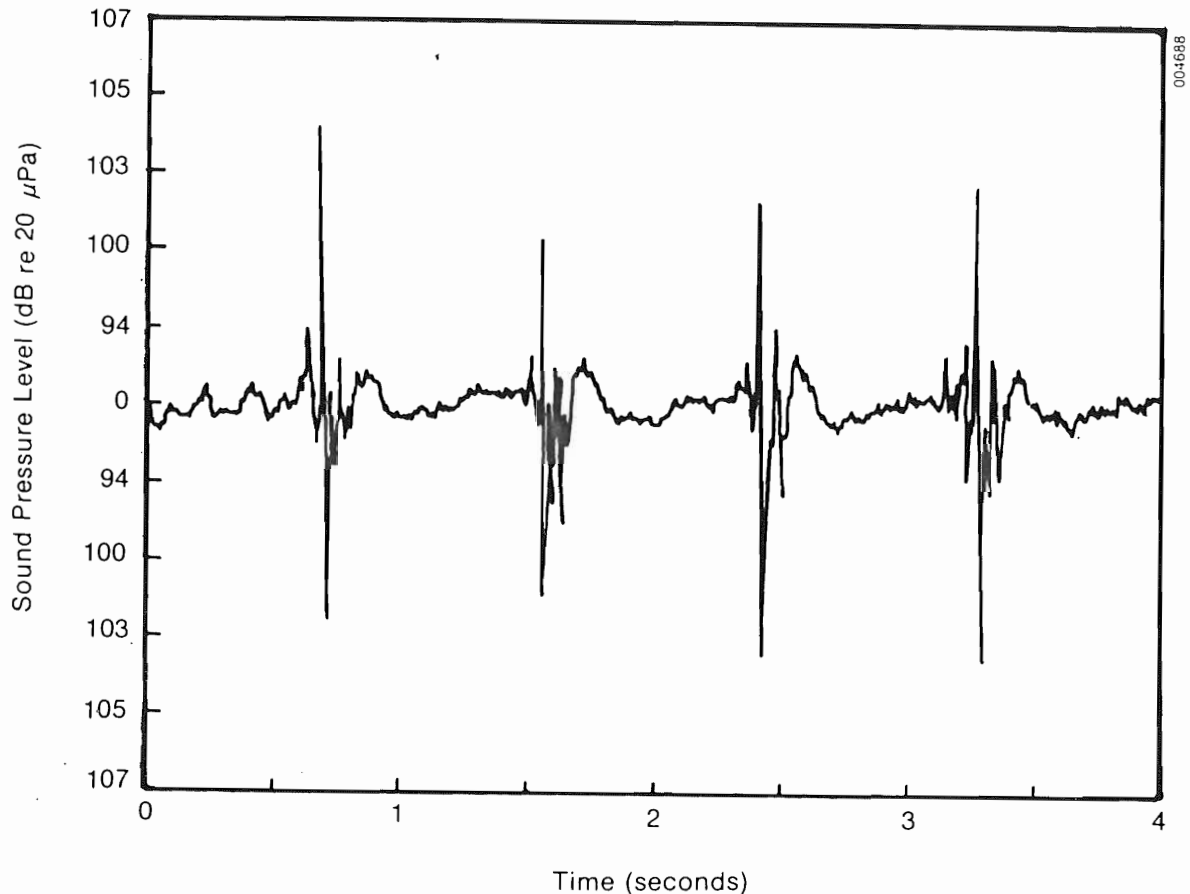


**Figure 3-3. Typical Pressure-Time Plot of MOD-1 Acoustic Emissions Containing Strong Period Impulses.** (Two complete rotor revolutions and four blade passages)

From this it was clear that whatever was producing these acoustic impulses was taking place in the lee of the 0.5-m-diameter tower legs. Furthermore, the impulses were also the most likely source of the low-frequency "thumping" sounds the residents reported. Impulsive waveforms of this type, when transformed into the frequency domain, generally resemble the  $(\sin x)/x$  or sinc function shape, as illustrated in Figure 3-9. The characteristic spectral shape of an impulse also indicates the distribution of acoustic energy as a function of frequency in the radiated emission, with the total impulse energy striking a surface defined as the energy intensity  $E_I$  (energy per unit area), or

$$E_I = \frac{1}{\rho c} \int_0^T (p(t) - p_0)^2 dt = \frac{1}{\rho c} \int_0^T \hat{p}^2(t) dt, \quad (3-1)$$

where  $\rho$  is the air density;  $c$ , the sound speed;  $p_0$ , the local atmospheric pressure;  $p$ , the total pressure;  $\hat{p} = p - p_0$ , the dynamic (over or under) pressure; and  $T$ , the impulse duration (Parseval's Theorem).

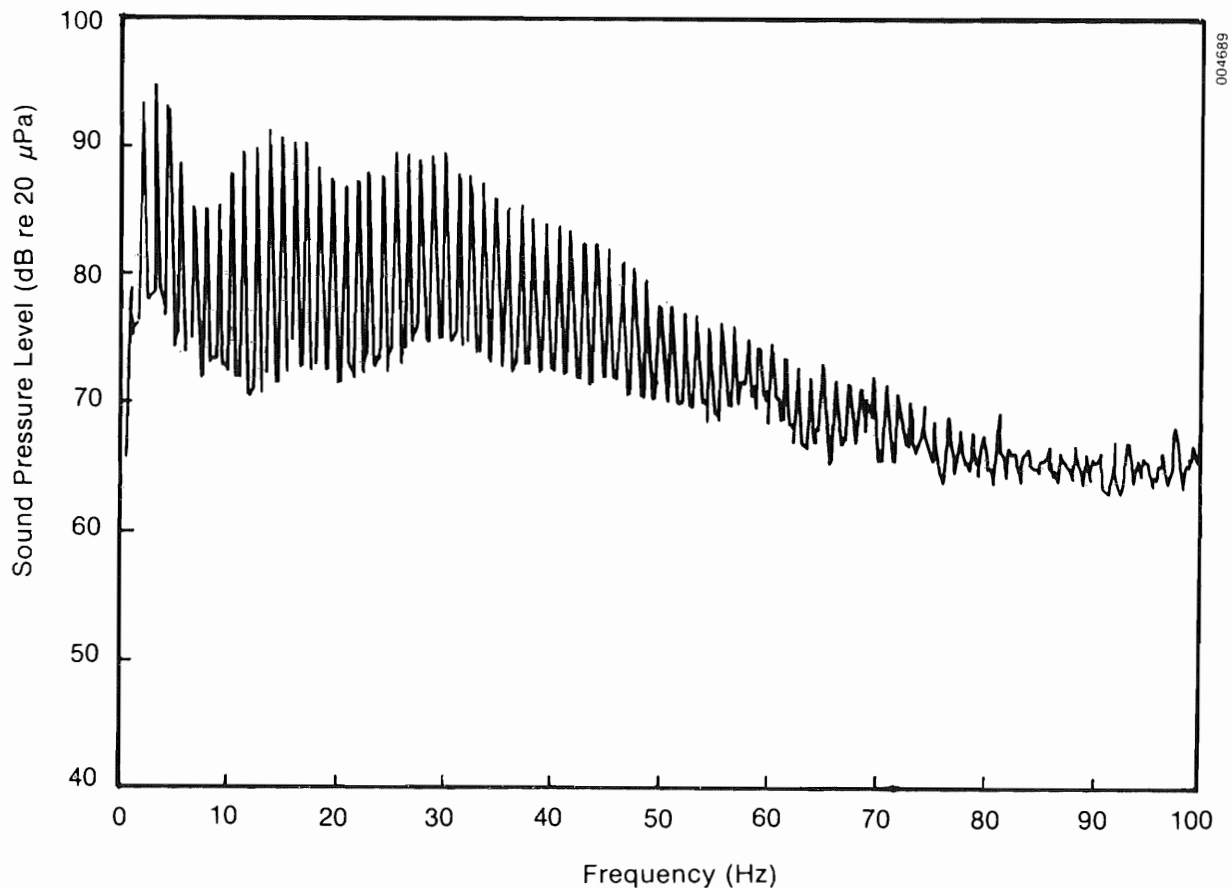
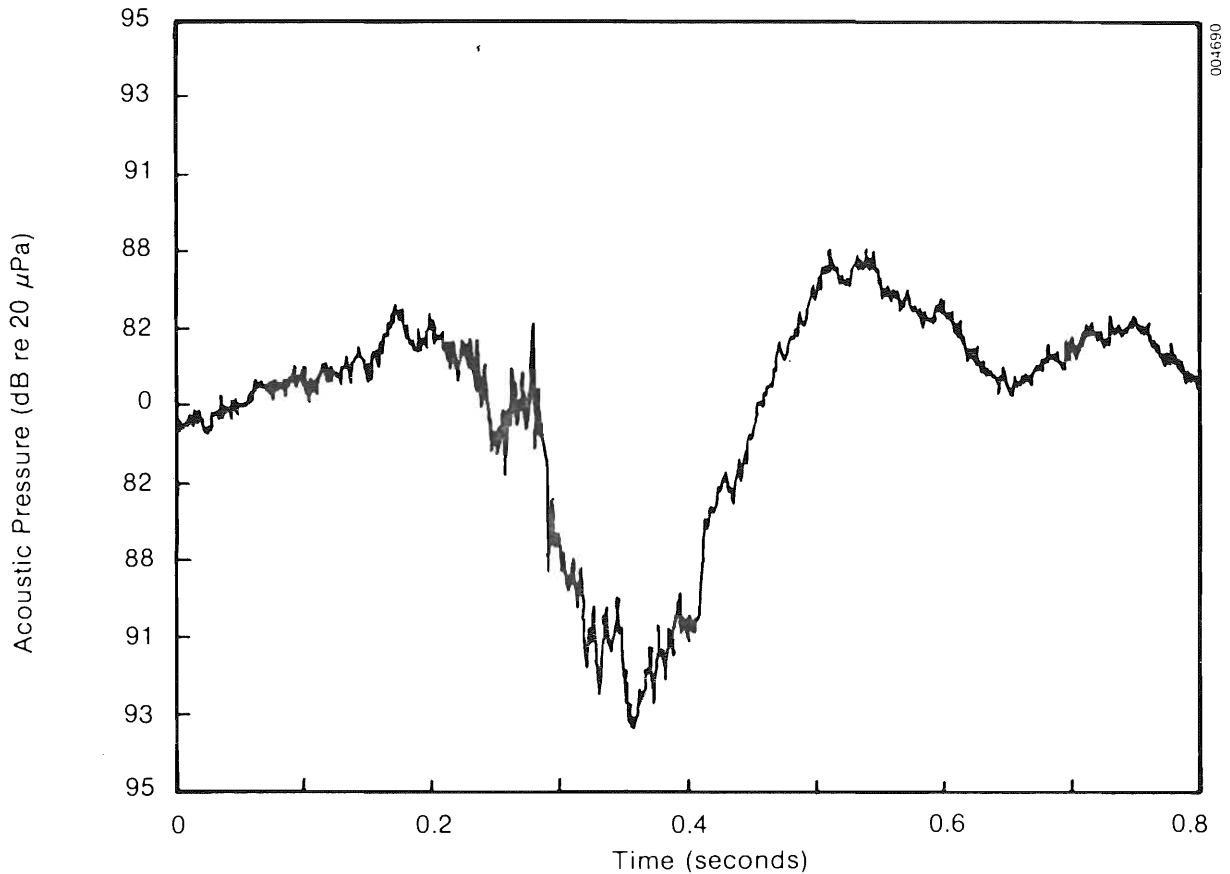


Figure 3-4. Averaged Sound Pressure Spectrum of MOD-1 Acoustic Emissions Containing Strong Periodic Impulses ( $B_e = 0.25$  Hz)



**Figure 3-5. Detail of Typical Pressure-Time Plot of MOD-1 Acoustic Emissions with No Periodic Impulse Present.** (Single blade passage by tower)

The spectral distribution of the acoustic energy of the impulse shown in Figure 3-9 is given by the Fourier transform of the dynamic acoustic pressure. To describe the energy distribution with frequency, both the magnitude and phase spectra are necessary. The magnitude spectrum shows how the energy is distributed as a function of frequency, and the phase spectrum indicates how energies in the frequency bands are related to each other in time (i.e., does it all appear at the same instant or does the energy in some bands lag or lead others with respect to some time reference?). The phase spectrum of Figure 3-9, which corresponds to the  $(\sin x)/x$  distribution of the magnitude spectrum,

indicates that by the zero phase angle at these frequencies the harmonic energy peaks are in phase with one another; i.e., they occur at the same instant in time. Thus, this type of impulsive acoustic radiation is usually referred to as coherent, a term borrowed from the study of optics, which infers that corresponding points on a propagating wavefront are in phase. This means the harmonic energy from an impulse arrives at the receiver at the same time or with a definite phase relationship, as opposed to an incoherent source which is composed of harmonic energies that are radiated with a random phase (time) relationship. In this regard, an impulsive source may be viewed as a much more efficient radiator in its ability to transfer energy to a receiver than a broadband, incoherent source (for a pure rectangular-shaped impulse, the phase angle is zero across the entire frequency spectrum), compared with the much longer time that is usually necessary to transfer the same total amount of broadband, incoherent energy.

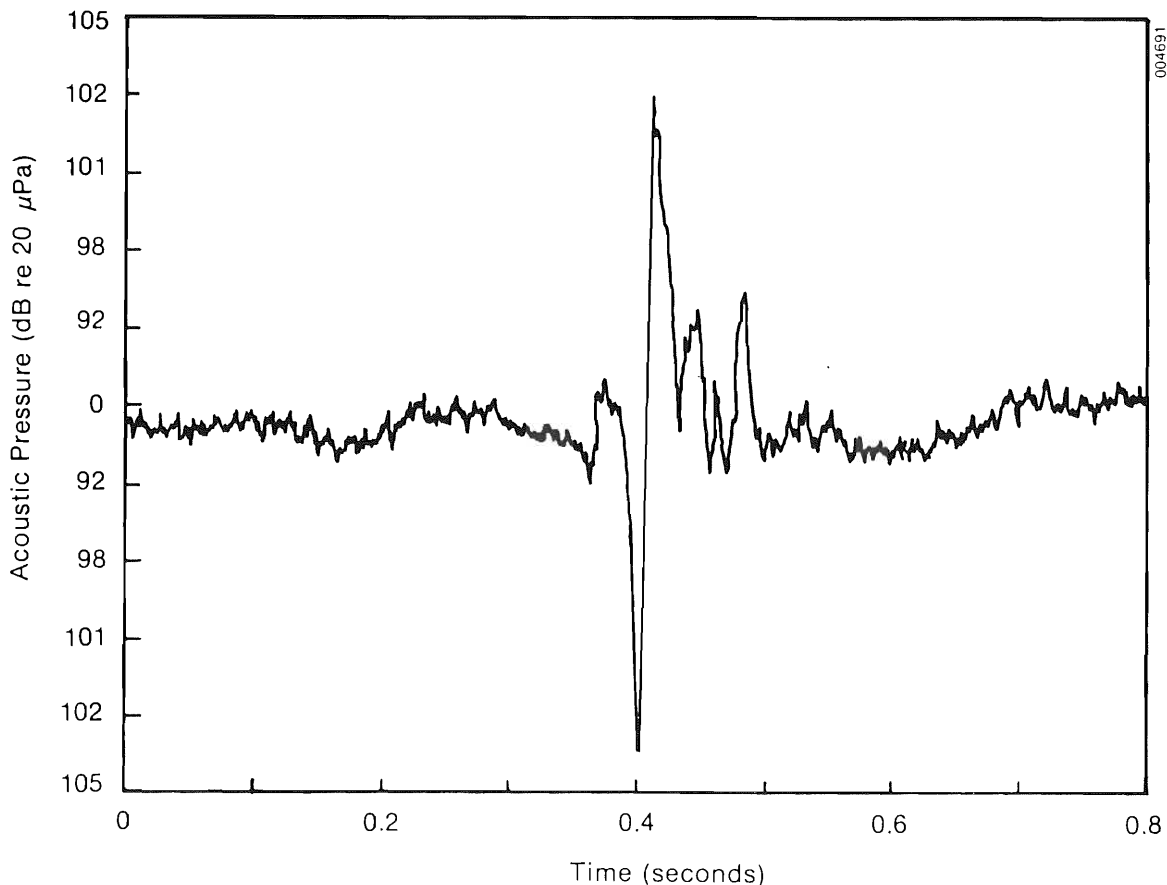


Figure 3-6. Detail of Typical Pressure-Time Plot of MOD-1 Acoustic Emissions Containing Strong Periodic Impulses. (Single blade passage by tower)

004682

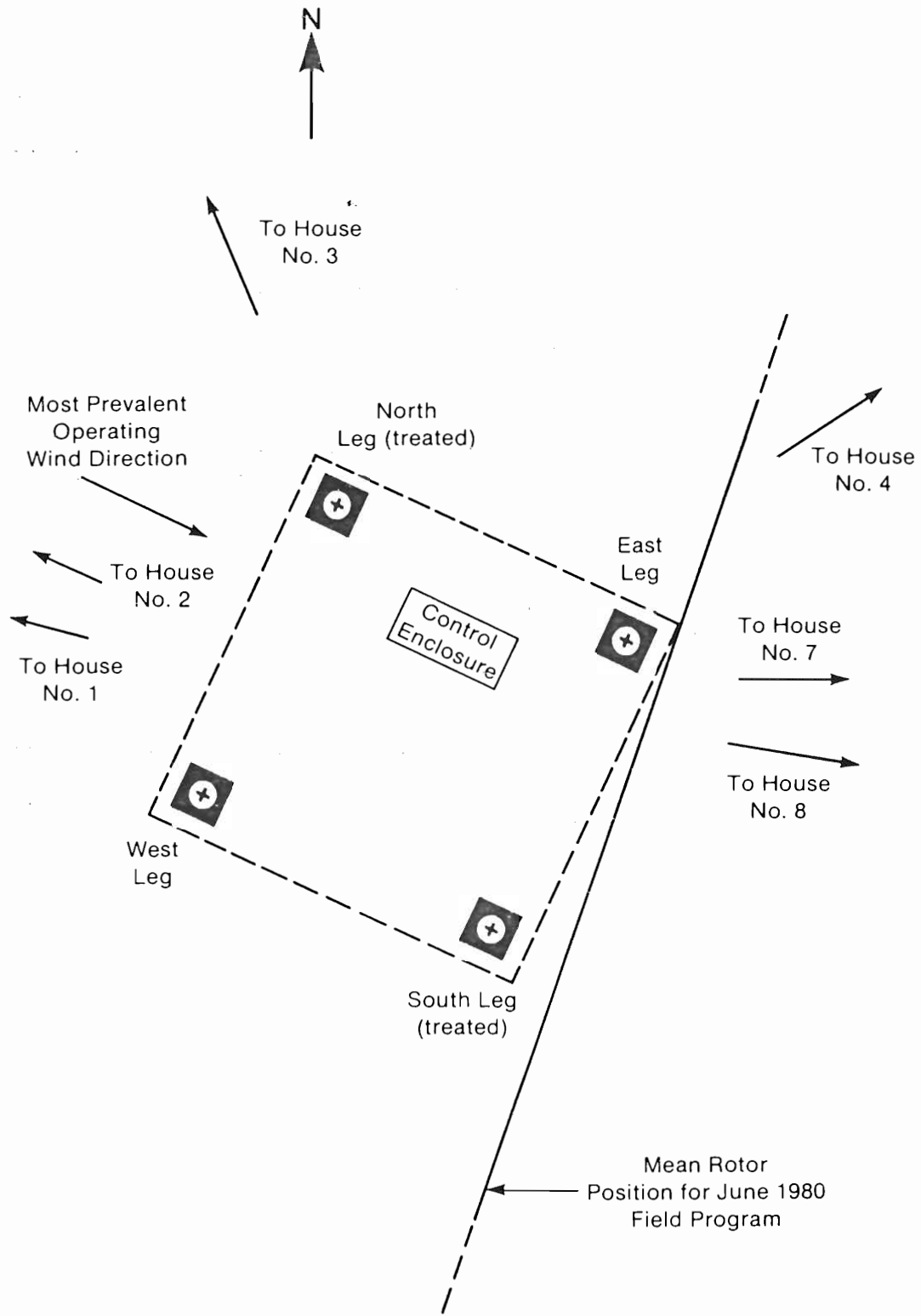
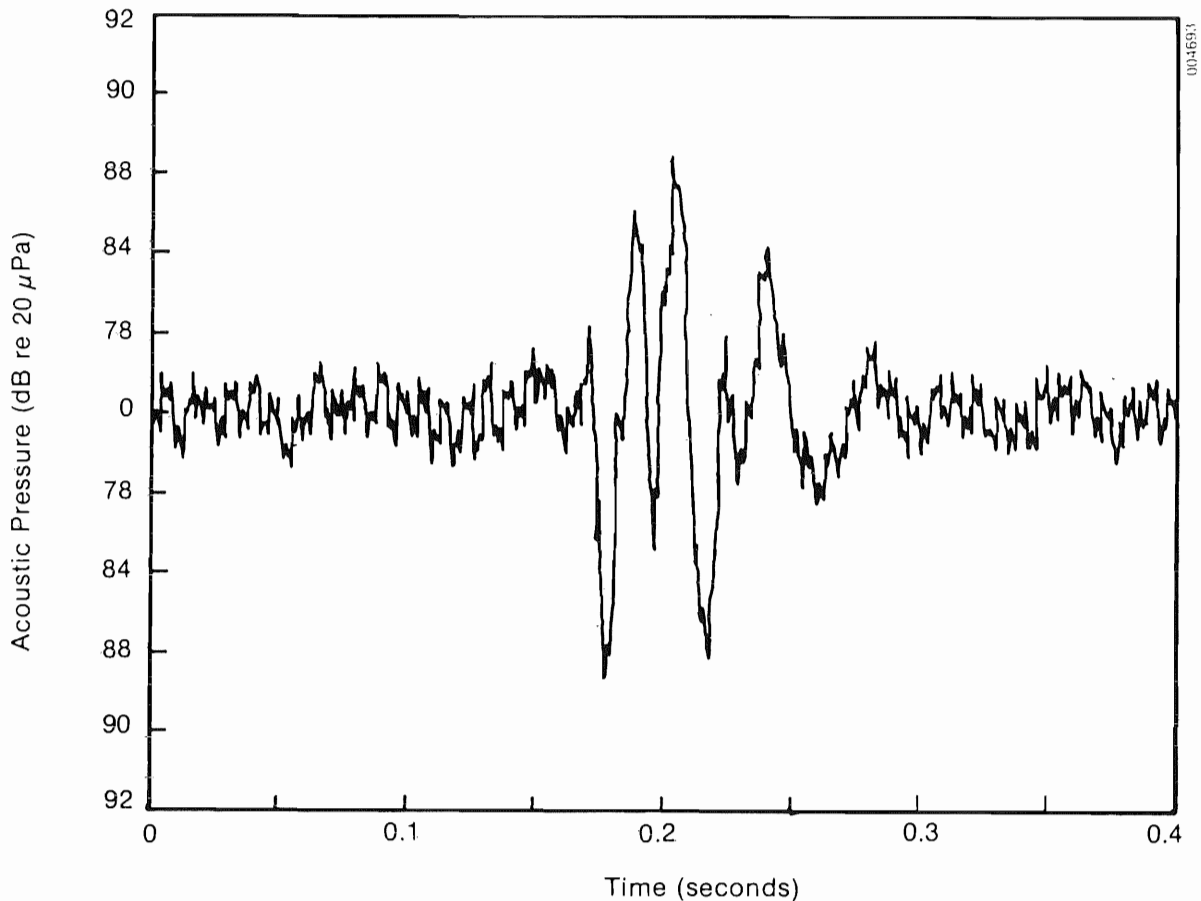


Figure 3-7. MOD-1 Tower Base Layout and Relationships to Rotor Plane, Prevalent Operating Wind Direction, and Orientations of Complainants' Homes





**Figure 3-8. Pressure-Time Plot of Moderate-to-Severe MOD-1 Acoustic Impulse Measured Outside House #8. (Single blade passage by tower)**

Coherent pulses of the type described above are best evaluated using energy techniques in both the time and frequency domains. The time domain is used to establish important waveform characteristics of the impulses; i.e., the rise time, rise rate, total energy content, and peak overpressure (underpressure or deviations from the local static pressure value). These are discussed more fully in Section 4.0. The frequency domain, through the application of the Fourier transform, provides the spectral or harmonic distribution of the impulse energy. Figure 3-10 plots the energy distribution for the impulse of Figure 3-8.

Thus, we have found that the impulsive character of the MOD-1 acoustic radiation related to the passage of the rotor blades through the downstream wakes of the cylindrical, vertical tower support members or legs is in some way responsible for the annoyance complaints.

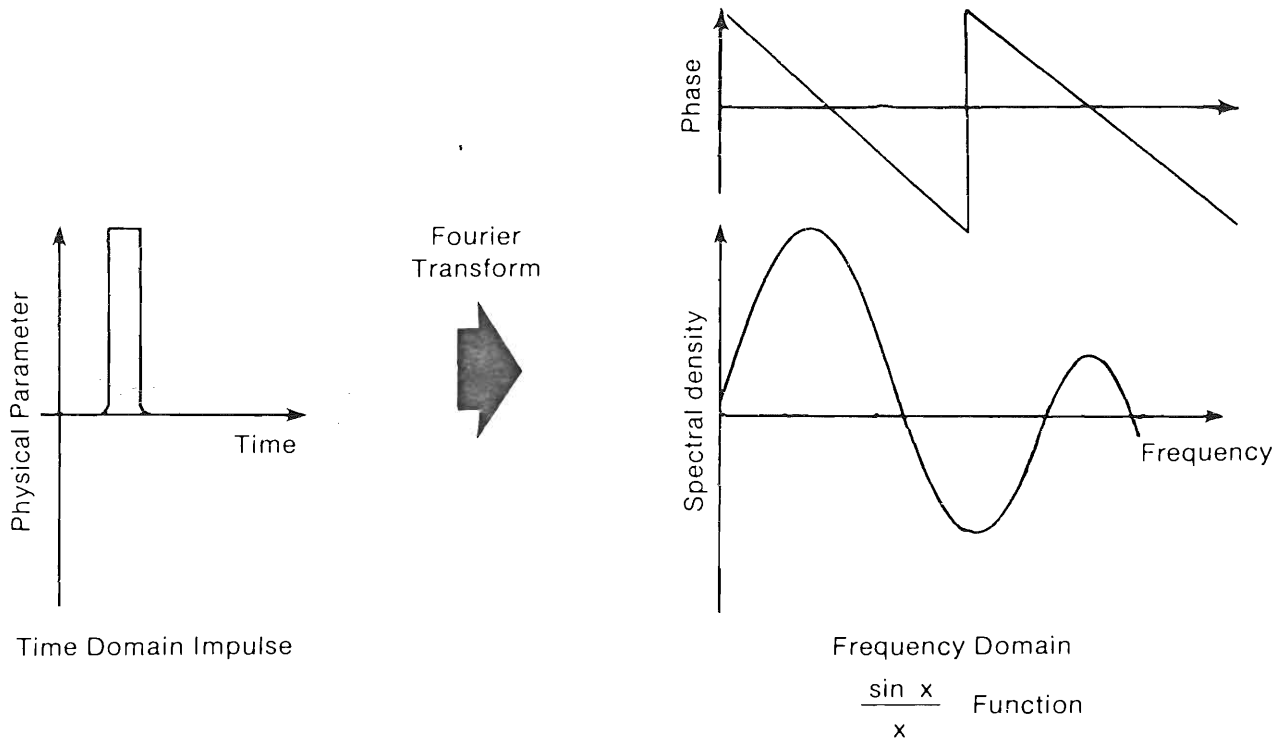


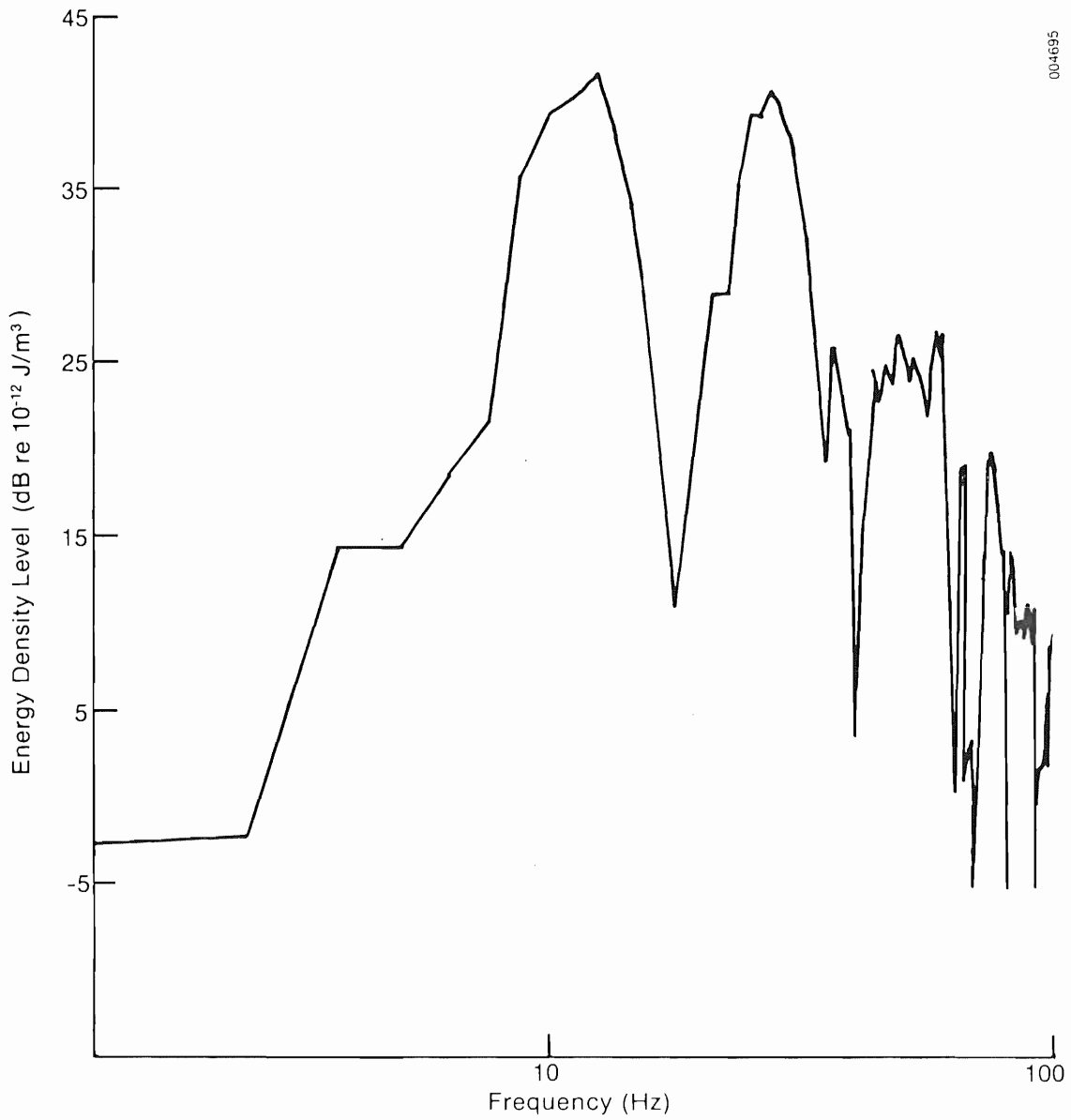
**Figure 3-9. Schematic Example of the Transformation of a Time Domain Acoustic Impulse into the Frequency Domain as a  $(\sin x)/x$  Function**

### 3.1.2 Annoyance and Acoustic-Structural Interaction

After the acoustic impulse was identified as a possible source of the annoyance associated with the MOD-1, it became important to understand the mechanism(s) prompting the noise complaints themselves, particularly because people generally appeared to be more annoyed inside their homes than out. To determine the physical basis of the complaints (i.e., thumping sounds and vibrations inside the affected homes), we instrumented two of the most frequently affected homes with acoustic and seismic equipment and recorded the range of severity of the turbine-induced impulsive noises.

#### 3.1.2.1 External/Internal Acoustic Fields Under Turbine-Induced Impulsive Excitation

Houses #7 (a double-wide mobile home) and #8 (a conventional 1-1/2 story frame structure) were instrumented with a pair of our VLF microphone systems, one outside the home and one in the room designated by the owners as the one in which the greatest annoyance occurred. In addition, a precision sound level meter was also installed in the room of the house to better document sounds



004695

Figure 3-10. Acoustic Energy Level Distribution of the Single Impulse Shown in Figure 3-8 Received at House #8

in the normal audible range. We noted that both homes were equipped with storm windows and that the conventional frame house was substantially tighter. Both affected rooms were bedrooms; the room in House #8 has a single window that faces the turbine site. House #7 has two windows that face in the direction of the machine, but it could not be seen because the house was near a steep grade at the base of Howard's Knob.

Figure 3-11 shows the external pressure excitation of the radiated impulse and the resulting indoor pressure trace in the 31.5-Hz octave frequency band in the bedroom of house #8 under moderate-to-severe impulsive annoyance. As shown, the indoor pressure impulse lasted for a period of over a second, in contrast to the two individual impulses outside the house which lasted for only a few milliseconds each (care was taken to ensure that there was no ringing of the filter). Further, there was a time delay between the arrival of the acoustic peak pressure at the outdoor microphone and the initial onset of the internal reaction in the 31.5-Hz band of about 125 ms. The physical separation between the two microphones was about 23 m, and the outdoor one was closer to the wind turbine. The separation at this altitude and air temperature would account for only 73 ms or only about 60%, of the observed delay, which indicated that some form of a dynamic process with storage was involved.

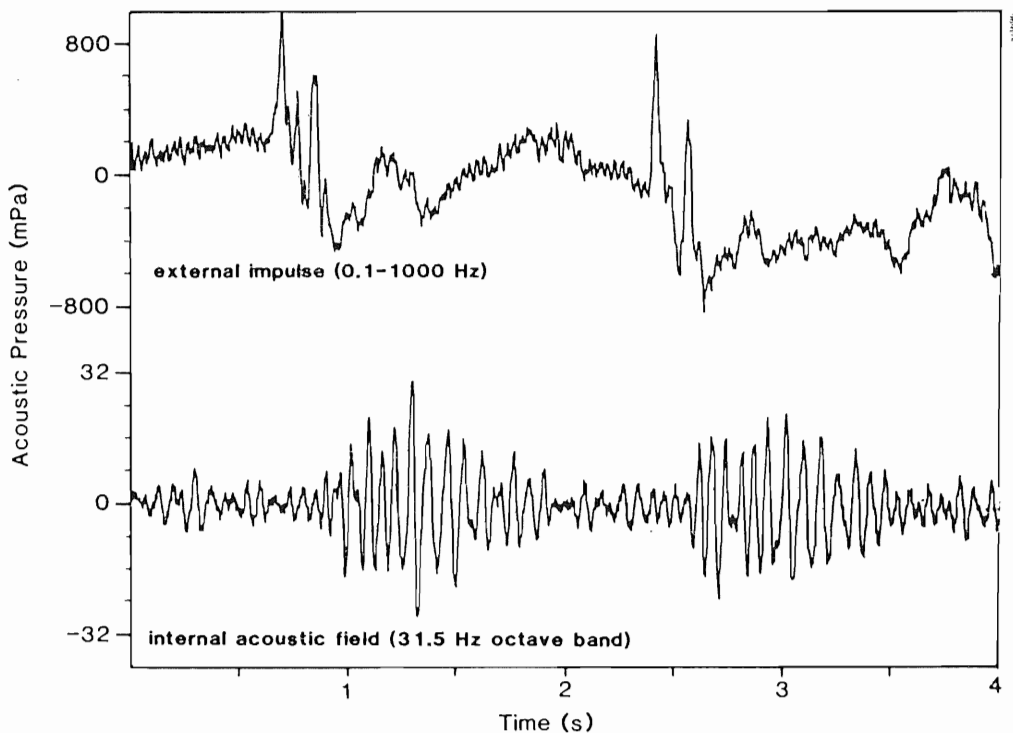
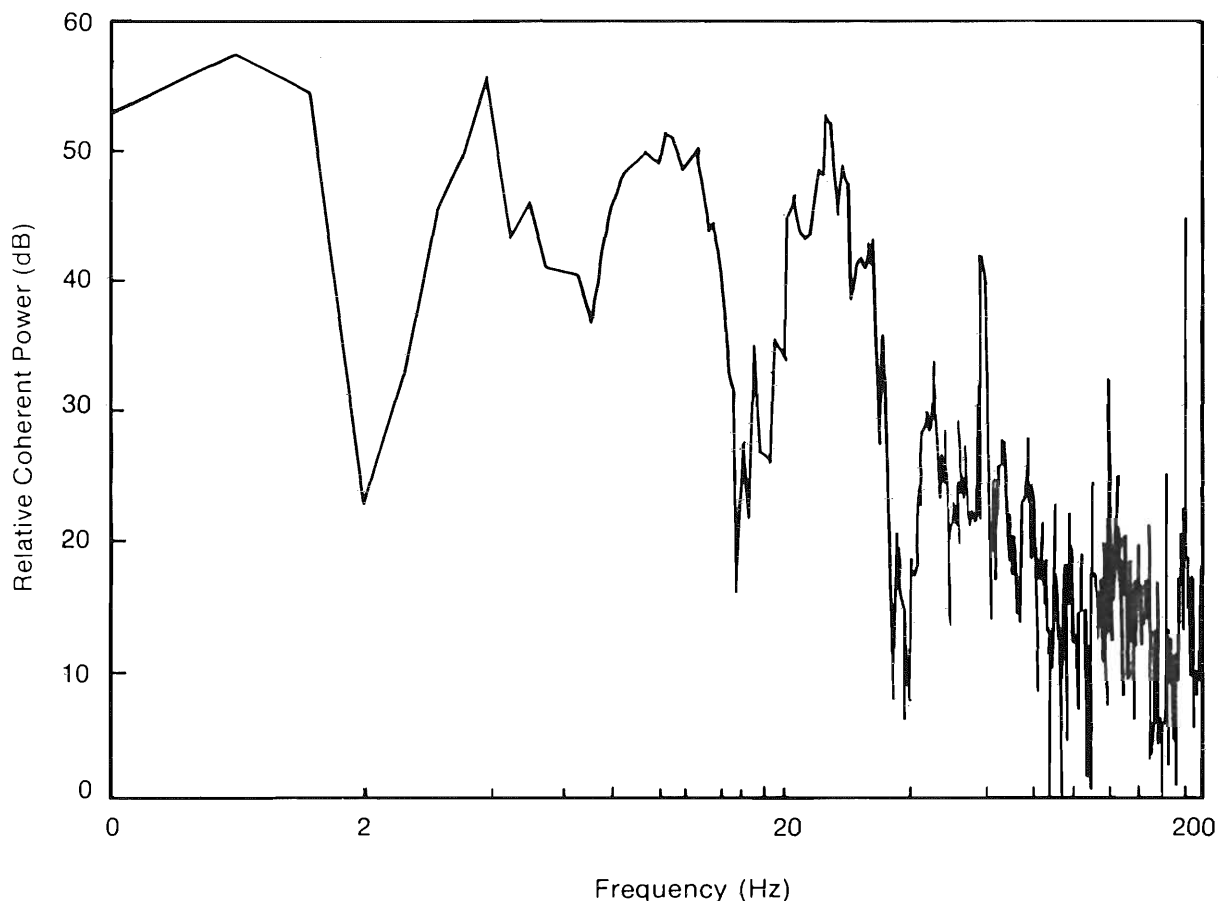


Figure 3-11. Plot Showing Time Delay between Arrival of Outdoor MOD-1 Impulse and Onset of 31.5-Hz Octave Band Acoustic Pressure

The coherent output power\* plots of Figures 3-12 and 3-13 for houses #7 and #8, respectively, indicate that the transmission of impulsive acoustic energy into the house was dispersive because of the observed frequency dependency and not simply a pure delay. The spectra of Figures 3-12 and 3-13 contain peaks at the power line frequency of 60 Hz and its harmonics, the source of which were humming transformers near both homes.



**Figure 3-12. External-Internal Acoustic Coupling Modes of House #7 under MOD-1 Impulsive Excitation**

\*Coherent output power is derived from the product of the squared coherence function and the measured output power spectrum (in this case the indoor acoustic pressure under the excitation of the external impulse) which is useful for determining dynamic interdependence when the output signal may be contaminated with signals containing energies at similar frequencies; e.g., it is the part of the output signal which is coherent with the excitation.

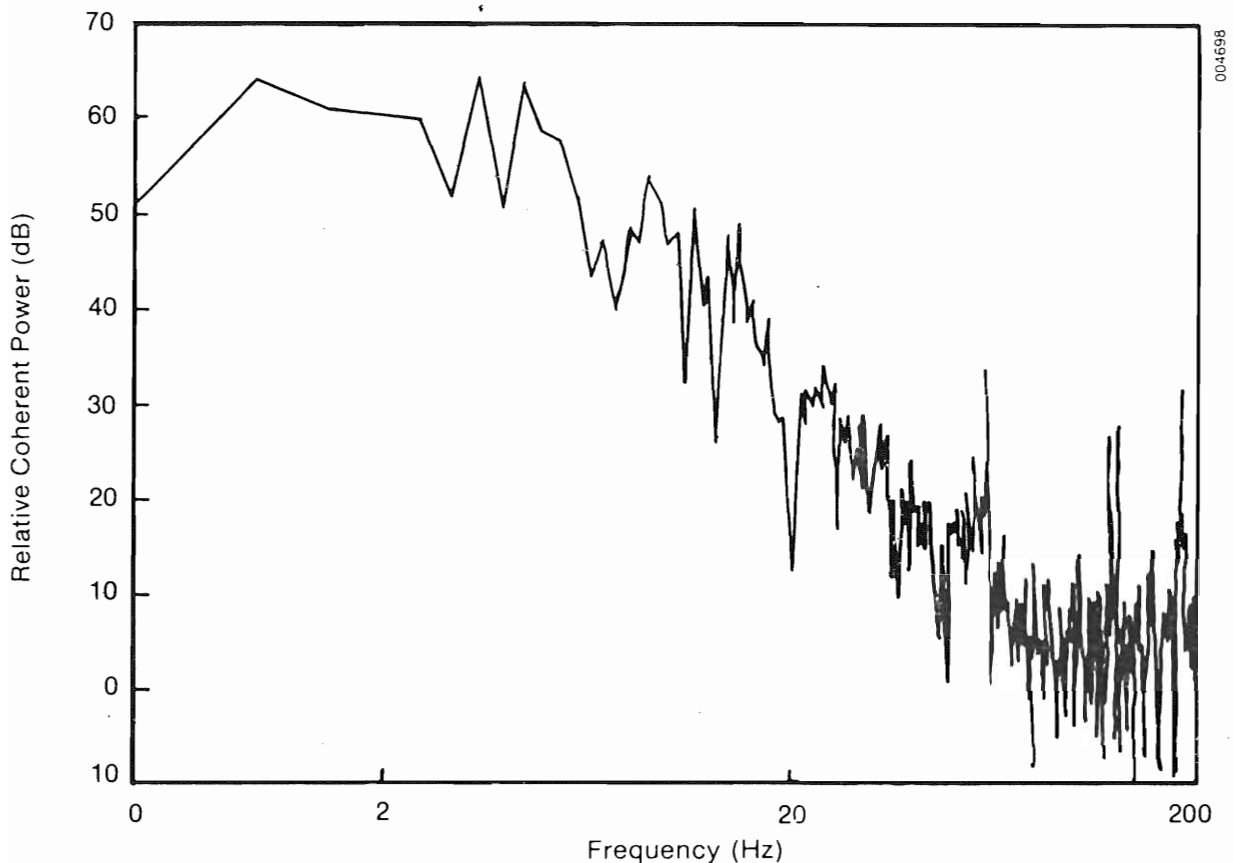


**Figure 3-13. External-Internal Acoustic Coupling Modes of House #8 under MOD-1 Impulsive Excitation**

To compare acoustic pressure fields accompanying moderate annoyance episodes in house #8 with the threshold perception measured at house #7, we analyzed the differences between indoor and outdoor sound pressure levels and the indoor levels as a function of the existing acoustic environment. These results are presented in Figures 3-14 and 3-15. The interior peak overpressures above background for moderate and threshold excitation levels forcing compared with peak outdoor levels are shown in Figure 3-16. Figure 3-17 presents the energy density level spectrum for a typical impulse striking house #7 that permits threshold perception. See, in comparison, the energy density level spectrum of a moderate-to-severe impulse at house #8 in Figure 3-10.

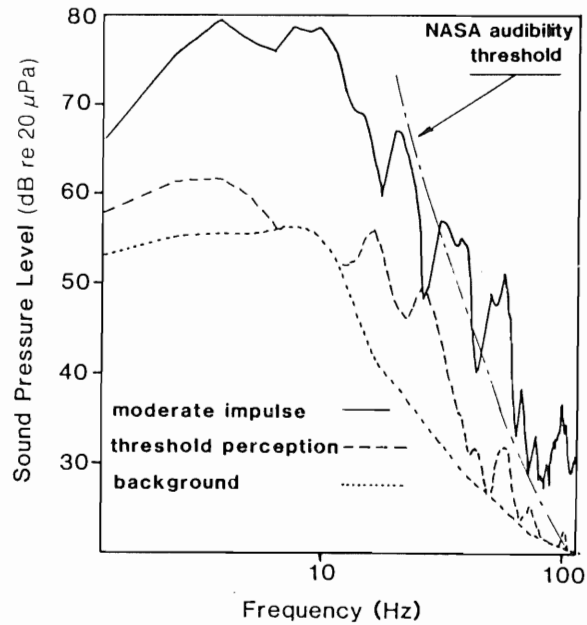


**Figure 3-14. Peak Interior South Pressure Levels Observed in Houses #7 and #8 during Threshold Perception and Moderate Impulsive Annoyance Conditions, Respectively ( $B_e = 1.25$  Hz)**

**3.1.2.2 Structural Response in Houses #7 and #8 under Turbine-Induced Impulsive Excitation**

Figures 3-18 and 3-19 plot the frequency spectra of the horizontal component of the floor vibration under moderate (house #8) and threshold (house #7) perception. In both cases, the sensitive axis of the accelerometer was parallel to the major floor supports, pointing toward the wind turbine. The relative transmissibility function  $T_r$ , defined by

$$T_r = \left\{ \frac{1 + [2\zeta f/f_n]^2}{[1 - (f/f_n)^2]^2 + [2\zeta f/f_n]^2} \right\}^{1/2} = \left[ \frac{G_p(f)}{G_a(f)} \right]^{1/2}, \quad (3-2)$$

(where

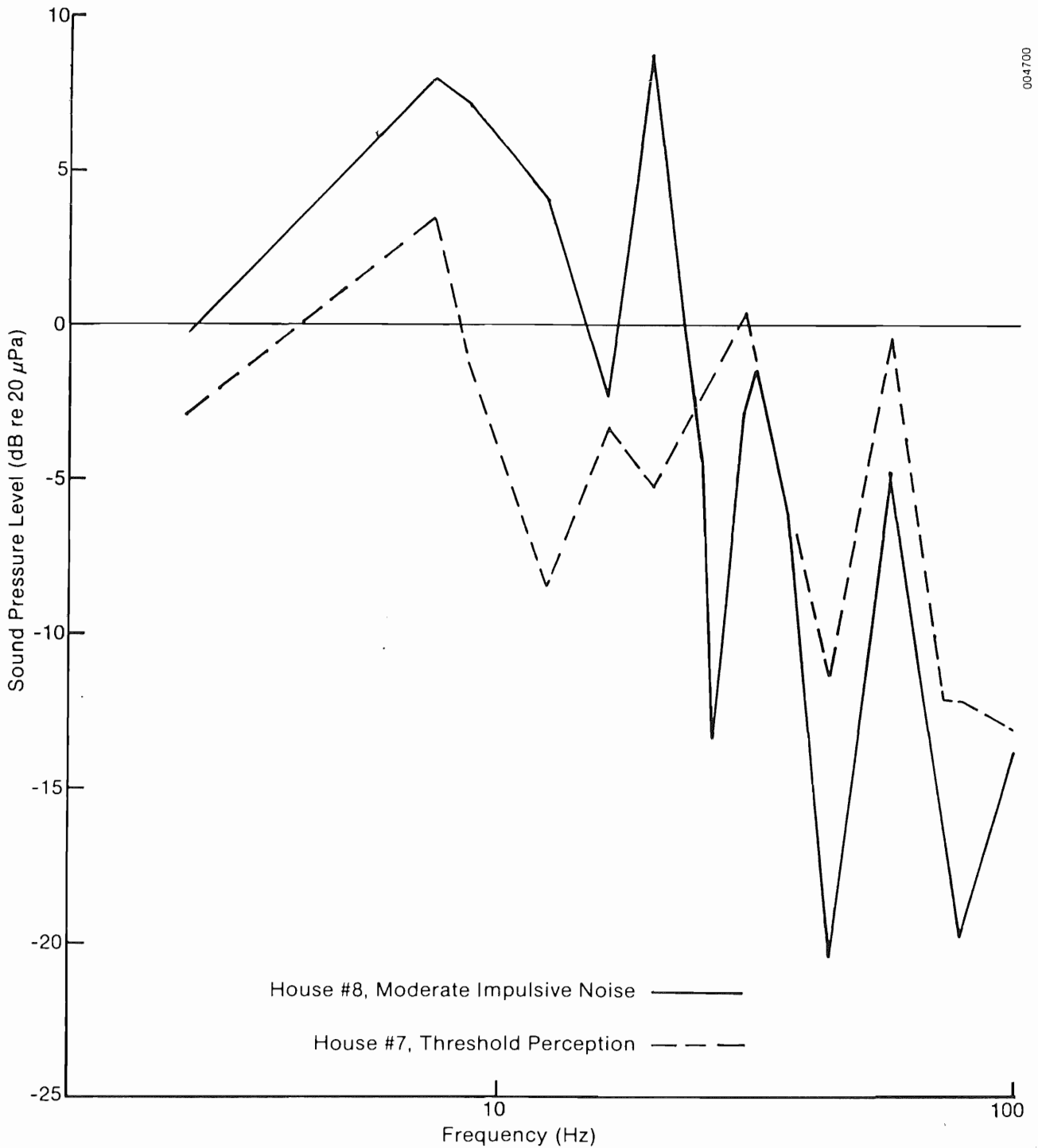
$\zeta$  is the damping ratio of the house mechanical/acoustic/elastic structure given by  $c/2(km)^{1/2}$  and  $c$ ,  $k$ , and  $m$  are the effective damping, stiffness, and mass

$f$  is the cyclic frequency

$f_n$  is the natural frequency of the structure

$G_p(f)$  is the power spectrum of the interior acoustic pressure field and

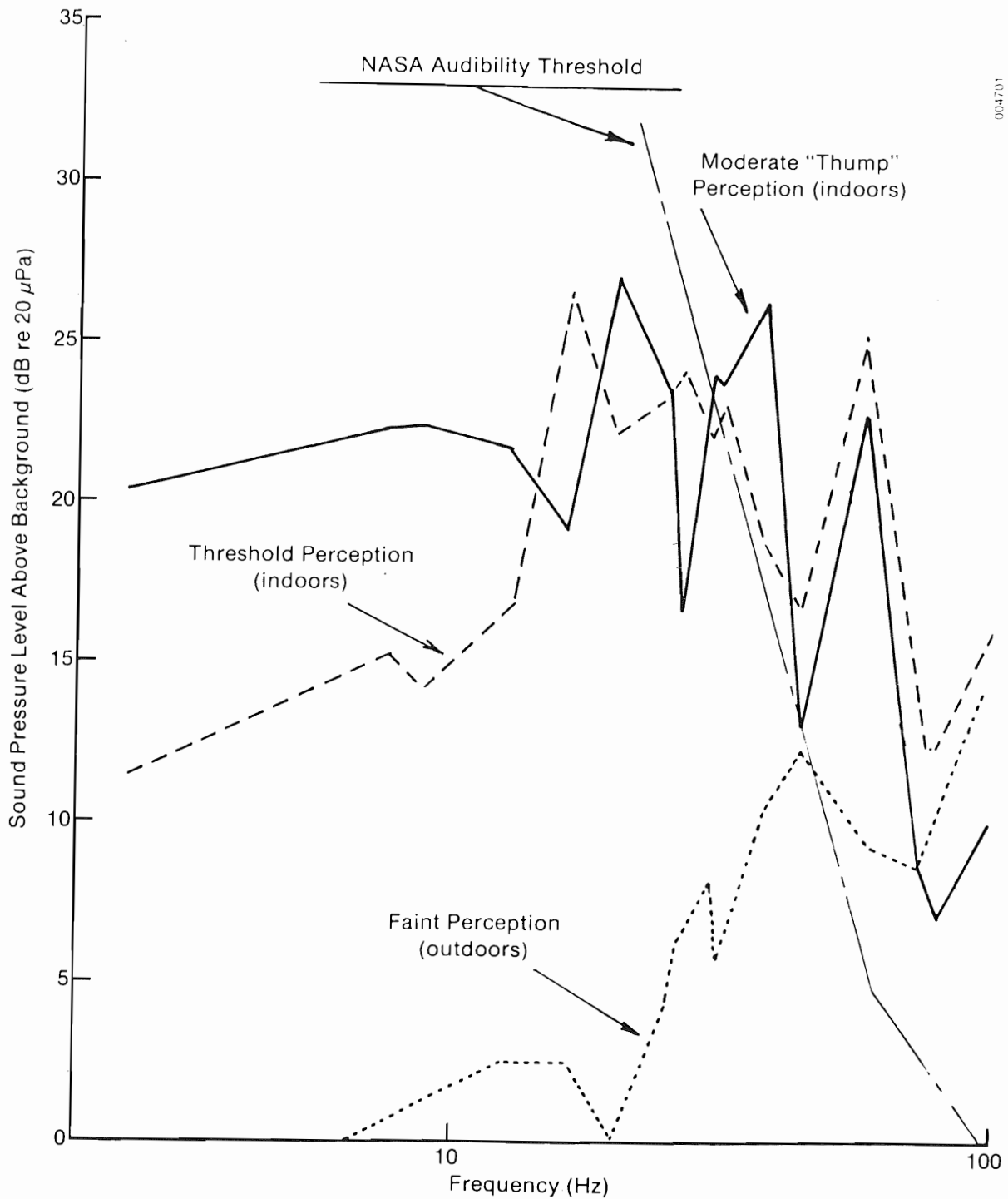
$G_a(f)$  is the floor/wall acceleration power spectrum),



004700

**Figure 3-15. Peak Internal-External Sound Pressure Level Differences for Moderate Annoyance and Threshold Perception in Houses #7 and #8 ( $B_e = 1.25$  Hz)**





004701

Figure 3-16. Peak Sound Pressure Levels above Background for Moderate Impulsive Excitation (Outdoors and Indoors, House #8) and Threshold Perception (Indoors, House #7) ( $B_e = 1.25$  Hz)

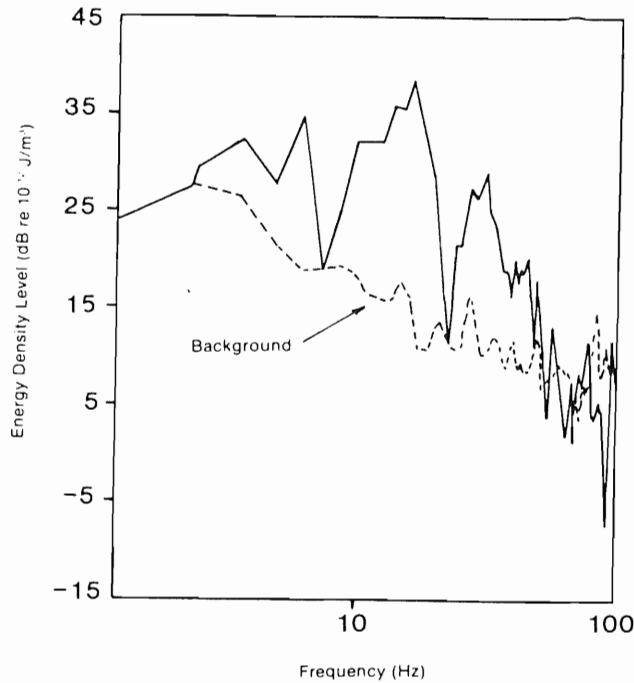


Figure 3-17. External Acoustic Energy Density Level Narrowband Spectrum for Single Impulse Corresponding to Threshold Perception in House #7 ( $B_e = 1.25$  Hz)

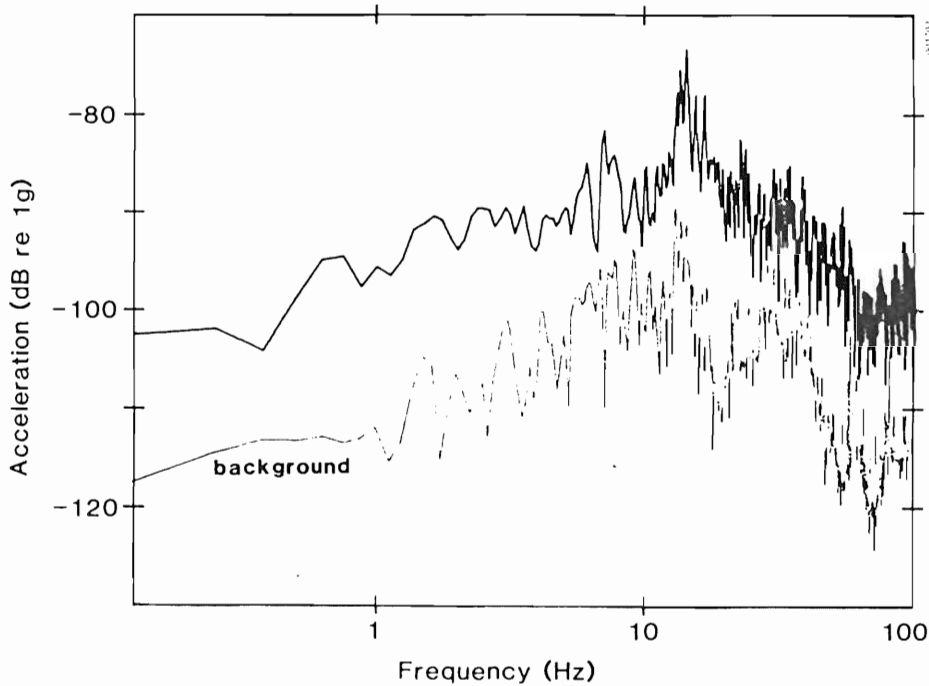
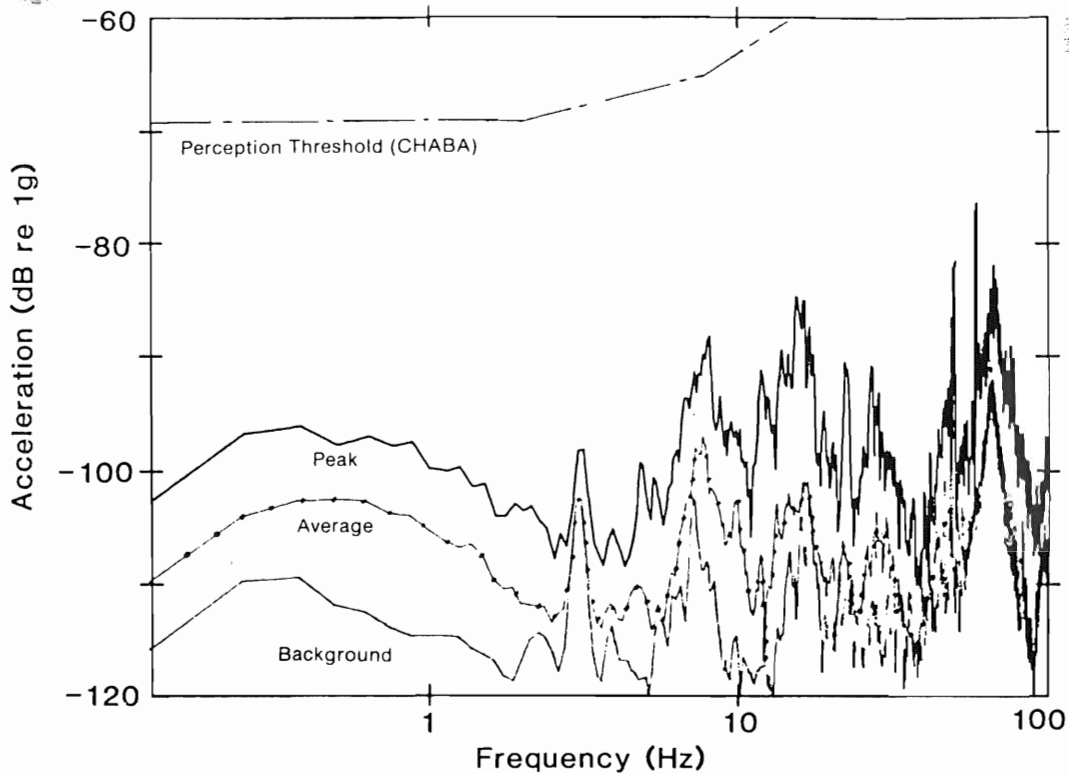


Figure 3-18. Background and Peak Horizontal Floor Acceleration Levels in House #7 during Perception-Level MOD-1 Impulsive Excitation ( $B_e = 1.25$  Hz)



**Figure 3-19. Peak, Average, and Background Horizontal Floor Acceleration Levels in House #8 during Moderate Annoyance MOD-1 Impulsive Excitation ( $B_e = 1.25$  Hz perception threshold: see Ref. [50])**

is plotted in Figure 3-20 for the acoustic pressure field of the affected room of house #8, using both the vertical and horizontal floor accelerations as the forcing (made relative by setting the levels equal, or 0 dB at  $f = 0.2$  Hz). Equation (3-2) describes the dynamic interaction between the walls and air volume contained within the affected room and, in this case, indicates the level of dynamic coupling between the mechanical forcing of the floor vibration (displacement) and the room acoustic pressure. As shown in Figure 3-20, the horizontal floor motion is coupled more to the pressure field in several frequency bands than the vertical mode is. This agrees with the low acceleration levels measured in the vertical orientation, plotted in Figures 3-18 and 3-19 for houses #7 and #8. Note the dynamic relationship between the external pressure forcing by turbine-generated impulses and the elastic response of the vertical floor acceleration plotted in Figure 3-21; the maximum occurs in the 10-20 Hz frequency band, with less prominent effects in the 20-40 and 40-80 Hz bands.

### 3.1.2.3 Groundborne (Seismic) Propagation/Excitation by Turbine

At the beginning of the field measurement program, we did not know if groundborne noise propagation from the MOD-1 turbine was a factor in the disturbance of residents living near the base of what was thought to be a solid granite mountain. To answer this question, the Penn State Group installed two Hall-Sears Model HS-10-1 seismometers (geophones) to record any ground excitation by the turbine that might occur near the foundations of houses #7 and #8.

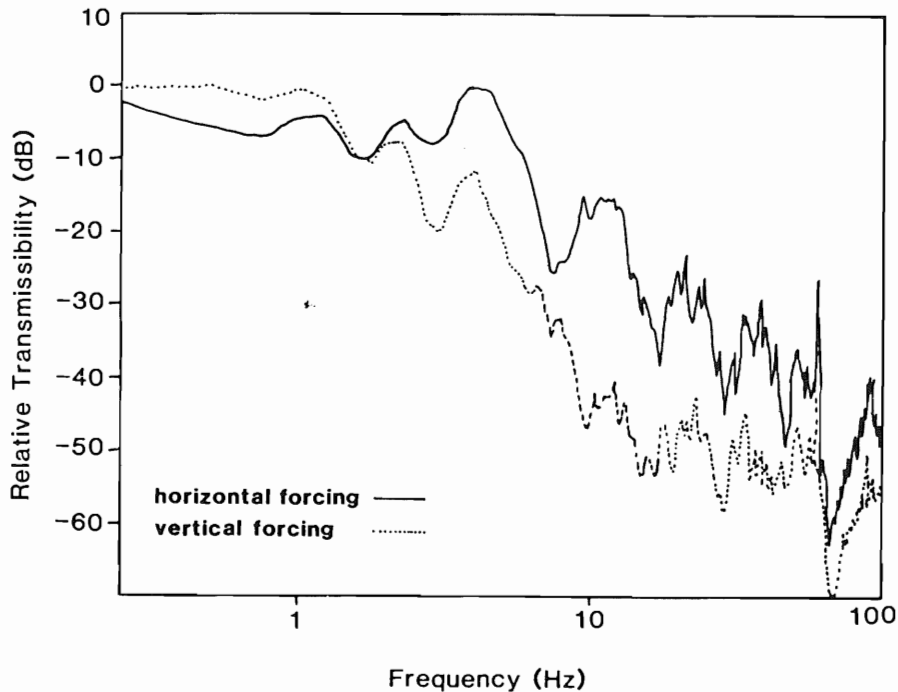
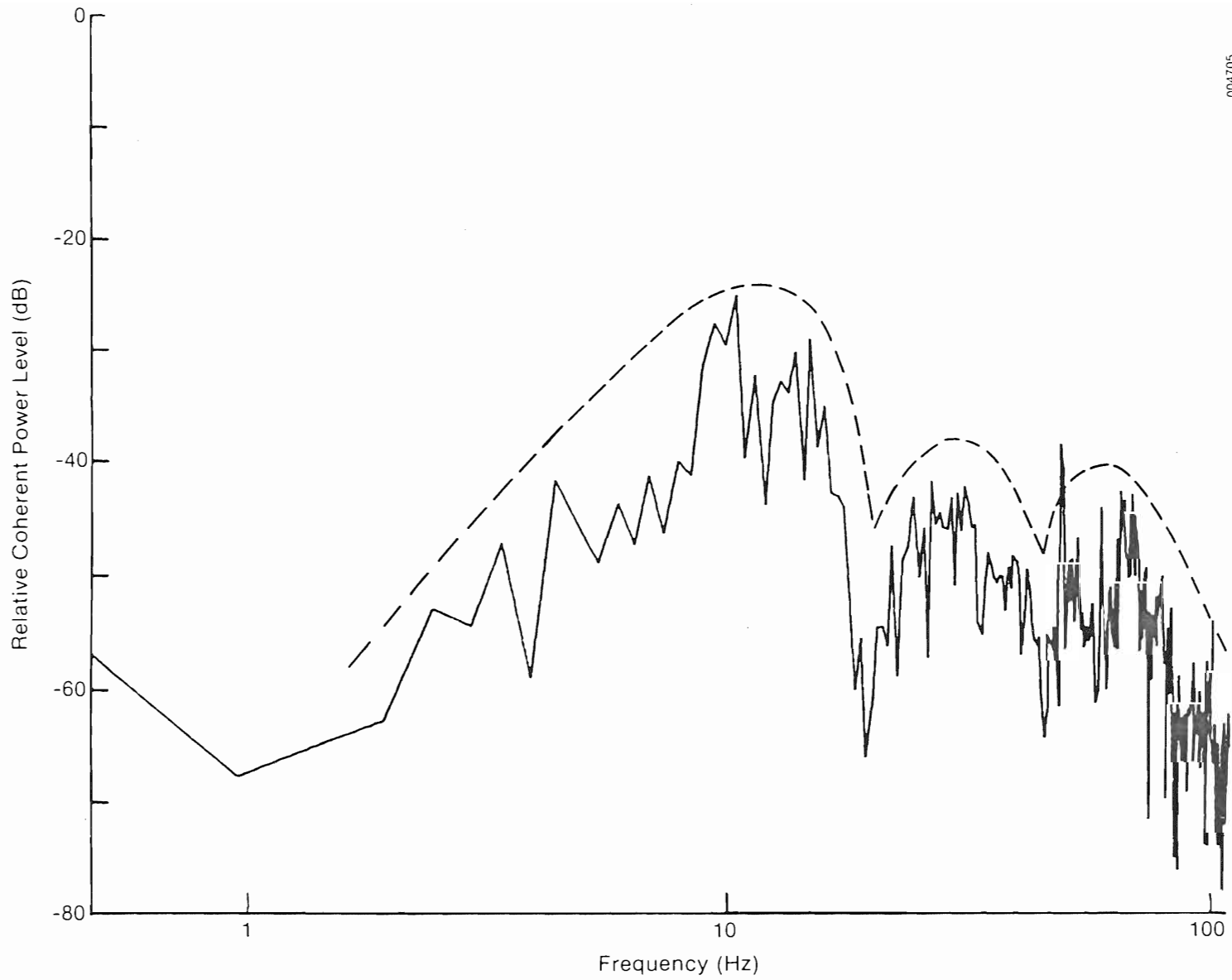


**Figure 3-20. Horizontal and Vertical Plane Acceleration (Deformation)-Forced Internal Acoustic Pressure Transmissibility for House #8 under Moderate Impulsive Excitation ( $B_e = 1.25$  Hz)**

During the recording period, footsteps of persons in the vicinity were much more prominent than the turbine impulses, which indicated that the disturbance was being transmitted by airborne propagation. Ground velocities measured when the turbine was operating and when annoyances were being reported were less than  $0.16 \mu\text{m}\cdot\text{s}^{-1}$  ( $0.4 \mu\text{-inch}\cdot\text{s}^{-1}$ ). Figure 3-22 plots typical ground motion velocity spectra for a period at house #8 when residents were reporting impulsive annoyance [3].

### 3.2 FACTORS AFFECTING NOISE GENERATION

When we discovered that the annoyance was associated with the strong acoustic pressure impulses produced as the turbine's blades passed behind the large, cylindrical tower legs, we directed our attention to the air flow around the legs, the truss-lattice tower as a whole, and the resulting downstream wakes through which the blades passed. A NASA wind tunnel study of the wake characteristics of a 1/40th-scale model of the MOD-1 [4] showed that pronounced mean velocity deficits existed in the lee of the vertical leg members. The shape and magnitude of the deficits depended in part on the orientation of the wind flow into the turbine tower structure. Unfortunately, the characteristics of these wakes had been measured at an equivalent distance of about 40 leg diameters downstream, but the actual blades can come as close as 4 leg diameters. While the study did provide a basis for more investigation, details about the wake structure could not be ascertained from reported data.



004705

Figure 3-21. Elastic (Deformation) Response of Floor Vertical Plane in House #8 under Moderate, External Impulsive Acoustic (Pressure) Loading ( $B_e = 1.25$  Hz)

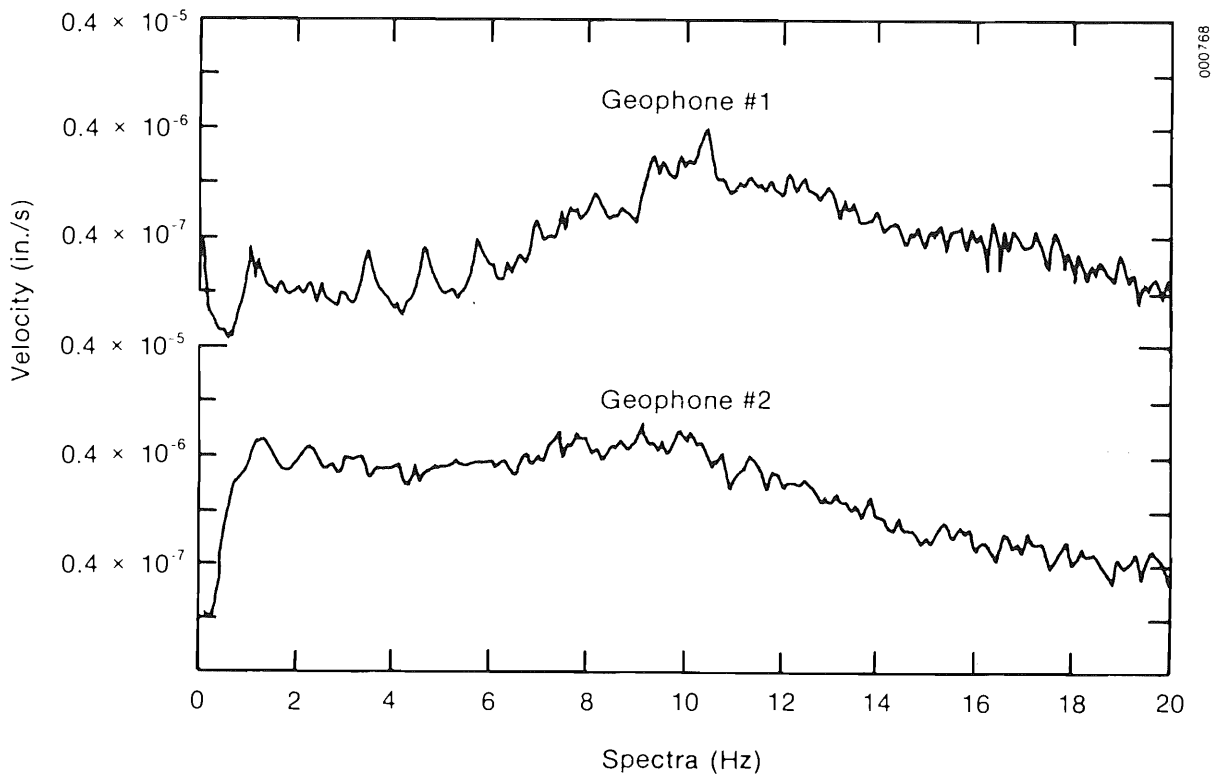


**Figure 3-22. Ground Motion Velocity Spectra Measured near House #8 when Undergoing Moderate Impulsive Annoyance ( $B_e = 1.25$  Hz)**

The conclusions we drew at this point in the investigation were that (1) the leg wakes were the primary source of the impulsive noise generation; (2) the orientation of the turbine nacelle might be partly responsible (per Ref. [4]) and (3) the actual physical process was aerodynamic (aeroacoustic) because of the variation in lift experienced by the blades passing through the tower leg wakes. The third conclusion helped us to realize that the rotor speed (principally the tip speed, which was known to be a major design parameter in aerodynamic noise generation) and perhaps the commanded electrical load as well were also factors to be considered--particularly the former, since a reduction in tip speed reduced noise output from propeller and fan blades.

### 3.3 FACTORS AFFECTING THE PROPAGATION OF THE TURBINE NOISE

From our first visit to the MOD-1 site in October 1979, we recognized the role atmospheric propagation could play in annoying the surrounding families. The isolated peak is surrounded by deep valleys that can trap layers of colder, still air, while strong winds were prevalent at the turbine site. Such a situation is highly conducive to strong atmospheric refraction of sound waves from the turbine down into the valleys below. The Penn State Group found that the vertical wind shear, particularly to the east of Howard's Knob, is the primary factor in conjunction with ground reflection in the enhancement of the turbine impulse levels received at houses #7 and #8 [3, 30]. They have also

found that the low-frequency components of the impulse could also be propagated upwind of the site, which resulted in frequent annoyance of the residents in house #2 (see Figure 1-2). Thus, the factors controlling the propagation of sound away from the turbine include (1) the complex terrain surrounding the site; (2) the vertical wind shear plus the thermal structure in the layer bounded by the area immediately above the elevation of the turbine to the valley floors below; and (3) the wind direction that prevailed when the turbine was operating.

### 3.4 INITIAL CONCLUSIONS BASED ON FIELD MEASUREMENTS

After the first three field surveys were completed, we reached the following conclusions about the MOD-1 noise situation:

- The residents' annoyance in several homes near the turbine was real and not imagined.
- Acoustic and vibration measurements supported the residents' observations, at least as to time if not always in terms of accepted annoyance levels.
- The physical mechanism responsible for the impulsive noise generation was related to the dynamic characteristics of the wakes downstream of the large, vertical tower legs and some form of a transient lift fluctuation, and the attendant acoustic pressure impulse radiated as the rotor blades passed downwind of the tower.
- The greater part of the impulse acoustic energy responsible for the annoyance was very low frequency, and the observed peak was generally below the "normally" audible lower limit of 20 Hz.
- The physical mechanism responsible for the complaints, particularly the higher levels observed in the homes, was the considerable energy contained in the impulses, their coherent characteristics, and the dynamic interaction with the building structures discussed in Section 3.1.2.
- The source of the annoyance was the acoustic pressure impulses propagated through the air rather than through the ground.
- Some sort of enhancement of the impulses at homes in the valleys below the turbine was taking place through the mechanism of terrain and atmospheric refraction which depended upon meteorological conditions in the complex terrain surrounding the site.
- Measures had to be taken to reduce the generated impulses below detection levels, given that the source was aerodynamic and that reducing the blade tip speed had met with some success in other cases of propeller or fan noise.

We preferred to begin solving this problem by understanding the physical mechanisms involved in the noise generation, propagation, and resulting subjective impact on the families affected. In that way we could identify the physical parameters responsible, including both important turbine design and critical environmental parameters that needed to be pointed out to planners and designers of second- and third-generation machines. In the following sections, we summarize the results of this effort.

## SECTION 4.0

### ANALYSIS AND INTERPRETATION

In this section, we discuss the results of our investigation into the physical parameters of the generation, propagation, and impacts of the acoustic noise associated with the operation of the MOD-1 turbine. The conclusions are based on the results of the five field measurement periods undertaken at the MOD-1 site and on supporting experimentation performed with models under controlled conditions in wind tunnels and with full-scale turbines operating in the natural environment. We also briefly discuss the results of analytical modeling done at MIT's Fluid Dynamics Research Laboratory and at Penn State in aerodynamic noise generation and atmospheric sound propagation, respectively.

#### 4.1 AEROACOUSTIC NOISE GENERATION MECHANISMS

As discussed in Section 3.1.1, the source of the residents' complaints was traced to the acoustic impulses being generated as the rotor blades passed through the wakes of the large, cylindrical tower legs. While the NASA wind tunnel study [4] gave some clues as to the physical aeroacoustic mechanisms involved, the far-wake position of the profile measurements and the presentation in terms of averaged quantities were limited in applicability to the situation in Boone, N.C. Examination of the characteristics of the waveshape and the severity of the impulses generated under a range of conditions revealed not only the cases sited in Section 3.1.1 (from no impulses present to the most severe situation) but impulses whose waveforms varied considerably. Closer study revealed that while the impulse waveform shape varies from blade to blade passage in some detail, it also tends to take on a more or less specific shape over a few minutes in a given situation.

##### 4.1.1 Aeroacoustic Mechanism for Impulse Noise Generation

To understand the pertinent physical characteristics present in the tower leg wakes and to determine what is responsible for the severe impulsive action, we need to review the aerodynamic (aeroacoustic) process that is functioning to radiate the acoustic pressure field. Acoustic impulses similar to those found with the MOD-1 have also been observed with the rotors of helicopters in which the physical mechanism is believed to be the interaction of the rotor with a vortex shed by the passage of a previous blade. The impulsive noise from a helicopter rotor can be very annoying and, of course, clearly gives away the aircraft's presence. Fortunately, except for the detectability problem, the period of impulsiveness is generally short and related to certain maneuvers of the aircraft. Understandably, this has been and continues to be an area of considerable research.

##### 4.1.1.1 Rotor Noise Characteristics

Wind turbines exhibit many of the noise generation mechanisms associated with low-speed rotating blades utilizing aerodynamic lift, particularly those



using high lift airfoil shapes. Rotating blade noises are generally classified into three major mechanisms that effectively function as acoustic dipoles at low Mach numbers: noises caused by steady forces on the blades, noises emanating from periodic sources, and those coming from random or nonperiodic sources.

**Steady Forces.** Steady forces of lift and drag produce noise that, as first pointed out by Gutin [52], is modulated in frequency by the motion of the blade at a fixed observer location by the Doppler effect. These sources account for noise that contains relatively high energy at discrete frequencies close to the blade passage frequency (when viewed in terms of an average of several blade passages) but suffers from poor radiation efficiency [5,6]. It is usually impossible to identify the steady load noise, particularly in the case of a full-scale wind turbine, because it is masked by other, more effective sources.

**Unsteady Forces.** Unsteady forces on the blades as they move around the rotor disk can be classified as either periodic or non-periodic. Periodic sources arise from fluctuating asymmetric disk loading resulting from blade-to-blade interactions, vortex interactions (helicopter blade slap), etc. These reflect coherent sources (see Section 3.1.1 for a definition of coherency) and are characterized by discrete noise with high energy and moderate radiation efficiency, which results in the extension of the discrete noise to relatively high frequencies in an averaged acoustic spectrum. If sufficiently strong, these can be most annoying. Nonperiodic or random fluctuating loads, in contrast, are brought about by sources such as wind shear, inflow turbulence, and blade vortex shedding. These sources are usually characterized by broadband, incoherent noise having high energy and moderate radiation efficiency. Such sounds are often described as the "swishing" noise associated with the blade passage of a wind turbine. The unsteady forces are usually sufficient to mask noise being created by the steady blade loads. Figures 3-1 and 3-4 illustrate the averaged sound pressure spectra that contain a predominance of periodic or nonperiodic sources.

#### 4.1.1.2 Physical Basis for Impulsive Noise Generation

This discussion follows that of George [7] in which he discusses the physical mechanisms that lead to acoustic radiation from rotor blades employing aerodynamic lift. Lighthill [8] showed that the equations of mass and momentum conservation, while they allow for mass sources and applied forces in the fluid, could be put in the form of wave equation on the left-hand side with all other terms on the right, or

$$\frac{\partial^2 \rho}{\partial t^2} - c_0^2 \frac{\partial^2 \rho}{\partial x_i^2} = \frac{\partial Q}{\partial t} - \frac{\partial F_i}{\partial x_i} + \frac{\partial^2 T_{ij}}{\partial x_i \partial x_j}, \quad (4-1)$$

where

$\rho$  = density

$c_0$  = the undisturbed sound speed

$$\begin{aligned}
Q &= \text{mass source strength, mass/volume} \times \text{time} \\
F_i &= \text{force/volume} = \text{momentum/volume} \times \text{time} \\
T_{ij} &= \text{Lighthill stress} = \rho u_i u_j + (p - c_0^2 \rho) \delta_{ij} - \sigma_{ij} \\
\sigma_{ij} &= \text{viscous stress tensor.}
\end{aligned}$$

For the wind turbine situation, the operating tip Mach number ( $\sim 0.3$ ) and observed radiated frequency range (i.e., acoustic wavelengths  $\gg$  rotor blade physical dimensions) may allow mass (thickness) and viscous stress effects to be ignored and the source may be considered a point dipole (compact assumption). By applying the equation of state one can obtain the pressure as the desired dependent variable. Equation (4-1) now becomes, for the acoustic far-field,

$$p - p_0 = \hat{p} = \frac{x_i}{4\pi c_0 r^2} \frac{\partial F_i}{\partial t} \left( t - \frac{r}{c_0} \right), \quad (4-2)$$

where  $r$  is the distance to the observer from the compact dipole source and  $\partial F_i / \partial t$  is evaluated at  $t - r/c_0$ , the "retarded time." Following the development of Leverton and Amor [9], we define a blade loading per unit span,  $\lambda_s(x, t)$ , perpendicular to the plane of rotation, or

$$\delta F_i \equiv \delta F_n = \lambda_s \delta x, \quad (4-3)$$

where  $\delta x$  is a small increment over which  $\lambda_s$  acts; then,

$$\delta \hat{p} = \frac{x_n}{4\pi c_0 r^2} \frac{\partial \lambda_s}{\partial t} (t - r/c_0) \delta x. \quad (4-4)$$

If we now integrate over the span  $x = 0$  to  $x = \text{span}$  assuming that the differences in retarded time over the span can be neglected (i.e., either  $\lambda \gg \text{span}$  or for on-axis noise), then,

$$\hat{p} = \frac{x_n}{4\pi c_0 r^2} \frac{d}{dt} \int_0^{\text{span}} \lambda_s(x, t) dx, \quad (4-5)$$

which shows that the radiated sound depends on the net correlated lift over the span. If  $\lambda_s(x, t)$  is of the form  $L(t) f(x)$ , then,

$$\hat{p} = \frac{x_n}{4\pi c_0 r^2} \frac{dL(t)}{dt} \delta_c, \quad (4-6)$$

where the effective correlated span length is defined as

$$\delta_c \equiv \int_0^{\text{span}} f(x) dx. \quad (4-7)$$

This indicates that acoustic pressure radiated from a blade undergoing lift fluctuations is a function of the span length simultaneously involved. Another way to view the concept is as a spanwise (line) source of simple point dipoles radiating in-phase or coherently. From the discussion in Section 3.1.1, we see that this situation corresponds to a very efficient acoustic radiator. Thus, the more spanwise correlated is the lift, the more coherent is the radiated acoustic pressure field. Using Eq. (3-1), we can now write the expression for the energy intensity of the radiated impulse for an observer in a fixed location as

$$E_I(t) = \frac{1}{\rho c_0} \int_0^T \hat{p}^2(t) dt = \frac{X_n^2 \delta_c^2}{16 \pi^2 \rho c^3 r^4} \int_0^T \left[ \frac{dL(t)}{dt} \right]^2 dt \quad (4-8)$$

Equation (4-8) now directly relates the energy content of the radiated acoustic impulses to the coherent or spanwise correlated lift fluctuations on the blade surface. The blade loading function  $l(t)$  for each increment of the correlated span length can be expressed in terms of a series of loading harmonics through the use of the Fourier Transform, or

$$\tilde{L}(f) = \int_{-\infty}^{\infty} L(t) e^{-i2\pi ft} dt = \left| \tilde{L}(f) \right| e^{i\phi(f)}, \quad (4-9)$$

where the far right expression relates to the amplitude or magnitude loading spectrum and the phase spectrum  $\phi(f)$ , both of which are required to completely define  $L(f)$ . In terms of the time domain utilizing the inverse transform,

$$L(t) = \frac{1}{\pi} \int_0^{\infty} \tilde{L}(f) e^{i2\pi ft} df, \quad (4-10)$$

where the integration is carried out over a period  $T$  corresponding to an impulsive lift fluctuation for (4-10) and an upper frequency limit of interest for (4-11). Similarly, the same transform may be applied to the square of the dynamic pressure  $p^2(t)$  to acquire the harmonic acoustic energy  $P(f)$ .

With the use of the Fourier Transform, both sides of Eq. (4-8) can be viewed in terms of the frequency domain or observed acoustic pressure harmonics that have their origins in the harmonics of the unsteady blade loads. This relationship is reasonable for impulsive-type noise where Doppler modulation has very little influence due to the very short time periods and small segments of the rotor disk involved. Wright [5,6], for example, has shown that the essence of the blade loading spectrum is carried through to the acoustic spectrum even when the Doppler effect cannot be disregarded. Equations (4-8) and (4-10) now give us a tool for additional insight into the nature of the unsteady lift fluctuations occurring on the blades of the MOD-1 for they allow us to examine both the time-pressure signature (Eq. 4-8) and the instantaneous and averaged frequency spectra (Eq. 4-10).

#### 4.1.1.3 Impulse Waveform Analysis and Interpretation

The discussion of the previous section pointed out that the essence of the lift transients responsible for the impulsive radiation can be interpreted from the acoustic pressure time signature. To see this more clearly, we repeat Eq. (4-6):

$$\hat{p}(t) = \frac{X_n}{4\pi c_0 r^2} \frac{dL(t)}{dt} \delta_c .$$

This equation indicates that the dynamic pressure field is proportional to the rate of change of the lift correlated in time over a given portion of the blade. The resulting acoustic pressure wave form can be interpreted in terms of the effect on the radiated frequency spectrum as follows:

1. Impulse rise time (seconds): this is the time required for the pressure to rise (or fall) from 10%-90% of peak pressure change. The smaller the value, the greater the amount of energy present at higher frequencies; i.e., this has a major influence over the radiated spectral shape, the location of spectral band energy.
2. Impulse peak dynamic (over or under) pressure (dB re 20  $\mu$ Pa): this parameter controls the level of impulse energy present across the spectral bands specified by the rise time.
3. Impulse rise rate (rate of change of radiated acoustic pressure, Pa/s): this parameter combines the spectral influences of (1.) and (2.) above (i.e., both the spectral shape and energy content) and is more convenient to measure particularly when the impulse period is very small.
4. Total impulse energy intensity ( $\text{mJ}/\text{m}^2$ ): this is defined in Eq. (3-1), which describes the total dynamic pressure energy per unit area contained in the impulse.

In summary, the impulse rise time controls the spectral frequency distribution; the peak dynamic pressure controls the level of energy in the various spectral bands; and the total impulse energy intensity controls the total energy available to be distributed spectrally by the first two. In terms of the unsteady, transient lift on the turbine, Eq. (4-6) tells us that the peak dynamic pressure is determined by the maximum rate of lift change and the rise rate by the period of time in which this change takes place. Equation (4-8) indicates the energy intensity is the area under the impulse pressure curve. Thus, by examining the impulsive waveshapes, quantified in terms of the parameters above, we have a basis for understanding what may be occurring aerodynamically on the blade itself, the severity of the occurrence in terms of energy content and spectral distribution, and we find grounds for comparing different operating conditions and the effectiveness of various amelioration techniques.

## 4.2 MULTIVARIATE STATISTICAL ANALYSIS OF PARAMETERS RELATED TO IMPULSIVE NOISE GENERATION

In order to isolate the parameters influencing the impulsive noise associated with the MOD-1, a data analysis technique was developed to correlate three of the impulse waveform parameters: peak dynamic (over) pressure, rise rate, and energy intensity (the operational parameters were believed to be in some way responsible). These operational parameters included the hub-height windspeed, nacelle azimuth angle, generator output power, blade attack and pitch angles, and rotor rotational speed. These data, plus one or two additional parameters discussed below, were then synchronized in time with acoustic impulse information and input to a multivariate, linear regression analysis to identify important correlations. The results of this analysis are discussed in Section 4.2.2.

### 4.2.1 Impulse and Operational Data Reduction

#### 4.2.1.1 Impulse Data Reduction

Data from the March and June 1980 field studies were stratified into about 3-minute records that exhibited relatively stationary statistics. This was necessitated by the fact that the MOD-1 noise situation (including generation, propagation, and impact) was a nonstationary process. Impulses found in the acoustic signal (derived from the on-axis, upwind microphone) were processed with the spectrum analyzer in the time domain mode and under the control of an external computer. Special software was developed to obtain sample estimates of the populations of the three waveform parameters plus a reference nonimpulsive sound pressure level. The sample statistics of these parameters were then assembled for each 2- to 3-minute record of interest including the sample mean, variance, and peak and minimum values, and a frequency distribution was plotted of each. The process could also be synchronized to obtain statistical summaries of the impulses generated in the lee of each tower leg for comparison.

#### 4.2.1.2 Operational Data Reduction

The periods to be analyzed for the impulse data reduction process discussed in the previous section were chosen from one-second samples of turbine operational data that had been digitized and scaled by a specially programmed mini-computer system. After the periods for analysis had been identified, the one-second samples that composed these segments were processed to acquire sample statistics of each. Impulse data and operational sample statistics were then merged into a single data file for each record segment analyzed.

### 4.2.2 Analysis Results

A series of bivariate correlations were calculated for the master data file. The independent variables included the nacelle azimuth (essentially the mean wind direction), wind speed, rotor rotational speed (rpm), generator output power, and the pitch and attack angles.

We recognized early that the position of the rotor blade in terms of its downstream distance from the tower legs was also a factor to be considered and a function of the nacelle azimuth angle. The closest approach of rotor blades to a tower leg occurred when the nacelle was oriented along the structure's diagonal [about 4 leg diameters, or 2.1 m (see Figure 3-7)]. The following expressions were derived to locate the rotor plane in terms of the downwind distance from each of the tower legs, in leg (cylinder) diameters, identified as the north, east, south, and west legs in Figure 3-7:

$$\begin{aligned}D_n &= 12 \cos (\psi + 315) + 16 \\D_e &= 12 \cos (\psi + 225) + 16 \\D_s &= 12 \cos (\psi + 135) + 16 \\D_w &= 12 \cos (\psi + 45) + 16 \quad ,\end{aligned}\tag{4-11}$$

where n, e, s, and w are the distances in leg diameters downstream of the identified tower leg and  $\psi$  is the nacelle yaw angle in degrees (differs from the true azimuth (w.r.t. geographic north) by addition of 28 degrees or 0.49 rad).

Figures 4-1 through 4-12 present representative bivariate distributions of the waveform parameters with a range of independent variables, including the nacelle azimuth angle (w.r.t. to true north), hub-height wind speed, blade pitch angle, minimum blade-to-leg distance, generator output power, and blade rotational speed (rpm). With the exception of one or two to be discussed separately, these bivariate distributions generally show little in the way of correlation. Figures 4-1 and 4-2 do indicate the azimuthal preference for impulse generation, but these directions only reflect the site power wind rose as shown in Figure 4-13. Figure 4-5 does demonstrate the blade rotational speed influence on the impulse rise rate versus blade pitch angle plot, however. The peak dynamic or acoustic overpressure is usually the dependent variable, since it is a good reflection of the impulse severity.

The bivariate distributions that indicate a relationship are Figures 4-10, 4-11, and 4-12. Figure 4-10 plots the nonimpulsive or reference sound pressure level as a function of hub-height wind speed which increases monotonically. The acoustic signal depicted here contains not only the increase in wind noise at the turbine site but also reflects an overall turbine noise output outside of the rotor disk segment in which the tower structure resides and, in fact, dominates this measurement. Thus, as shown in Figure 4-10, the general noise SPL rises approximately 14 dB (or a factor of 5 in acoustic pressure) from cut-in to normal cut-out windspeed [ $6.7 \text{ ms}^{-1}$  (15 mph) to  $15.6 \text{ ms}^{-1}$  (35 mph)].

The dependence of impulse severity on windspeed is shown in Figures 4-11 (March 1980) and 4-12; in Figure 4-11, 35 rpm runs for June and March 1980 are plotted. It is clear from Figure 4-11 that for the same wind speed, the impulses generated by the turbine's operation during June were generally much more severe than those recorded in March; in fact, the slopes of the linear regression lines are quite different, though they tend to converge at high wind speeds. Figure 4-14 indicates the relationship of rotor rotational speed to the mean impulse peak dynamic pressure bivariate sample population. As can be seen, the 35-rpm cases generally cluster around the upper regression line

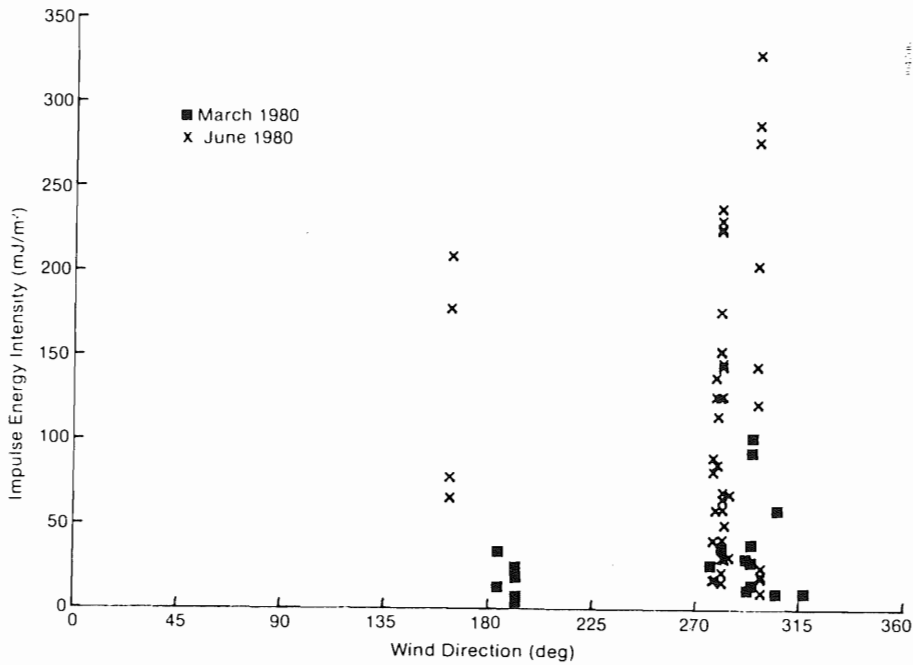


Figure 4-1. Scatter Diagram of Impulse Energy Intensity vs. Hub-Height Wind Direction for March and June 1980 Field Surveys

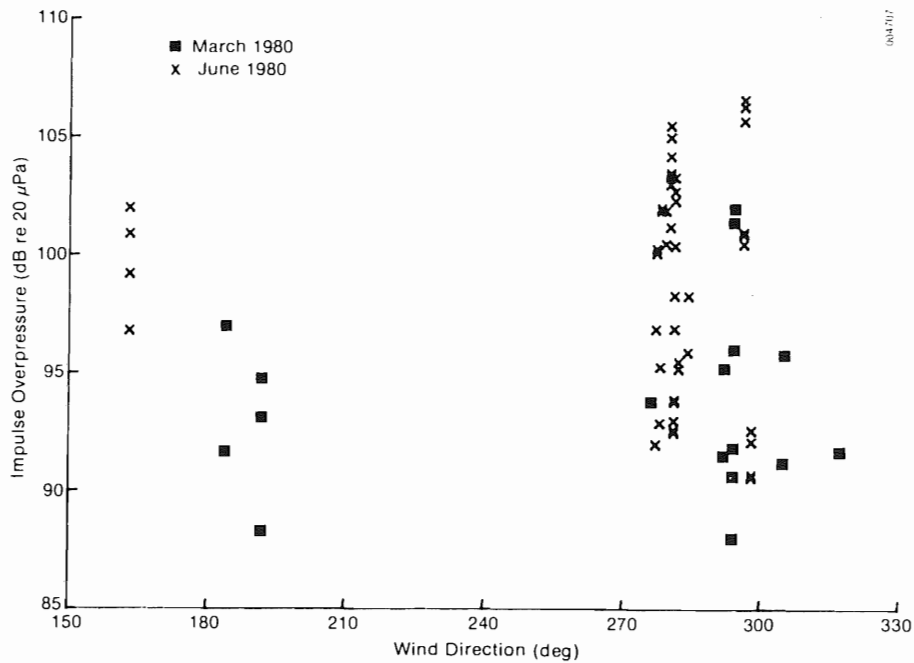


Figure 4-2. Scatter Diagram of Impulse Overpressures vs. Hub-Height Wind Direction for March and June 1980 Field Surveys

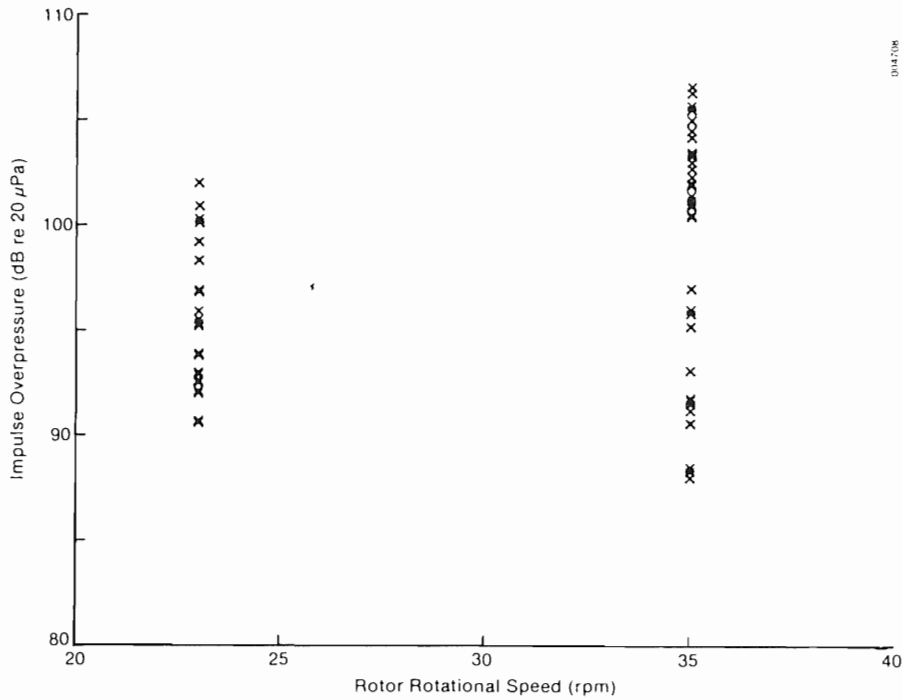


Figure 4-3. Scatter Diagram of Impulse Overpressure vs. Blade Rotational Speed (rpm)

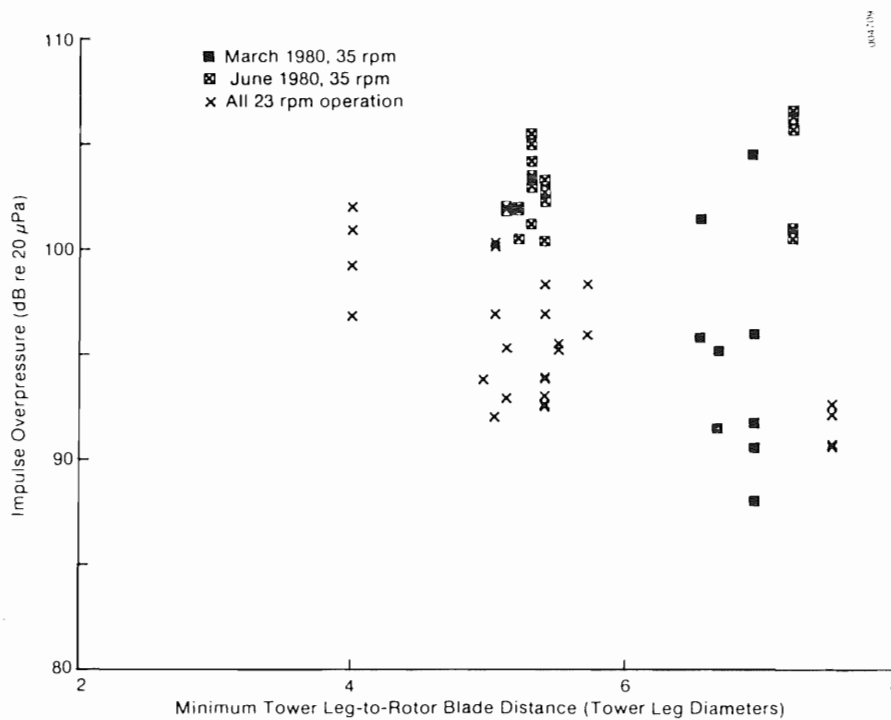


Figure 4-4. Scatter Diagram of Impulse Overpressure vs. Minimum Tower Leg-to-Rotor Blade Distance (in Tower Leg Diameters) as a Function of rpm and Survey Period



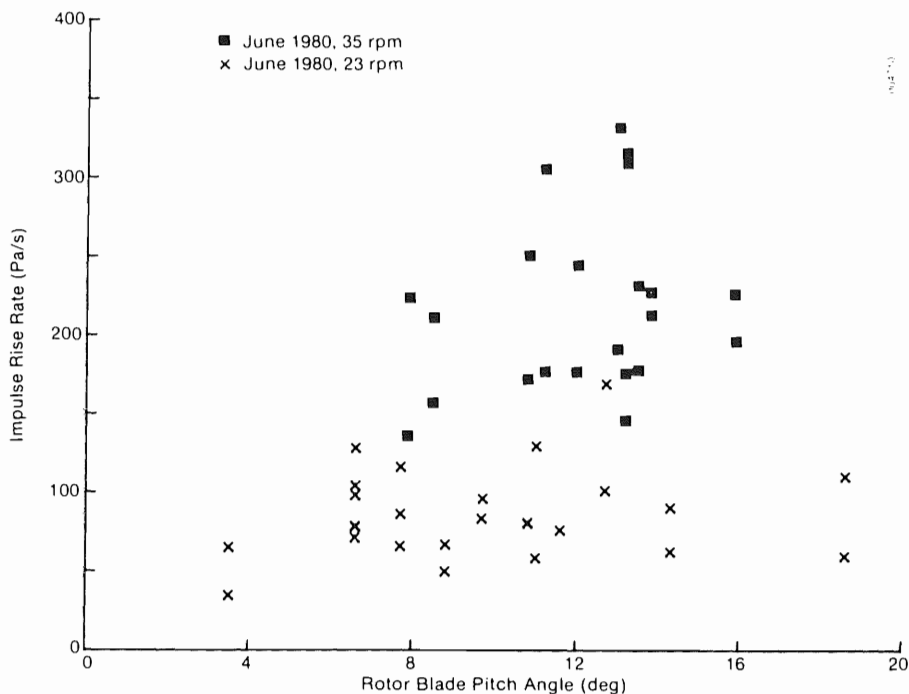


Figure 4-5. Scatter Diagram of Impulse Rise Rate vs. Rotor Blade Pitch Angle as a Function of Blade rpm for June 1980 Survey

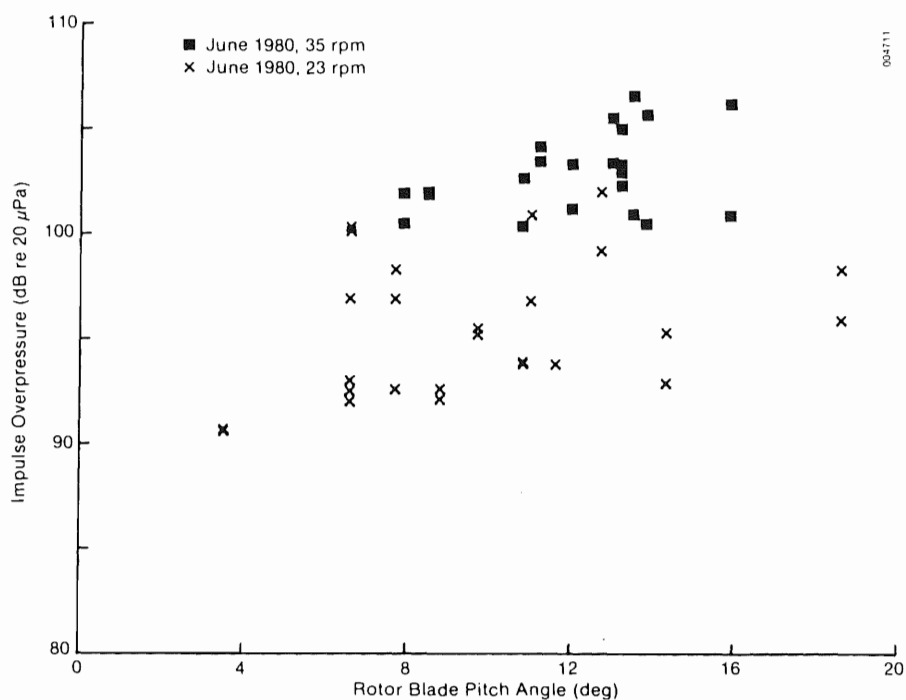


Figure 4-6. Scatter Diagram of Impulse Overpressure vs. Rotor Blade Pitch Angle as a Function of Blade rpm for June 1980 Survey

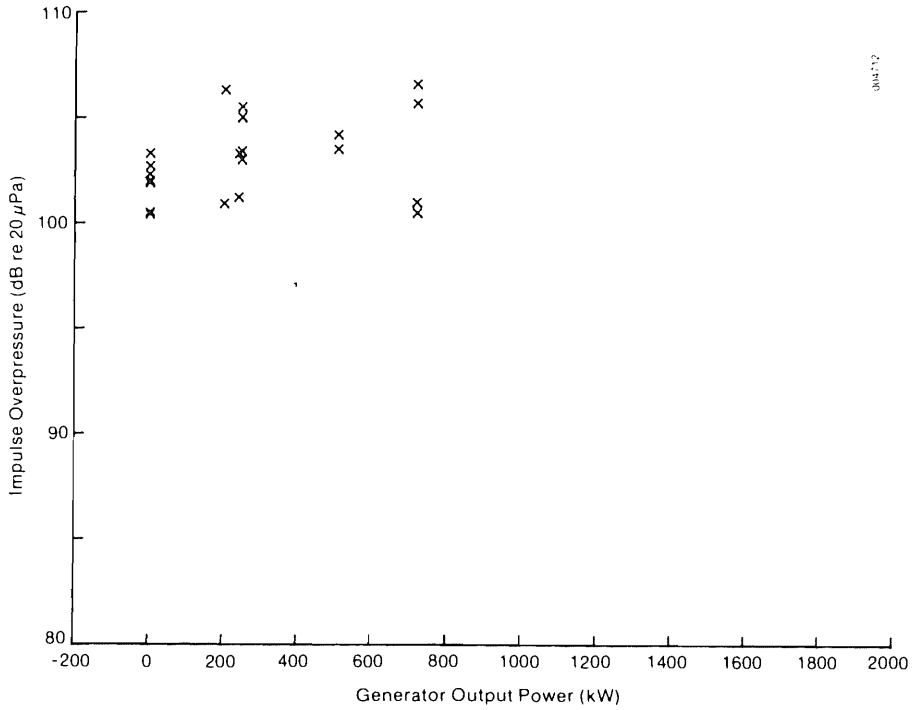


Figure 4-7. Scatter Diagram of Impulse Overpressure vs. Generator Output Power for 35 rpm Operation during June 1980 Survey

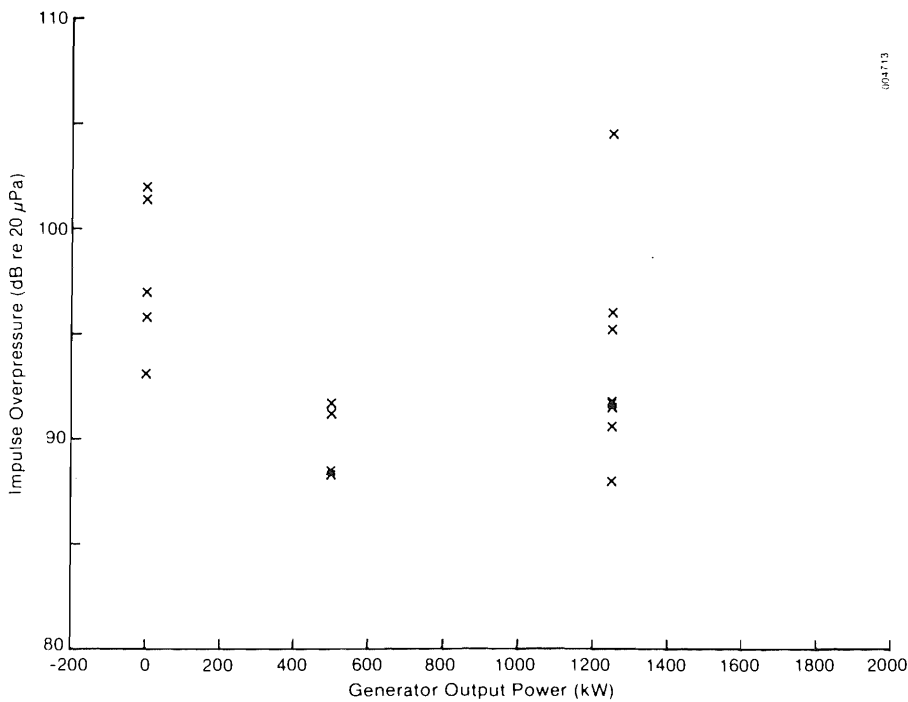
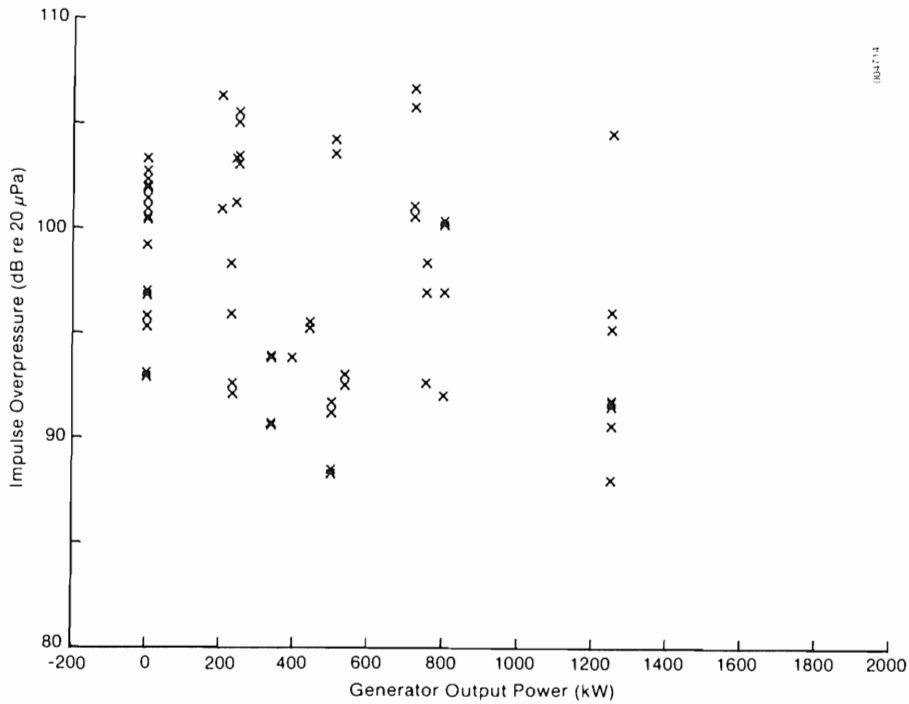
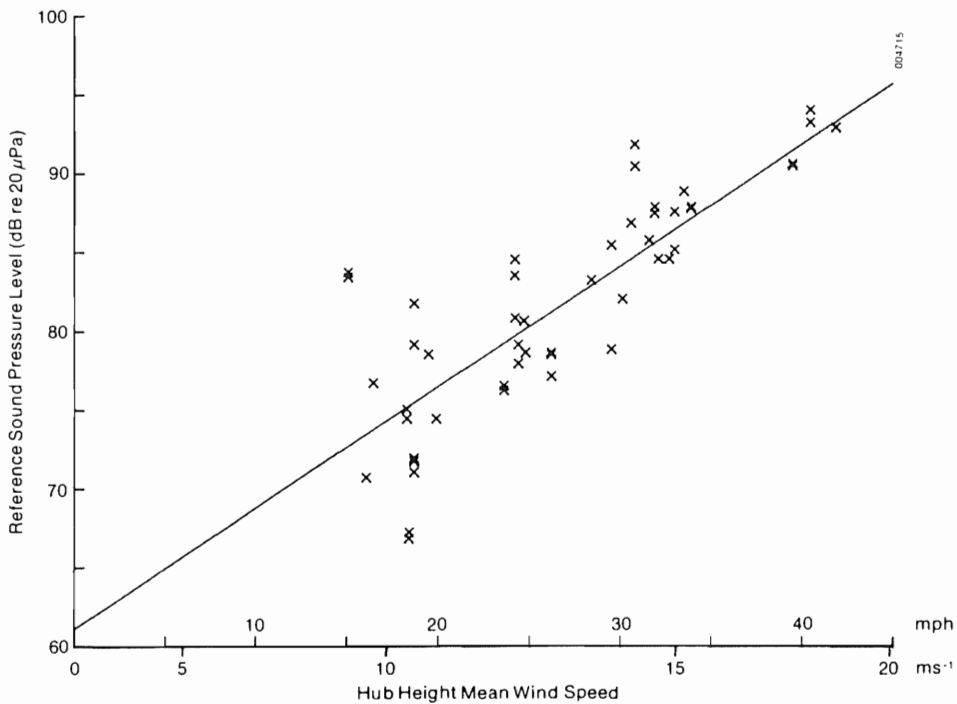


Figure 4-8. Scatter Diagram of Impulse Overpressure vs. Generator Output Power for 35 rpm Operation during March 1980 Survey



**Figure 4-9. Summary Scatter Diagram of Impulse Overpressure vs. Generator Output Power under 35 rpm Operation for Both March and June 1980 Surveys**



**Figure 4-10. Scatter Diagram with Linear Regression Line of Reference Sound Pressure Level (at 1.5 Rotor Diameters Upwind of Turbine) as a Function of Hub-Height Wind Speed**

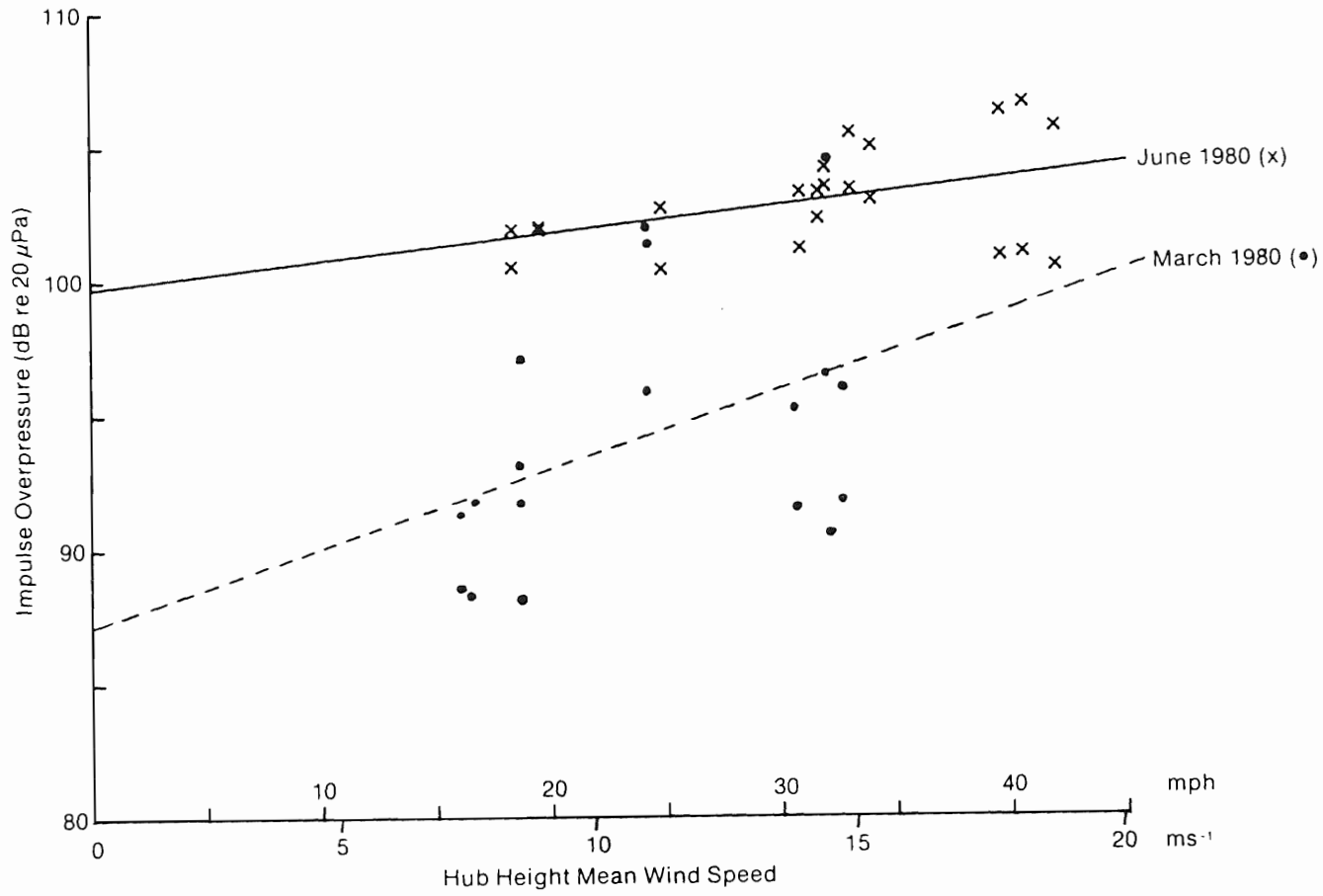
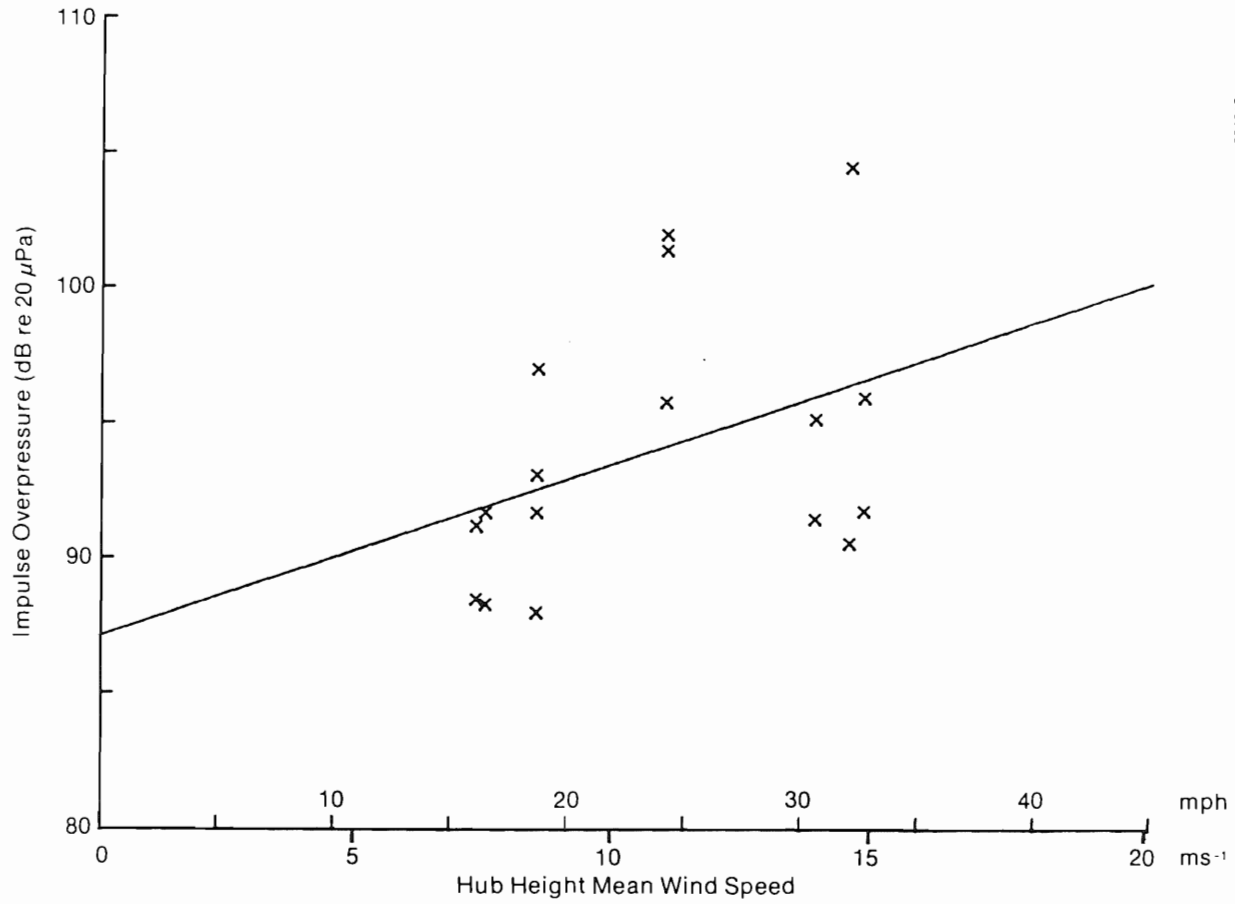


Figure 4-11. Scatter Diagram with Linear Regression Lines for Impulse Overpressure vs. Hub-Height Mean Wind Speed (35 rpm Operation) for March and June 1980 Survey Periods



004717

Figure 4-12. Scatter Diagram with Linear Regression Line of Impulse Overpressure vs. Hub-Height Wind Speed for 35 rpm Operation during March 1980 Survey

004718

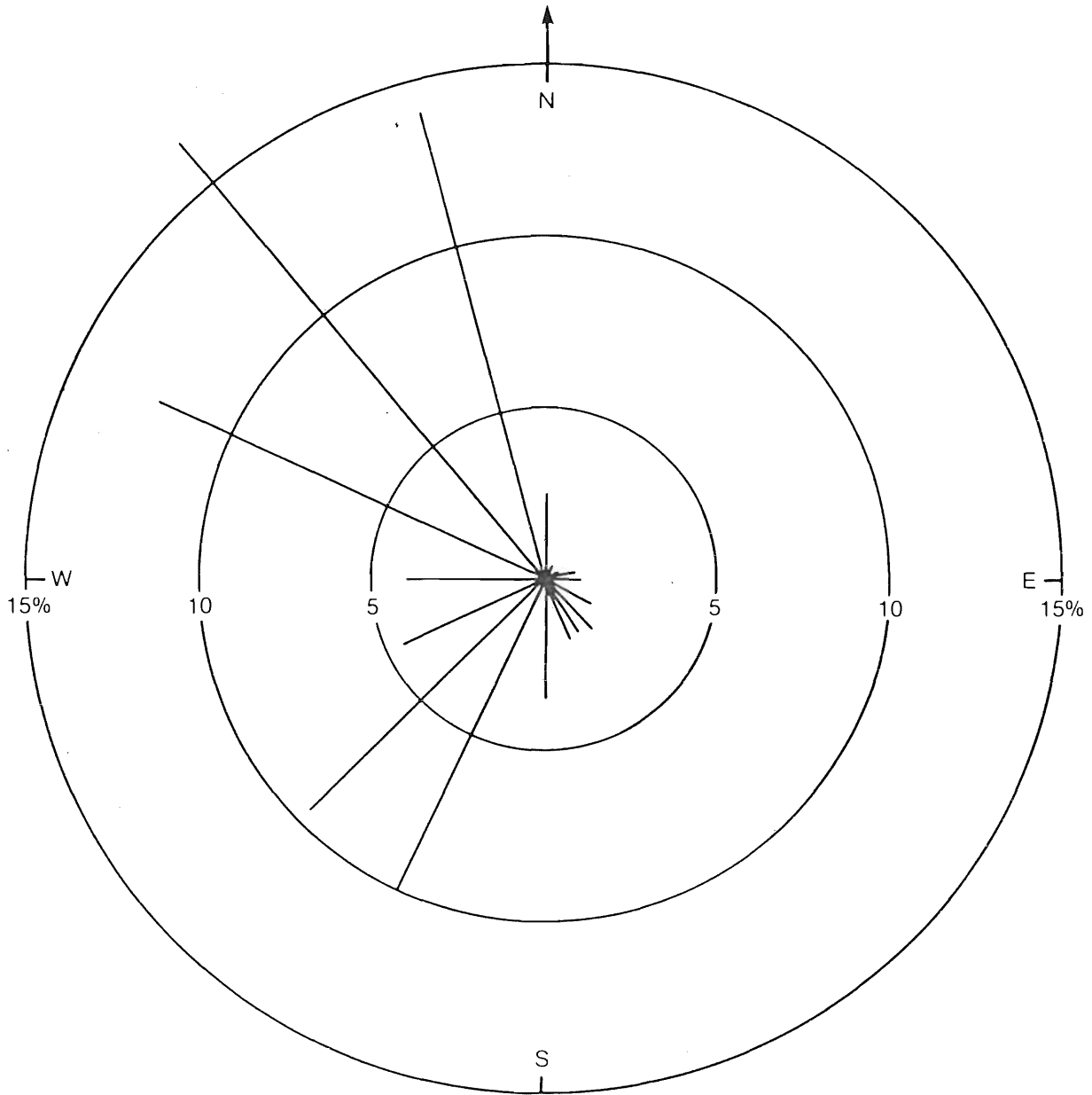
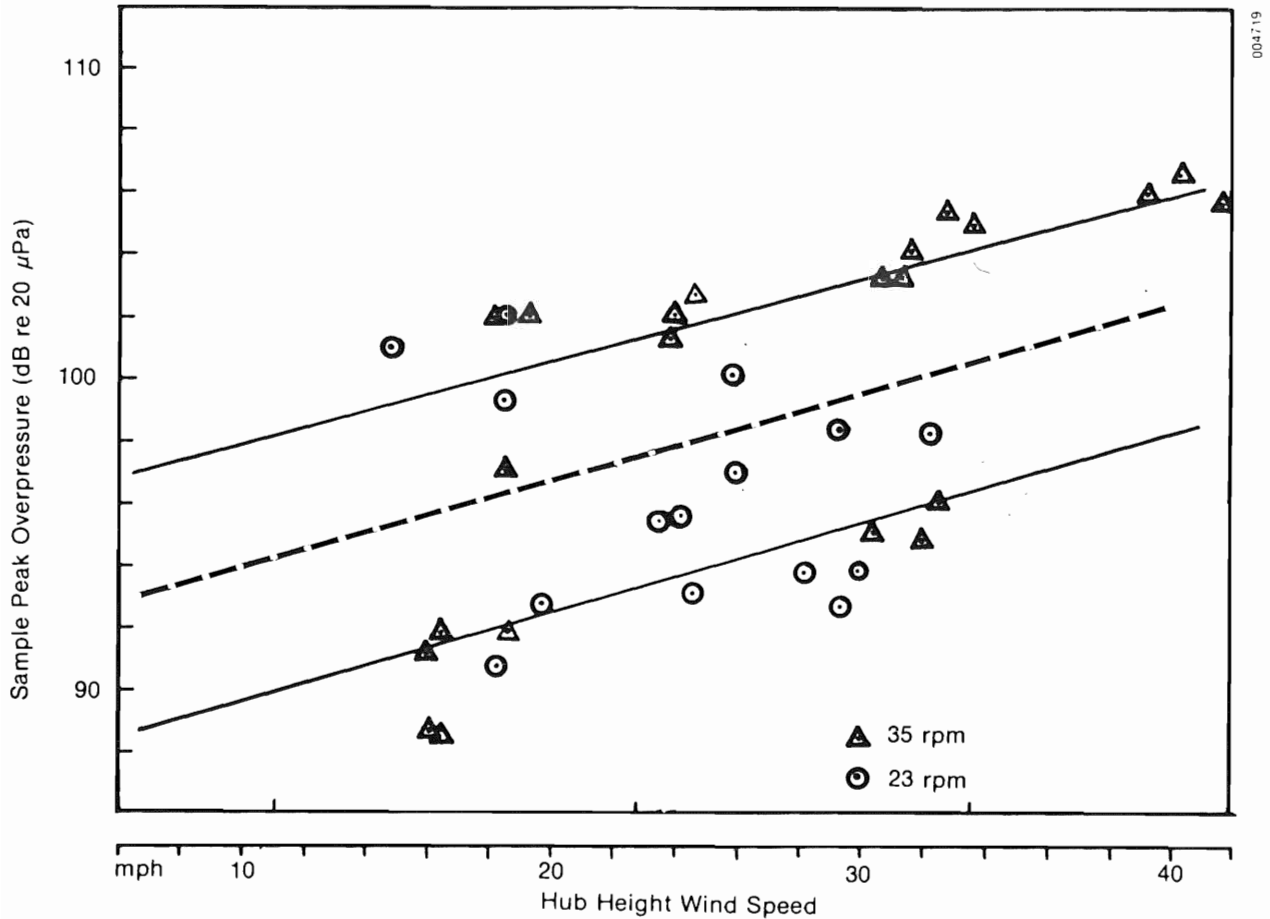


Figure 4-13. "Power" Wind Rose—Directional Probability of Receiving Hub-Height Wind Speeds between Turbine Cut-In and Cut-Out Values—for MOD-1 Site



004719

**Figure 4-14. Scatter Plot of Impulse Peak Overpressure vs. Hub-Height Wind Speed as a Function of Rotor rpm.** (Solid lines represent best fits for upper and lower groups of points and the dashed line was chosen as an approximate divider in between.)

and the 23-rpm cases, around the lower. However, on closer examination, we find that this is not always the case. In this figure, the few 23-rpm data points collected during the January 1981 field survey are included, about half of which cluster around the upper, more severe line.

From an examination of these figures and a number of similar ones, we have reached the following conclusions:

1. More than two parameters are necessary to describe a statistically significant correlation between variables and the observed impulse characteristics.
2. The wind direction in itself is a factor only because of the site wind rose, in which winds sufficient for power generation tend to cluster around two azimuths; i.e.,  $180 \pm 25^\circ$  and  $290 \pm 20^\circ$ . The stronger and more persistent winds blow from the latter.
3. A high sensitivity to the rotational speed of the blade and the hub height wind speed has been shown, but it is not consistent.
4. The impulses generated by the turbine's operation during the June 1980 study were generally more severe than those measured in March 1980.
5. The severity of the few impulses that could be recorded and processed from the January 1981 study at 23 rpm indicated that about half reached levels as severe as those observed in June 1980 at the same rotational speed.

#### **4.2.3 Multivariate Statistical Analysis**

The impulse data set described in the previous sections was analyzed using a multivariate, linear regression technique as a response to the obvious interaction between more than two independent variables, which was also discussed in the previous section. The purpose of this analysis was twofold: (1) to establish correlation factors and regression coefficients for the list of operational variables in order to assess the sensitivity of the impulse generation process to these particular parameters; and (2) to establish a statistical model in which different cases could be compared, albeit somewhat crudely. The latter could also serve as a basis for assessing the effectiveness of trying abatement procedures, such as roughening one of the tower legs with wire mesh or reducing the rotor rotational speed.

##### **4.2.3.1 Methodology**

As explained earlier, 2- to 3-minute sample periods of both acoustic and operational parameters were selected based on relatively stationary statistics in the latter. The operational data summaries, compiled from samples at one-second intervals, were assembled and merged with the results of the associated impulse analysis and placed on a computer disk file. This master file then was sorted several times, allowing a subfile structure to be developed which included, as examples, all cases stratified in terms of rotational speed (35 or 23 rpm), survey period (March or June 1980 or January 1981), and the specific tower leg with which the impulse was associated. This stratification allowed details in the statistical distributions to be brought out more clearly.

A standard set of statistical estimates including means, variances, coefficients of variation, skewness, and kurtosis were obtained for the entire data set and many of the subfiles. Correlation matrices and cumulative probability



distributions were also obtained and will be discussed in the next section. Both bivariate, polynomial regressions and multivariate, linear regression models were used to compare the stratified data sets.

#### 4.2.3.2 Analysis Results

As discussed above, the data were stratified into different operational categories: the two rotational speeds (35 and 23 rpm); the survey period during which the data were collected (March 1980, June 1980, or January 1981); and whether or not the impulse was associated with either the east or south leg of the support tower. The effect of the various operational parameters, including rotor rotational speed, nacelle azimuth angle, hub-height wind speed, blade pitch and attack angles, the blade downwind distance from a tower leg, and the electrical load (generator output power) are discussed below in terms of the overall data set and for the two major field surveys (March and June 1980) individually.

**Effect of Rotor Rotational Speed on Impulse Generation.** Table 4-1 presents the correlation matrices for the three mean impulse characteristics of energy intensity, overpressure (peak dynamic pressure), and rise rate for 39 sample periods at 35 rpm and 26 at 23 rpm. Figures 4-15, 4-16, and 4-17 present the cumulative probability distributions for impulse energy intensity, overpressure, and rise rate, respectively, for 35 and 23 rpm operation. Figure 4-16 also displays the reference sound pressure level taken when no impulse was present.

**Table 4-1. Correlation Matrix of Mean Impulse Characteristics and Operational Parameters**

	Energy Intensity	Overpressure	Rise Rate
35 rpm (39 sets of observations)			
Nacelle azimuth angle	0.258	0.157	0.184
Hub height wind speed	0.654	0.565	0.460
Blade pitch angle	0.515	0.392	0.231
Blade attack angle	0.051	-0.076	-0.084
Blade distance from nearest leg	-0.141	-0.389	-0.434
Generator output power	-0.307	-0.454	-0.521
23 rpm (26 sets of observations)			
Nacelle azimuth angle	-0.750	-0.622	-0.490
Hub height windspeed	-0.330	-0.023	0.008
Blade pitch angle	0.224	0.332	0.188
Blade attack angle	-0.437	-0.364	-0.187
Blade distance from nearest leg	-0.600	-0.680	-0.598
Generator output power	-0.282	-0.072	0.017

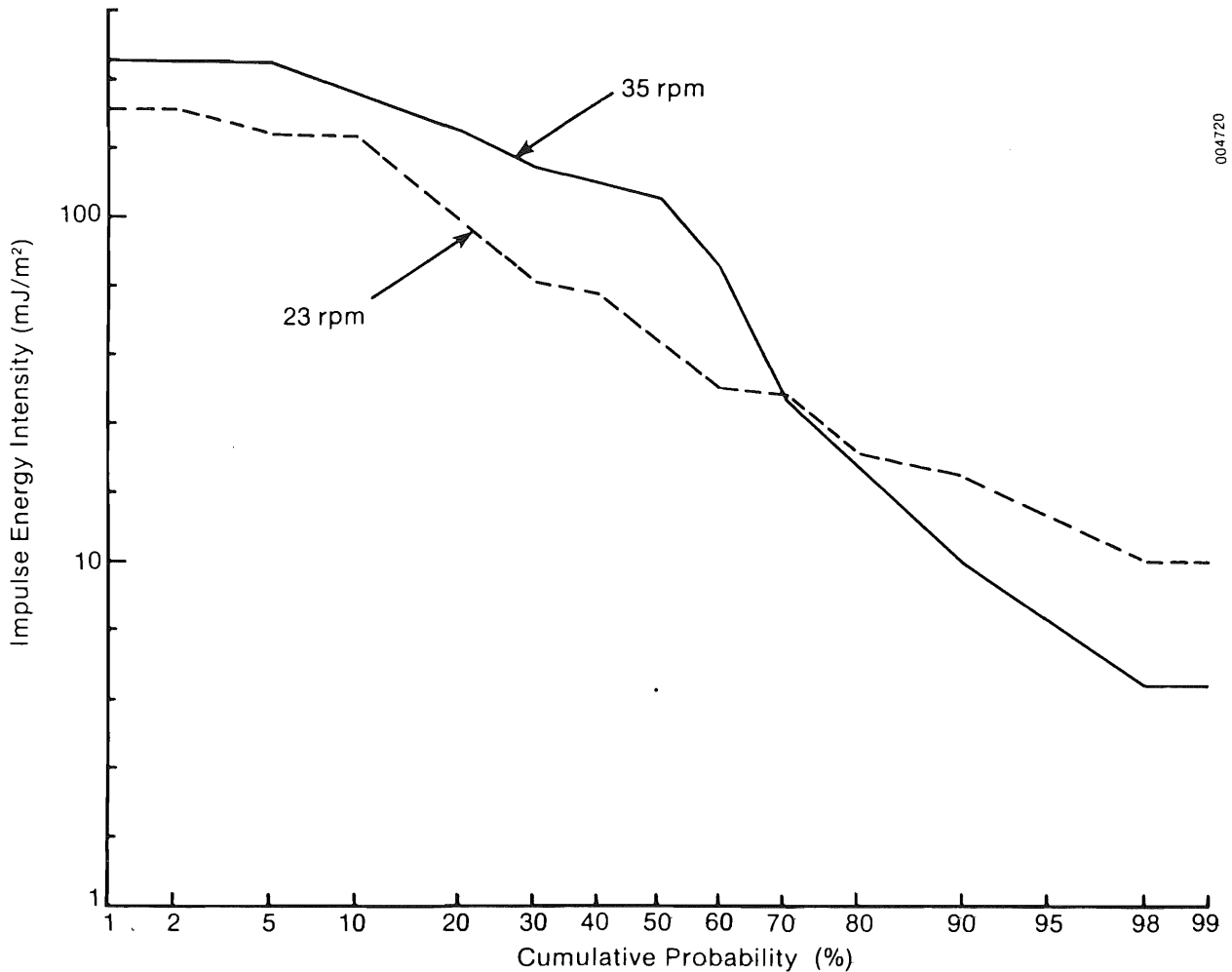


**Figure 4-15. Cumulative Probability Plot of Impulse Energy Intensity as a Function of Rotor rpm**

The effect of the blade rotation speed is graphically illustrated in the cumulative probability plots. In terms of energy intensity, as shown in Figure 4-15, the 35-rpm-derived impulse contained 25 times more acoustic energy than the 23-rpm operation 10% or less (90th percentile) of the time; i.e., the fraction of time the rotor blades spend in the tower wake. A similar contrast is seen in Figure 4-16 in which the mean impulse overpressure observed at 35 rpm was 106 dB, versus 101.5 dB at 23 rpm for the same percentile. Both Figures 4-15 and 4-16 indicate that the 35-rpm impulses tend to be persistent, as evidenced by the probability of higher levels extending out to the 40th-percentile (60%) level. Figure 4-17 also illustrates the

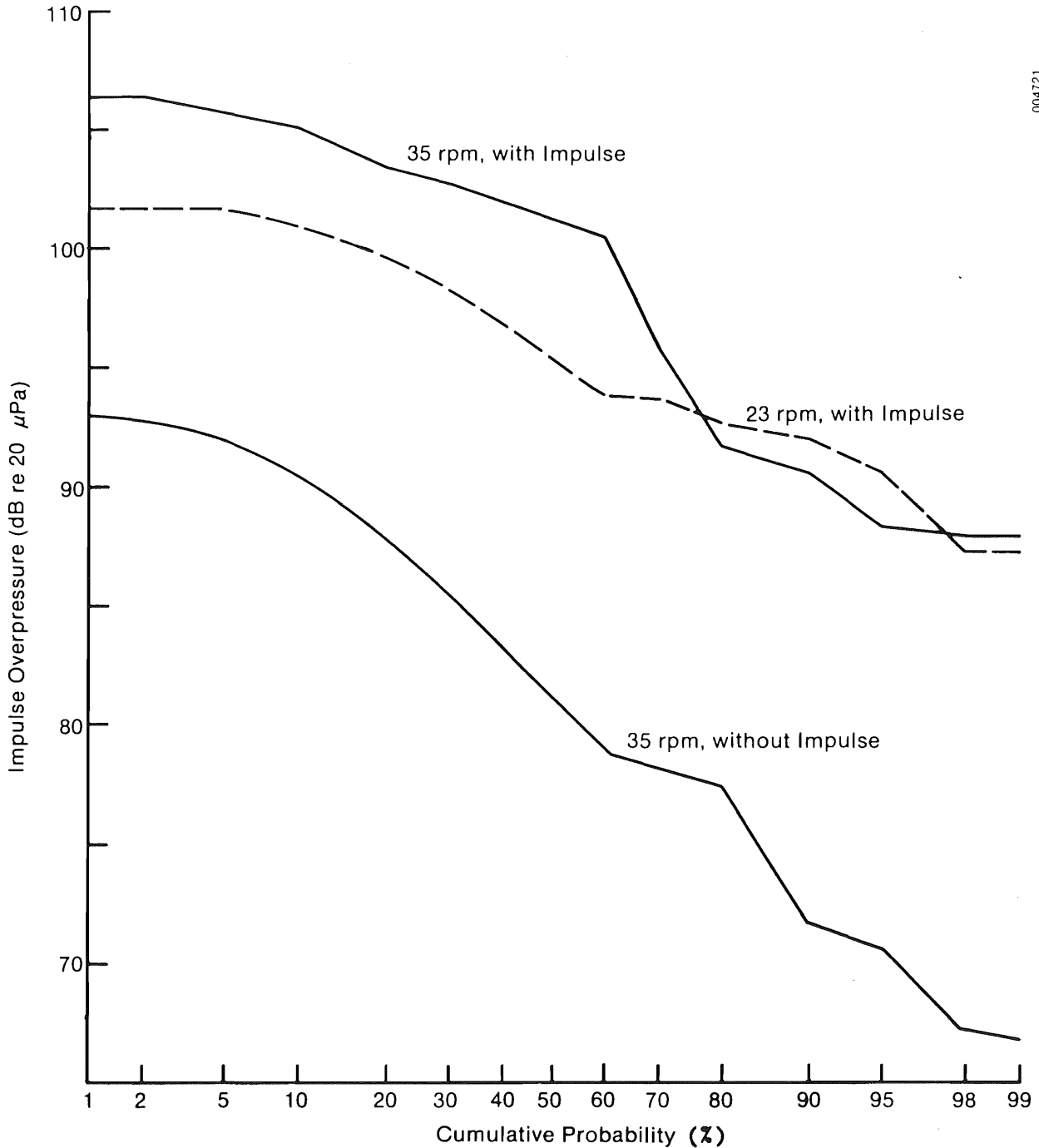
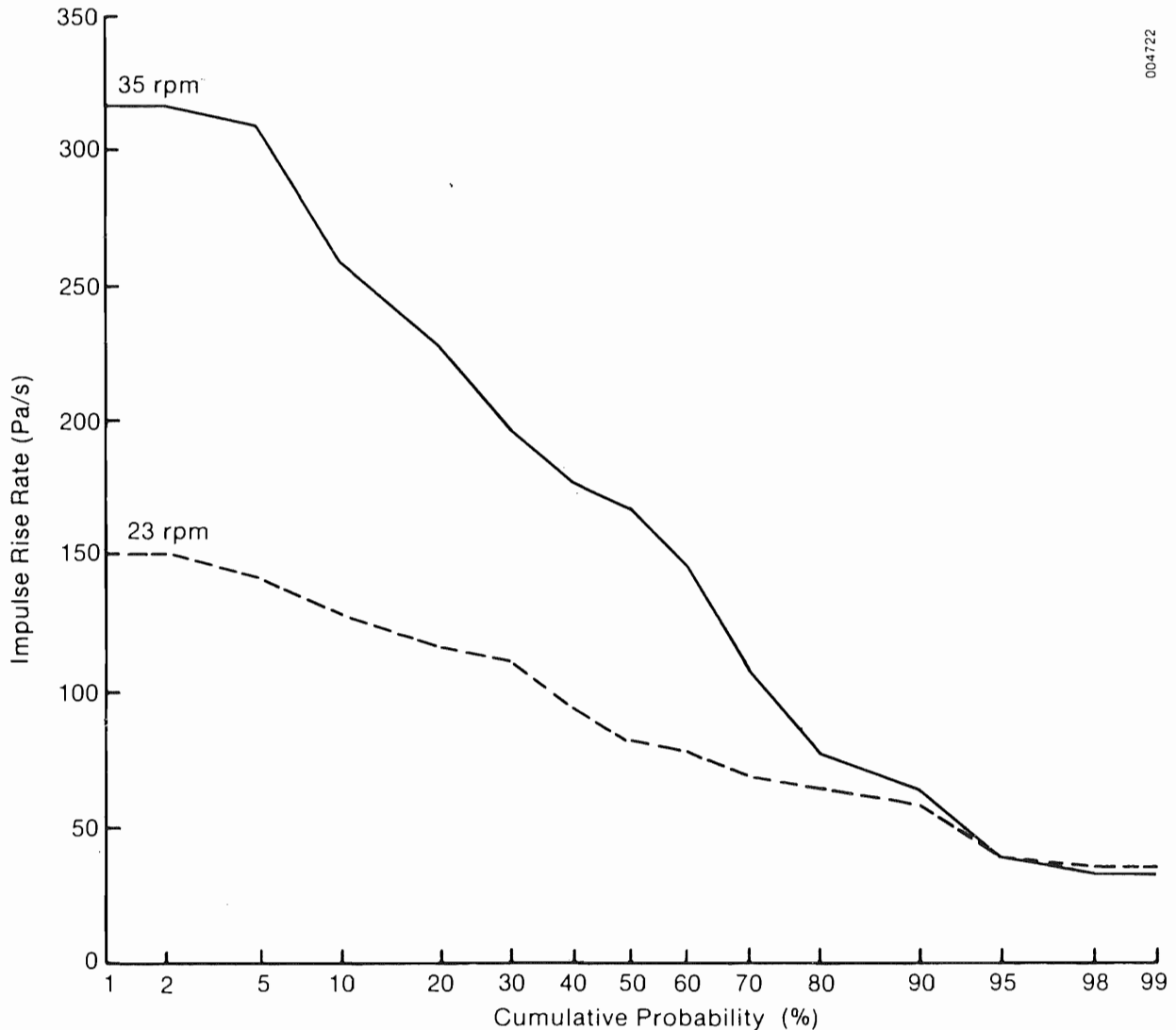


Figure 4-16. Cumulative Probability Plot of Impulse Overpressure as a Function of Rotor rpm. (The probability of acoustic pressure levels without an impulse present is shown for comparison.)



**Figure 4-17. Cumulative Probability Plot of Impulse Rise Rate as a Function of Rotor rpm**

severity of the 35-rpm impulse which exhibits a rise rate over twice that of the 23-rpm case at the 95th-percentile (5%) level. Table 4-1 indicates that at 35 rpm there are significant levels of positive correlation with the impulse characteristics with hub-height wind speed and blade pitch angle and negative correlation with the distance to the nearest tower leg and generator load. The 23-rpm data indicate a significant negative correlation with the nacelle azimuth and blade attack angles, and the distance from the tower leg, as well as a lesser positive correlation with the blade pitch angle. In contrast to the 35-rpm operation, little correlation existed with wind speed.

Some of the correlations (or lack thereof) are somewhat surprising at first glance. A partial explanation lies in the bias of the two data set divisions, i.e., 35 and 23 rpm operations. Generally, with one or two exceptions, the 35-rpm operation of the turbine occurred at higher wind speeds, the choice of the supervising field director. This is reflected in the sensitivity of the impulse parameters to wind speed. Further, the June 1980 data, which encompass a large percentage of the available information, also reflect the severe off-design operation of the turbine when connected to the resistive loadbank (the loadbank had an actual capacity of about 750 kW in contrast to the grid-connected capacity of 2 MW). This off-design influence is seen in the correlation of the mean attack angle; i.e., a negative correlation in the impulse parameters in the 23-rpm case when one would expect a positive relationship (higher attack angle equating to an increased airload on the rotor blades). The limited capacity of the loadbank necessitated a reduction in the attack angle for the generator output to stay within limits at high wind speeds or commanded load level. The same argument (negative correlation instead of the expected positive one) also applies to the correlation with the generated load.

Table 4-2 summarizes the key statistics for the March 1980 study of the mean impulse characteristics and operational parameters for the 39 and 26 sample periods for 35-rpm and 23-rpm operations, respectively. An examination of these figures generally supports previous comparisons, that the 35-rpm-generated impulse generally can be expected to be more severe, but not always as indicated by the extremes listed in Table 4-2 and the probability plots of Figures 4-15, 4-16, and 4-17. The stochastic nature of the impulse radiation and its relationship to the turbine operating parameters are evident in these figures and table. However, some positive statements can be made such as attributing the lesser severity of the 23-rpm-generated impulse to the increased residence time of the rotor blade in the leg wake, which is reflected principally in the smaller rise rate statistics in Table 4-2.

**Effect of Blade Passage Distance from Tower Leg.** The distance the rotor blades pass downwind from the tower legs was believed to be an important operational influence on the characteristics and severity of the generated impulses. Available data were divided into two major classifications: i.e., the impulses generated downwind of both the east legs and the south legs of the support tower (see Figure 3-7). The data were further classified into March and June 1980 survey periods to compare these two series of experiments and to evaluate the effects of the wire mesh that had been placed on the south and north tower legs for the June experiments.

Tables 4-3 and 4-4 summarize statistics from the sample periods of the March and June 1980 surveys in terms of the impulses generated in the lee of the east and the south tower legs. We can see that the impulse severity associated with both tower leg wakes was far more intense for June than for March. In both cases, the rotor blades were passing closer to the east tower leg in the mean, but the impulse characteristic statistics indicate that more severe impulses were being generated by the wake associated with the south leg. The south leg wake was being intersected by the blade at about twice the downwind distance of that of the east leg. This indicates that the mean wake velocity deficit was not a major contributor, since it decreases as downstream distance increases.

**Table 4-2. Summary Statistics of Mean Impulse Characteristics and Operational Parameters for March 1980 Data**

	Mean	Coef. of Var. (%) <sup>a</sup>	Maximum	Minimum	Median
35 rpm (39 sets of observations)					
Parameter					
Impulse energy intensity (mJ/m <sup>2</sup> )	112.2	80.5	329.5	4.43	115.1
Impulse overpressure (dB)	99.1	5.7	106.6	88.0	101.2
Impulse rise rate (Pa/sec)	163.8	48.4	331.7	32.9	169.2
Nacelle azimuth angle (deg)	307.8	30.5	350.0	007.0	342.0
Hub-height wind speed (m/s)	12.5	29.1	18.7	7.2	13.8
Blade pitch angle (deg)	12.1	19.0	15.9	7.9	13.0
Blade distance from nearest leg (diam.)	6.1	14.2	7.2	5.1	5.4
Generator output power (kW)	455.4	103.4	1250.0	0.0	248.0
23 rpm (26 sets of observations)					
Impulse energy intensity (mJ/m <sup>2</sup> )	67.8	90.1	235.1	10.3	41.6
Impulse overpressure (dB)	95.9	4.0	102.0	87.3	95.4
Impulse rise rate (Pa/sec)	89.9	35.4	168.9	34.7	82.1
Nacelle azimuth angle (deg)	326.7	13.7	360.0	225.0	343.0
Hub-height wind speed (m/s)	11.0	21.4	15.0	6.7	11.0
Blade pitch angle (deg)	9.7	39.8	18.6	3.5	9.3
Blade attack angle (deg)	8.0	50.1	12.1	1.7	8.6
Blade distance from nearest leg (diam.)	5.4	19.0	7.5	4.0	5.4
Generator output power (kW)	387.3	75.4	799.0	0.0	338.0

<sup>a</sup>Coefficient of variation = (standard deviation/mean) x 100.

Tables 4-5 and 4-6 present the correlation matrices for the two leg impulses and study periods. The blade pitch and attack angles are missing from the March survey; they were not available because of an insufficient number of available SERI recording channels. All the data taken in March and used in this table were recorded with the turbine operating at 35 rpm. These matrices indicate that impulse severity was correlated more with wind speed for the south leg during both observational periods than the east leg. The correlation with leg-to-tower distance shifts from high positive during March to low negative during June for the south leg for all impulse characteristic parameters. A mixed picture emerges from the east leg correlations. Table 4-6 indicates the high degree of sensitivity of impulse severity to blade rotational speed, which was discussed previously. The correlations with the mean blade pitch and attack angles are almost a mirror image, particularly for the south leg. This is to be expected, since the attack angle was derived from the pitch and the wind speed and is an artifact of the off-design operating condition.

**Table 4-3. Summary Statistics of Mean Impulse Characteristics and Operational Parameters for March 1980 Data**

	Mean	Coef. of Var. (%) <sup>a</sup>	Maximum	Minimum	Median
East Leg Impulse (10 observations)					
Impulse energy intensity (mJ/m <sup>2</sup> )	25.0	65.7	58.7	4.43	26.9
Impulse overpressure (dB)	91.8	3.4	97.0	88.0	91.6
Impulse rise rate (Pa/sec)	17.9	42.5	169.2	38.1	76.4
Nacelle azimuth angle (deg)	286.4	38.0	356.0	007.0	181.5
Hub-height wind speed (m/s)	11.1	27.1	14.6	7.2	10.9
Blade pitch angle (deg)	--	--	--	--	--
Blade attack angle (deg)	--	--	--	--	--
Blade distance from leg (leg diam.)	7.8	28.3	11.7	6.7	6.9
Rotor rotational speed (rpm)	32.6	15.5	35.0	23.0	25.7
Impulses processed	200				
South Leg Impulse (9 observations)					
Impulse energy intensity (mJ/m <sup>2</sup> )	37.7	93.7	101.8	9.5	24.5
Impulse overpressure (dB)	95.2	4.2	102.0	91.2	94.8
Impulse rise rate (Pa/sec)	93.4	41.3	146.9	32.9	94.4
Nacelle azimuth angle (deg)	244.7	57.2	356.0	007.0	254.0
Hub-height wind speed (m/s)	10.6	28.2	14.6	7.2	10.8
Blade pitch angle (deg)	--	--	--	--	--
Blade angle of attack (deg)	--	--	--	--	--
Blade distance from leg (leg diam.)	13.9	70.0	27.2	5.2	8.1
Rotor rotational blade speed (rpm)	35.0	0.0	35.0	35.0	35.0
Impulses processed	180				

<sup>a</sup>Coefficient of variation = (standard deviation/mean) x 100.

**Comparison of Treated and Untreated Tower Legs.** During the June 1980 field studies, the large vertical members of two bays on the north and south tower legs were wrapped with several layers of wire mesh. This was done to see if the dynamics of the flow around these cylindrical elements could be altered to decrease the severity of the impulses. The purpose of treating the legs on a diagonal was to provide an "A-B" comparison; i.e., to compare treated versus untreated legs under the same operating conditions. The wind direction during this phase of the experimentation positioned the rotor blade downwind of the southeast face or flat of the tower and allowed us to compare the treated south and untreated east legs.

Table 4-7 summarizes the observed mean impulse characteristics and associated operational parameters for both tower legs in the March and June 1980 field studies. The coefficient of variation for each parameter is shown in parenthesis. The greater severity of the impulses observed in June are again evident in the table. Examining the March statistics shows that while the blades, in the mean, were passing farther away from the south tower leg

Table 4-4. Summary Statistics of Mean Impulse Characteristics and Operational Parameters for June 1980 Data

	Mean	Coef. of Var. (%) <sup>a</sup>	Maximum	Minimum	Median
East Leg Impulse (10 observations)					
Energy intensity (mJ/m <sup>2</sup> )	121.9	61.8	238.4	20.4	122.1
Overpressure (dB)	99.4	4.3	105.5	90.6	100.9
Rise rate (Pa/sec)	173.2	52.1	331.7	34.7	168.9
Nacelle azimuth angle (deg)	335	12.7	360	225	343
Hub-height wind speed (m/s)	12.4	56.8	18.7	6.7	11.7
Blade pitch angle (deg)	10.9	32.3	18.6	3.5	11.0
Blade attack angle (deg)	6.2	57.2	12.1	1.7	4.8
Blade distance from leg (diam.)	6.7	45.8	16.0	5.0	5.4
Rotor rotational speed (rpm)	28.7	21.3	35.0	23.0	23.0
Impulses processed	460				
South Leg Impulse (treated with wire mesh)					
Energy intensity (mJ/m <sup>2</sup> )	103.5	89.1	329.5	10.3	78.5
Overpressure (dB)	98.9	5.0	106.6	90.7	100.1
Rise rate (Pa/sec)	126.5	47.1	232.0	49.8	104.2
Nacelle azimuth angle (deg)	335.5	10.6	360.0	225.0	343.0
Hub-height wind speed (m/s)	12.4	27.2	18.7	6.7	11.7
Blade pitch angle (deg)	10.9	33.1	18.6	3.5	11.1
Blade attack angle (deg)	6.0	58.8	12.1	1.7	4.6
Blade distance from leg (diam.)	11.4	46.8	28.0	7.5	5.4
Rotor rotational speed (rpm)	28.7	21.3	35.0	23.0	23.0
Impulses processed	440				

<sup>a</sup>Coefficient of variation = (standard deviation/mean) x 100.

(16.1 leg diameters versus 7.8 for the east), the impulse characteristics were not much different, indicating that the wake from the south leg was inherently more energetic than that from the east leg or that its unsteady characteristics persisted farther downstream. The coefficients of variation for the impulse characteristics for the south leg tend to indicate a more consistent generation process.

The statistics for the June 1980 data set show the rotor position closer to both tower legs than in March, but again, the blades are passing about twice the downstream distance from the south leg than the east. This time, however, the mean statistic characteristics show that the impulses tended to produce similar dynamic peak (overpressures), but those from the treated south leg contained less total energy and exhibited a less severe rise rate. Also, in this case, the south leg impulses tended to be less consistent, as indicated by the larger variation coefficients, compared with the east leg impulses.



**Table 4-5. Correlation Matrix of Mean Impulse Characteristics and Operational Parameters for June 1980 Data**

	Energy Intensity	Impulse Overpressure	Rise Rate
<b>East Leg Impulse</b>			
Nacelle azimuth angle	-0.318	-0.211	0.035
Hub-height wind speed	0.300	0.331	0.416
Blade pitch angle	0.453	0.457	0.407
Blade attack angle	-0.671	-0.636	-0.568
Blade distance from leg	0.253	0.055	-0.149
Rotor rotational speed	0.704	0.764	0.876
<b>South Leg Impulse</b>			
Nacelle azimuth angle	0.183	0.073	0.278
Hub-height wind speed	0.732	0.623	0.682
Blade pitch angle	0.473	0.495	0.399
Blade attack angle	-0.385	-0.496	-0.394
Blade distance from leg	-0.193	-0.076	-0.282
Rotor rotational speed	0.748	0.845	0.912

**Table 4-6. Correlation Matrix of Mean Impulse Characteristics and Operational Parameters for March 1980 Data**

	Energy Intensity	Impulse Overpressure	Rise Rate
<b>East Leg Impulse</b>			
Nacelle azimuth angle	0.434	0.083	-0.335
Hub height wind speed	0.362	0.253	-0.107
Blade pitch angle			
Blade attack angle			
Blade distance from leg	-0.138	0.070	0.588
Rotor rotational speed			
<b>South Leg Impulse</b>			
Nacelle azimuth angle	0.321	0.292	0.199
Hub height wind speed	0.884	0.934	0.949
Blade pitch angle			
Blade attack angle			
Blade distance from leg	0.870	0.919	0.841
Rotor rotational speed			

Table 4-7. Summary Statistics for a Comparison of Leg Wake Mean Impulse Characteristics

Parameter	Untreated East Leg (Mar. 1980)	Untreated South Leg (Mar. 1980)	Untreated East Leg (June 1980)	Treated South Leg (June 1980)
Impulse energy intensity ( $\text{mJ}/\text{m}^2$ )	21.3 (57.1) <sup>a</sup>	20.5 (53.4)	121.7 (61.8)	107.1 (86.5)
Impulse overpressure (dB)	91.3 (3.2)	93.4 (2.1)	99.4 (4.3)	99.1 (5.0)
Impulse rise rate (Pa/sec)	84.8 (44.0)	78.1 (35.3)	173.1 (52.1)	128.6 (60.1)
Nacelle azimuth angle (deg)	255.5 (19.6)	248.8 (22.4)	273.5 (13.0)	273.1 (13.3)
Hub-height wind speed (m/s)	11.1 (28.6)	10.5 (32.7)	12.4 (27.2)	12.3 (27.9)
Blade attack angle (deg)	n.a.	n.a.	6.2 (57.2)	6.0 (58.8)
Blade downwind distance (diam.)	7.8 (30.1)	16.1 (61.3)	6.7 (45.8)	11.5 (47.7)
Rotor rotational speed (rpm)	35.0 (0.0)	35.0 (0.0)	28.7 (21.3)	29.0 (21.2)
Number of impulses processed	180	140	460	440

<sup>a</sup>Coefficient of variation (%) in parentheses.

While the mean values and variation coefficients of Table 4-7 are revealing, the stochastic nature of the impulse generation process is demonstrated in the cumulative distributions of Figures 4-18, 4-19, and 4-20 of the sample mean impulse energy intensity, overpressure, and rise rate parameters, respectively. As before, greater impulse severity is evident in the June data compared with the impulses generated in March. What these distributions also show, with one exception, is the tendency for the 90th percentile (or 10% cumulative probability level) of the observed south leg impulses to be more energetic and exhibit higher peak dynamic pressures than those associated with the east leg in both surveys. The exception occurs in the rise-rate characteristic for the south (treated) leg impulses in the June data. Here, the rise rate is about 30% less than that observed for the east leg impulse, though energy and overpressure are greater for the south leg than the east 10% or less of the time. One interpretation is that the wake is becoming wider and blade residence time is increasing, resulting in a less abrupt rate of change in lift but extending over a greater period of time which increases the energy content as defined by Eq. 3-1. A similar conclusion can be drawn from the June mean and probability data, but obviously a more energetic process is at work than we observed in March, with the stronger impulses coming off the south tower leg. There is evidence, however, that the wire mesh did influence the wake characteristics from the south tower leg. We believe the mesh may have caused a more rapid spreading or diffusing of the wake turbulence as evidenced by the reduced rise rate and greater variation in the observed impulses.

**Multiple Linear Regression Models.** As discussed previously, we noted the interactions of operational variables and their combined effect on the severity of the observed impulses. The somewhat confusing picture painted by the bivariate correlations in Tables 4-5 and 4-6 bear this out. In order to overcome this difficulty, we computed a multiple linear regression model of each of the subclassified data sets discussed above. Table 4-8 lists the regression coefficients associated with each of the data set classifications; i.e., survey period and tower leg wake location. Of major interest are the correlation coefficients. These reflect the degree to which the regression model has explained the observed variance, 0 for totally random and 1 for a complete explanation. With the exception of the east leg mean impulse energy intensity and overpressure during March, the model correlations are very good, explaining more than 90% of the observed variance in most cases. The regression coefficients of the subclassifications of Table 4-8 now can be used to compare the sensitivities of the impulse characteristics for the different cases. For example, the greater sensitivity of the mean energy intensity with the tower leg-to-blade distance for the south leg impulse, compared with the east leg, is evident both for March and June, and the latter is far more sensitive.

Having established the multiple linear regression models summarized in Table 4-8, we can now use these tools to assess the interdependence of the major operational variables on the observed acoustic impulse characteristics of energy intensity, overpressure, and rise rate and try to relate them to what may be happening physically through the equations developed in Sections 4.1.1.2 and 4.1.1.3. From an examination of Tables 4-5, 4-6, and 4-8, we see that the most influential operational parameters are the blade rotational speed (rpm), the hub height wind speed, and the blade-to-tower-leg distance.

Table 4-8. Multiple Linear Regression Coefficients

	Nacelle Azimuth	Hub Wind Speed	Attack Angle	Leg Distance	RPM	Correlation Coefficient	Impulses Processed
Energy Intensity ( $\text{mJ/m}^2$ )							
Untreated east leg impulse (Mar. 1980)	-0.096	1.398		-0.327	*	0.588	180
Untreated south leg impulse (Mar. 1980)	0.384	0.976		-2.478	*	0.934	140
Untreated east leg impulse (June 1980)	-1.704	2.597	-0.607	-4.049	9.273	0.919	460
Treated south leg impulse (June 1980)	-26.566	6.765	5.034	-170.452	9.878	0.935	440
Overpressure (dB)							
Untreated east leg impulse (Mar. 1980)	-0.053	0.403		-0.067	*	0.594	180
Untreated south leg impulse (Mar. 1980)	-0.241	0.277		-1.316	*	0.986	140
Untreated east leg impulse (June 1980)	-0.135	0.148	-0.050	-0.897	0.538	0.951	480
Treated south leg impulse (June 1980)	-0.156	0.310	0.177	-0.644	0.637	0.938	460
Rise Rate (Pa/s)							
Untreated east leg impulse (Mar. 1980)	-0.382	4.905		13.299	*	0.811	180
Untreated south leg impulse (Mar. 1980)	-4.635	3.883		-22.696	*	0.836	140
Untreated east leg impulse (June 1980)	-1.976	2.053	-0.492	-16.017	12.721	0.945	480
Treated south leg impulse (June 1980)	-6.246	2.915	3.617	-38.777	8.814	0.970	460

\*All runs at 35 rpm.

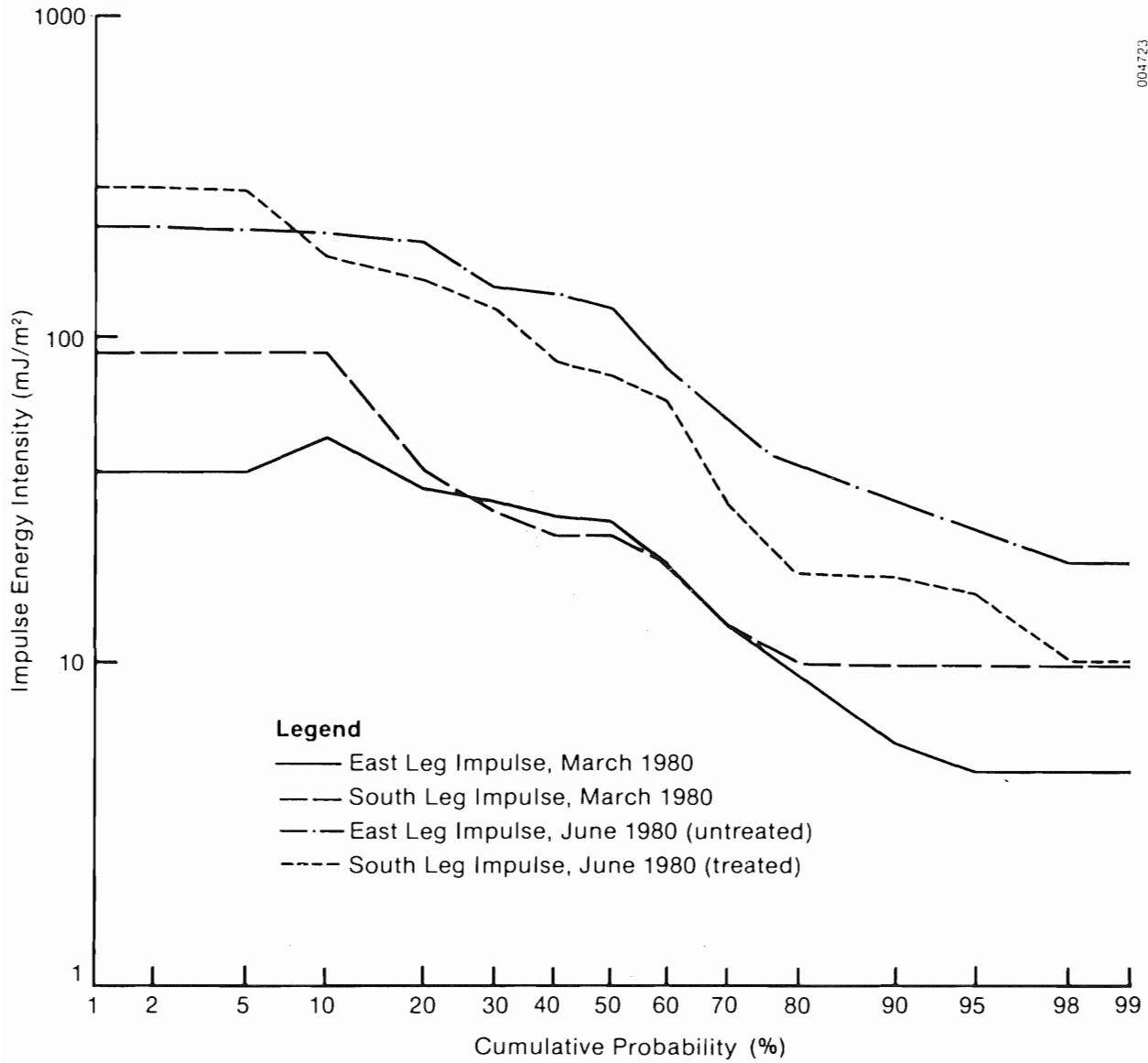
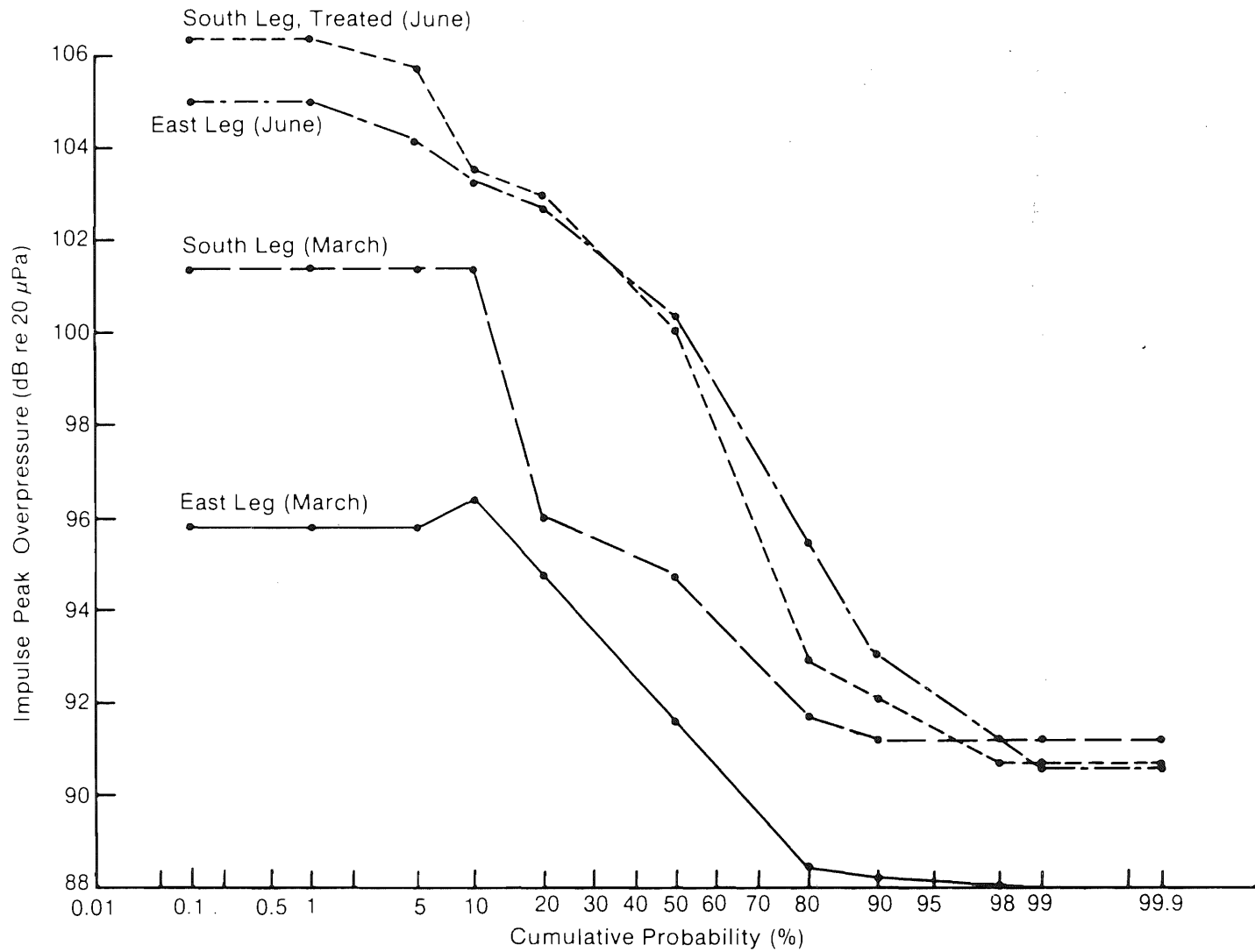
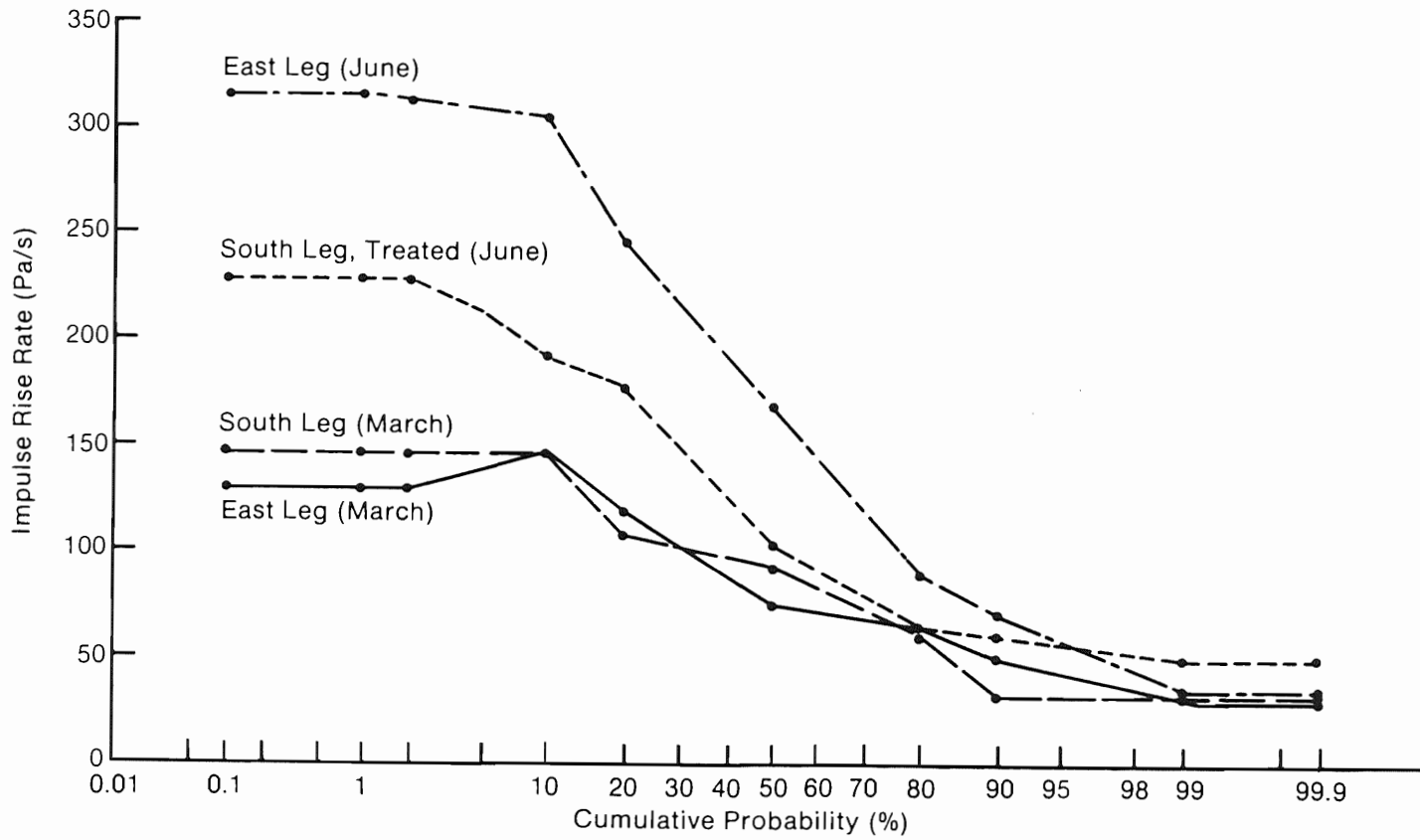


Figure 4-18. Cumulative Probability Plot of Impulse Energy Intensity as a Function of Survey Period and Specific Tower Leg Wake (East or south)



004724

Figure 4-19. Cumulative Probability Plot of Impulse Peak Overpressure as a Function of Survey Period and Specific Tower Leg Wake (East or south)



004725

Figure 4-20. Cumulative Probability Plot of Impulse Rise Rate as a Function of Survey Period and Specific Tower Leg Wake (East or south)

When adding variables to the models, we generally found the addition of the pitch and/or attack angles made little difference in reducing the unexplained variance as did just including only the nacelle azimuth but no leg-to-blade distances. Therefore it was decided to fix the pitch, attack, and nacelle azimuth angles at their median values and allow the rotor speed, wind speed, and leg-to-blade distance to vary as inputs to the models to examine the influence on the mean impulse characteristics.

Figures 4-21, 4-22, and 4-23 display the resulting variation of the three impulse characteristics as a function of leg-to-blade distance and hub height wind speed for the impulses associated with the east and south tower legs at a constant rotational speed of 35 rpm for the June 1980 study. The curves are plotted only over the ranges of leg-to-blade distances actually encountered. Figure 4-21 shows that the average impulse energy falls with increasing leg-to-blade distance for the east leg (solid lines) but does increase with hub-height wind speed. In contrast, the impulse energy associated with the south, mesh-treated leg peaks when the blade passes about 8 leg diameters from the tower and, for the same wind speed, radiates a much more energetic impulse compared with the east leg at that distance. It is interesting to note as the leg-to-blade distance increases, the curves representing radiations from both legs appear to approach parallelism, but the south leg impulses remain stronger at the same wind speed.

The plots of impulse overpressure and rise rate in Figures 4-22 and 4-23 show somewhat similar distributions, but the most severe impulse characteristics are found closest to the east tower leg. The south leg impulse overpressures also appear to reach a peak similar to the energy intensities in Figure 4-21, but somewhere between 11 and 13 diameters downstream instead of 8. The rise rate distribution in Figure 4-23 also peaks at approximately the same downstream distance as the energy intensity curves. This plot graphically displays the differences between the east and south leg-generated impulses. There also appears to be a possible discontinuity in the spacing of the 11.1 and 13.4 m/s (25 and 30 mph) wind speed isopleths, indicating what could be a non-linear increase in rise rate in this speed regime. Nothing similar is indicated in the east leg family of curves.

The same impulse characteristic distributions are displayed in Figures 4-24, 4-25, and 4-26 for the March 1980 field survey. The energy intensity (Figure 4-24) and overpressure (Figure 4-25) follow the same shapes as the June data with peaks at about 8.5 and 11-12 diameters downstream of the south leg and the closest passage for the east leg. One difference is that greater overpressures are found near the peak at all wind speeds for the south leg impulses, compared with those from the east. There is a considerable shift in the rise rate distribution for the east leg impulses in the March data, compared with those observed in June, as evidenced by Figures 4-23 and 4-26. The March data tend to indicate peak rise rates beyond 10 leg diameters downstream of a similar magnitude for both leg impulses. But the June results show the east leg peak is closest and is much more severe than those associated with the south leg at that distance.

A comparison of the effects of changing the blade rotational speed is demonstrated in Figures 4-27, 4-28, and 4-29 for the June data at a hub wind speed of  $12.3 \text{ m s}^{-1}$  (27.5 mph) and an attack angle of 6 degrees. The chief result



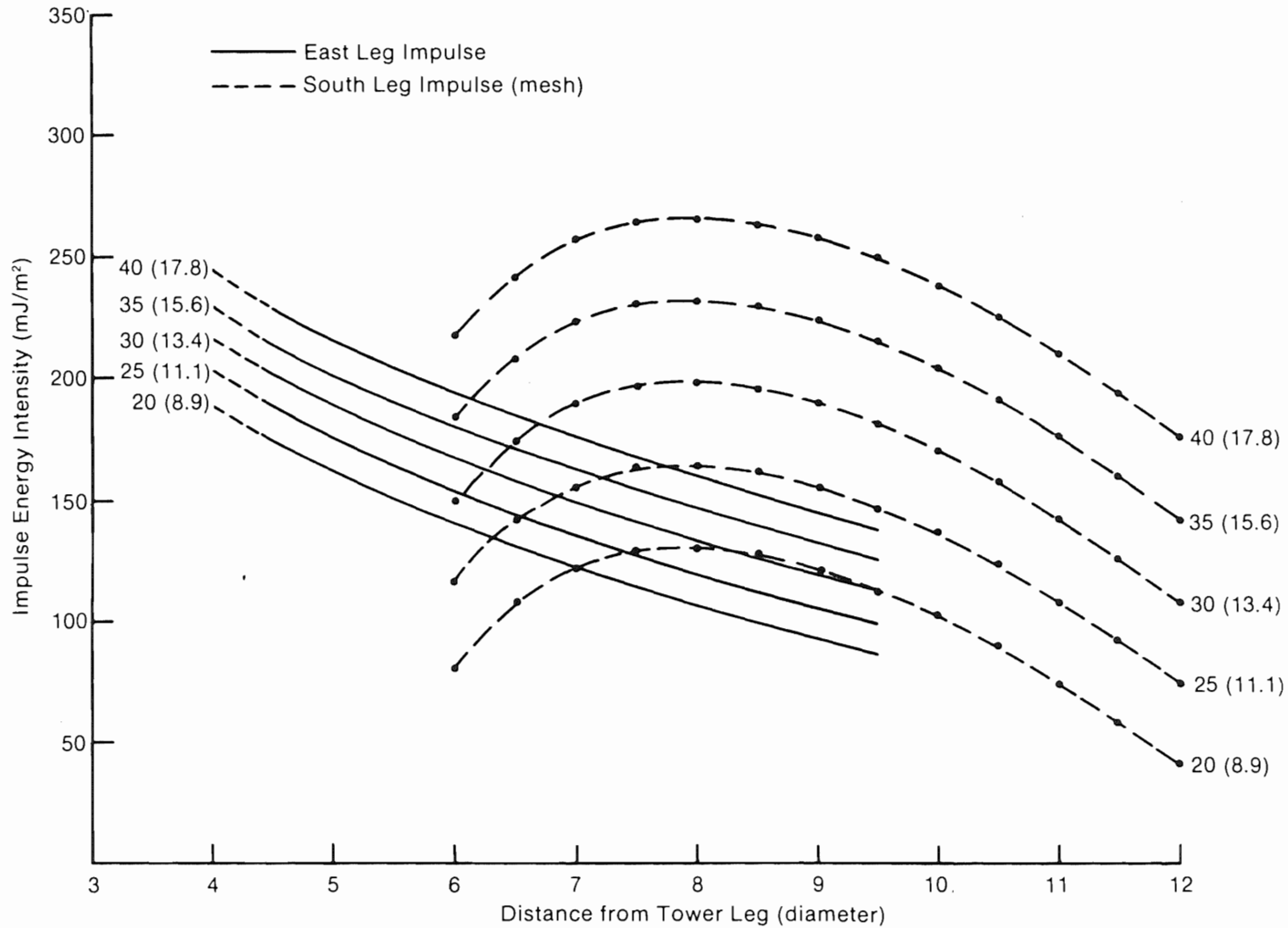


Figure 4-21. Impulse Energy Intensity as a Function of Tower Leg-to-Blade Distance (in leg diameters) and Hub-Height Wind Speed for June 1980 Survey Period (Shown in mph with  $\text{ms}^{-1}$  in parentheses)

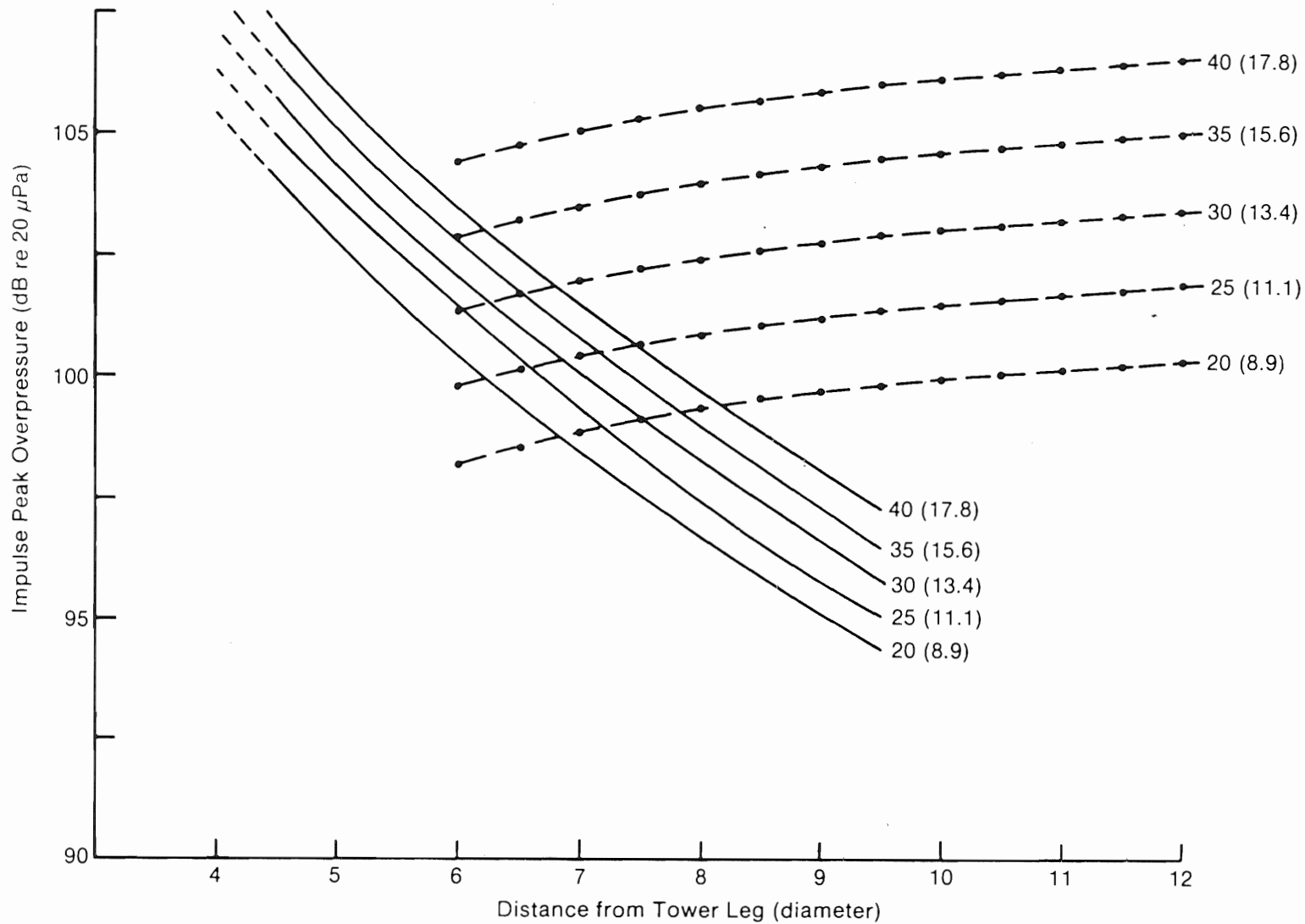
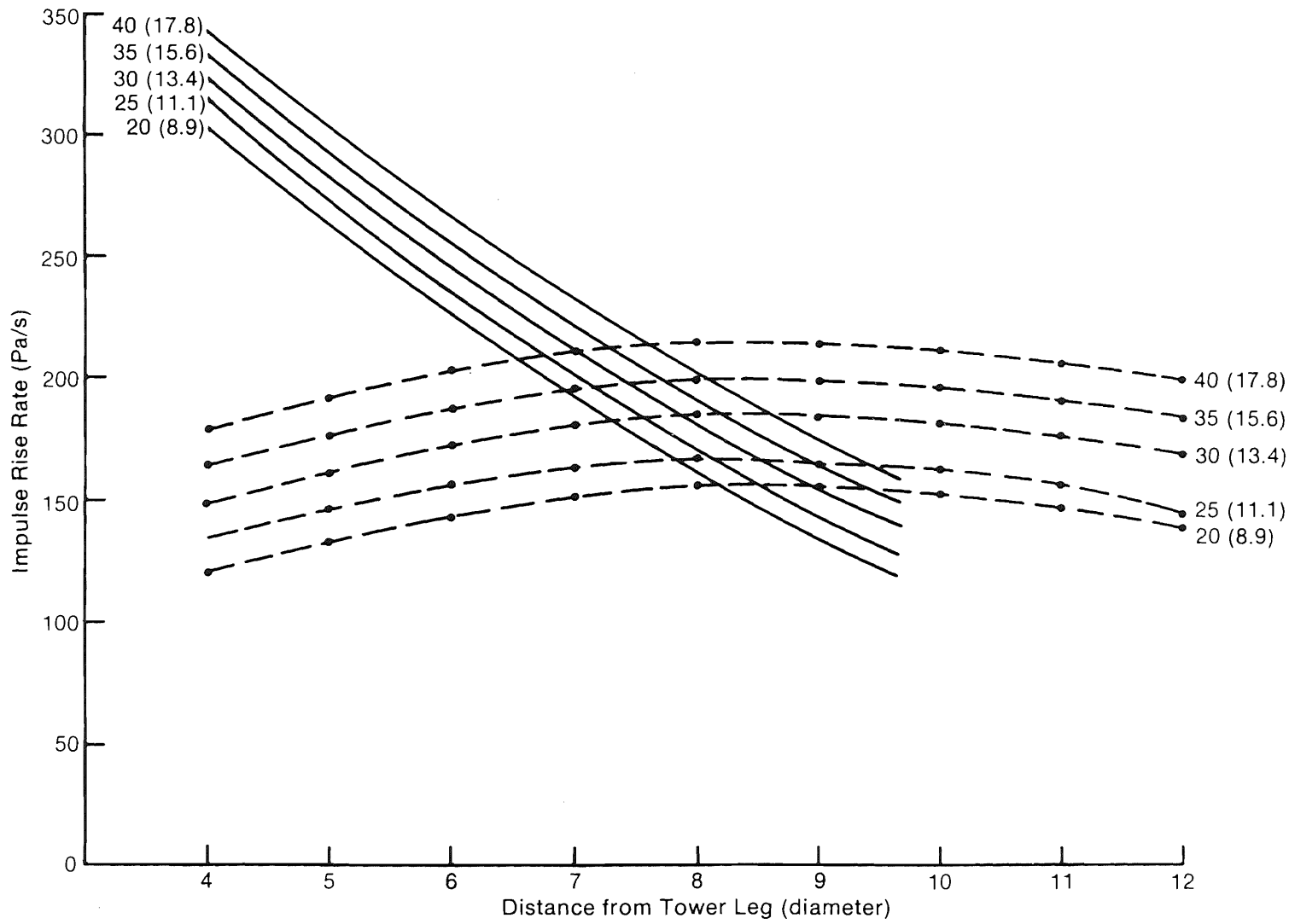


Figure 4-22. Impulse Peak Overpressure as a Function of Tower Leg-to-Blade Distance and Hub-Height Wind Speed for June 1980 Survey Period (East, solid curves; south, dashed curves)

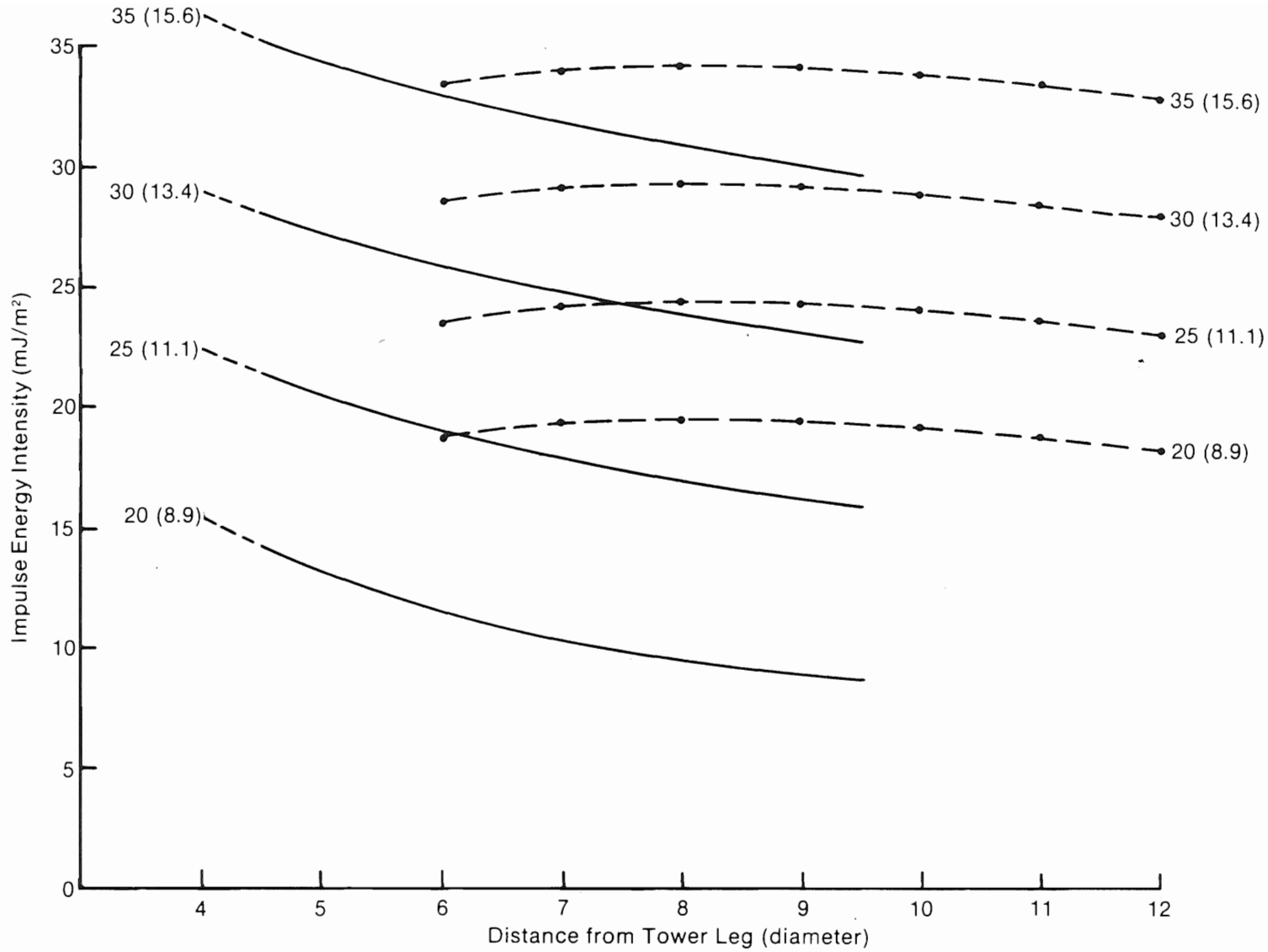


70

004728



Figure 4-23. Impulse Rise Rate as a Function of Tower Leg-to-Blade Distance and Hub-Height Wind Speed for June 1980 Survey Period (East, solid curves; south, dashed curves)



00-729

Figure 4-24. Impulse Energy Intensity as a Function of Rotor Distance from Tower Leg and Hub-Height Wind Speed for March 1980 Survey Period (East, solid curves; south, dashed curves)

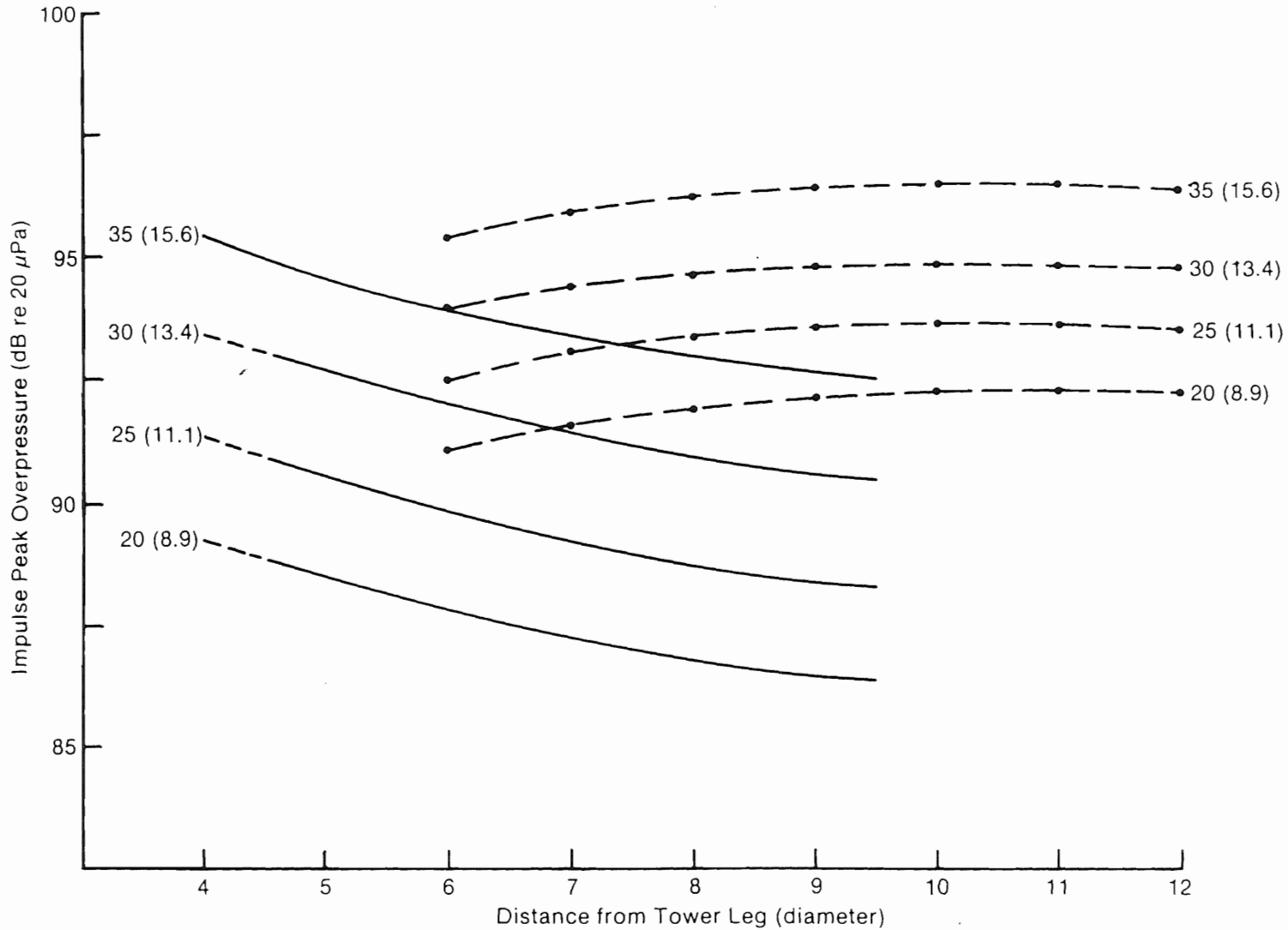
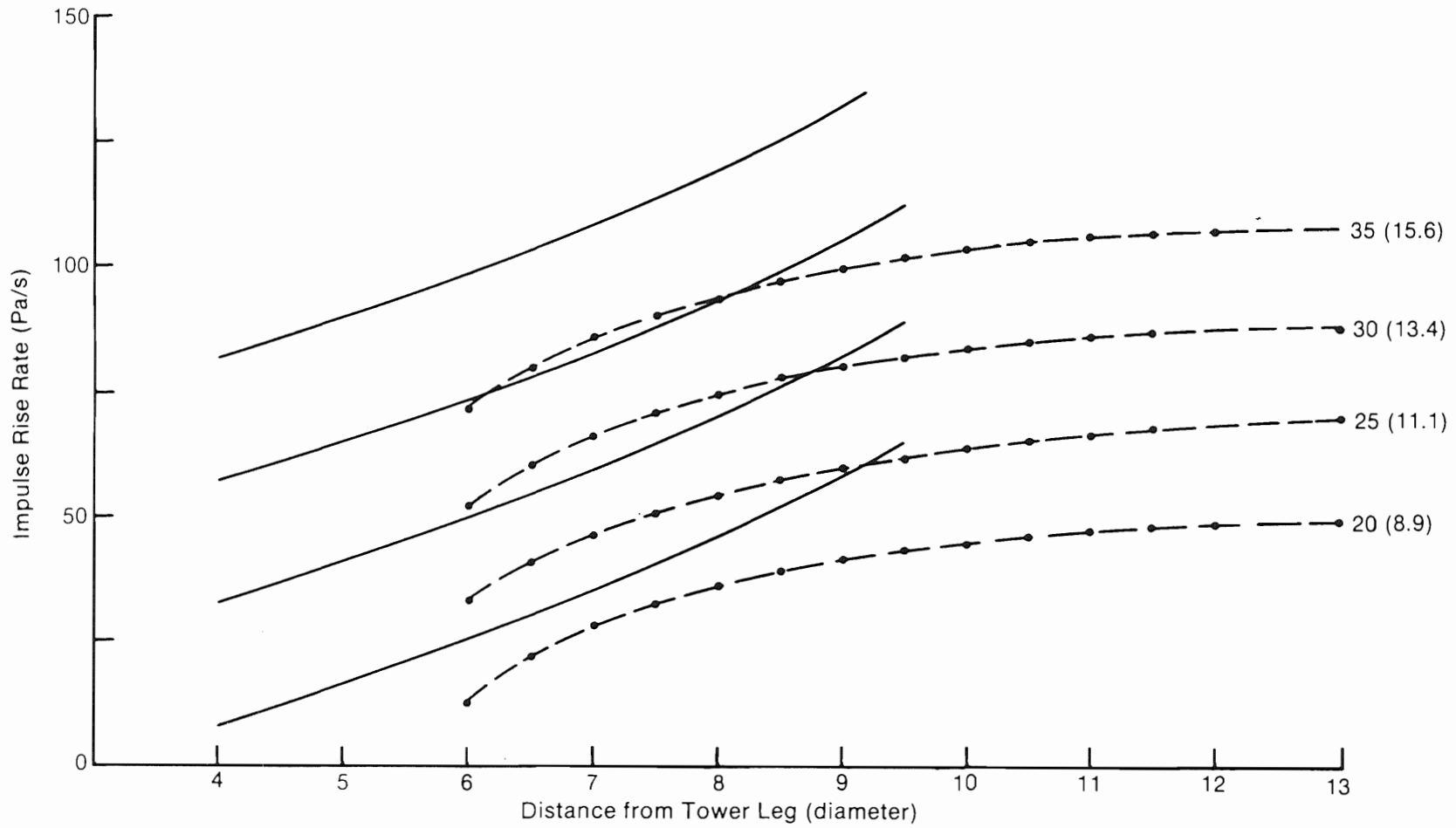


Figure 4-25. Impulse Peak Overpressure as a Function of Rotor Distance from Tower Leg and Hub-Height Wind Speed for March 1980 Survey Period (East, solid curves; south, dashed curves)



004731

Figure 4-26. Impulse Rise Rate as a Function of Rotor Distance from Tower Leg and Hub-Height Wind Speed for March 1980 Survey Period (East, solid curves; south, dashed curves)

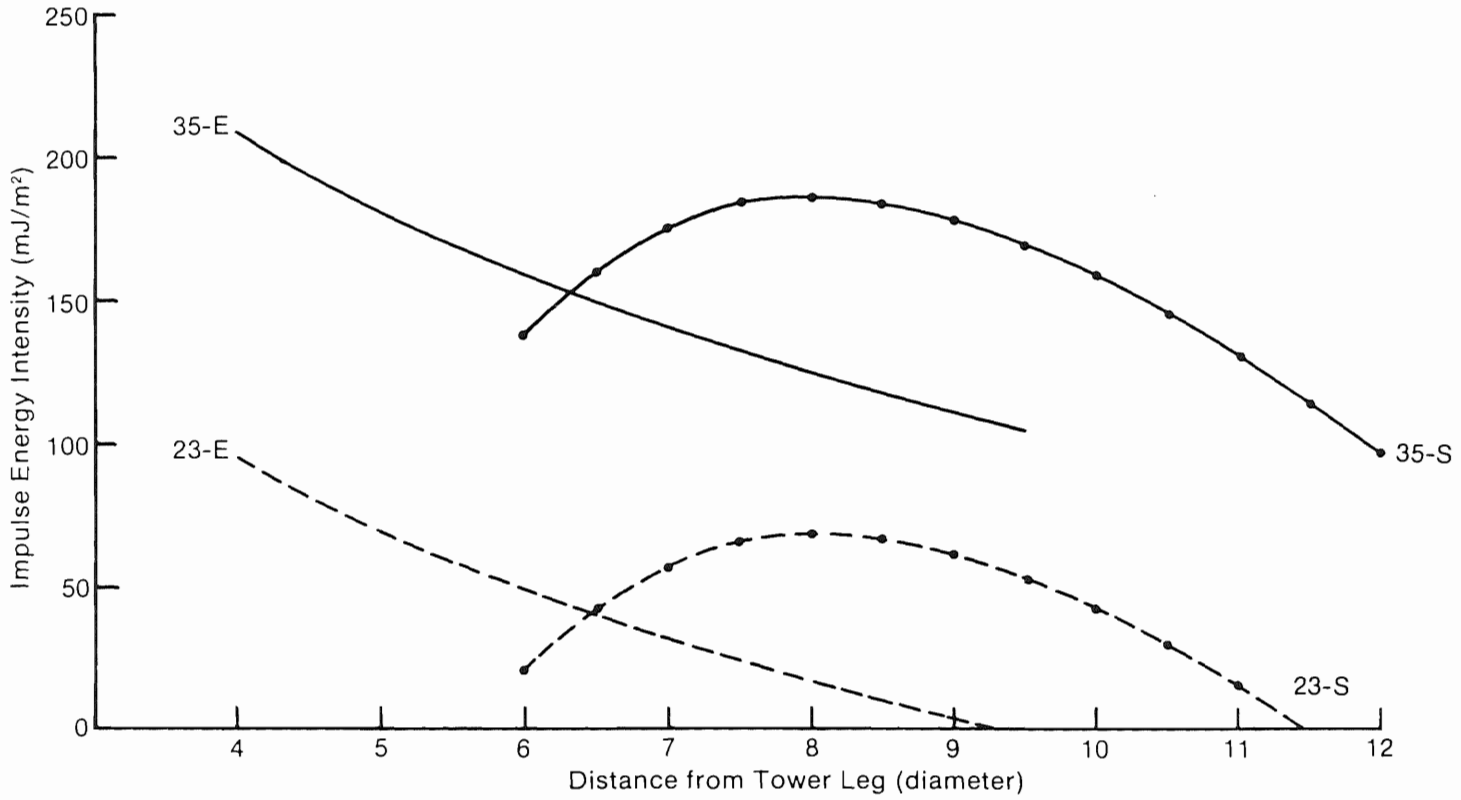
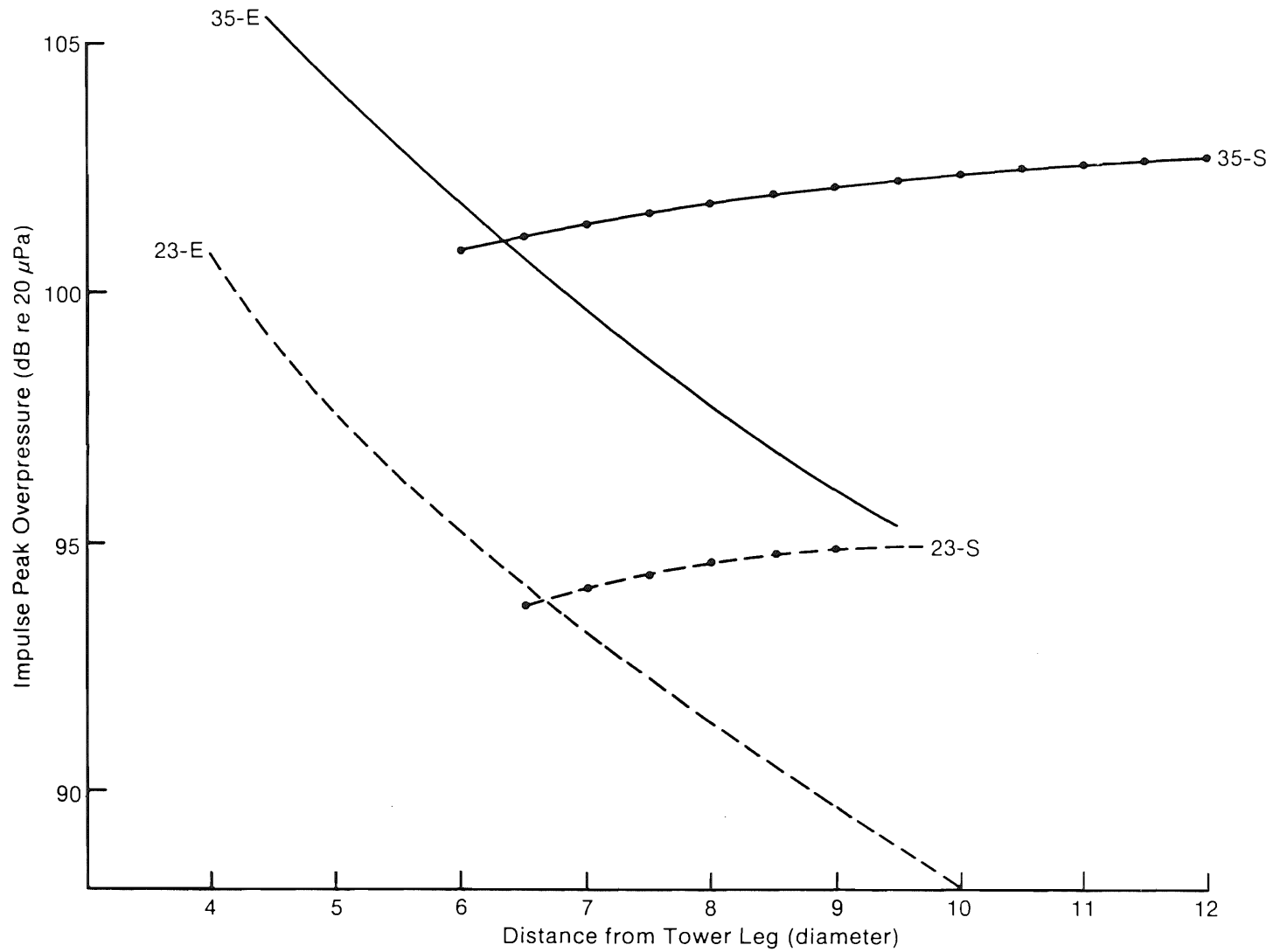


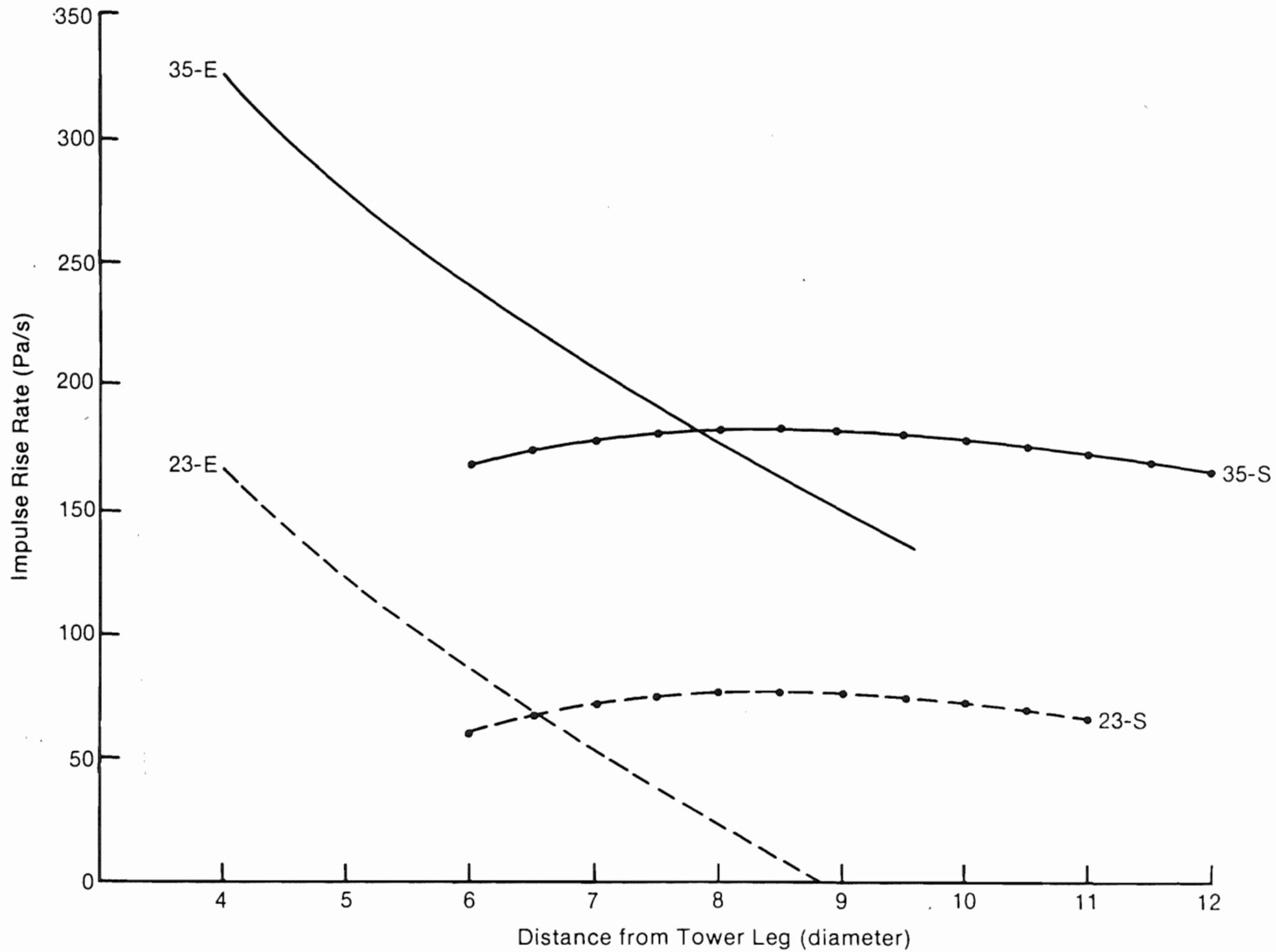
Figure 4-27. Comparison of Energy Intensity of Impulses Associated with the East Tower Leg as Function of the Rotor rpm and Tower Leg-to-Blade Distance (June 1980)



004733

Figure 4-28. Comparison of Peak Overpressures of Impulses Associated with the East Tower Leg as Functions of the Rotor rpm and Tower Leg-to-Blade Distance (June 1980)





004734

Figure 4-29. Comparison of the Rise Rate of Impulses Associated with the East Tower Leg as a Function of Rotor rpm and Tower Leg-to-Blade Distance (June 1980)

of lowering the rotational speed is to reduce the relative blade speed, often referenced to the speed at the blade tip. As shown, the average decrease in energy intensity for the south and east induced impulses are 63% and 57%, respectively. The average decreases in the impulse overpressures for the south leg impulses is 57% versus 52% for the east. The rise rate decrease is 61% and 64% for the same legs, respectively. Thus, reducing the rotational speed from 35 to 23 rpm, or 34%, results in about a 60% decrease in the average impulse characteristic levels, apparently through the increased residence time of the rotor blades in the tower leg wakes.

#### **4.2.3.3 Impulse Analysis Interpretation and Conclusions**

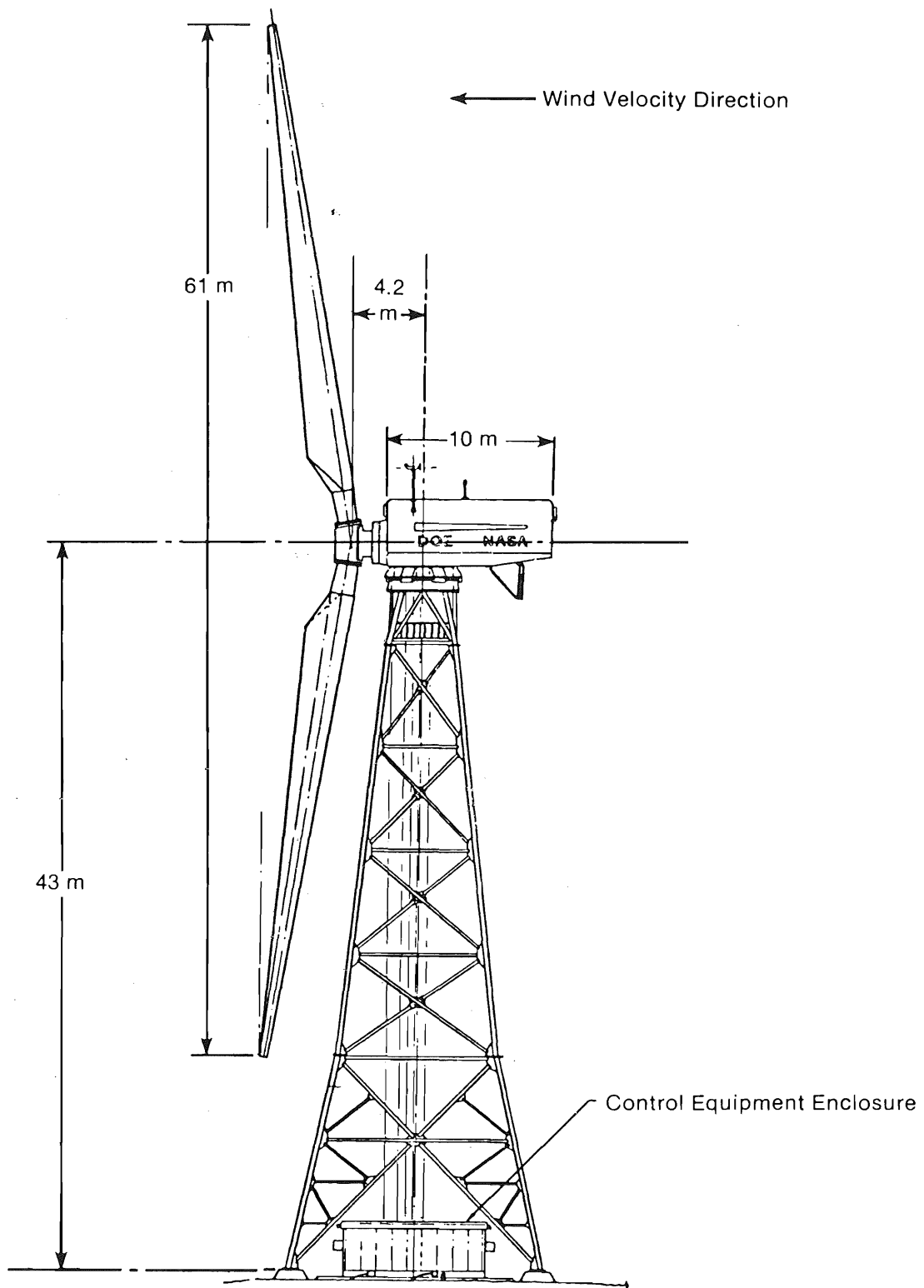
The results of the acoustic impulse analysis presented in the previous section have shown that the sensitivity of the impulse generation process is related to a complex interaction of several operational parameters, including the rotor rotational speed, wind speed, and blade passage distance from the tower support legs. In particular, the following results have been found:

1. The average characteristics of impulses generated in the wake of the east and south tower legs demonstrate strong differences which are similar for both the March and June surveys in form if not in severity.
2. The hypothesis that the impulse generation is strictly a function of wake velocity deficits (or a function of wind speed and separation distance) is not borne out by the marked differences in the severity of levels of impulses generated in the east and south leg wakes plus the unexplained overall increase in severity of the impulses observed during the June experiments over much the same wind-speed range experienced in March.
3. Reducing the rotor rotational speed from 35 to 23 rpm results in an approximately 60% decrease in the average levels of the three impulse characteristic parameters; i.e., the energy intensity, peak dynamic or overpressure, and rise rate.
4. The variation in impulse characteristic parameters with the two leg wakes, particularly the rise rate, indicates that the dynamics of the two wakes must be substantially different in some important aspects.
5. The effect of the wire mesh on the south tower leg appears to have had minimal influence on the generated impulses, the principal effect being a decrease in observed rise rates (Figures 4-16, 4-23, and 4-26) and an average attendant shift in the impulse energy to somewhat lower frequency bands.

The results listed here have strengthened our belief that the acoustic impulse generation process is the result of a complex, unsteady aerodynamic interaction between downstream wakes emanating from various tower structural members, from the large, 0.5-m vertical legs in particular, and the dynamics of the aerodynamic lift being developed by the turbine rotor blades, as described by Eq. (4-5). We also believe that the shape and characteristic parameters of the observed impulses are indicative of the wake dynamics present at the time of blade passage and therefore describe a stochastic process or processes.

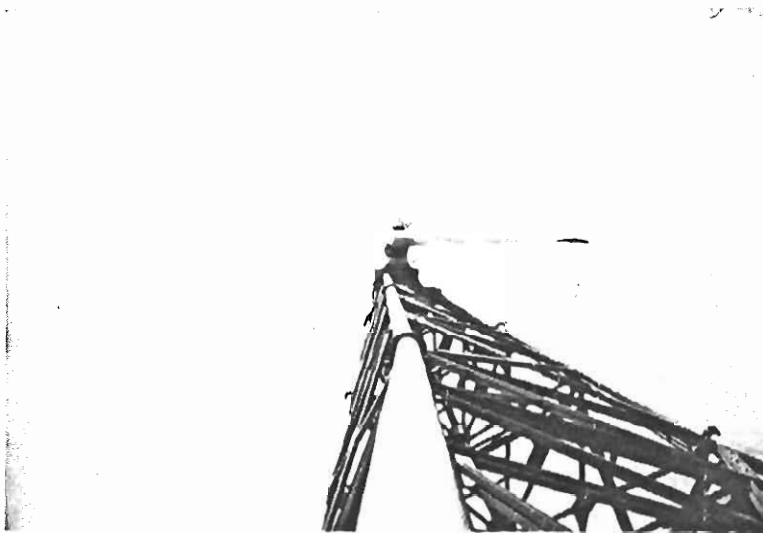
The evidence accumulated so far points to the need for understanding the development of, and downstream dynamics of, the wakes of the tower legs in three dimensions since the rotor blades parallel the legs as they pass the tower, as shown in Figure 4-30. The role of the upstream tower members must be also considered. The peaks in many of the characteristics of impulses generated in the lee of the south leg occurred when the rotor was close to paralleling the SE flat of the tower, a time when the west and north legs were immediately upstream and may have influenced the wake development of the downstream members.

In addition to developing an understanding of leg wake dynamics, it is also necessary to assemble a body of knowledge regarding the effects of the transient, unsteady lift fluctuations forced on the rotor blades as they pass through the tower leg wakes. Understanding both of these processes is essential to the development of abatement procedures that could keep impulses from reaching annoyance levels. These matters are discussed in the following sections.



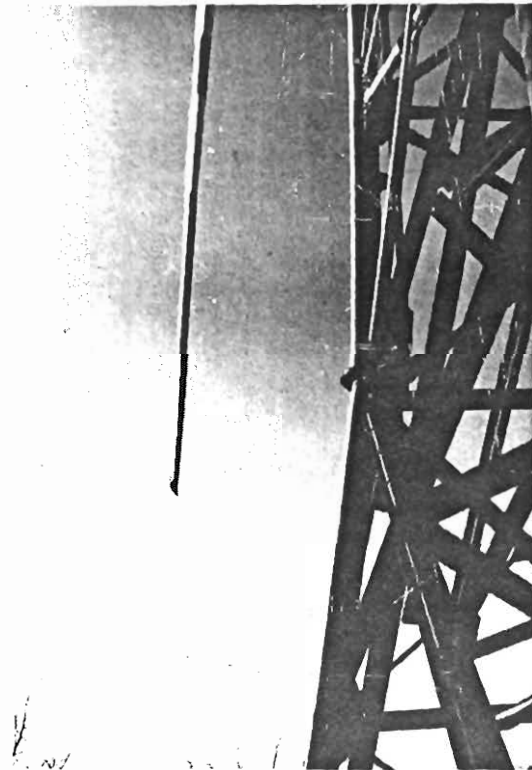
004735

Figure 4-30a. Schematic of MOD-1 Tower and Rotor Structure Showing Small Tower Leg-to-Blade Clearances and 9° Coning Angle



004737

Figure 4-30b. Tower Leg-to-Blade Clearance with Rotor Nominally Parallel to Southeast Flat



004736

Figure 4-30c. Vertically Oriented View, Similar to Figure 4-30b

## SECTION 5.0

### AERODYNAMIC NOISE-GENERATING MECHANISMS

It is evident that the ultimate source of the annoying acoustic impulses being generated in the lee of the MOD-1 tower legs is aerodynamic in origin. In this section, we discuss the physical processes that are responsible for the observed transient, unsteady rotor blade loads which are radiated as acoustic impulses containing considerable pressure energy. Figure 5-1 summarizes the physical processes leading up to the radiated acoustic emissions from a rotating, lifting blade. While both broadband incoherent and discrete emissions are indicated in the figure, we are presently interested only in the latter. From Figure 5-1, we see that the following factors need to be considered in developing an understanding of the MOD-1 noise problem, in particular, and Wind Energy Conversion Systems (WECS) acoustic noise emissions, in general:

- The role of the upwind fetch and the vertical hydrodynamic stability of the atmospheric surface layer in shaping the freestream turbulent structure entering the rotor disk of an upwind turbine design or influencing the wake shedding characteristics of a tower structure ahead of the rotor blades in the case of a downwind design such as the MOD-1
- Aerodynamic processes that control the generation and unsteady structure of downstream wakes from upwind tower elements such as the large cylindrical legs of the MOD-1
- The unsteady aerodynamic response of the airfoil of a turbine rotor blade to the turbulent structures encountered as the blade moves around the rotor disk, resulting in an unsteady airload pressure spectrum on the blade surfaces
- The partitioning of spectral energy derived from the unsteady aerodynamic loading, e.g., that fraction aeroelastically extracted by the blade mechanical structure in the form of dynamic stresses and the small amount  $[O(10^{-5} \text{ J})]^*$  radiated as acoustic emissions with various temporal and frequency domain characteristics; i.e., the degree of coherency.

In this section we examine each of these processes with respect to its influence on the MOD-1 noise situation. Note that some of the material was derived from SERI experimentation which has not been completely analyzed, but appears in more complete form in several other reports. The areas to be considered here, not necessarily in this order, include physical factors influencing the generation of wakes and the unsteady aerodynamic response of airfoil sections similar to those used in WECS applications.

#### 5.1 WAKES FROM CYLINDRICAL BLUFF BODIES

Although wakes from cylindrical bodies have been studied from the time of Archimedes to the present, there are still gaps in our knowledge about this

---

\* $O(10^{-5}) \equiv$  order of  $10^{-5}$  J.

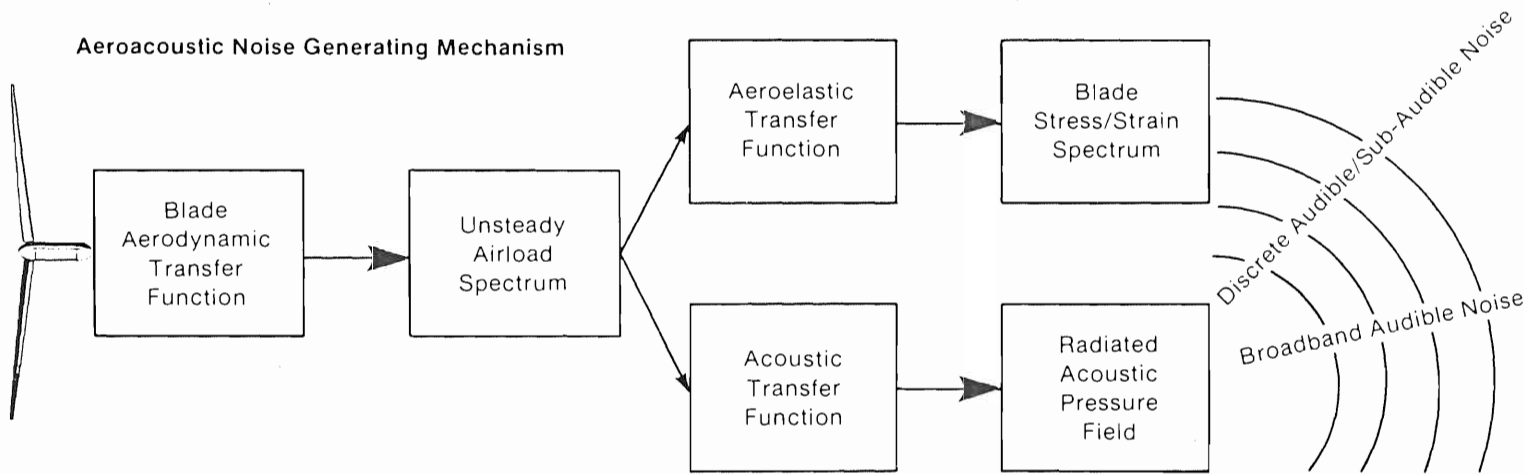
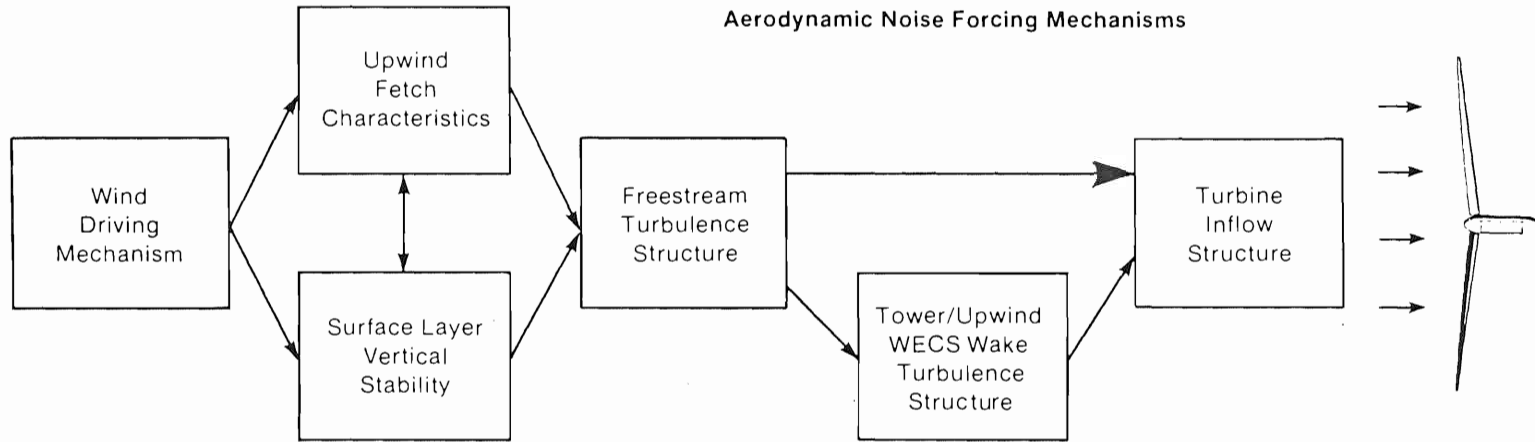


Figure 5-1. Physical Mechanisms Responsible for Noise Generation by Wind Energy Conversion Systems (WECS)

physical phenomenon. The general characteristics of cylinder wakes, which are usually studied as a two-dimensional (2-D) problem, include such parameters as mean velocity deficits (shadowing effects), wake lateral spreading with distance, and the existence of a mean return flow circulation in the near wake region close to the cylindrical body. Dynamic parameters of interest include the shape, frequency, and persistence of vortex sheets, and free shear layer-induced and overall turbulence characteristics. Figure 5-2 highlights some of the major features of cylinder wake flows. Greene [45] made an initial study of the concepts discussed in this section.

The dynamic characteristics of cylinder wake flows are of primary interest to the MOD-1, and all downwind WECS, since the events described in Section 4.0 occur with each blade passage forcing the resulting impulse characteristics to form random variables. Physical factors that influence cylinder wake characteristics include

- the freestream velocity
- freestream turbulence levels and spatial structure
- surface roughness
- the physical diameter of the body itself.

The boundary layer dynamics, which are viscous in nature and therefore a function of the Reynolds number based on the diameter, or

$$Re = \frac{\rho U_{\infty} D}{\mu} = \frac{U_{\infty} D}{\nu}, \quad (5-1)$$

where

$U_{\infty}$  = freestream velocity

$\rho$  = air density

$D$  = cylinder diameter

$\mu$  = absolute viscosity

$\nu$  = kinematic viscosity =  $\mu/\rho$

determine the wake structural characteristics; i.e., a periodic vortex street or a random shedding of vortices, for example. The frequency at which vortex shedding occurs is related to the cylinder boundary layer stability and expressed in terms of the Strouhal number,  $St$ , or

$$f_s = \frac{St U_{\infty}}{D}, \quad (5-2)$$

where  $f_s$  is the cyclic or Strouhal (vortex) shedding frequency.

Critical to the MOD-1 problem is the relevant cylinder Reynolds number range, because the boundary layer viscous forces influence the wake structure the



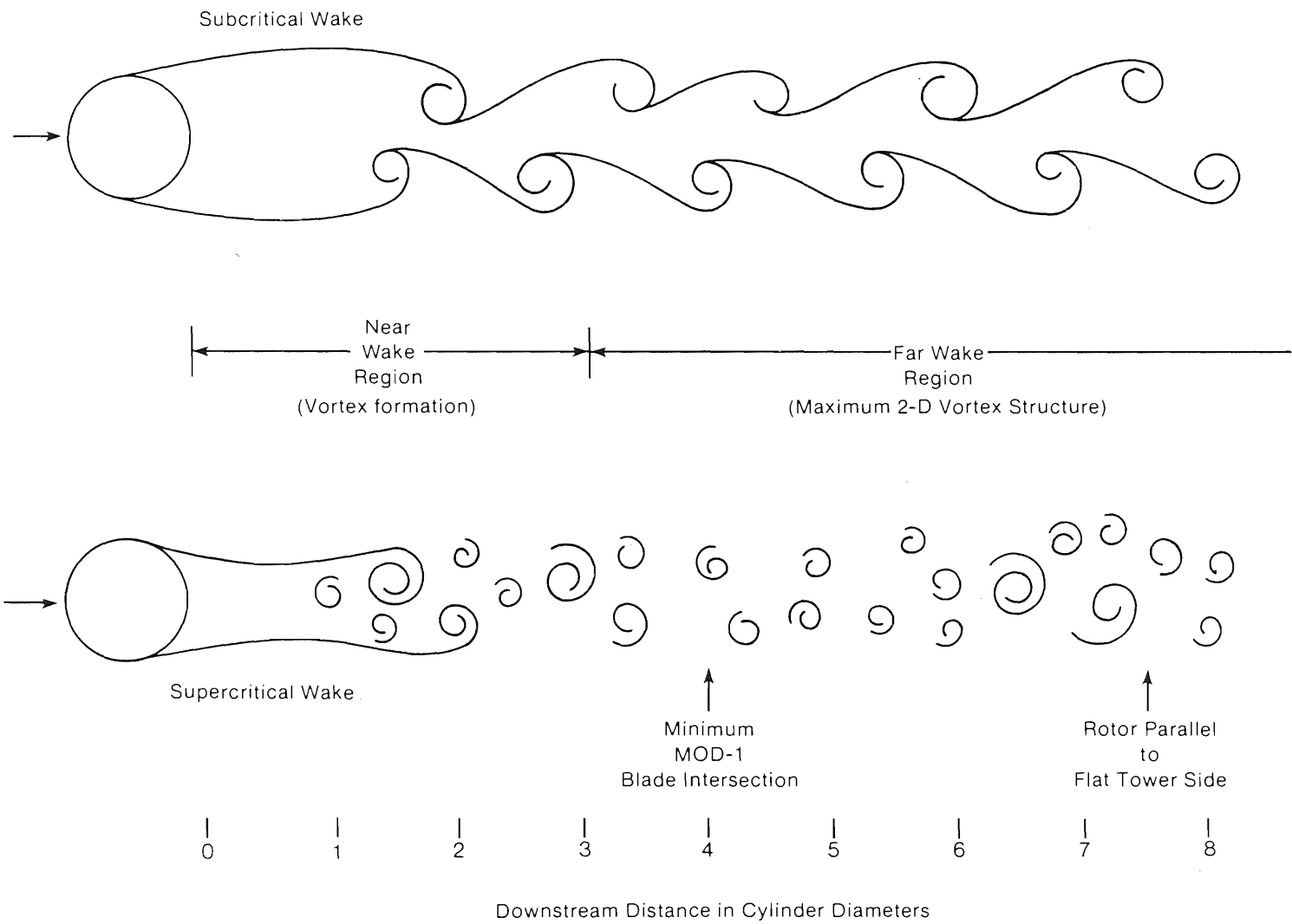
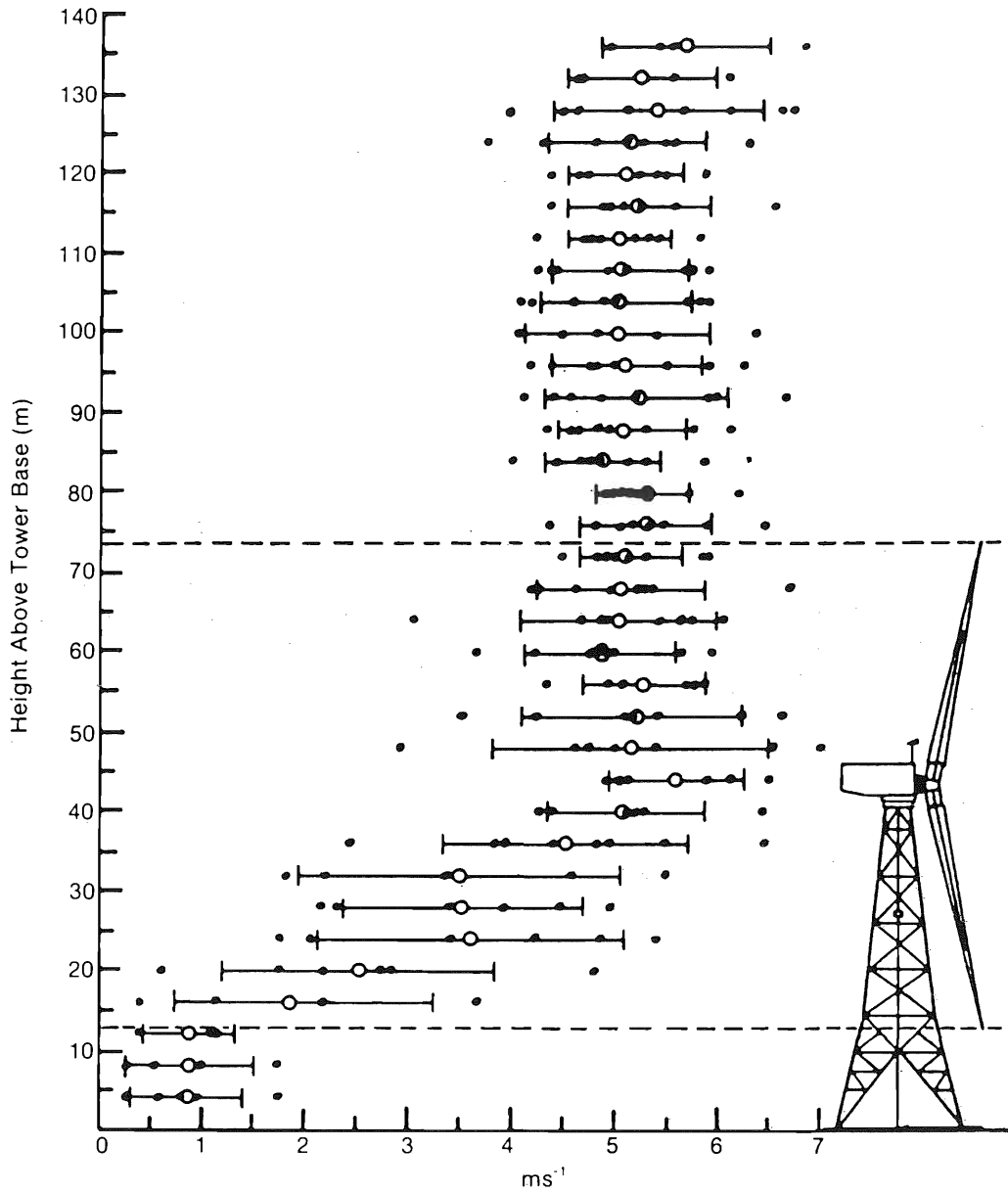


Figure 5-2. Schematics of Cylinder Wake Flows in the Subcritical and Supercritical Regimes

blades are passing through. It is clear that the freestream velocity, particularly as seen by the downstream tower legs (the east and south numbers immediately responsible for the impulse generation as discussed in Section 4.0) do not normally see the hub height values due to the vertical shear existing below the hub and above the forest canopy. The canopy, which reaches the lowest extent of the blade tips, the upwind fetch of complex, mountainous terrain, and drag losses in the tower structure itself all contribute to the generation and maintenance of this shear zone at the rotor disk. Figure 5-3 indicates the level and variability of this shear layer below hub height. This shear is also enhanced by tower blockage effects which are dependent on the approach angle of the wind, as shown by Savino et al. [4]. Garstang et al. [10] have found, from a series of measurements taken during March 1979, that the mean inflow velocity entering the west flat of the tower is typically 15%-25% less than the hub value at the height of the two lower tower structural bays, which are immediately upwind of the rotor blades. Therefore, the downwind tower legs experience a wide range of freestream velocities, often much less than hub value. Translating the turbine operating wind speed range of about 7 to 18  $\text{ms}^{-1}$  (15-40 mph) measured at hub height, we would expect the freestream values at the downwind legs to vary from 50% to 90% of those figures or 3.5 to 16  $\text{ms}^{-1}$ , depending on conditions. For the 0.5-m diameter legs, the Reynolds number can range from 280,000 to 1,260,000 at the altitude of the turbine and an air temperature of  $10^{\circ}\text{C}$ , with a nominal value of 350,000 at an assumed freestream value of 10  $\text{ms}^{-1}$  at this tower height, and with a hub figure estimated to be 25% greater or 13  $\text{ms}^{-1}$ . The expected shedding frequency range, defined by Eq. (5-2) for a Strouhal number of 0.21, would be 1.5 to 6.7 per second and 4.2 at the 10  $\text{ms}^{-1}$  windspeed expressed above. Therefore, a wide Reynolds number range and vortex shedding frequency can be experienced. A frequent intersection of the blade with a vortex is certain since the shedding frequency range, in all cases, is greater than the blade passage frequency of 1.17 per second at 35 rpm and 0.77 at 23 rpm.

#### 5.1.1 Effect of Reynolds Number on Wake Characteristics

Roshko [11] has shown with cylinder flows at Reynolds numbers less than about 200,000, or in the "subcritical" regime, that the resulting downstream wake forms with a dominant shedding periodicity whose frequency is given by Eq. (5-2) and a nominal Strouhal number of 0.21. Above a "critical" Reynolds number (the exact number depends on the roughness characteristics of the surface of the cylinder and the turbulent structure of the inflow), a noticeable narrowing of the wake occurs as a turbulent reattachment of the boundary layer takes place, causing the dominant periodicity of the subcritical regime to cease but strong vortex shedding to continue. This later flow condition, what Roshko refers to as the "supercritical" regime, has been described as "wide-band" and not completely random [12], as well as being very sensitive to freestream turbulence levels, surface roughness and three-dimensional disturbances. The Strouhal shedding frequency  $f_s$  has been observed to vary considerably from a nominal value of 0.21 in subcritical flows, but ranging as high as 0.42 in the supercritical regime. Thus, the freestream flows surrounding the downwind legs of the MOD-1 tower were probably transcending the critical Reynolds number at various times which, as a consequence, influenced the characteristics of the leg wakes to introduce yet another stochastic degree of freedom into the noise generation process.



004739

Figure 5-3. Example of the Vertical Windshear Variability Immediately Upwind of the MOD-1 Turbine

Source: Ref. [10].

### 5.1.2 Three-Dimensional Aspects of Cylinder Vortex Shedding

An examination of Figure 4-29a, b, and c shows, because of the coning angle, how parallel the rotor blade is to the vertical, cylindrical tower members. We noted in Sections 4.1.1.2 and 4.1.1.3, the dependence of coherent, impulsive acoustic radiation on the spanwise lift correlation function, defined as

$$\delta_c = \int_0^{\text{span}} f(x) dx , \quad (5-3)$$

which is related to the radiated dynamic pressure field by

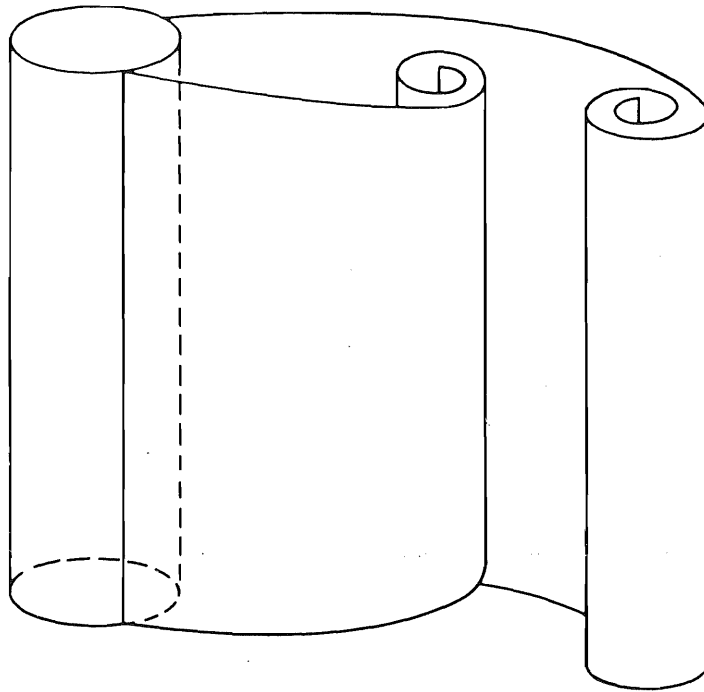
$$\hat{p}(t) = \frac{X_N}{4\pi c_0 r^2} \frac{dL(t)}{dt} \delta_c . \quad (5-4)$$

It is clear that, due to the positioning of the rotor blade with respect to the cylindrical tower leg shown in Figure 4-29, a 2-D cross section of the wake containing vortex elements may also extend into the third dimension or vertically along the leg. The intersection of a turbine blade with such a vertically coherent wake structural element would most certainly produce a lift fluctuation over a sizable portion of the span, as defined by Eq. (5-3).

The three-dimensional (3-D) aspects of cylinder vortex shedding have been studied by Naumann and Quadflieg [13]. From a series of experiments, they concluded that what amounts to a periodic "vortex tube" develops in the wake of a cylinder, as shown in Figure 5-4, initially along a separation line which is parallel to the cylinder major axis. Should the separation line become distorted along the cylinder surface, circulation differences develop and, at a short distance downstream, the 2-D vortex structure breaks down into generally chaotic, 3-D turbulence. Therefore, a physical mechanism potentially exists which is capable of producing a vertically coherent turbulent wake structure and which, if intersected by a turbine blade, could produce large values of  $\delta_c$  as defined by Eq. (5-3) and large, radiated acoustic pressure fluctuations as expressed by Eq. (5-4).

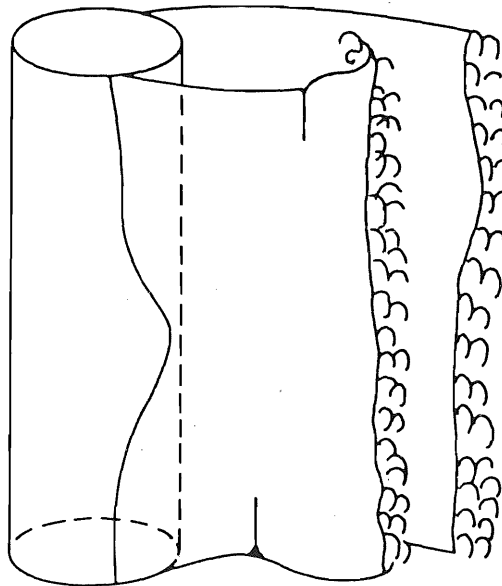
### 5.1.3 Cylinder Far Wake Characteristics

The major elements of a 2-D cylinder wake flow are shown in Figure 5-2. Many investigators have found that this 2-D structure is generally most fully developed downstream of the formation region (about 3-4 cylinder diameters) and extending 10-12 diameters or more before viscous vortex decay and the entrainment of freestream turbulence converts the 2-D structure to 3-D chaotic. Stability factors are also known to control this rate of decay. Under stable, low freestream turbulence conditions, discrete cylinder wakes have been detected out to 50 diameters. Recently, Snyder and Wentz [14] conducted a study of the wake characteristics of cylindrical bluff bodies, including both true circular and 12-sided, polygonal-shaped cylinders. They found that the mean wake profile expands laterally an included angle of about  $1.5^\circ$  from the wake centerline for subcritical flow and only about  $1^\circ$  for the supercritical regime.



004740

Vortex Shedding from a Linear and Parallel Separation Line



Shedding from a Distorted Separation Line

Figure 5-4. Sketch of Cylinder Vortex Shedding from a Vertical Separation Line Parallel to Major Axis and when this Line is Distorted

Source: Ref. [13].

#### 5.1.4 Field Verification of Vertical Coherency of Cylinder Wake Structures in Natural Flows

To verify the existence or nonexistence of vertically coherent structures in the downstream wake of a cylindrical tower element, an experiment (which was part of a larger effort) was performed at the Rocky Flats Wind Energy Research Center during the summer of 1981. A cylindrical section 2.4 m long and 0.5 m in diameter (same as a MOD-1 leg) was mounted approximately 10 m above the ground on a small wind turbine support tower. Two constant-temperature, hot-film anemometers with measuring elements 50  $\mu\text{m}$  in diameter were mounted on a boom support mount attached to the arm of a lift truck, as shown in Figure 5-5. The two anemometers were mounted approximately one meter apart vertically and placed in the wake of the cylindrical element on the tower at various downstream distances.

Figures 5-6 and 5-7 plot the resulting averaged cross spectrum and standard coherence function for the two wake velocity signals. The two probes saw a correlated shedding signal at a frequency of 1.244 Hz. The mean freestream velocity was  $3.6 \text{ ms}^{-1}$  with a peak coherent wake velocity of  $1.10 \text{ ms}^{-1}$  or 31% of the freestream value at that frequency. The calculated Strouhal shedding frequency ( $St = 0.21$ ) for this mean freestream velocity is 1.51 Hz, compared with the 1.244 Hz measured. The peak coherence was 0.591, indicating that the two velocities can be considered partially vertically coherent in the mean.

These and other similar measurements have confirmed the existence of wake structures that are partially coherent along a dimension parallel to the major axis being shed from vertically mounted cylindrical bluff bodies in a natural wind. Figure 5-8 further confirms the periodic shedding attribute through a comparison of the local wake dynamic pressure amplitude spectrum, as measured at the base of the cylinder and 2 cm from its surface (upper trace), with a corresponding wake velocity spectrum 1-1/2 cylinder diameters downstream.

#### 5.2 IMPULSIVE NOISE GENERATION MECHANISM(S)

Because of the extreme difficulty of making detailed aerodynamic measurements near the MOD-1 turbine, as well as the highly nonstationary conditions surrounding the impulse generation process itself, we performed a series of supporting experiments to aid us in developing a more clear understanding of what physical processes were operating but under conditions in which some control could be exerted. These ancillary experiments included field measurements using both the full-scale DOE/NASA MOD-0 experimental turbine at Plumbrook, Ohio and a small downwind turbine installed at the Rocky Flats Wind Energy Research Center near Golden, Colorado. Two wind tunnel experiments were also performed using the MIT Anechoic Wind Tunnel and the University of Colorado-Boulder subsonic wind tunnel facilities. Due to the incompleteness of much of the analyses of these supporting studies, only excerpts from the results obtained so far can be presented in this document; the remainder is to be included in future SERI reports.

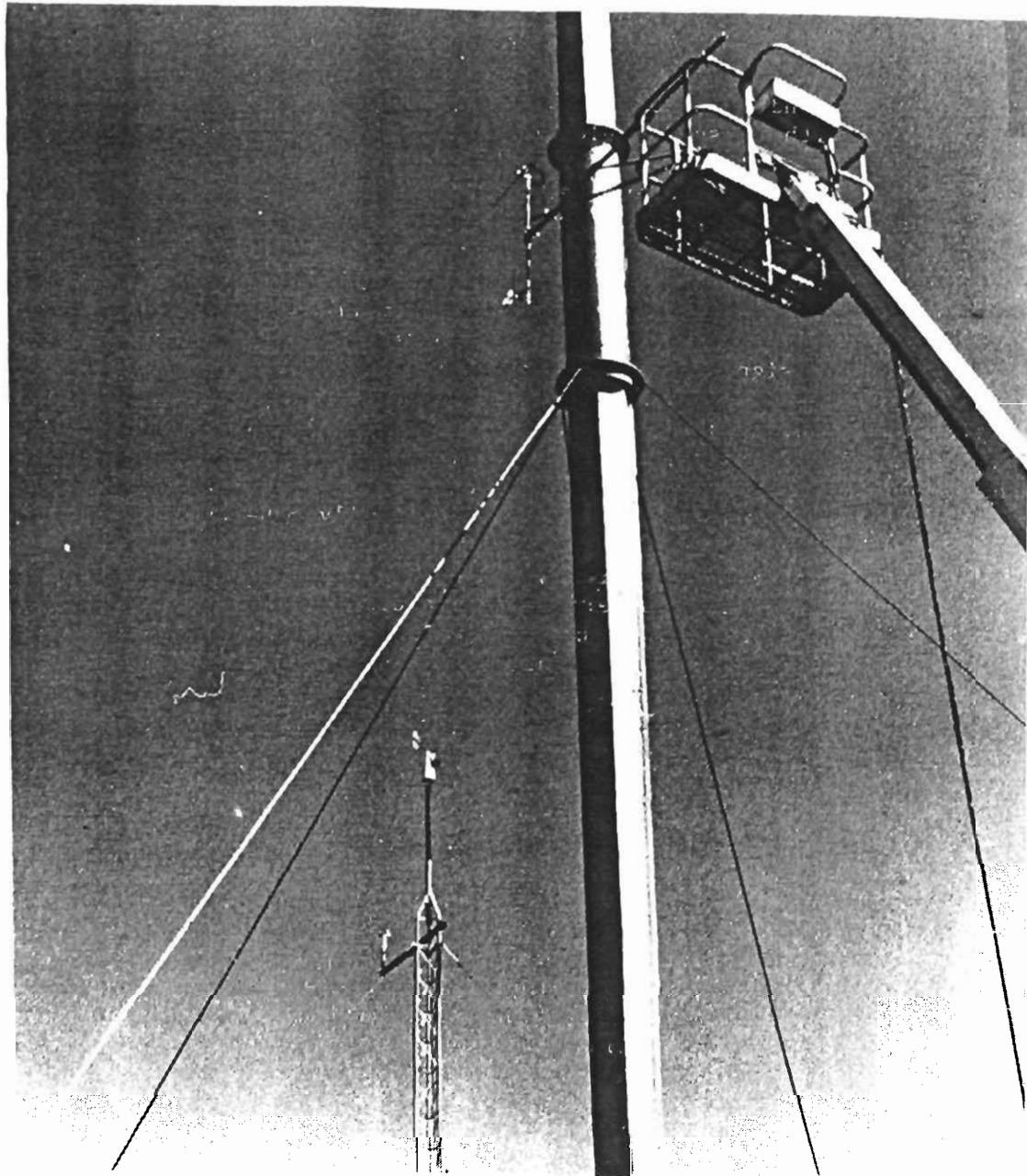


**Figure 5-5. Vertically-Separated, Dual Hot-Film Anemometer Configuration for Measuring Cylinder Wake Characteristics in Natural Turbulent Flow**

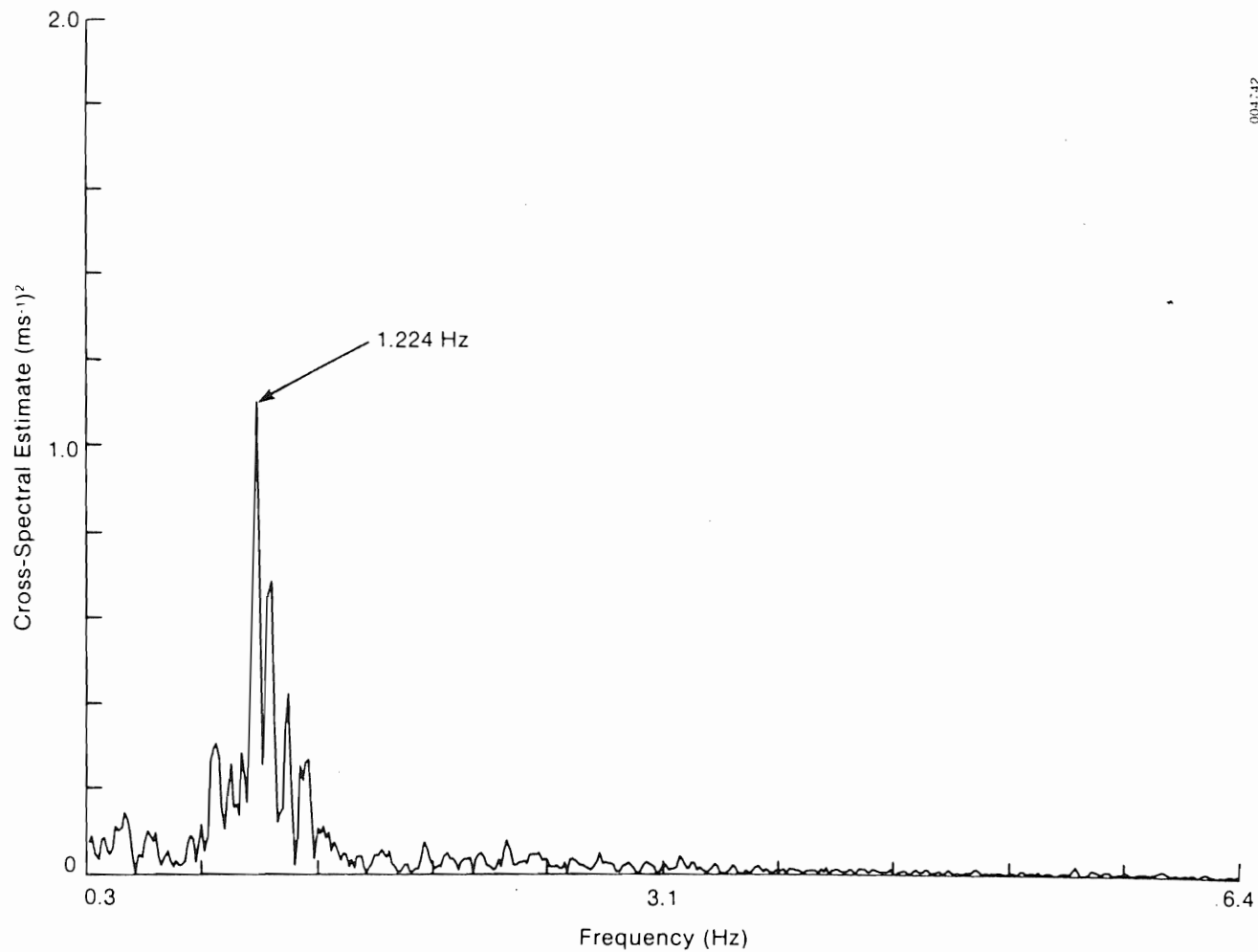
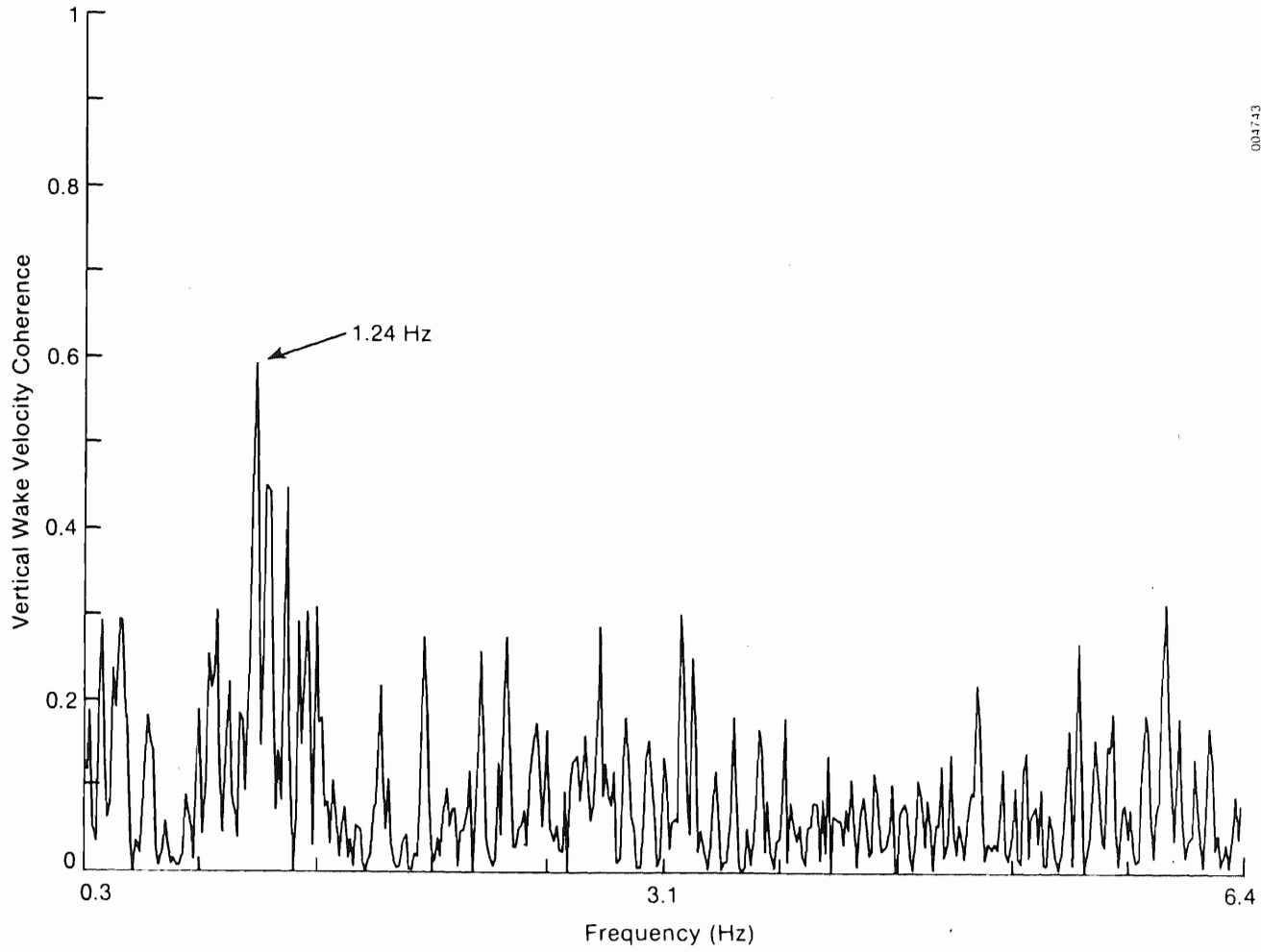


Figure 5-6. Cross-Spectral Estimate of the Upper and Lower Bare Cylinder Wake Velocities as Measured by the Technique Shown in Figure 5-5





001743

Figure 5-7. Vertical Coherence of Bare Cylinder Wake as Determined by Measurements of Figure 5-5

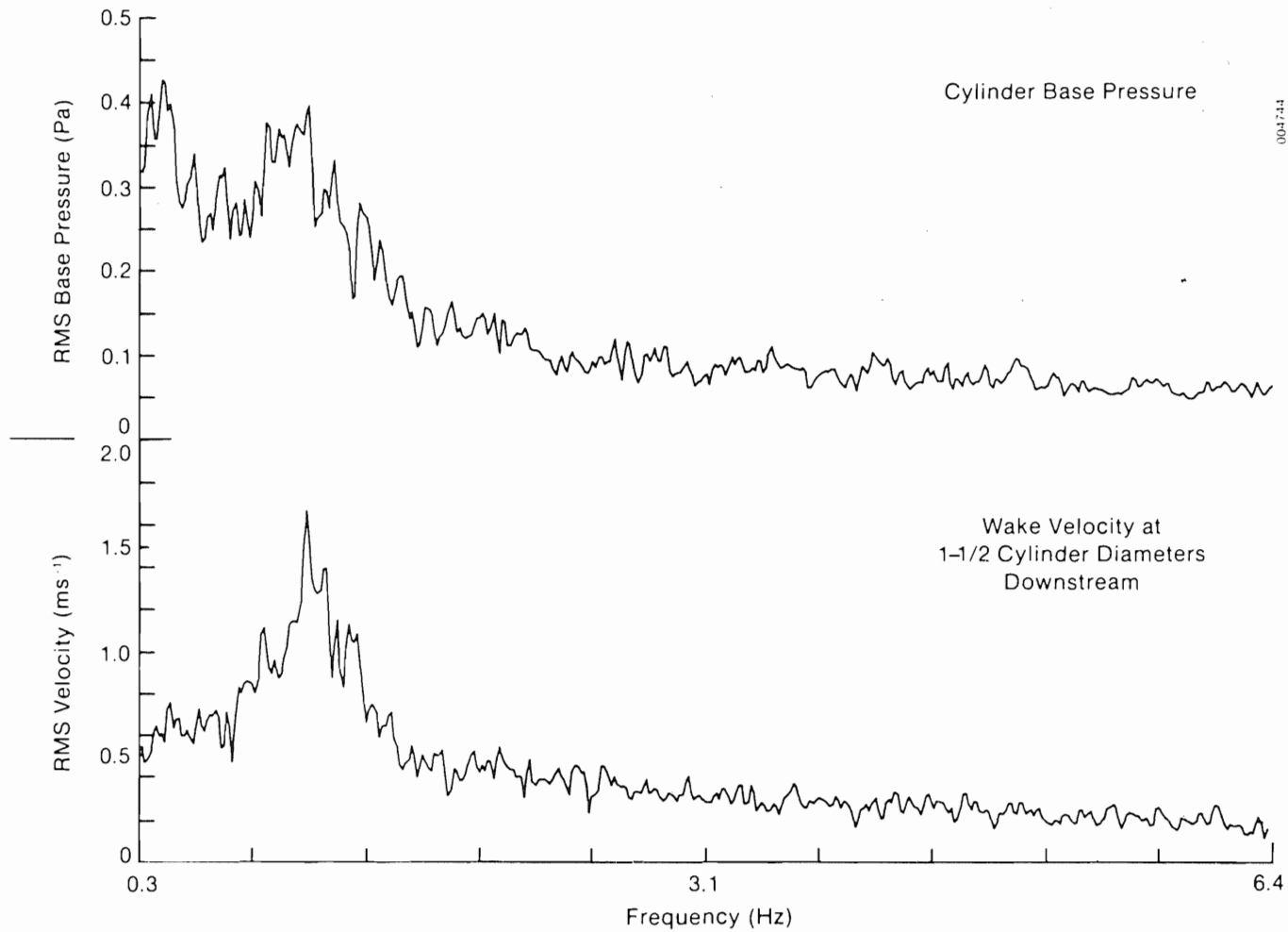


Figure 5-8. Comparisons of Cylinder Base Pressure and Wake Velocity RMS Spectra for Bare Cylinder Tower Element

### 5.2.1 Wind Tunnel Verification of Tower Leg Wakes as the Principal Cause of Impulse Generation

The purpose of using the MIT anechoic wind tunnel was to confirm, at least on a semiquantitative basis, the role of tower leg downstream wakes in the generation of acoustic impulses and as the source of homeowner complaints. Figure 5-9 is a sketch of the experimental setup. Details of the actual experiments are discussed in Refs. [15] and [16]. Essentially, the experiments consisted of placing a series of cylinders of varying diameters in the inflow of an unloaded, two-bladed rotor operating at a tip speed ratio of between 9 and 10. Cylinder diameters were chosen based on diameter/blade-chord ratios of 0.31, 0.63, 1.0, and 2.5 to simulate upstream tower structural element diameters ranging from the MOD-1 (0.31) to the Hamilton-Standard Model WTS-4 turbine (2.5) and including two intermediate values, 0.63 and 1.0. The leg-to-blade distance was also varied by moving the blocking cylinder to upstream positions normalized by the cylinder diameter ( $D$ ), i.e., 3, 5, 10, and 15 $D$ . When there was sufficient clearance, a second cylinder identical to the first was placed upstream at a distance of 17 $D$  to evaluate the effects of augmenting the inflow of the cylinder immediately ahead of the rotor disk. The purpose of this was to simulate a quasi-periodic turbulent structure containing disturbances related to the cylinder Strouhal frequency similar to that found on a pipe truss tower when the downstream legs are emersed in the wake from those immediately upstream. In the case of the MOD-1, this arrangement corresponded to the most common rotor azimuth position, a result of the prevalence of a WNW wind direction. A constant-temperature, hot-wire anemometer was placed in the cylinder wake at a distance slightly ahead of the rotor plane to measure the turbulent structure actually entering the blades. Two SERI VLF microphone systems were used to measure the acoustic emissions of the blade-wake interaction, one on-axis and one in the rotor plane in the acoustic far field. Unfortunately, dynamic similarity with the MOD-1 could not be achieved with this arrangement. The 5.5-cm constant-chord rotor achieved a blade speed of 50  $\text{ms}^{-1}$  at 80% span for a chord Reynolds number of 160,000, compared with the MOD-1 80%-span-speed of 88  $\text{ms}^{-1}$  at 35 rpm and a chord Reynolds number of  $10^7$ . Similarly, the maximum cylinder Reynolds numbers ranged from 14,000 for the smallest diameter to 115,000 for the largest, compared with a value of about 350,000 for the MOD-1 at a freestream velocity of 10  $\text{ms}^{-1}$ .

#### 5.2.1.1 Acoustic Results

Some of the acoustic results of these tests are summarized in Figure 5-10 in terms of the peak SPL measured by the on-axis microphone at a freestream velocity of 13.4  $\text{ms}^{-1}$ . The smallest cylinder (which is the same cylinder-diameter/chord ratio as the MOD-1 at 80% span) radiates the most severe impulse levels compared with the larger cylinder wakes, a full 11 dB above background. The effect of placing an identical cylinder 17 $D$  upstream of the first was to intensify the impulses being emitted by the blade-wake interaction. Figure 5-11 shows two pressure-time plots of a single blade passage through the wake of the smallest cylinder 3.5 $D$  upstream and with and without a second cylinder 17 $D$  upstream of the first. The impulse generated by the augmented wake has a peak dynamic pressure almost four times or 12 dB greater than the single-cylinder-induced impulse. The acoustic pressure-time

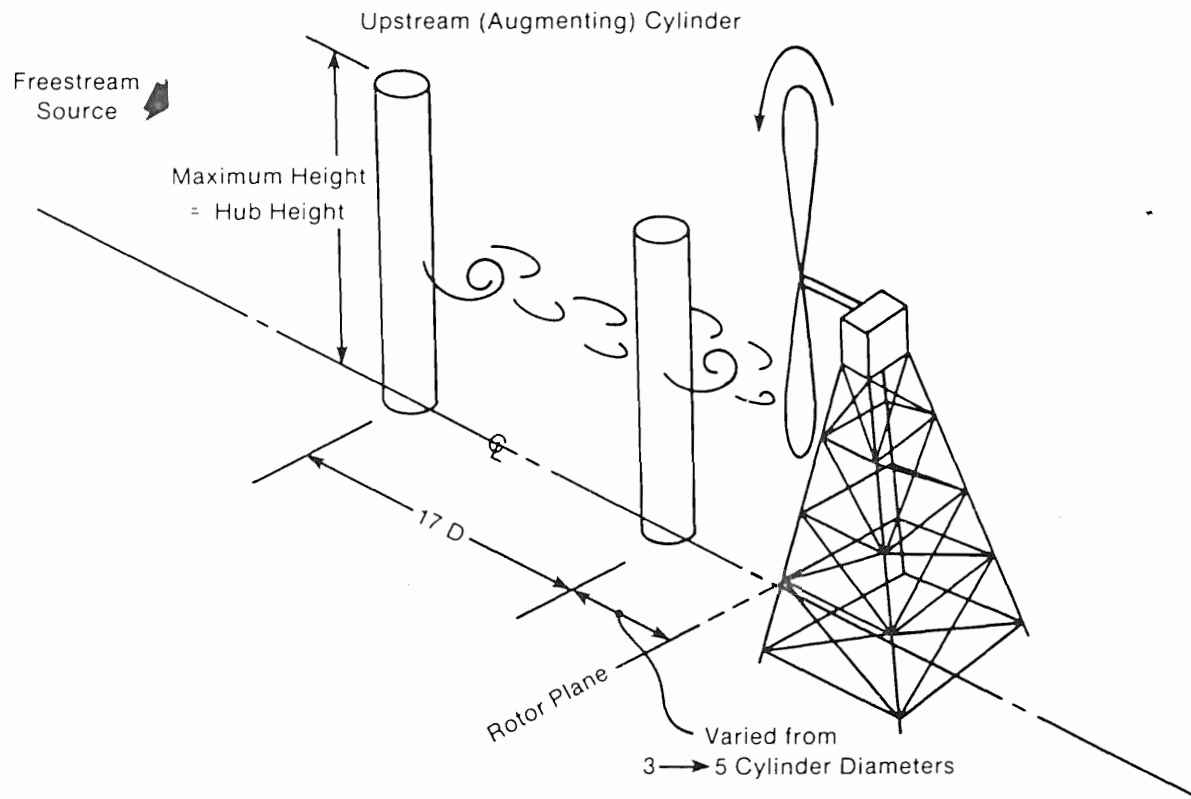
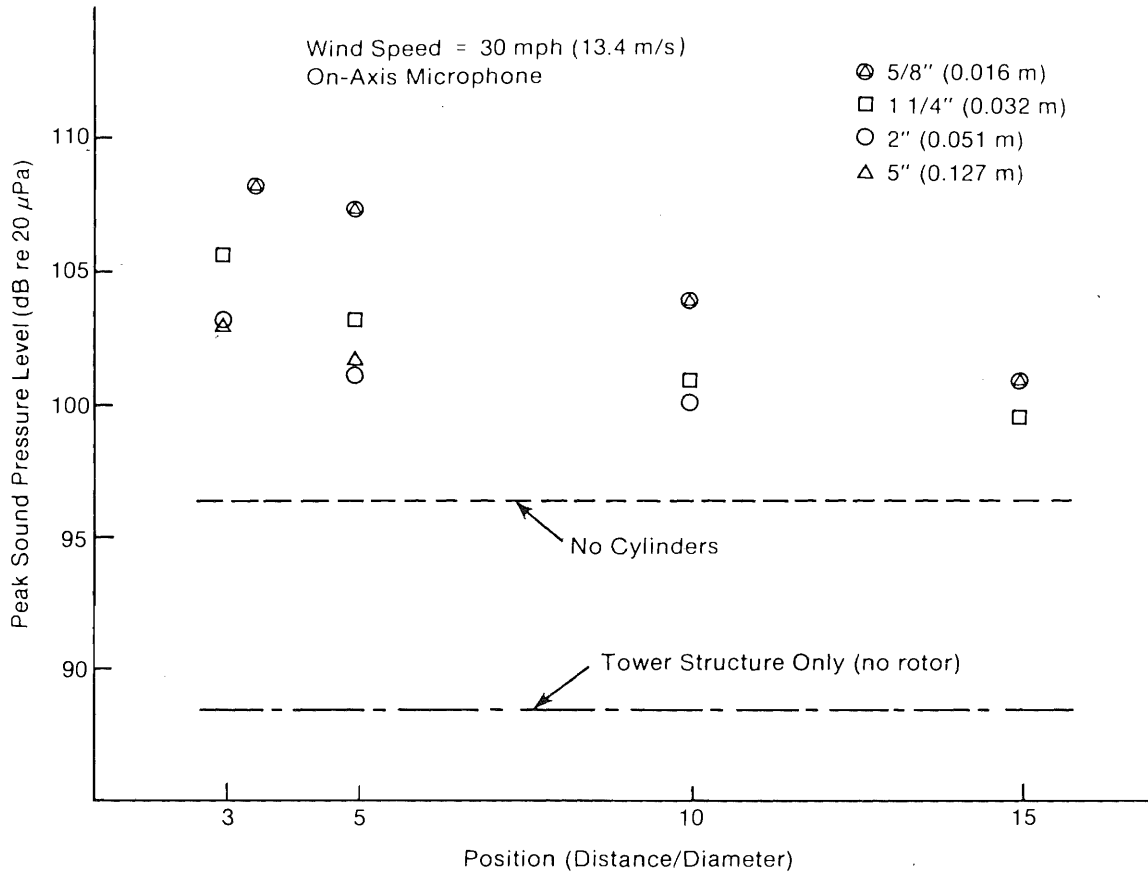


Figure 5-9. Experimental Configuration Used in the MIT Anechoic Wind Tunnel Testing



**Figure 5-10. On-Axis Peak Impulse Pressure as a Function of Cylinder-to-Rotor Distance and Upstream Cylinder Diameter**

Source: Ref. [15].

histories of three blade passages for the dual and individual cylinder wakes are plotted in Figure 5-12, which again show the variability of the impulse signatures and the increased severity of the impulse associated with the augmented wake, even under controlled wind tunnel conditions.

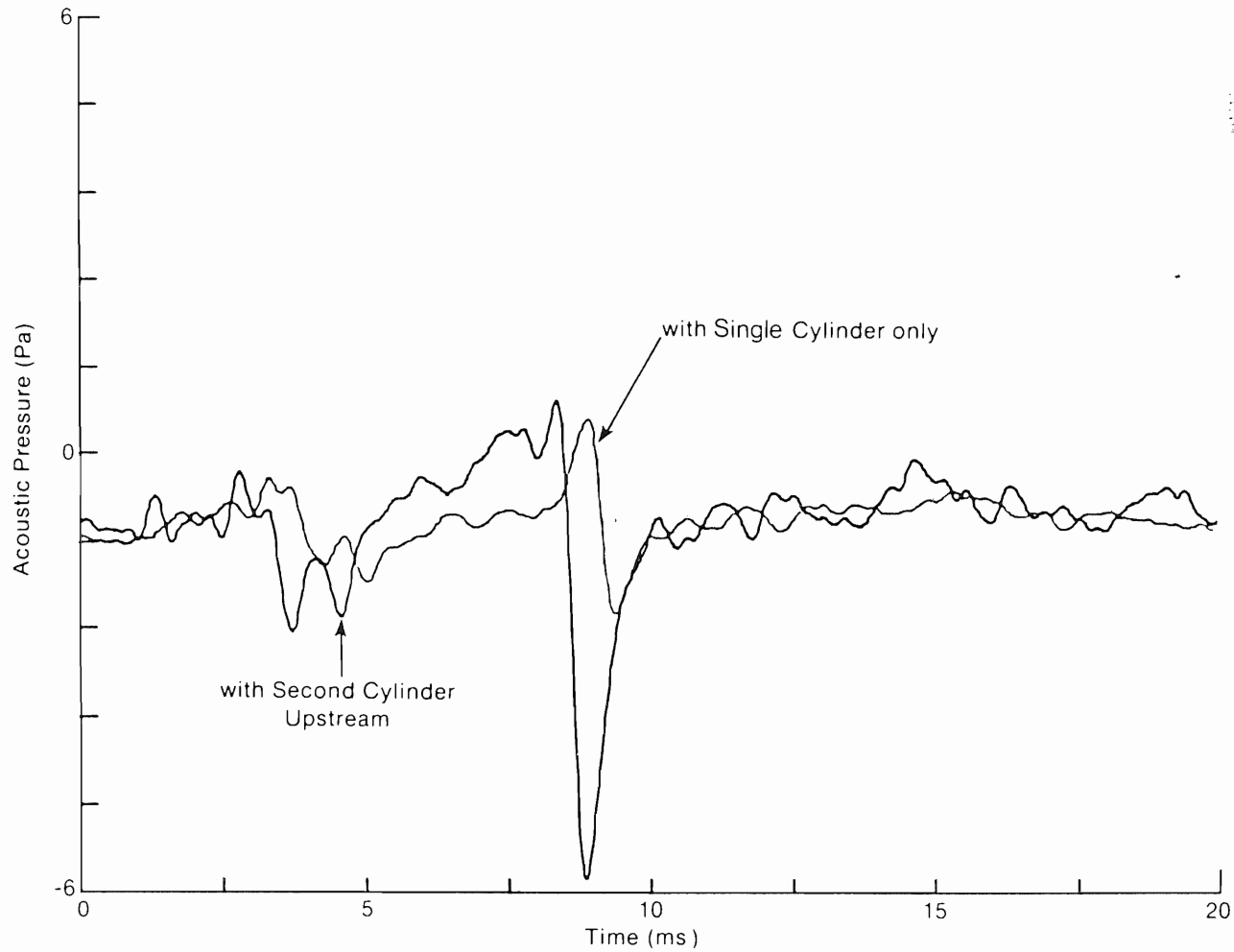


Figure 5-11. Acoustic Pressure-Time Plot of Impulses Emitted from Cylinder Wake-Blade Interaction with a Single Upstream Cylinder and with a Second Augmenting Cylinder Present

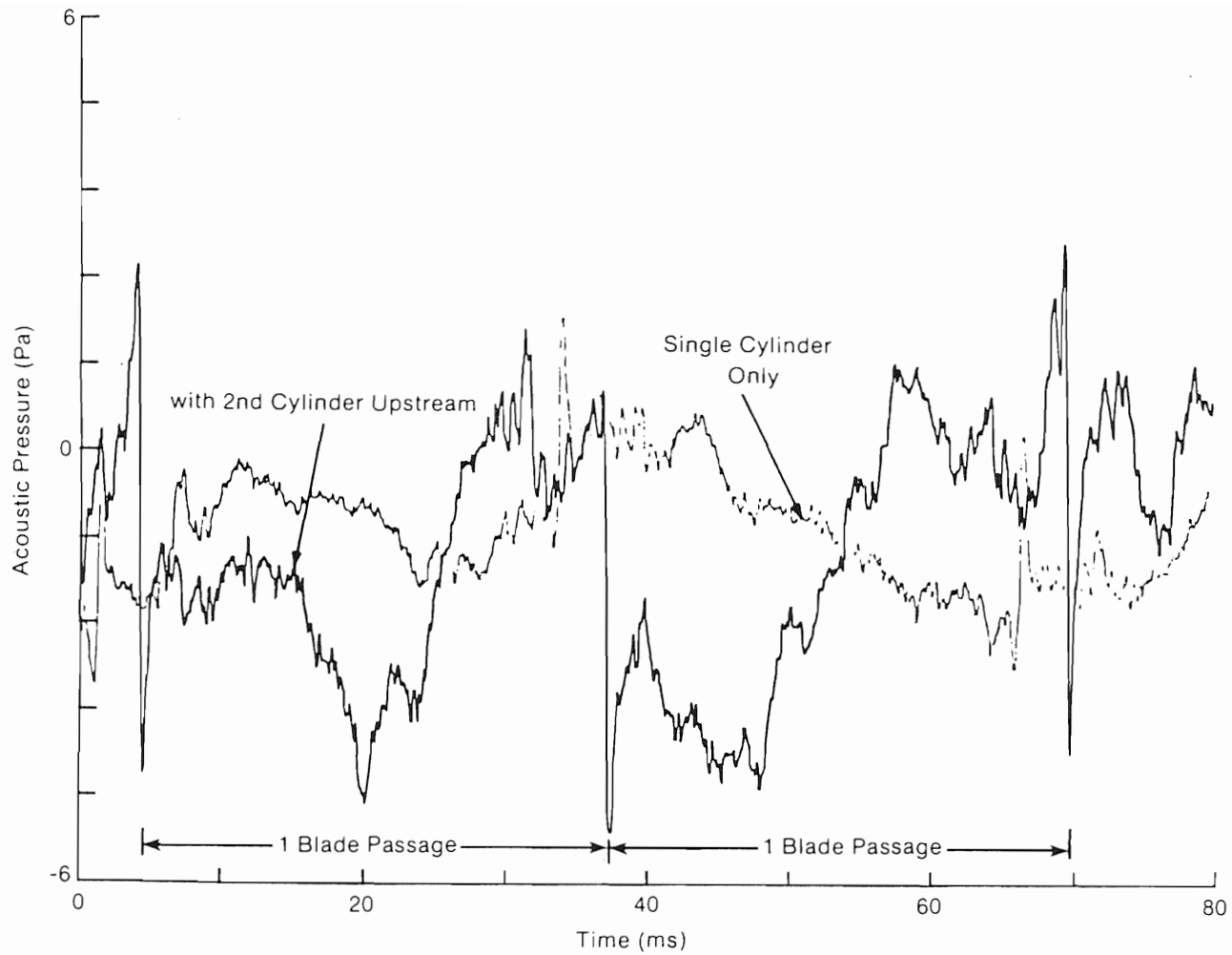


Figure 5-12. On-Axis Acoustic Pressure-Time Plot of Impulses Generated by Three Passages through Wakes Produced by Single and Dual Upstream Cylinders

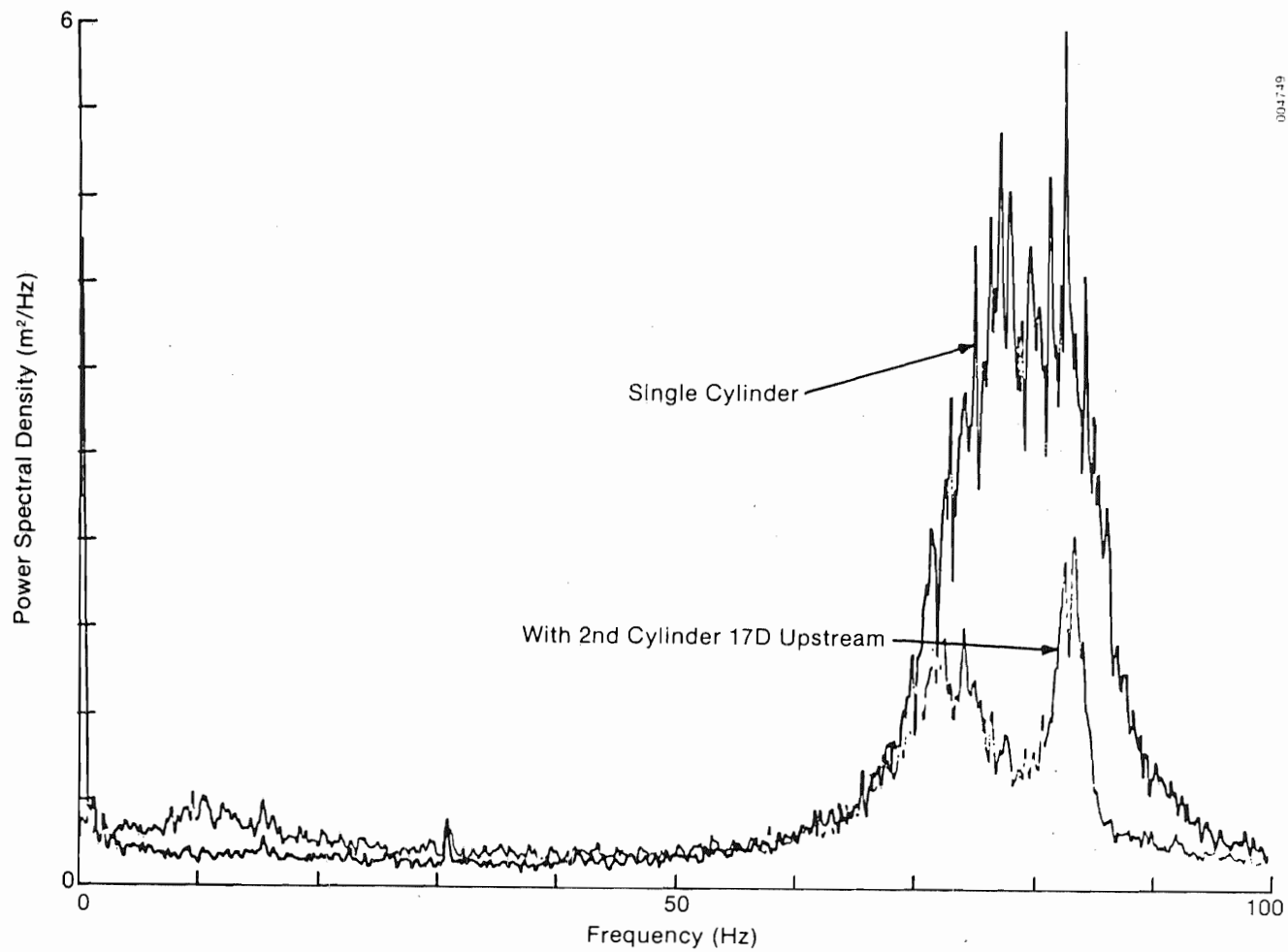
### 5.2.1.2 Aerodynamic Results

The advantage of this experiment, when compared with actual field measurements of the MOD-1, is that we gain at least a partial knowledge of the turbulent structural characteristics of the cylinder wakes entering the rotor disk while being able to compare the induced acoustic effects on the same time base. Under these conditions, we are also able to examine the features of the single- and upstream-cylinder-augmented wakes to gain insight into why the latter were intensified. Figure 5-13 plots the averaged velocity power spectral density spectrum of the smallest cylinder wake with and without upstream augmentation (which corresponds to the acoustic impulses shown in Figures 5-11 and 5-12). The spectrum of the augmented wake is seen to be less energetic and more discrete than that of the single-cylinder wake. The probability density curves of Figure 5-14 for these two time series (which have been passed through a bandpass filter whose 3 dB breakpoints reside  $\pm 20$  Hz of the shedding frequency of 87 Hz) show that the single-cylinder wake is not only more broadband but also exhibits a more-or-less uniform density distribution in the wake vortex shedding frequency range. The augmented wake, in contrast, not only is more discrete but tends to be more Gaussian. From this we find that the more intense acoustic impulses are being generated in a wake containing a greater number of discrete vortices and exhibiting narrowband properties, compared with the single-cylinder wake which inherently exhibits a wideband characteristic. Thus, the disturbances present in the wake of the upstream bluff body will tend to intensify the unsteady aerodynamic process related to the wake generation of a downstream cylinder, the latter being directly responsible for the rapid lift fluctuations and impulse radiation from a passing turbine blade.

These characteristics are difficult to see in an actual sample time series of the wake velocity. However, because of the nature of this experiment, i.e., what may be called stationary in the wide sense due to the external conditions imposed, underlying wake structures both containing and not containing a predominance of these qualities may be viewed in Figure 5-15a and 5-15b. Here, two wake velocity signals representing the augmented and unaugmented cases have been ensemble-averaged over a period of 100 seconds using a once-per-revolution synchronizing pulse. A close study of these two statistical ensembles reveals many of the structural characteristics described by the frequency and probabilistic presentations of Figures 5-13 and 5-14. In particular, the wideband nature of the unaugmented wake is clearly evident (the excess of signal peaks over the augmented signature), and the greater range over which this wake velocity can be found in comparison with the two-cylinder case bears out the uniform density distribution of Figure 5-14.

One additional interpretation of the statistical ensembles of Figure 5-15a and 5-15b can be made in terms of the mean distribution of the eddies or vortices present in the wake flow. In the unaugmented wake (Figure 5-15a) many more such elements exist than in the augmented case, supporting the position that the latter situation contains fewer but more discrete vortices than the former. One parameter unfortunately missing in this experiment is the vertical coherence,  $\delta_c$ , defined by Eq. 4-7. Hence, we can only speculate on the effects on  $\delta_c$  by the augmented and unaugmented wake flows present.





004749

Figure 5-13. Power Spectral Density of Wake Velocities Associated with Single and Dual Upstream Cylinders

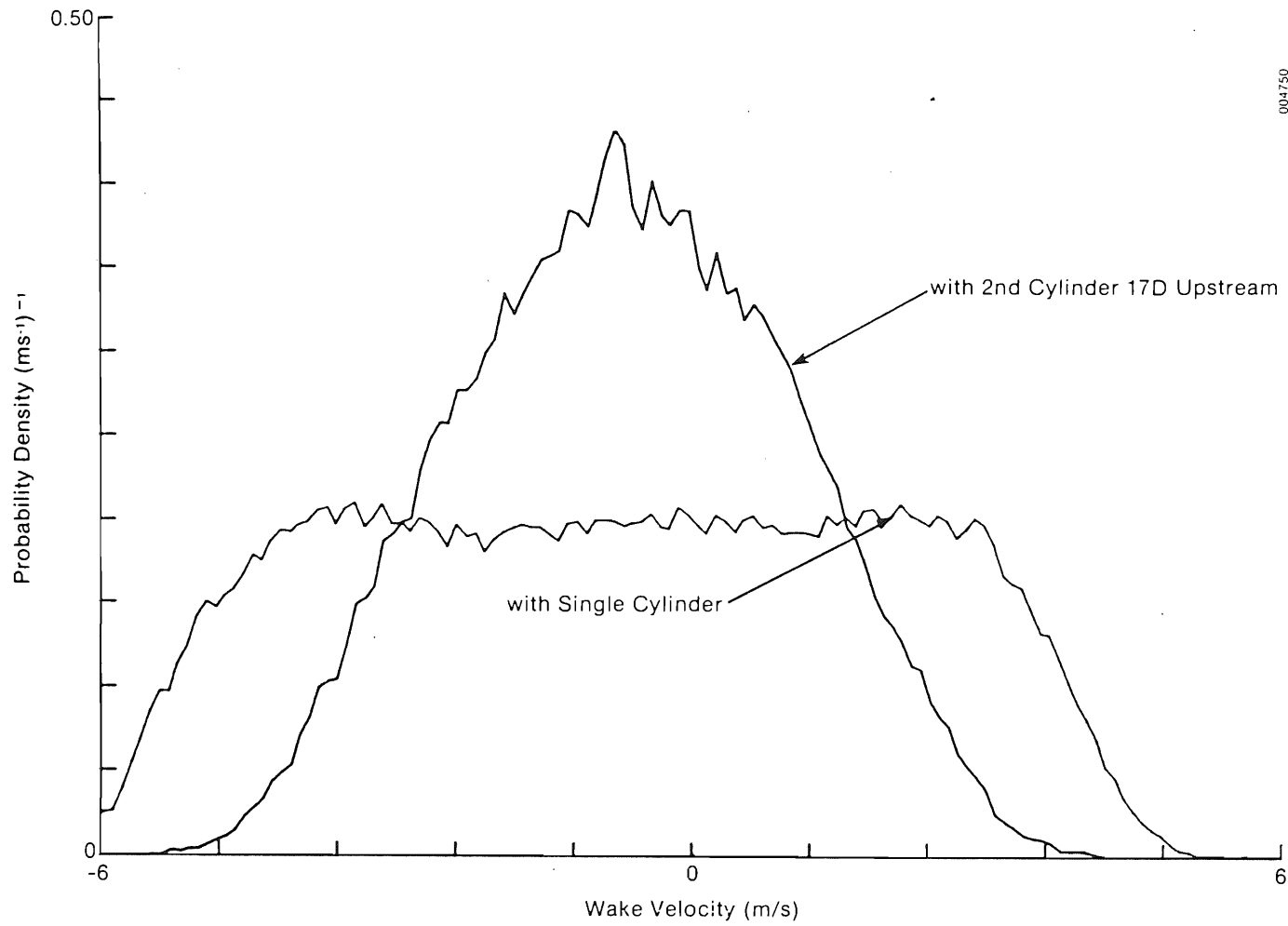
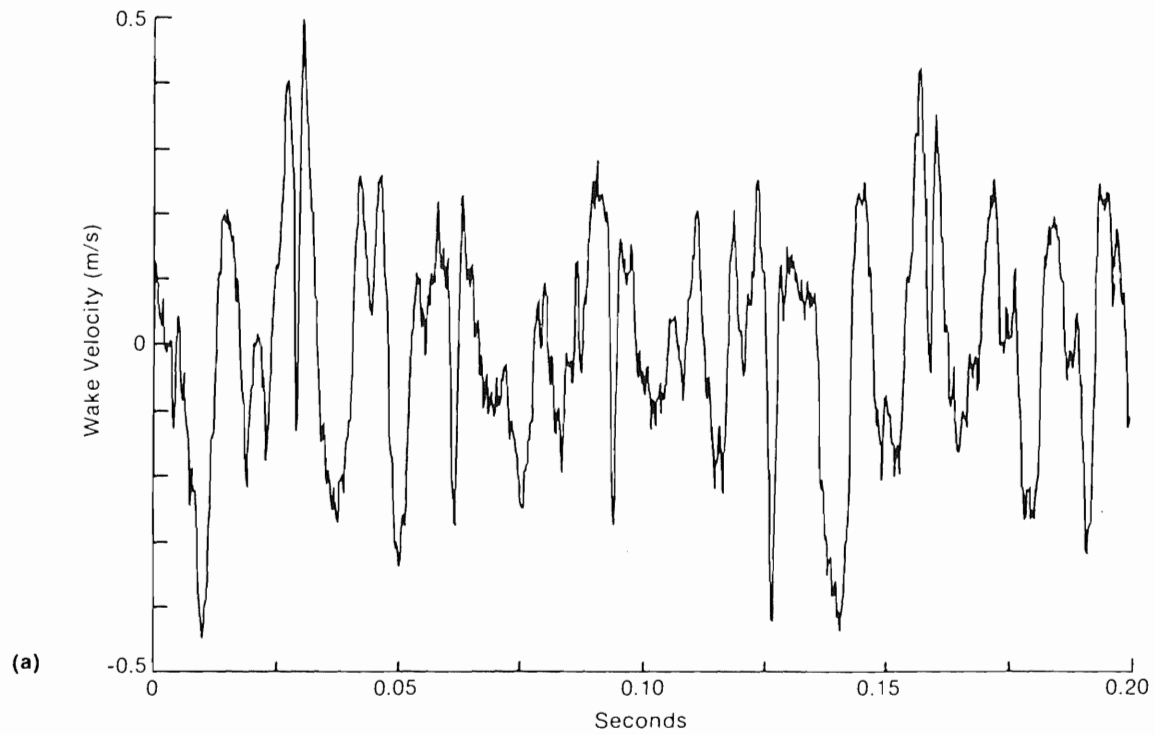


Figure 5-14. Wake Velocity Probability Densities for Both Single and Dual Upstream Cylinders (dc component removed)



004751

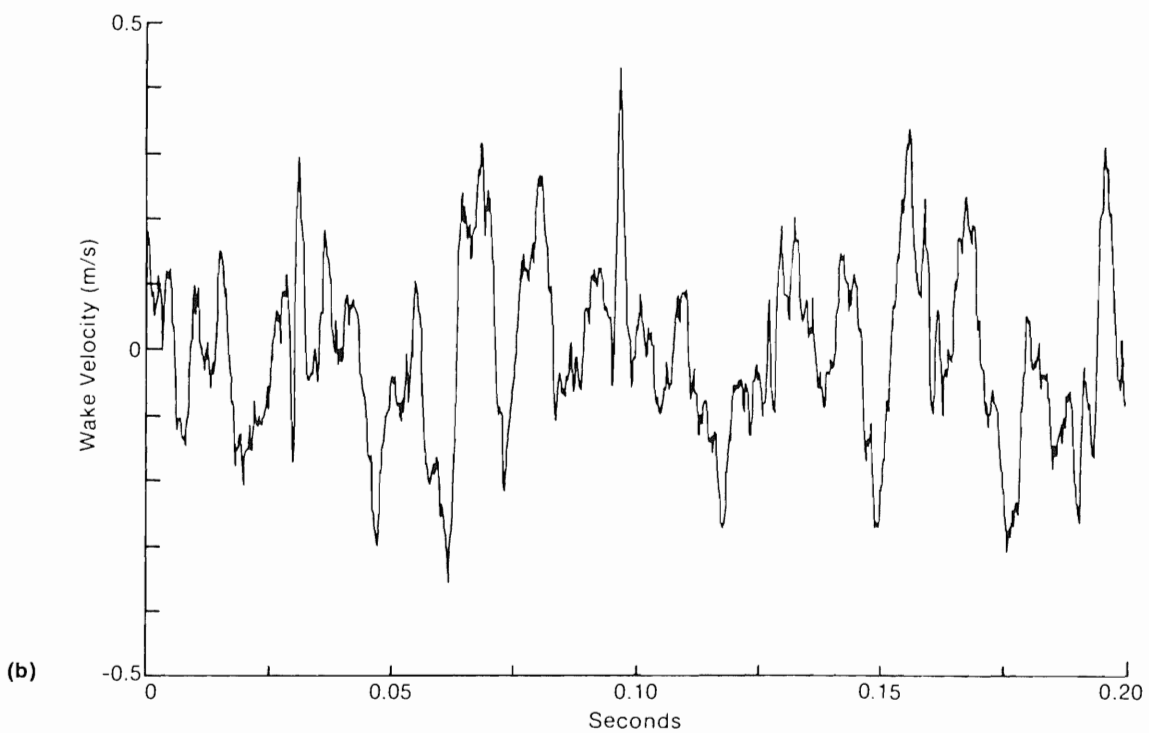


Figure 5-15. Statistical Ensemble Averages of a Single-Cylinder Wake (a) and a Wake Augmented by a Second Cylinder Installed 17D Upstream (b)

### 5.2.1.3 Conclusions from the Anechoic Wind Tunnel Experiment

The results of this experiment, including conclusions reached by Park and Harris [15] and from a follow-on experiment based on the same experimental procedure by Marcus and Harris [16], have indicated the following:

1. Aerodynamically generated acoustic impulses associated with downwind wind turbine designs can, at least qualitatively, be reproduced in an anechoic wind tunnel environment.
2. The strong on-axis or dipole directionality of the impulse radiation predicted by numerical models [2] has been confirmed.
3. The severity of the observed impulse becomes less as the cylinder-to-blade distance increases, indicating a change in the character of the cylinder wake and emulating a similar decrease found in the impulses derived from the MOD-1 east leg wake discussed in Section 4.2.3.
4. The most intense impulses associated with the interaction of a wake from a solid upstream cylindrical body were produced with the smallest cylinder-diameter/chord ratio (0.31), indicating the importance of vortex elements whose dimensions are the order of the chord in this process.
5. Adding a second cylinder of the same physical dimensions  $17D$  upstream of the one immediately ahead of the blade plane increases the severity of the observed impulses.
6. Augmentation by a second upstream cylinder significantly alters the turbulent wake structure of the downstream cylinder by changing the vortex shedding from essentially a wideband to a narrowband stochastic process with an attendant increase in acoustic impulse severity as the turbine blades pass through the altered wake.
7. The statistical nature of the rotor/wake impulse generation process has again been demonstrated, this time under controlled laboratory conditions, underscoring the need for employing stochastic as well as deterministic analysis tools in order to achieve a reasonably complete understanding of the physical processes involved and to lay the groundwork for the development of effective amelioration procedures and techniques.

### 5.2.2 The Role of Freestream Turbulence in Influencing Severity of Impulse Generation

The results of the previous section have shown that the wake of an upstream cylinder when it intersects a similar downstream cylinder can alter the turbulent wake structure of the latter. Such a mechanism could be important in determining the severity of acoustic impulse generation from downwind turbines employing pipe-truss towers since, for certain wind directions, the downwind legs closest to the rotor plane are being similarly influenced, as is true of the MOD-0, MOD-0A, and MOD-1 turbine designs. This may also be true for single-column towers (WTS-4) if the natural inflow contains a sizable proportion of turbulent eddies whose spatial dimensions translate close to the Strouhal shedding frequency when intersecting a cylindrical tower structure.

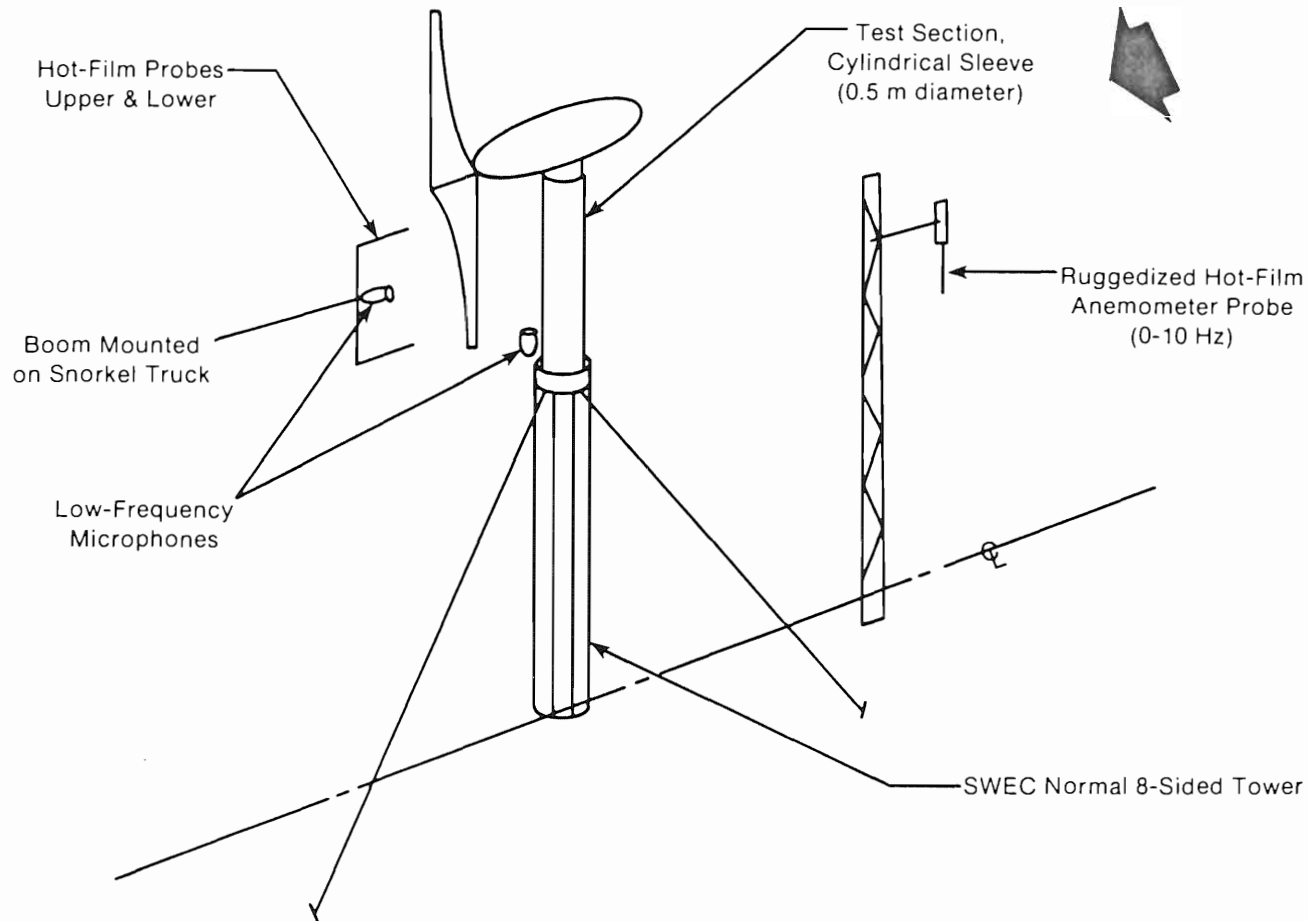
### 5.2.2.1 Field Experimentation

To investigate the possibility of tower-turbulence interaction, we designed our experiment at the Rocky Flats Wind Energy Research Center to measure the influence of natural inflow turbulent energy in a spectral frequency band defined by a Strouhal shedding frequency range for the 0.5-m (20-inch) bare cylinder and the compass of wind speeds encountered. Figure 5-16 sketches the physical arrangement. A rugged, constant-temperature, hot-film anemometer with a maximum frequency response of 10 Hz was installed upwind of the small wind turbine tower to measure the horizontal turbulence component. It was located about 15 m upstream and at a height equivalent to the center of the cylindrical test section, about 12 m. Two VLF microphone systems were used, one installed at the base of the cylinder on the tower to measure the pressure field near the cylinder surface and the other on the boom of the lift truck which was positioned as close to the rotor axis as practical to capture the radiated impulses. The vertically coherent shedding characteristics of the bare cylinder were discussed in Section 5.1.4.

Figure 5-17 shows an averaged sound pressure level spectrum as measured by the microphone mounted at the foot of the test section for an impulsive episode with the bare cylinder in place. The level of the discrete bands (tones) are a measure of the severity of the impulses being generated. Because the frequencies associated with these averaged tonal peaks are principally a function of the constant rotational rate of the turbine and therefore subject to little or no frequency variation, we chose the average narrowband (0.125 Hz) pressure levels of six of these discrete tonal frequencies (including 23.5, 27.35, 31.25, 35.25, 39.125, and 43.0 Hz) as quantitative measures. While clearly discernible tones could occasionally be found at frequencies as high as 100 Hz and perhaps more (a function of the impulse shape and intensity), these six tone levels could almost always be identified above background, particularly at the higher wind speeds. The tone levels were determined by averaging 2-minute acoustic records simultaneously with sample records of the freestream velocity and the mean-square turbulence inflow in the 2.5-8.0 Hz frequency band, the Strouhal shedding or excitation range. Thus, the wind speed and 2.5-8.0 Hz band mean-square turbulence values were used as forcing functions, and the acoustic tonal peaks as the output of the process under investigation. A total of 35 2-minute records were assembled from the available data covering a wind speed range of 4.7 to 10.9  $\text{ms}^{-1}$ . Table 5-1 summarizes the observed statistics of these 2-minute samples.

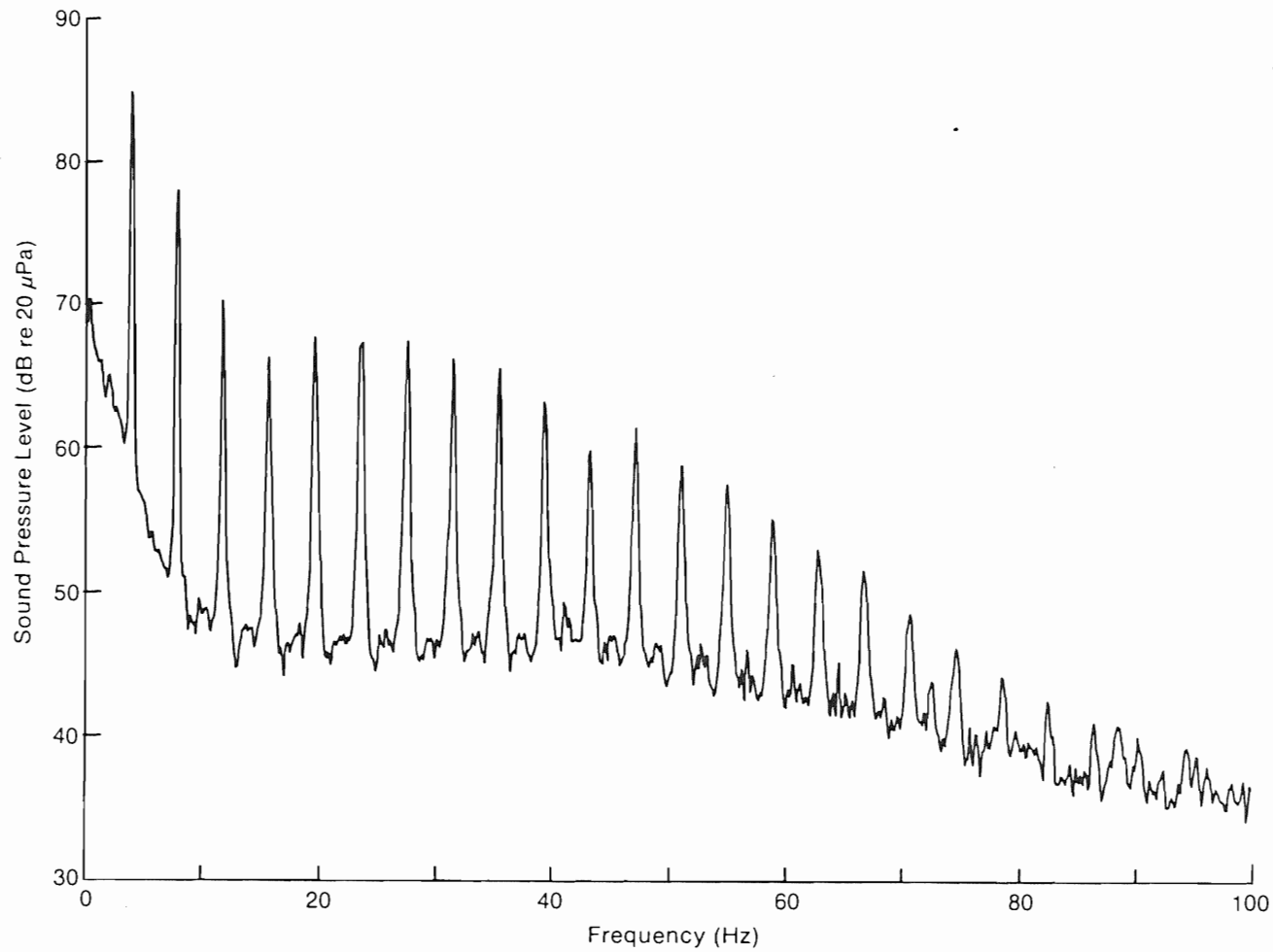
### 5.2.2.2 Results

Figure 5-18 plots the relationship between the freestream velocity and the turbulent energy in the 2.5-8.0 Hz Strouhal excitation band. The correlation coefficient for the indicated linear regression is 0.787 with a standard error of estimate of  $\pm 0.385 (\text{ms}^{-1})^2$ . Figure 5-19, as an example, plots the observed bivariate relationship between the freestream velocity and the mean 35.25 Hz tone level (dB). The correlation coefficient for the indicated linear regression is 0.671 with a standard error of estimate of  $\pm 4.15$  dB. A similar plot of the 23.5 to 43.0 Hz tone, root-sum-square equivalent bandwidth tone level (BPL) is presented in Figure 5-20, with the regression explaining 65% of the



004752

Figure 5-16. Sketch of Experimental Setup Used for Acoustic/Aerodynamic Studies of Small Wind Turbine and Various Test Section Configurations



004753

Figure 5-17. Averaged Acoustic Spectrum as Measured by a VLF Microphone Mounted at the Base of the Cylindrical Test Section (See Figure 5-16)

**Table 5-1. Summary Statistics of Natural Strouhal Excitation of Acoustic Impulses for 0.5-m Cylinder (35 samples)**

Parameter	Mean	Maximum	Minimum	Coefficient of Variation (%)
Freestream velocity (m/s)	7.31	10.9	4.7	20.0
2.5-8 Hz band <sup>a</sup> Mean-sq. velocity (m/s) <sup>2</sup>	1.15	3.33	.077	53.6
23.5 Hz BPL <sup>b</sup> (dB)	63.3	71.6	50.9	7.5
27.35 Hz BPL (dB)	61.3	69.4	49.4	8.2
31.25 Hz BPL (dB)	60.2	68.5	48.0	8.4
35.25 Hz BPL (dB)	58.1	67.2	45.3	9.5
39.125 Hz BPL (dB)	55.8	64.7	41.9	10.0
43.0 Hz BPL (dB)	54.5	63.2	41.2	10.5
Total <sup>c</sup> BPL (dB)	67.5	80.0	55.5	7.5

<sup>a</sup>Strouhal excitation band.

<sup>b</sup>0.125 Hz bandwidth tone level.

<sup>c</sup>Root-sum-square of individual 0.125 Hz tone levels.

observed variance and a standard error of estimate of  $\pm 3.89$  dB. Table 5-2 summarizes the results of both a bivariate regression analysis using the freestream velocity and the 2.5-8.0 Hz (Strouhal excitation) band mean-square turbulence level, and a trivariate model incorporating both parameters. Figures 5-21a,b plots the trivariate regression model for the root-sum-square band pressure total as a function of the freestream velocity and Strouhal excitation turbulence band energy. As indicated in Figures 5-21a,b and Table 5-2, the latter model explains 75% of the observed variance with a standard error of estimate of  $\pm 3.3$  dB.

### 5.2.2.3 Interpretation and Conclusions

The influence of natural turbulent energy in the Strouhal excitation band (2.5-8.0 Hz, corresponding to a shedding frequency defined by Eq. (5-2) and a Strouhal number of 0.21 for a range of 4 to 12  $\text{ms}^{-1}$ ) has been demonstrated. The physical significance of Strouhal number is related to a cylinder boundary layer instability that controls the vortex shedding characteristics of the wake. At subcritical Reynolds numbers encountered by operating wind turbines, the cylinder Strouhal number is within 5% of 0.21 but may vary as much as 100% higher in the low supercritical flow regime, depending on local environmental conditions [12]. The relationship between the freestream velocity and the



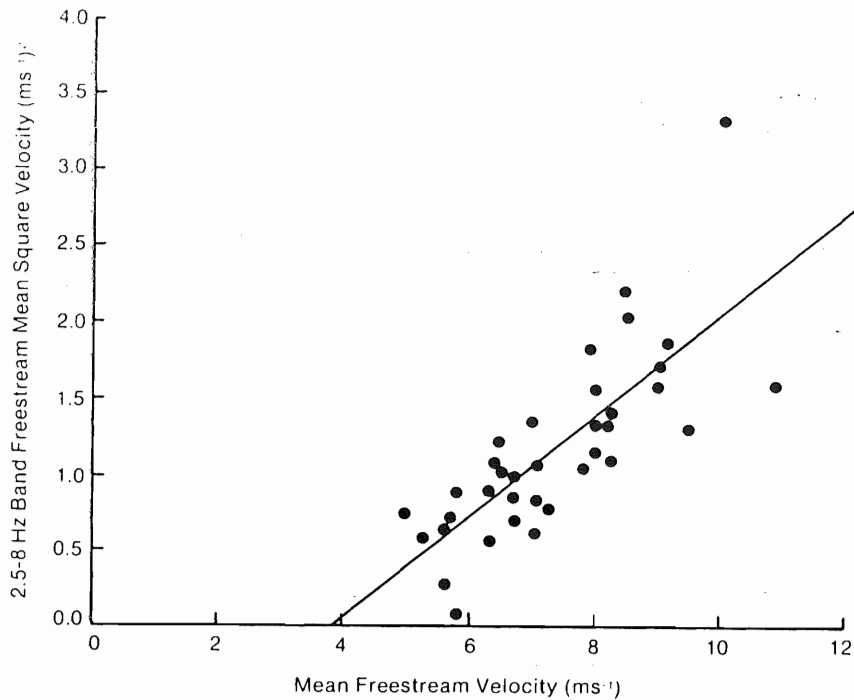


**Figure 5-18. Scatter Plot and Indicated Linear Regression for the Mean-Square Velocity in the 2.5-8.0 Hz (Strouhal Excitation) Band vs. the Mean Freestream Velocity**

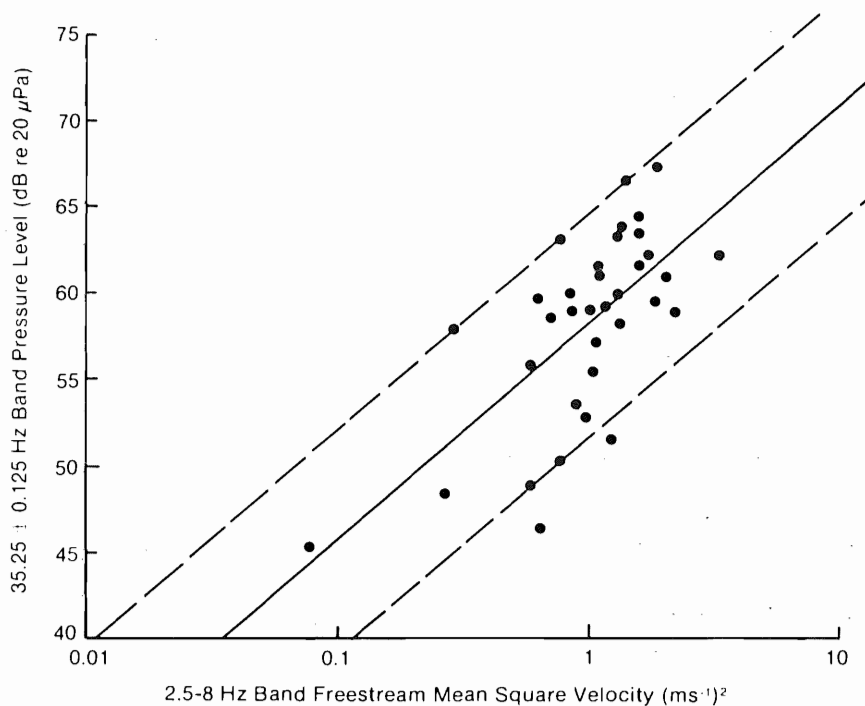


**Figure 5-19. Scatter Plot of the 35.25 ± 0.125 Hz Tone Band Pressure vs. the Strouhal Excitation Band (2.5-8.0 Hz) Mean-Square Inflow Velocity. (Solid curve is the linear regression and the dashed curves represent ± one standard error.)**

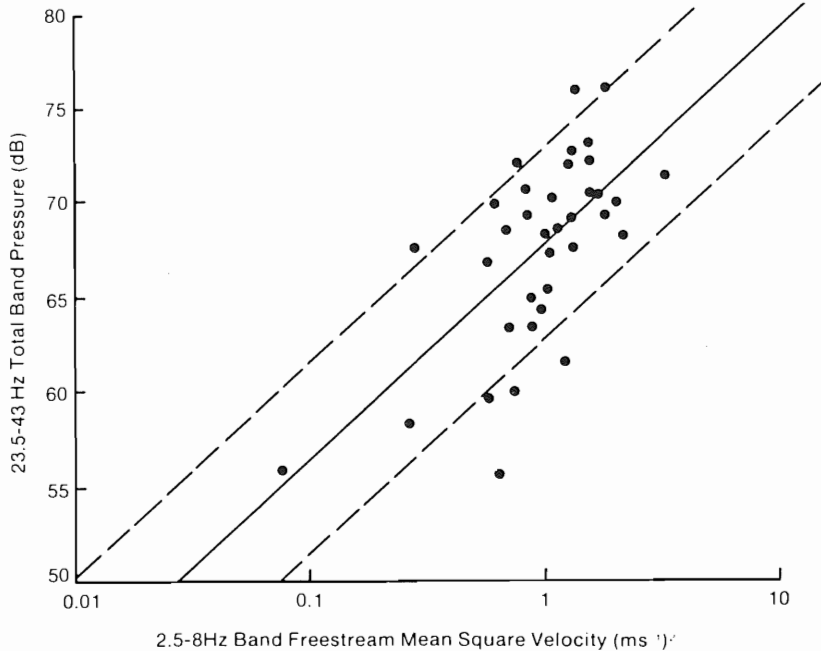


**Figure 5-20. Same as Figure 5-19, but for the 23.5-43.0 Hz Root-Sum-Square Tone Pressure Sum vs. the Inflow Strouhal Excitation Band Mean-Square Velocity**

turbulent energy present in this particular frequency band (disturbance space scale) for this experiment (shown in Figure 5-18) indicates a more or less monotonic increase with windspeed. Although almost 80% of the variance is explained by the linear regression, the relationship will probably not hold, in general because (a) it reflects the available data set, which is biased by the acoustic impulses observed; and (b) the dynamic stability of the local atmospheric surface layer undoubtedly also plays a role. The stability, which may account for some of the unexplained variance, was unavailable as an observable parameter.

The data set analyzed here was collected on two separate days, each in the late afternoon between 1530 and 1716 hours local standard time. The data sets used in this analysis contained 22 and 15 sets of two-minute observations, respectively, but the impulse statistics were quite different for each. Table 5-3 lists the pertinent statistics of each of these series of observations. On the surface there appears to be not much difference in the aerodynamic forcing parameters, the wind speed and the 2.5-8.0 Hz band turbulence; in fact, one would expect the second (August 24) to show a tendency toward more severe impulse generation. This is not the case, however, as the August 20th impulse levels average 4-5 dB higher. The answer may lie in the correlation statistics of the Strouhal excitation band turbulence and the freestream velocity. In the August 20th case, the correlation coefficient

Table 5-2. Impulse Generation Relationship with Natural Tower Strouhal Excitation:  
Correlation Analysis Results

Tone (Hz)	Bivariate Correlation Coefficient				Trivariate Regression Analysis			Correlation Coefficient	Standard Error (dB)
	Wind Speed	2.5-8 Hz	Log Mean Square Velocity	Wind Speed Coefficient	Log Mean Square Coefficient	Constant			
23.5	0.708	(3.41) <sup>a</sup>	0.638	(3.71)	1.68	4.34	51.1	0.731	3.33
27.35	0.740	(3.44)	0.638	(3.93)	2.01	3.74	46.6	0.756	3.40
31.25	0.722	(3.56)	0.633	(3.99)	1.92	4.07	46.0	0.740	3.52
35.25	0.765	(3.60)	0.671	(4.15)	2.23	4.50	41.7	0.765	3.54
39.125	0.768	(3.62)	0.727	(3.89)	1.93	6.66	41.7	0.806	3.41
43.0	0.793	(3.53)	0.725	(3.99)	2.20	5.90	38.4	0.820	3.37
Total Band <sup>b</sup>	0.749	(3.39)	0.651	(3.89)	2.01	4.01	52.9	0.766	3.34

<sup>a</sup>Standard error of estimate (dB).

<sup>b</sup>Root-sum-square equivalent of the six individual tone (0.125 Hz band) pressure levels.

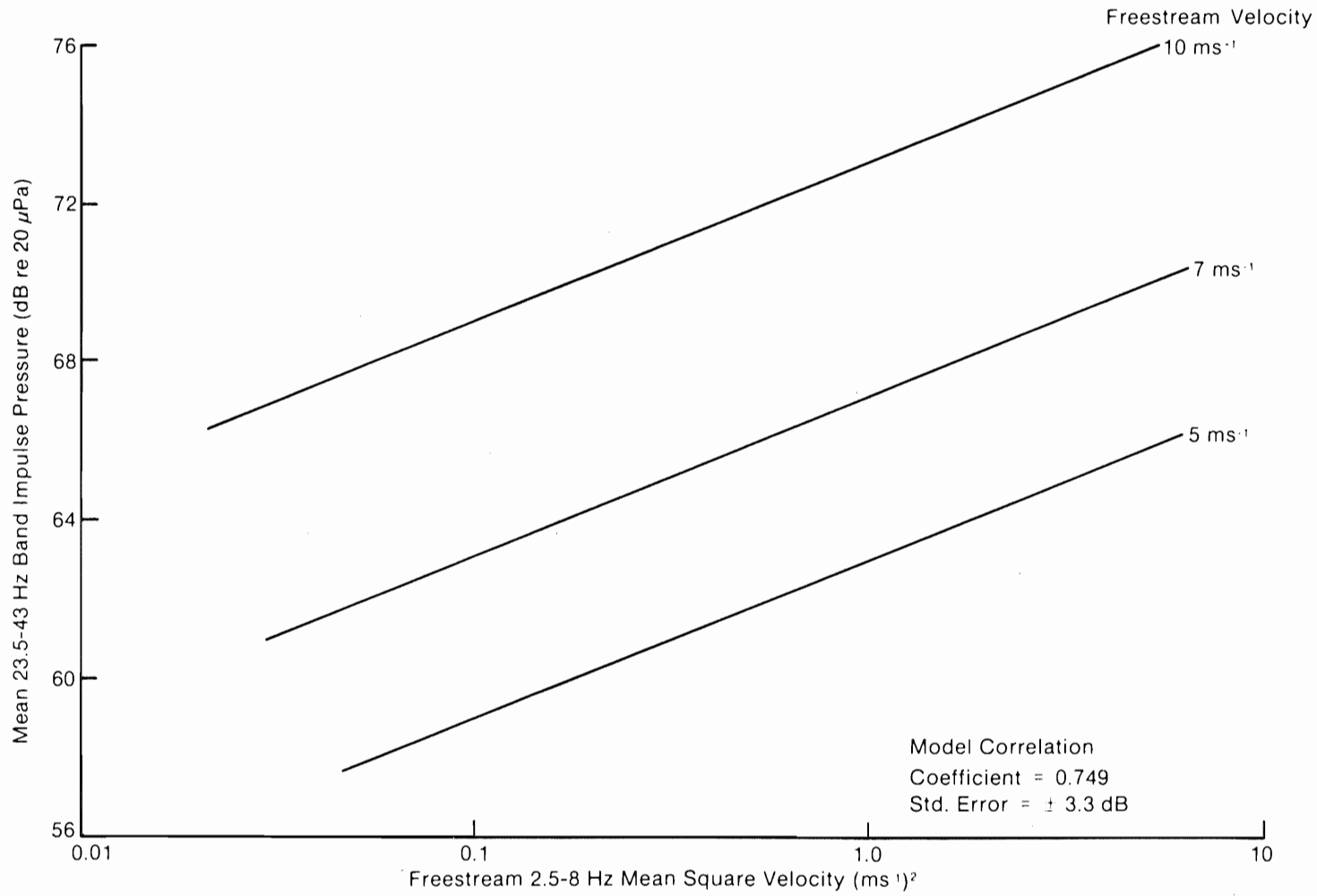


Figure 5-21. Results of Trivariate Linear Regression Model Relating the Mean 23.5-43.0 Hz Total RSS Acoustic Band Pressure to the Inflow Strouhal Excitation Band Turbulence Level and Velocity

Table 5-3. Statistical Summary of Aerodynamic and Acoustic Impulse Parameters for Observations made on August 20 and 24, 1981

Period/Parameter	Mean	Maximum	Minimum	Coefficient of Variation (%)
August 20, 1981 (1614 - 1716 MST)				
Freestream velocity (m/s)	7.00	9.2	5.6	14.8
2.5-8 Hz band mean-sq. velocity (m/s) <sup>2</sup>	0.969	1.87	0.284	43.1
23.5 Hz BPL <sup>a</sup> (dB)	65.8	71.6	61.5	5.7
27.35 Hz BPL (dB)	64.1	69.4	59.6	4.6
31.25 Hz BPL (dB)	63.0	68.5	57.1	5.1
35.25 Hz BPL (dB)	61.2	67.2	55.8	5.6
39.125 Hz BPL (dB)	58.3	64.7	53.1	6.7
43.0 Hz BPL (dB)	56.8	63.2	51.3	7.4
Total BPL <sup>b</sup> (dB)	69.9	76.0	63.4	5.2
August 24, 1982 (1531 - 1625 MST)				
Freestream velocity (m/s)	7.54	10.9	4.7	22.4
2.5-8 Hz band mean-sq. velocity (m/s) <sup>2</sup>	1.27	3.34	0.078	55.2
23.5 Hz BPL (dB)	61.5	67.4	50.9	8.0
27.35 Hz BPL (dB)	59.6	65.8	49.4	9.0
31.25 Hz BPL (dB)	58.4	64.4	48.0	9.1
35.25 Hz BPL (dB)	56.3	63.4	45.3	10.2
39.125 Hz BPL (dB)	54.2	61.0	41.9	11.1
43.0 Hz BPL (dB)	53.0	60.5	41.2	11.6
Total BPL (dB)	65.9	72.2	55.5	8.0

<sup>a</sup>0.125 Hz tone level.

<sup>b</sup>Root-mean-square of tone levels.

between these two parameters was 0.836 compared with a value of 0.764 for the August 24th case. From this we conclude that the vortex shedding of the second period was somehow less coupled to the freestream energy in the Strouhal excitation band, possibly due to a less stable surface layer environment, since the observational period took place almost an hour earlier than the data collected on August 20th. There is some support for this interpretation in the increased scatter of the 2.5-8.0 Hz band mean-square velocity with increasing freestream velocity as shown in Figure 5-22b. In comparison, the August 24th observations plotted in Figure 5-22a show the opposite effect. From our experience in the field, we have noted consistently that increased and more severe impulsive action occurs during the cool outflows of thunderstorms in the vicinity, a fact we depended on while performing the experiments during the light winds of the summer months at the Rocky Flats site.

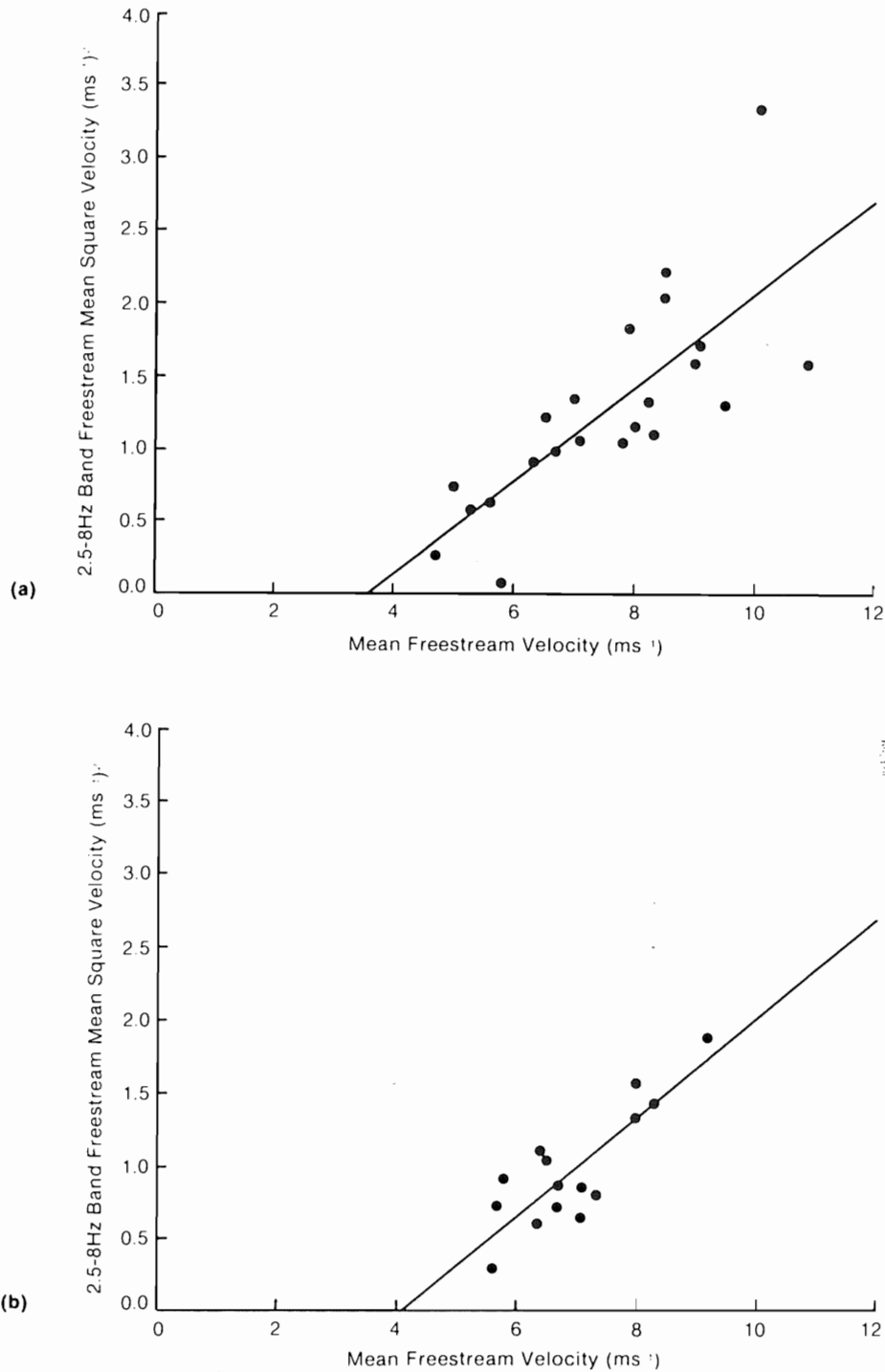


Figure 5-22. Scatter Diagrams for Inflow Strouhal Excitation Band Turbulence Levels vs. Freestream Velocity for (a) August 24, 1981, and (b) August 20, 1981

The influence of the freestream Strouhal excitation band in the tower-wake impulse generation process is summarized in Figure 5-21 using the trivariate regression model listed in Table 5-2. The sensitivity to both the freestream velocity, which determines the aerodynamic load on this fixed-pitch machine, and the Strouhal excitation band level, is evident. We have therefore concluded that turbulent energy in the Strouhal band influences the dynamic characteristics of the downstream wake by exciting a boundary layer instability in the cylindrical, bluff body. We also suspect the hydrodynamic stability of the atmospheric surface layer, in which the turbine and its support tower reside, also exerts a definite, but so far undefined influence, on this process as well. We also believe the combination of the level or energy content of the Strouhal band turbulence and the vertical stability are the missing factors that may well account for much of the unexplained variance in the multivariate regression model of the MOD-1, discussed in Section 4.2.3.2. The identification of this process continues to underscore the stochastic nature of the physical processes providing the excitation for the MOD-1 impulsive noise generation.

### **5.2.3 Role of Blade Unsteady Aerodynamic Response in Impulsive Noise Generation**

In the previous sections, we discussed the role of the cylindrical tower legs in modifying the turbulence inflow to the turbine rotor and, to some extent, the freestream parameters exerting influence on the leg (cylinder) wakes entering the rotor plane. It is now important to examine the physics of the actual impulse generation process experienced by the rotor blades as they transversely slice through what we have identified as vortex tubes being shed by each tower leg in order to further establish a physical basis for the design of appropriate abatement procedures. Efforts to achieve this understanding have been derived largely from the University of Colorado wind tunnel experiment and the full-scale tests performed at the Rocky Flats Wind Energy Research Center. Since neither of these experiments have been fully analyzed, the results here, while correct and indicative, represent only a small fraction of the total information that should eventually be obtained. Our previous discussion has established that the annoying impulses are being produced as the rotor blades pass through the leg wakes. We have also shown the importance of the wake turbulent structure; e.g., vertical coherence, discreteness, and possibly, existing hydrodynamic stability, among others, in determining the level of impulse severity. We have not, however, examined what dynamic, physical process actually occurs that causes the blade pressure field to radiate such intense and coherent pressure waves, nor have we identified the corresponding dominant physical parameters responsible. These matters are addressed in this section.

#### **5.2.3.1 A Physical Description of the Turbine-Radiated Acoustic Impulse**

A number of examples of observed impulse pressure-time plots have been given previously that have been taken from actual wind turbine measurements or the model turbine in the MIT anechoic tunnel. The instantaneous impulse depicted in Figure 5-23 (taken from the MIT tests for the smallest cylinder diameter at a freestream velocity of  $13.4 \text{ ms}^{-1}$ ) is typical. Figure 5-24 plots the

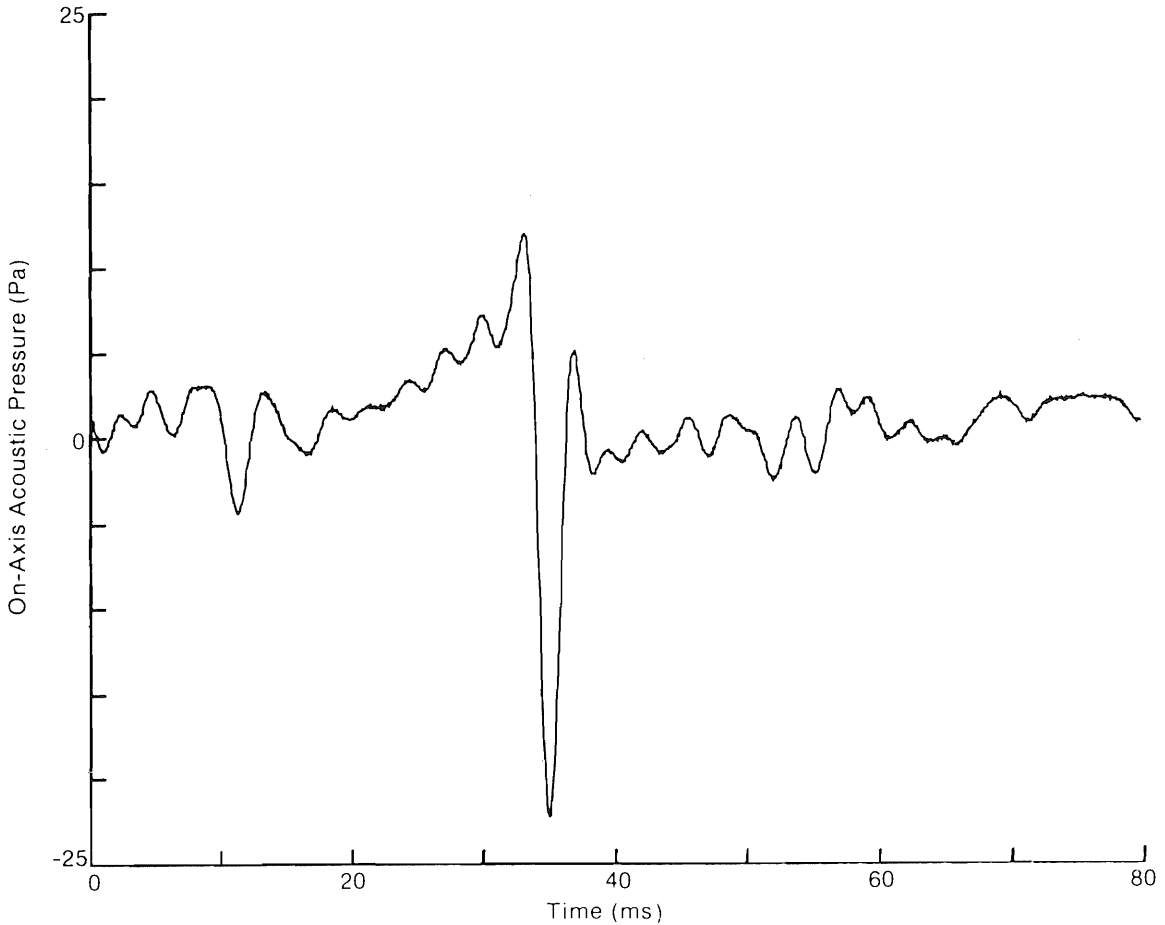


**Figure 5-23. On-Axis Acoustic Pressure-Time Plot of Impulse Generated by 1.6-cm Cylinder Wake at a Freestream Velocity of  $13.4 \text{ ms}^{-1}$  in MIT Anechoic Tunnel**

pressure-time signature from two of our VLF microphone systems, one installed at the base of the test cylinder on the tower of the small downwind turbine at the Rocky Flats Wind Energy Research Center and the other on the instrument boom. The figure shows three passages of the rotor blade past the tower. Because the tower base microphone is installed on the upwind or pressure side of the rotor, the pressure rises (dashed curve) as the blade approaches the tower, reaches a peak as it passes, then falls back until the next blade comes within range. The solid curve of Figure 5-24 traces the suction or downwind side acoustic field (boom-mounted microphone), revealing the gradual pressure decrease as the blade approaches the tower, then positive peaking as it passes, and finally increasing again as the blade moves toward the horizontal.



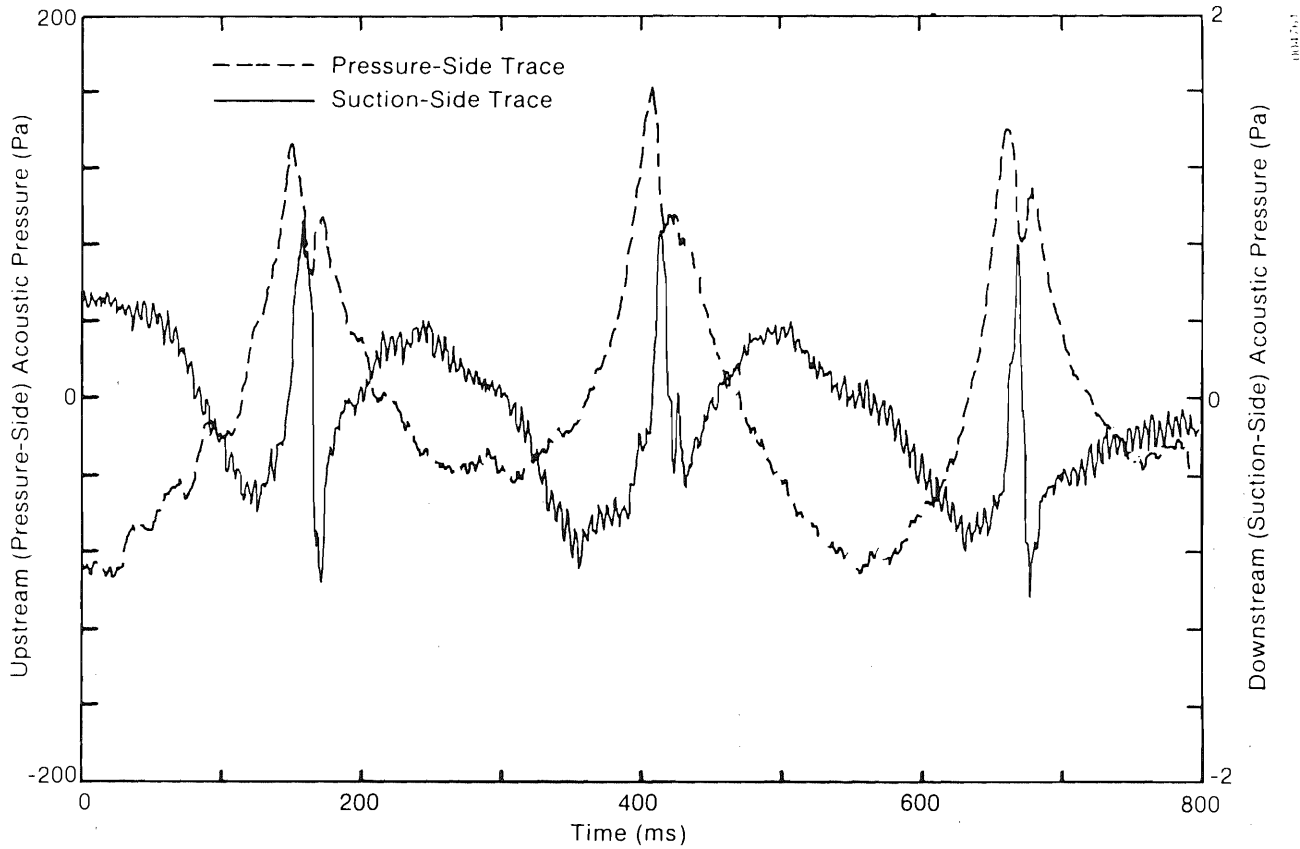


Figure 5-24. Acoustic Pressure-Time Plots Made on Both the Pressure (Upwind) and Suction (Downwind) Sides of a WECS Rotor Periodic Unsteady Lift in the Wake of a Cylindrical Tower Element

As can be seen, there are sharp discontinuities or rapid drops in the pressure-side (base microphone dashed) traces as the peak is reached on all three passages while the suction-side (boom-mounted microphone, solid trace) pressure suddenly peaks positive at the same time or rotor position. Figure 5-25 is an exploded view of a single instantaneous impulse measured on both sides of the rotor blade which presents the important temporal relationships in greater detail. The expected out-of-phase cyclic relationship between these two acoustic pressure traces is also in evidence in Figure 5-24; i.e., a pressure rise at the tower mike and a decrease at the downwind, boom-mounted position.

We believe that these rapid fluctuations (durations of 10-15 ms) reveal that the rotor blade is undergoing what amounts to a form of transient stall as it passes through the tower wake. This is clearly indicated by the sudden changes in both the pressure and suction values over that short duration. We also believe we are not just seeing a wake momentum deficit effect, since the severity and overall shape of these transients change from blade passage to blade passage, as shown in the traces of Figure 5-26. Occasionally, there is no evidence of a stall-induced transient at all--even during periods when almost every other passage exhibits some form of an impulse. Figure 5-27 illustrates a single blade passage when no transient was produced even though the freestream velocity was  $17-18 \text{ ms}^{-1}$ . From this we must conclude that the concept of a wake deficit exists only in the mean, and the rotor blades of a turbine see only whatever is there each time they pass behind the tower! Based on this, we must also argue that the variation in the severity, shape, and duration of the observed lift transients must be a function of the instantaneous, turbulent structure of the wake; i.e., the strength and distribution of shed vortices that vary stochastically.

Based on the discussions of Sections 4.1.1.2 and 4.1.1.3, the essence of the time history of these transient lift fluctuations is reflected in the acoustic pressure traces described by Figures 5-23 through 5-27. For the model-generated impulse in Figure 5-23, the duration of the sharpest portion of the signature was about 2 ms, which corresponds to a linear travel distance of the blade tip of 5.4 cm or about one chord width (5.1 cm). The width of the wake at this position 5D downstream would be about 2 cm, according to Ref. [14], for the subcritical operating regime ( $Re \sim 14 \times 10^3$ ). Therefore, the spatial duration of the impulse is about equal to half the chord width. In the case of the small turbine and the cylindrical test section, the average impulse duration shown in Figures 5-24 through 5-26 is about 12 ms, which corresponds to a space scale of 0.75 m or 3.25 blade chords at the blade tips and 0.57 m or 2.5 chords, respectively, at 80% span. The lateral dimension of the mean wake at the point of intersection with the rotor (1.5D downstream), which is relatively insensitive to the Reynolds number due to the nearness of the cylinder (the near wake region), is estimated to be 0.80 m for supercritical flow and 0.79 m for subcritical. The MOD-1, in contrast, exhibited a typical impulse duration of about 0.008 s at the 35 rpm rotational rate, which translates to a space scale of 1.0-1.2 mean wake widths (subcritical) or about 40% of the blade chord at the 75% span position, intersecting the leg wakes at 7.5D downstream. It is clear from the preceding that whatever the true width of the wake is at the instant of blade passage, the transient lift fluctuation is taking place over a space scale on the order of the mean chord width of the outer 40% of the span. This is the region of the blade span that develops the maximum aerodynamic lift. Also, this transient scale is determined by the wake dimensions and not the blade chord width, at least for the examples here.

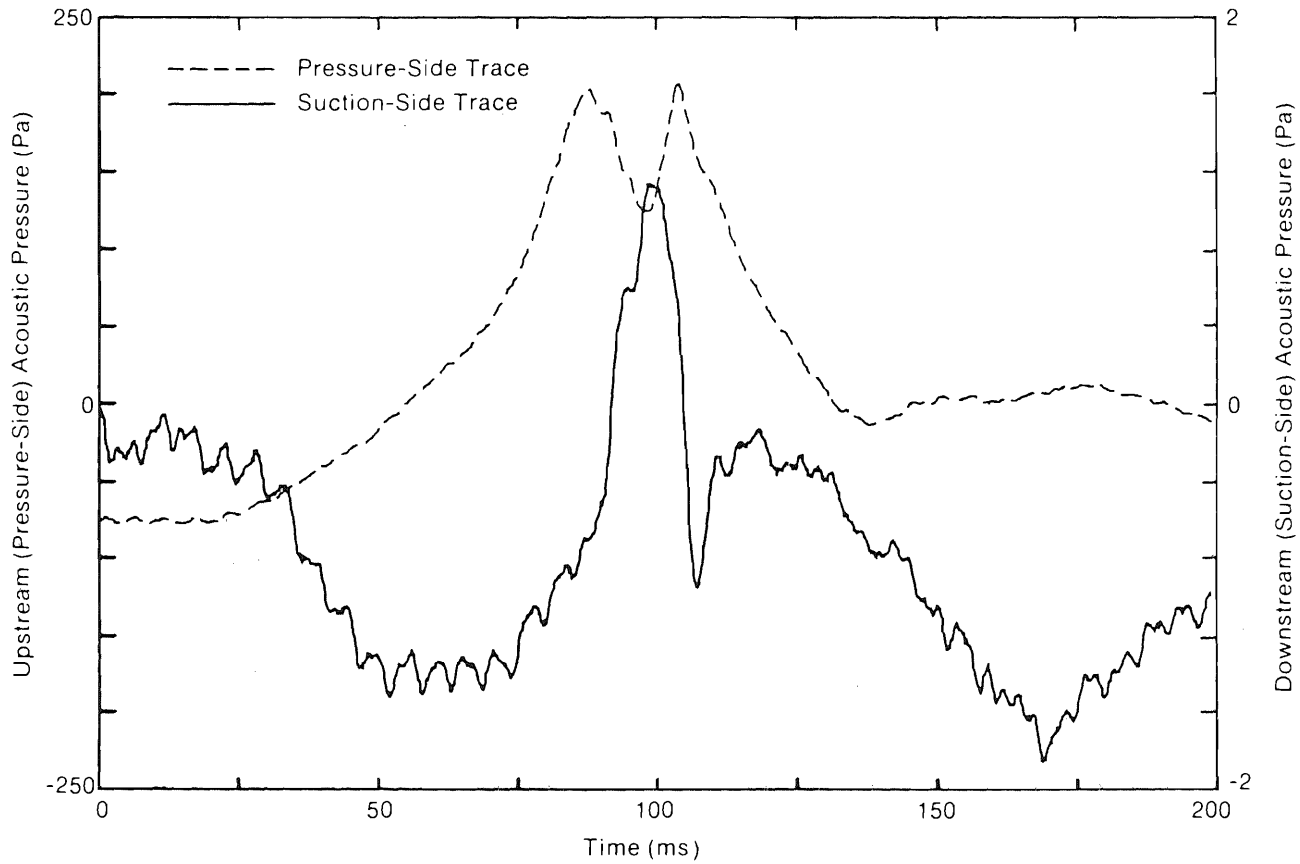


Figure 5-25. Acoustic Pressure Time Signature of a Single Blade Passage and Impulse Generation (Similar to Figure 5-24)

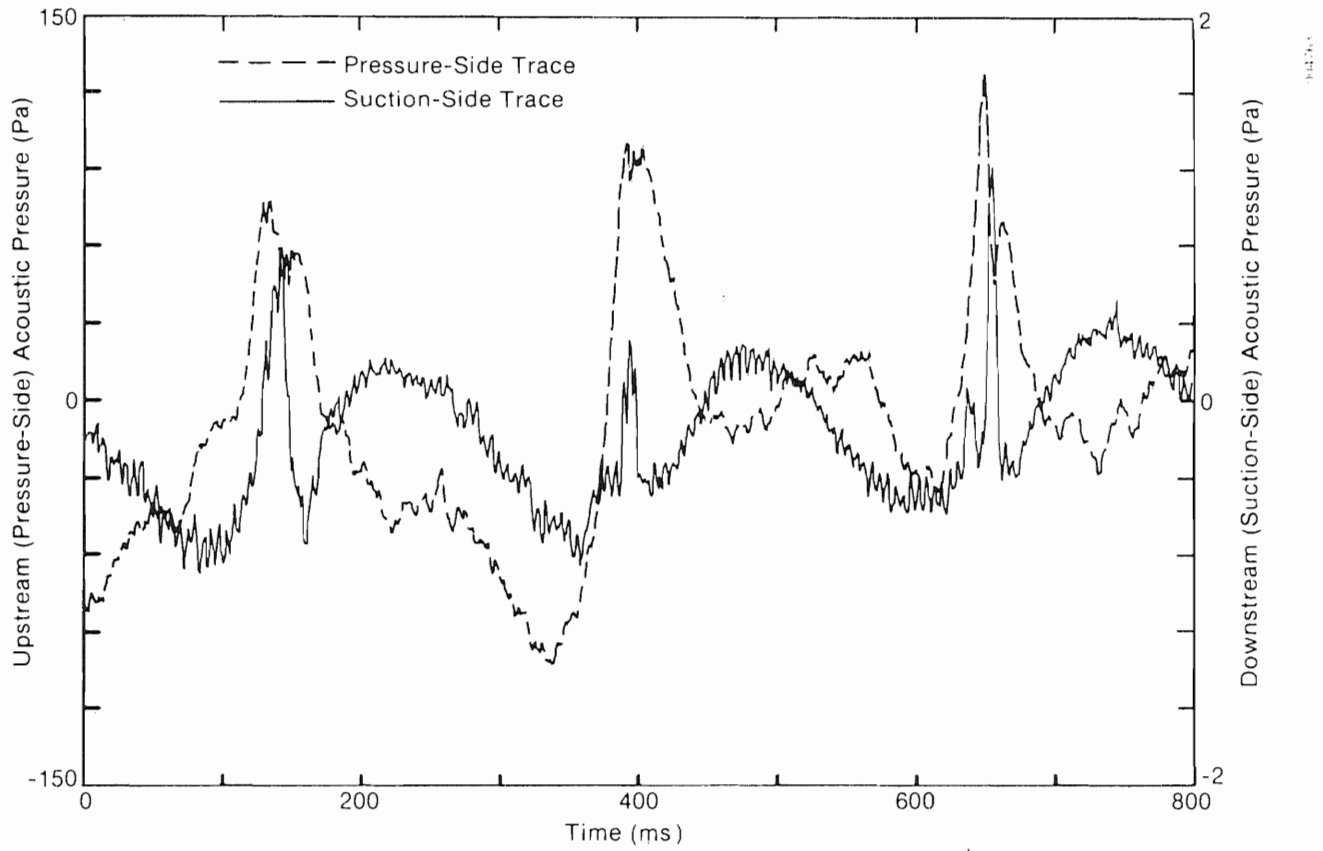


Figure 5-26. Acoustic Pressure-Time Trace Showing Variability from Blade Passage to Blade Passage through Tower Wake

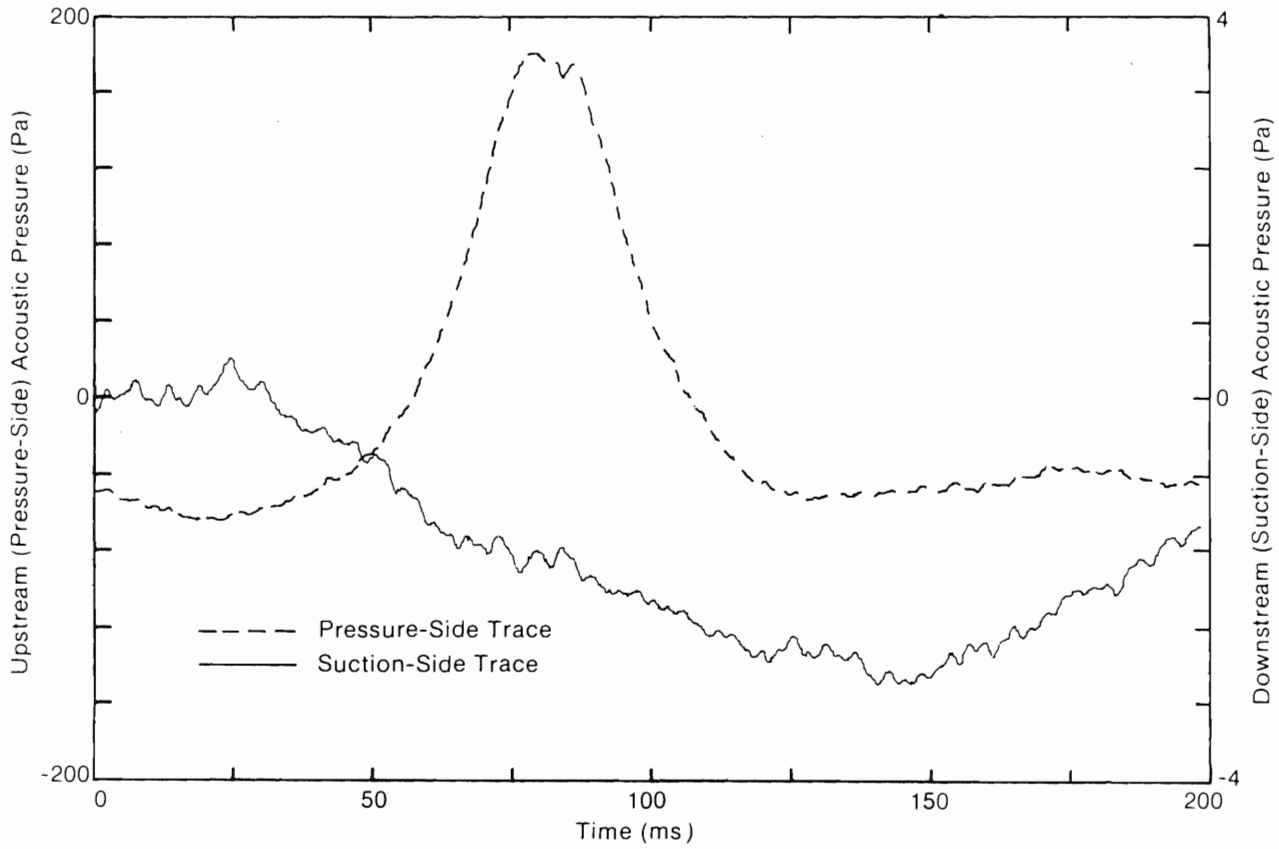


Figure 5-27. Acoustic Pressure Signature Showing No Evidence of Transient Lift Behavior and Impulse Generation

### 5.2.3.2 Proposed Unsteady Aerodynamic Mechanism Responsible for Impulse Generation

From the discussion in the previous sections, it is clear that the dynamic process responsible for creating the severe transient lift fluctuations that radiate as strong acoustic impulses is influenced by the following environmental parameters:

1. The magnitude of the freestream velocity
2. A space scale on the order of the rotor blade mean chord ( $\bar{c}$ ) dimension; i.e.,  $10 \leq \bar{c} \leq 0.1$ , with a dimension near the chord size apparently being the most acoustically sensitive
3. The degree of spanwise coherence in the turbulent structures encountered by the moving blade
4. The presence of narrowband turbulent flows; i.e., containing a predominance of discrete elements (eddies or vortices).
5. The fluctuating (unsteady) flow characteristics and not mean quantities making the process narrowband stochastic.

These parameters strongly suggest that the process is related to an unstable interaction between the blade viscous boundary layer and the coherent elements in the tower leg turbulent wakes. The condition for spanwise coherency brought about by the transverse intersection of the blade and the vortex tube structure being shed by the tower legs has already been discussed in Section 5.1.4 and accounts for one of the physical parameters necessary for impulse generation. At this point, we need to review the factors influencing airfoil boundary layer instabilities and observable consequences.

### 5.2.4 Airfoil Unsteady Boundary Layer Dynamics Applicable to the MOD-1 Situation

Much of the theoretical basis for the aerodynamic design of large wind turbine rotors such as the MOD-1 has been steady or quasi-steady lift generating processes. This has been the practical approach, since we can draw upon a relatively large body of available knowledge. The acoustically related process (or processes) we have described above is a direct result of the unsteady aspects of operational wind turbine aerodynamics and therefore may not follow the quasi-steady design models as closely as we would like (if at all, under some circumstances). At issue here are the physical consequences of unsteady flow over the airfoil surfaces of large wind turbine blades, particularly involving short-period, transient lift fluctuations that influence the characteristics of the radiated acoustic pressure field, the dynamic structural loads, and their interrelationship. The discussion here, by necessity, must be kept short. For a more complete review of the subject the reader is referred to the summary papers by McCroskey [17,18].

#### 5.2.4.1 Factors Influencing the Magnitude of Blade Airload Fluctuations

The airfoil section shape used in the MOD-1 blades, as in most wind turbine designs, was at least partially chosen, on the basis of its ability to develop high lift coefficients within the operational wind-speed envelope. In order to reach the design lift coefficients necessary to meet the load generation requirements, it is usually necessary to program the pitch (or blade) angle (referenced at 75% span) so that the blade encounters the incident flow at only one or two degrees below the static stall. This is particularly true below the rated wind speed to achieve maximum efficiency. The NACA 44xx-series airfoil sections, particularly the 15% thick section (4415) are known to be susceptible to a sudden leading edge separation (stall) under "rough" inflow conditions, whereas the quasi-static characteristic under a slowly increasing incidence angle exhibits a stall beginning at the trailing edge. Thus, the turbine blade normally operates at attack angles not far from static stall except at wind speeds near the cut-out value. The significance of this is discussed below.

A review of the literature concerning the causal factors influencing lift fluctuations in unsteady flow over an airfoil has identified the following physical characteristics of the airflow [19] and the flow it is passing through:

- the pressure distribution in the external flow
- the airfoil surface roughness
- the turbulent structure of the free flow the airfoil passes through.

We have already shown that the transient lift fluctuations responsible for acoustic impulse generation are a function of the spanwise coherency of the free-flow turbulent structure. The role of surface roughness in this situation remains unknown, since we have no direct information about it at this time. We believe, however, that it does not exert a major influence in the MOD-1 situation. The influence of the external pressure distribution does warrant a closer examination, however, as discussed in Section 5.2.4.2 below.

From our previous discussions regarding the downstream wake characteristics influencing the severity of impulses generated, we noted the distinct sensitivity of this unsteady process to the level of discreteness found in the wake velocity mean frequency spectrum. We also found this spectral characteristic was indicative of a flow containing a predominance of discrete elements or vortex circulations. A vortex superimposed on a mean flow imparts its own velocity and pressure distribution due to the effects of viscosity. It has already been noted that the space scale over which the lift transients are generated is on the order of the blade chord which, with perhaps one exception, corresponds very closely to the mean cylinder wake dimensions at the point of the blade plane intersection. Thus, if a vortex circulation exists within the wake boundaries, the blade section may experience an abrupt oscillatory inflow as it passes through. Therefore, in our search for the impulse physical generation mechanism, we must examine the effects of oscillatory excitations as a result of both velocity and pressure perturbations on the lift of a turbine blade operating not far from static stall.

McCroskey [18] has summarized the importance of unsteady fluid dynamic parameters influencing the onset of forms of dynamic stall (i.e., an abrupt stalling of an airfoil due to a sudden leading edge separation) that are listed along with observed effects in Table 5-4. As can be seen, the most critical parameters include the mean incidence (attack) angle, the Mach number (the MOD-1 tip Mach number is  $\sim 0.33$  at 35 rpm and 0.25 at 75% span), the airfoil shape, and the reduced frequency. The mean incidence angle is important because of its relationship to the peak excursions,  $\alpha_{max}$ , and increased airload hysteresis with an accompanying overshooting of the lift and moment coefficients, as illustrated in Figure 5-28. For these reasons, the dynamic airloads often far exceed the steady values and, if negative aerodynamic damping is present, energy is extracted from the airstream and dissipated in the blade mechanical structure, as indicated diagrammatically in Figure 5-1.

The role of blade speed (Mach number) has been investigated by Liiva et al. [20, referenced in 18] and illustrated in Figure 5-29 for Mach numbers of 0.2 and 0.4. The most noticeable effect of an increase in Mach number is a reduction in the negative aerodynamic damping, resulting in less aeroelastic but not much change in the normal force hysteresis. Thus, increasing the local Mach number along the turbine blade span may result in a stabilizing effect as the tips are approached, at least in terms of freestream aeroelastic excitation.

**Table 5-4. Relative Importance of Unsteady Fluid Dynamic Parameters in Leading Edge Stall Phenomena**  
(Source: Ref. [18])

Parameter	Effect
Airfoil shape	Large, in some cases
Mach number	Small (below $M_\infty \sim 0.2$ ), Large (above $M_\infty \sim 0.2$ )
Reynolds number	Small (?) at low Mach number, Unknown at high Mach number
Reduced frequency	Large
Mean incidence angle	Large
Type of motion	Virtually unknown
3-D effects	Virtually unknown



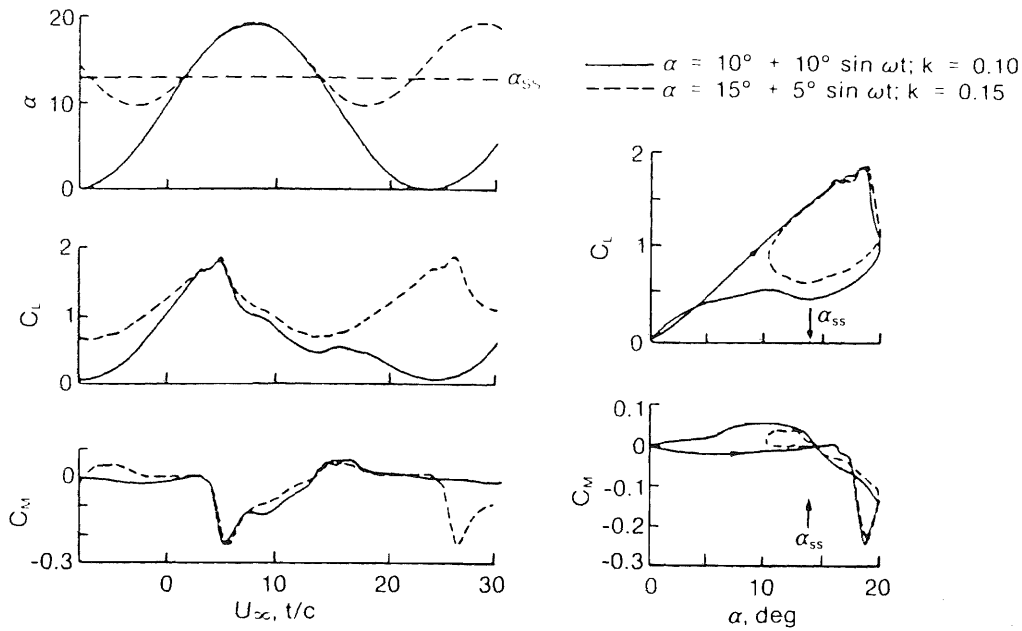


Figure 5-28. Effect of  $\alpha_{max}$  on Dynamic Airloads ( $\alpha = 10^\circ \pm 10^\circ$  and  $\alpha_{ss} = 15^\circ \pm 5^\circ$ )

Source: Ref. [18].

The influence of the airfoil shape has been found to be a major parameter in determining leading-edge separation characteristics. Particularly sensitive are sections that exhibit chordwise pressure distributions along the suction or upper surface which concentrate the greatest negative pressures very close to the leading edge and reach an extreme at high incidence angles. Figure 5-30 shows the development of this chordwise pressure distribution for half a cycle of an incidence angle oscillation of  $5^\circ$  above the steady value of  $10^\circ$  ( $3^\circ$  below static stall) for a NACA 0012 airfoil section. To the authors' knowledge, all commonly used airfoil sections employed in wind turbine designs (e.g., NACA 0012, 0015, 44xx-series, and the 230xx-series) possess similar chordwise distributions at the high incidence angles of normal operation (low blade or high pitch angles). The 44xx-series airfoil shape employed in the MOD-1 rotor will be discussed more fully below.

The reduced frequency parameter  $k$ , which is defined by

$$k = \frac{\pi f c_s}{U} = \pi \left( \frac{c_s}{\lambda} \right), \tag{5-5}$$

where

- $f$  = the cyclic frequency of the exciting perturbation
- $c_s$  = the section chord dimension
- $U$  = mean blade speed (or resultant velocity)
- $\lambda$  = wavelength of disturbance,

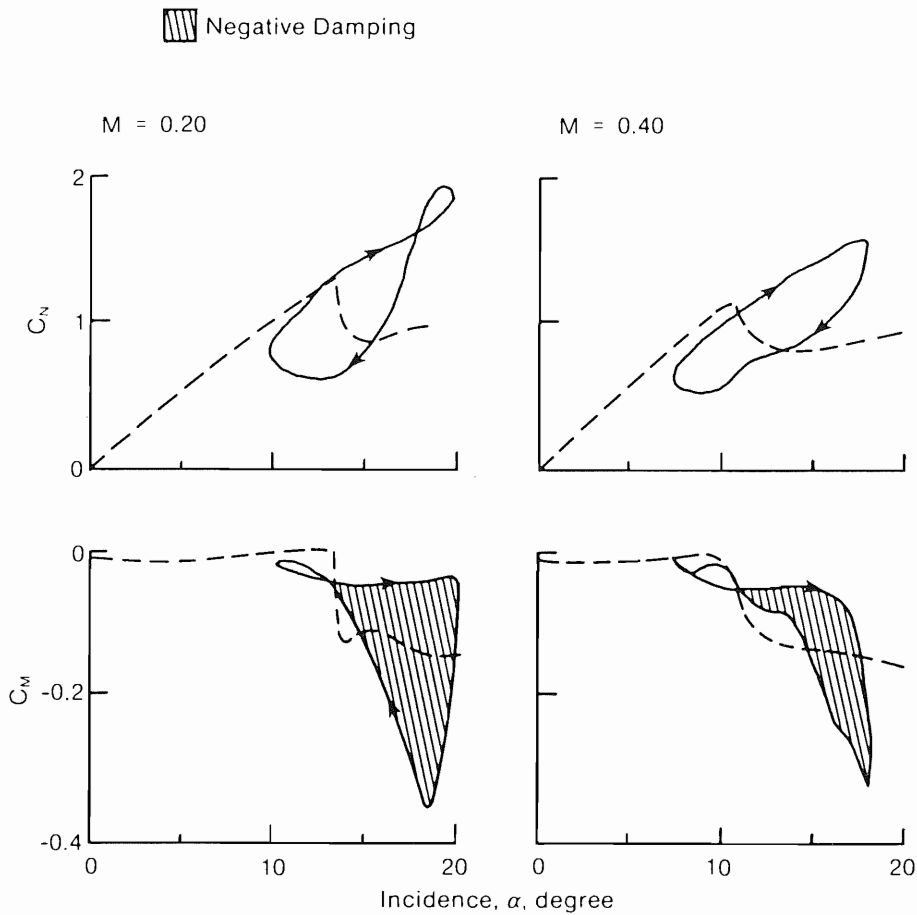


**Figure 5-29. Effect of Mach Number on Dynamic Normal Force and Moment Coefficients**

Source: Ref. [20].

represents the ratio of the section chord length to the wavelength of the disturbance encountered in the freestream. It relates how the perturbation is sensed by various parts of the section. Figure 5-31 shows the increase in the airload hysteresis and overshoot for an increasing reduced frequency for a NACA 0012 airfoil section oscillating  $\pm 5^\circ$  from a mean incidence angle of  $10^\circ$  at a Mach number of 0.30. It should be pointed out that the Strouhal number defined earlier may be thought to serve a similar function for perturbations affecting bluff body unsteady aerodynamics.

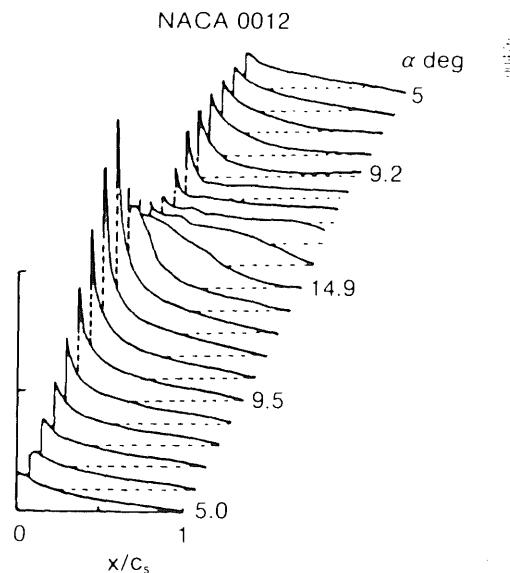


**Figure 5-30. Chordwise Pressure Distribution as a Function of the Incidence Angle for a NACA 0012 Airfoil**

Source: Ref. [18].

From the preceding it is apparent that the higher-order, nonlinear aspects of unsteady flows over various airfoil shapes is a complex subject with a number of fluid dynamic parameters exerting influence over the process (in comparison with static stall, where the incidence angle and airfoil shape are most important). McCroskey [18] has identified various transitory lift phenomena involving strong, viscous effects on airfoils being subjected to aerodynamic excitation by turbulent perturbations in the freestream, resulting in an oscillatory response in the airfoil boundary layer. If the angle of attack oscillates around a high mean value, the resulting aerodynamic excitation may lead to leading edge separation and transitory stall. The depth of the induced stall has been shown to be largely a function of the maximum incidence angle  $\alpha_{\max}$ . McCroskey [18] has classified the degree of stall severity into two regimes: light stall and deep stall. The former is characterized by sudden loss of lift and significant increases over inviscid values in the drag and nose-down pitching moments as the incidence angle  $\alpha$  exceeds a certain value. Also, this regime is subject to increasing airload hysteresis and the accompanying effects of negative aerodynamic damping. This condition is also highly sensitive to most of the unsteady parameters listed in Table 5-4, including, as McCroskey speculates, 3-D circulations (such as spanwise coherence).

The classification of the deep stall regime is characterized by a large excess in  $\alpha_{\max}$  accompanied by overshoot values of the lift, drag, and moment coefficients that far exceed their static values. Figure 5-32 compares the stall regimes. Particularly significant is the abrupt drop in the lift after the

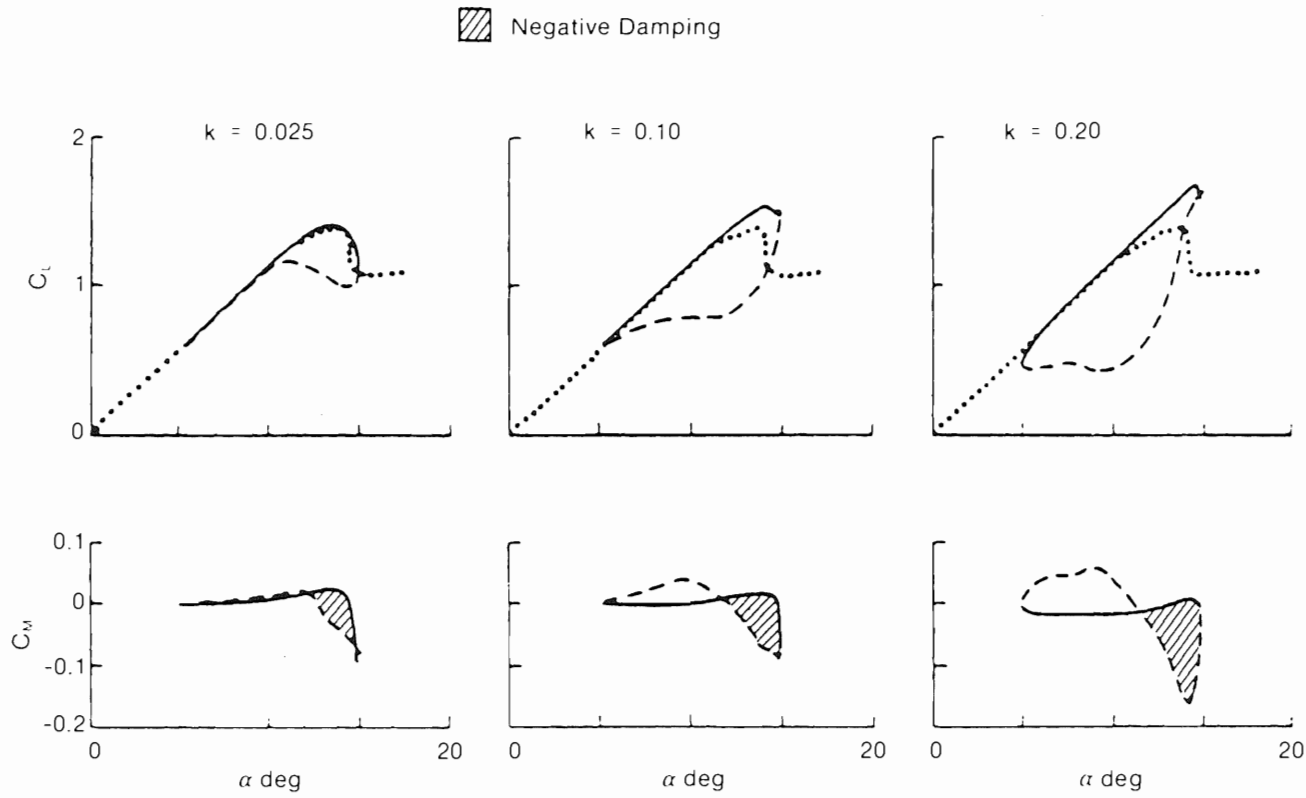
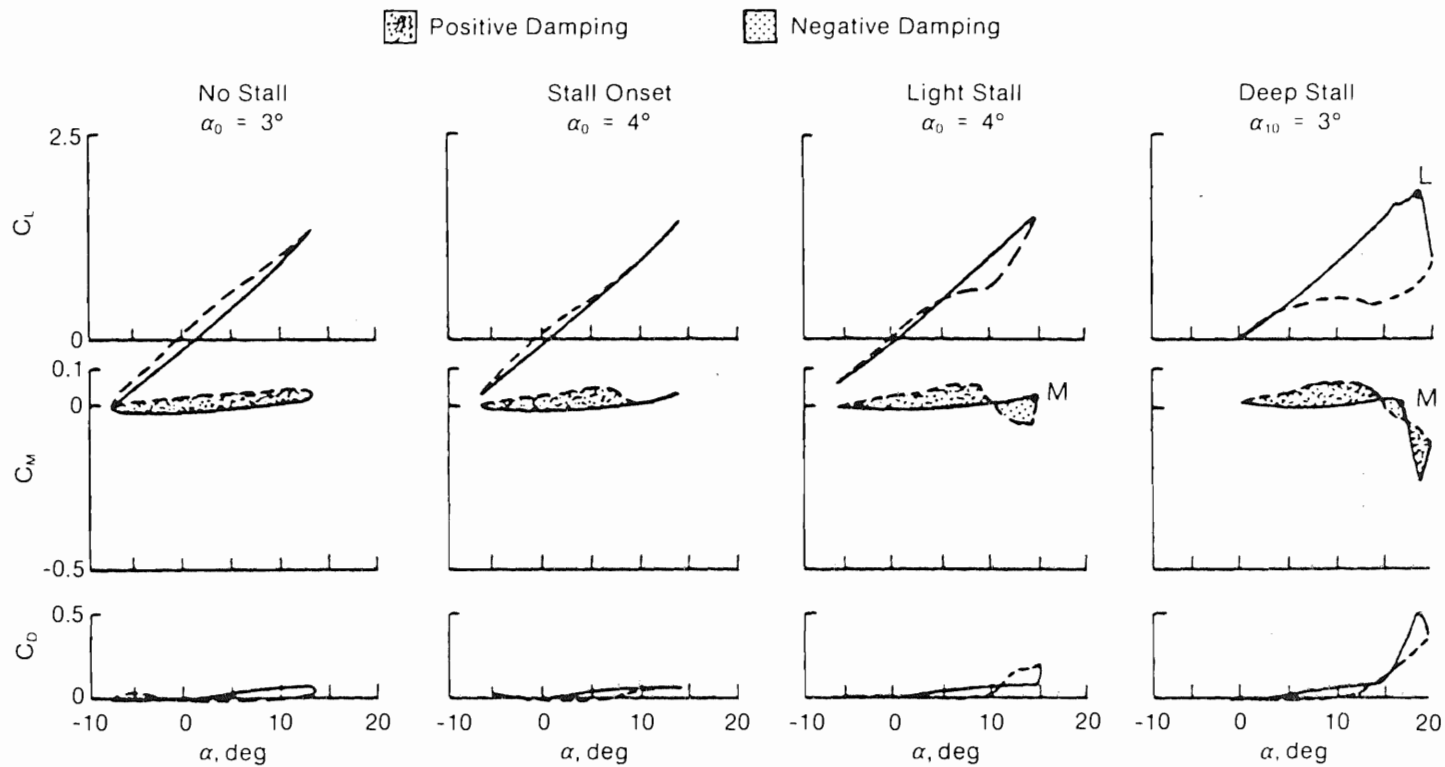


Figure 5-31. Effect of Reduced Frequency on the NACA 0012 Airfoil ( $M_\infty = 0.30$  and  $\alpha_{SS} = 10 \pm 5^\circ$ )  
 Source: Ref. [18].



**Figure 5-32. A Comparison of Dynamic Stall Regimes** (NACA 0012 airfoil,  $\alpha = \alpha_{SS} + 10^\circ \sin \omega t$ ,  $k = 0.10$ ; solid lines denote increasing  $\alpha$ , dashed lines decreasing  $\alpha$ )

Source: Ref. [18].

$CL_{max}$  value is reached in deep stall which is not noticeable in the light-stall case. Also, as McCroskey points out, large pitch change rates  $\dot{\alpha}$  and values of  $\alpha_{max}$  are necessary for deep stall. Ericsson and Reding [21] have qualitatively defined the overshoot  $\Delta\alpha_s$  as

$$\Delta\alpha_s = \left[ \frac{\partial}{\partial \left( \frac{c\dot{\alpha}}{U_\infty} \right)} \right] \frac{c\dot{\alpha}}{U_\infty}, \quad (5-6)$$

where  $\alpha_s$  is the static stall incidence angle and the quantity in brackets is the overshoot derivative. An example of the  $CL_{max}$  overshoot, defined as  $\Delta CL_{max} = CL_{\alpha} \cdot \Delta\alpha_s$ , is shown in Figure 5-33 for a NACA 2301x airfoil section (which is used on the MOD-0, MOD-0A, and MOD-2 turbines); a shape (like the NACA 44xx-series used on the MOD-1) which is susceptible to leading edge stall. McCroskey has also pointed out that the deep stall regime is relatively insensitive to airfoil motion and geometry as well as the flow Reynolds and Mach numbers as long as shock waves do not develop along the leading edge. The primary controlling factor is the incidence angle overshoot  $\Delta\alpha_s$ , defined by Eq. (5-6).

A reflection on the observed acoustic impulse shapes of Figures 5-23 through 5-26 in which an abrupt loss in lift is evident as the blade passes through the tower wake strongly suggests that the deep stall regime is being reached under these conditions primarily because of the suddenness and large change observed. However, we also know that the space scale over which this process is acting is on the order of the blade chord, a fact which will be treated next.

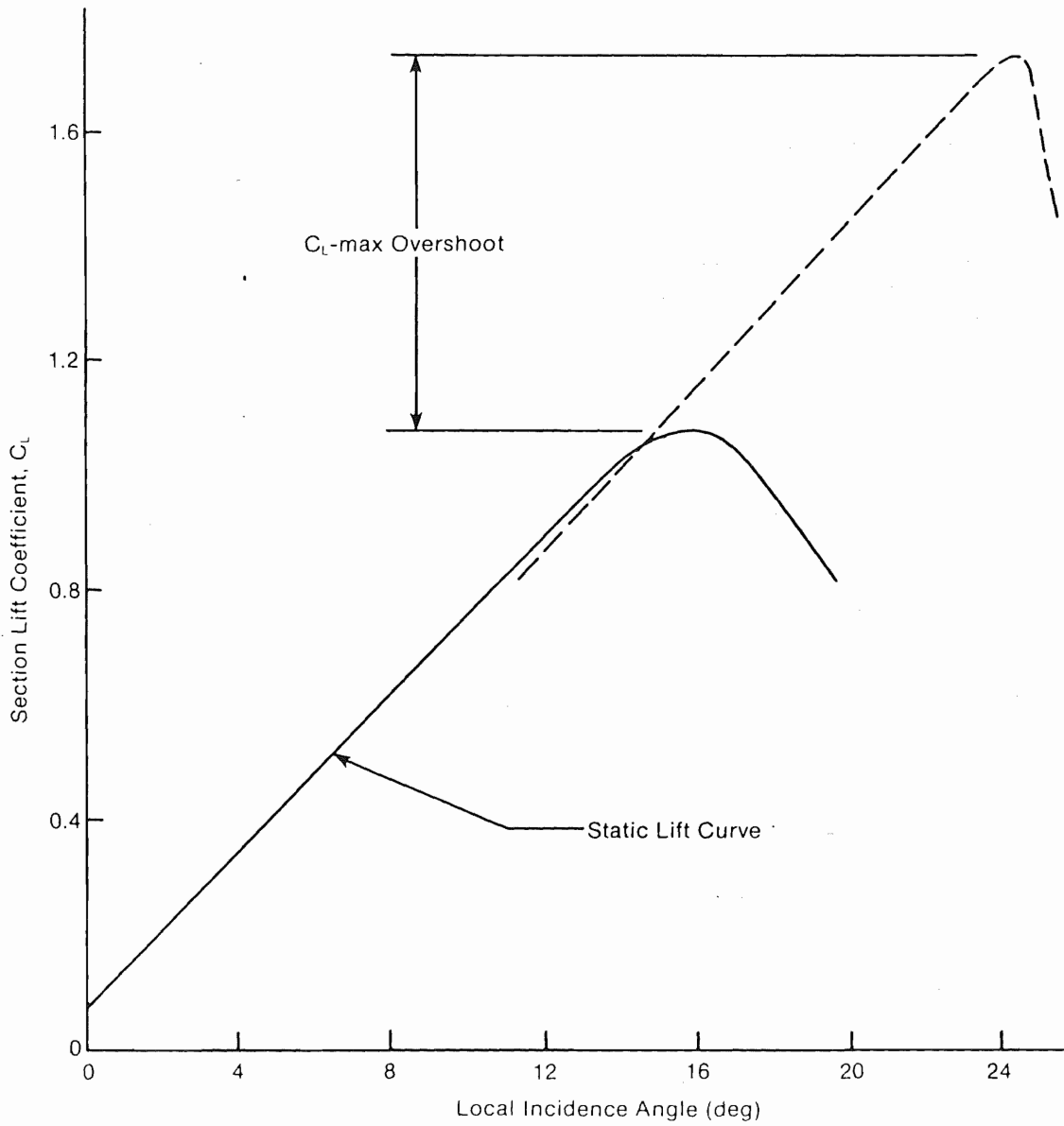
#### 5.2.4.2 Role of Blade-Vortex Interaction in Impulse Generation

In the previous section, we discussed the influence of various unsteady fluid dynamic parameters in the leading edge separation of airfoils causing abrupt losses of lift. While they are descriptive of the two-dimensional turbulent structure the blade is encountering, they do not address the existence of pressure perturbations existing in the inflow, which has also been listed in Section 5.4.2.1 as a potential factor. Wakes shed by circular cylinders are known to contain strong vortex elements, and the observed discreteness in the frequency domain is attributed to these circulation features. Before examining the potential role of the vortex shedding in the unsteady aerodynamics problem at hand, it is first useful to present a very brief review of vortex dynamics.

**Dynamics of Vortex Flows.** The rate of vorticity  $K$  being generated in a boundary layer separating from a body in 2-D flow has been shown by Birkhoff and Zaratonello [22, referenced in 23] as

$$K = \Gamma f_s = \Lambda U_\infty^2, \quad (5-7)$$

where  $\Gamma$  is the circulation of the vortex,  $f_s$  the cyclic shedding frequency, and  $\Lambda$  a dimensionless parameter relating the rate of vorticity generation to the freestream velocity  $U_\infty$  and most likely a function of the Reynolds number, body surface roughness, and inflow turbulence. We can rewrite Eq. (5-7) as



004771

Figure 5-33. Example of  $C_{l,max}$  Overshoot for NACA 2301x Airfoil  
 Source: Ref. [21].

$$\Gamma = \frac{\Lambda U_{\infty}^2}{f_s} , \quad (5-8)$$

which relates the vortex strength to the square of the freestream velocity. Vortices are the result of viscous phenomena and contain both a radially dependent velocity and pressure distribution. Figure 5-34 illustrates typical 2-D vortex velocity and pressure profiles. If the fluid in which the vortex exists is inviscid, irrotationality constraints require the radial velocity to become infinite at the center or core. In a real fluid, this does not occur, because the effects of viscosity prevent it from happening. Following Loth [24], the vortex is often modeled as a core region in constant solid-body rotation surrounded by an inviscid, irrotational region with a constant circulation  $\Gamma = 2\pi r U_{\theta_r}$ , where  $U_{\theta_r}$  is the tangential velocity at radius  $r$ . The maximum tangential velocity occurs at the edge of the solid rotating core ( $r = a$ ) or  $U_{\theta_a} = \Gamma/2\pi a$ . The flow inside the core is given by

$$U_{\theta_r} = U_{\theta_a} \cdot r/a = \Gamma/2\pi a \cdot r/a . \quad (5-9)$$

In the ideal or model vortex, there is no total pressure deficit beyond the core radius  $a$ , where the pressure is  $p_a = p - \frac{1}{2} \rho U_{\theta_a}^2$ .

At any radius within the core ( $r < a$ ), the total pressure,  $p_{t_r}$ , is given by

$$p_{t_r} = p_t - \rho U_{\theta_a}^2 [1 - (r/a)^2] . \quad (5-10)$$

From Eq. (5-10) it can be seen that the ideal vortex core has a pressure deficit that translates to a total pressure flux deficit of  $(\rho U_{\infty} \Gamma^2)/8\pi$  for the ideal vortex [24]. The total flux deficit for a real vortex has been found by Loth [24] to be  $0.78 (\rho U_{\infty} \Gamma^2/8\pi)$ . The decay of a vortex element, considered to behave like a single filament carried by the flow, is described by

$$U_{\theta_a}(t) = \frac{\Gamma}{2\pi a} \left( 1 - e^{-a^2/4\nu t} \right) , \quad (5-11)$$

where  $\nu$  is the kinematic viscosity [25]. Roshko [26] has found remnants of vortex circulations as far downstream as 40-50 cylinder diameters. Obviously, Eq. (5-11) is only an approximation, since it is also known that the entrainment of freestream vorticity is also a consideration.

**Vortices in MOD-1 Leg Wakes and Impulse Generation.** We are interested in assessing the potential of the perturbative velocity and pressures of the vertically coherent, vortex tube structures contained in the MOD-1 tower leg wakes as a contributory influence in the unsteady aerodynamic process responsible for the acoustic impulse generation. Much of our discussion in Section 5.4.2.1 was centered on the  $\alpha$  parameter derived from a time-varying upwash as a major factor controlling the depth of the transient stall observed. Another important physical parameter to be considered is the existence of a transient adverse pressure gradient encountered by the blade particularly at high incidence angles. We have already identified what we believe to be transient leading edge separation taking place within the leg wake boundaries, which we have found to contain vortex tubes extending more or less parallel to the blade span upon intersection. Because these vortex structures contain strong imposed pressure deficits as well as radial velocity fields, we believe both may be important in initiating the stalling process.



004772

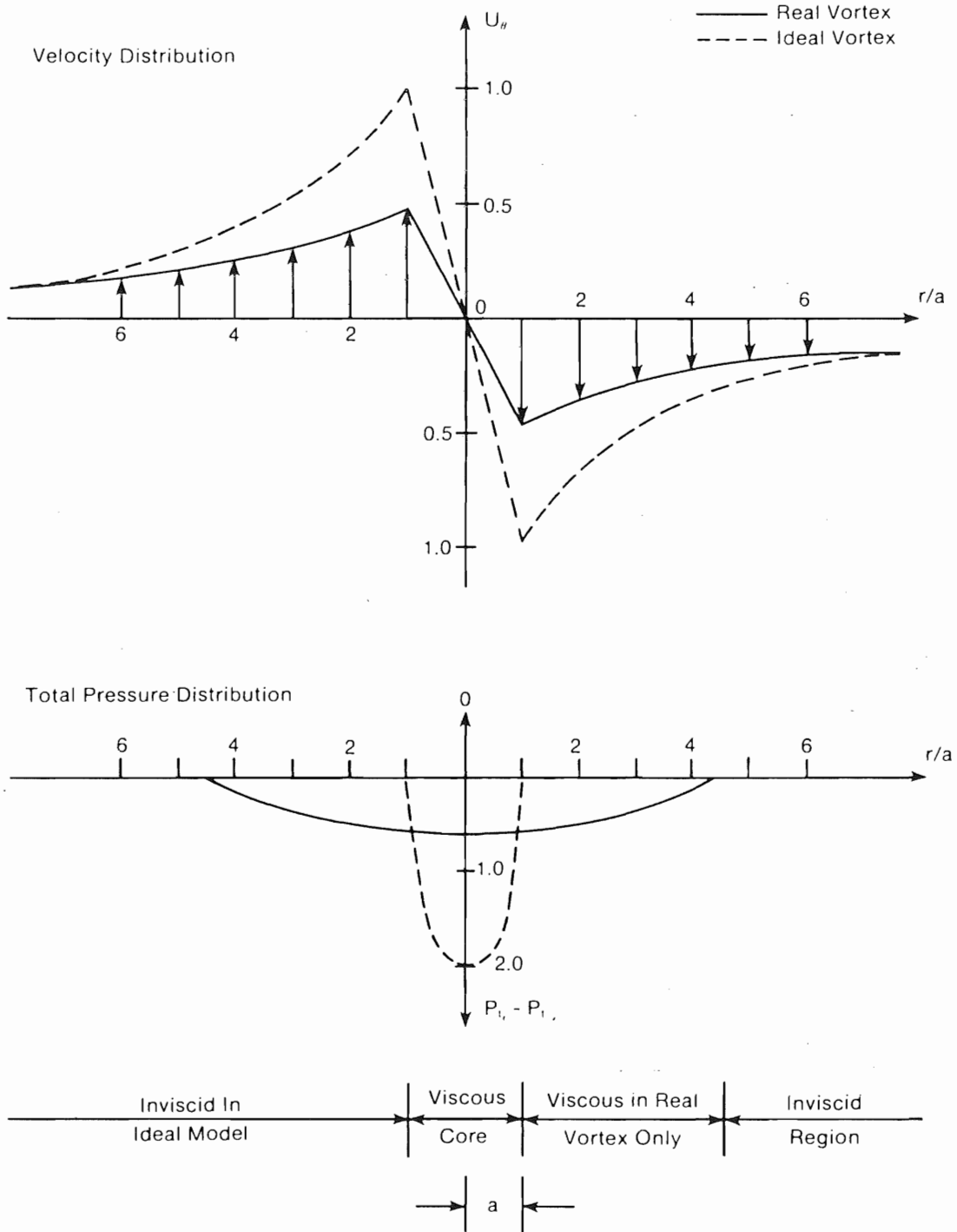


**Figure 5-34. Typical Vortex Radial Velocity and Pressure Distributions**  
 Source: Ref. [24].

It is well known that a positive or normal pressure gradient is a stabilizing influence on the boundary layer of an airfoil surface while, under the right conditions, an adverse gradient (decelerating flow) will promote separation. Figure 5-35 demonstrates the process. A normal gradient will allow a small region of laminar flow or "bubble" to exist near the leading edge of the suction side of an airfoil at a positive incidence angle. As the angle is increased, the laminar region contracts and the turbulent transition point moves forward toward the stagnation point. It should be noted that a turbulent inflow acts to favor transition and therefore delay separation. The  $c\bar{\alpha}/U_\infty$  term of Eq. (5-6) decreases the adversity of the pressure gradient, causing a lag to develop between the static and unsteady regimes and a delay in separation [21]. However, as previously discussed, there is a critical value of  $\alpha_{\max}$  at which an abrupt separation will occur.

Because of the leading edge separation sensitivity to adverse pressure gradients, and after considerable study of the characteristics of cylinder wake flows, we tentatively conclude that viscous interaction effects (primarily manifested as the pressure-deficit flux gradients in the viscous cores of shed vortices) may also be important. This point is illustrated by the two frequency spectra plotted in Figure 5-36. The mean frequency spectrum of the wake velocity measured at 1-1/2 diameters downstream of the bare cylinder on the small wind turbine tower is shown in the lower trace with the corresponding wake dynamic pressure spectrum, as measured by a boom-mounted VLF microphone, above. The coherence of these two spectra is quite noticeable. The sharp peaks of the pressure spectrum at one particular frequency, compared with a more broadband spectrum velocity with several discrete peaks, hints of pressure deficits in the cores of the vortices being convected past the measurement point. This strong, narrowband coherence between the wake dynamic velocity and pressure fields is further illustrated in Figure 5-37 by the sharp cross-spectral peak at 3.04 Hz derived from an intense and highly discrete wake flow from the same tower with a perforated shroud installed over the cylindrical surface.

The discrete, coherent relationship exemplified by Figures 5-36 and 5-37 suggests that the pressure deficit in the viscous cores of the shed vortices may be of sufficient intensity and spatial dimension to overcome the quasi-steady normal gradient (strengthened by the more broadband turbulence component of the wake) as the blade passes through. Because we know the impulse generating process is taking place within a space scale on the order of the blade chord, the relationship of the vortex viscous core dimensions in terms of its pressure deficit region and the dimensions of the positive pressure gradient on the leading edge of the blade airfoil may be quite important, particularly since (a) this positive gradient region decreases with increasing incidence angle; (b) the intensity of the peak core pressure deficit increases with enhanced vortex strength, which is proportional to the freestream velocity as indicated by Eq. (5-8); and (c) the positioning of the peak negative pressure is very near the leading edge of airfoil sections at high incidence angles.

In order to evaluate a plausible role for the vortex pressure distribution as a contributor in the causal relationship for leading edge separation, we must develop both the spatial and pressure deficit intensity aspects and their relationship to the dimensions of the cylinder wakes and blade chords. Roshko [26] has proposed a relationship for the vortex strength of a cylinder as

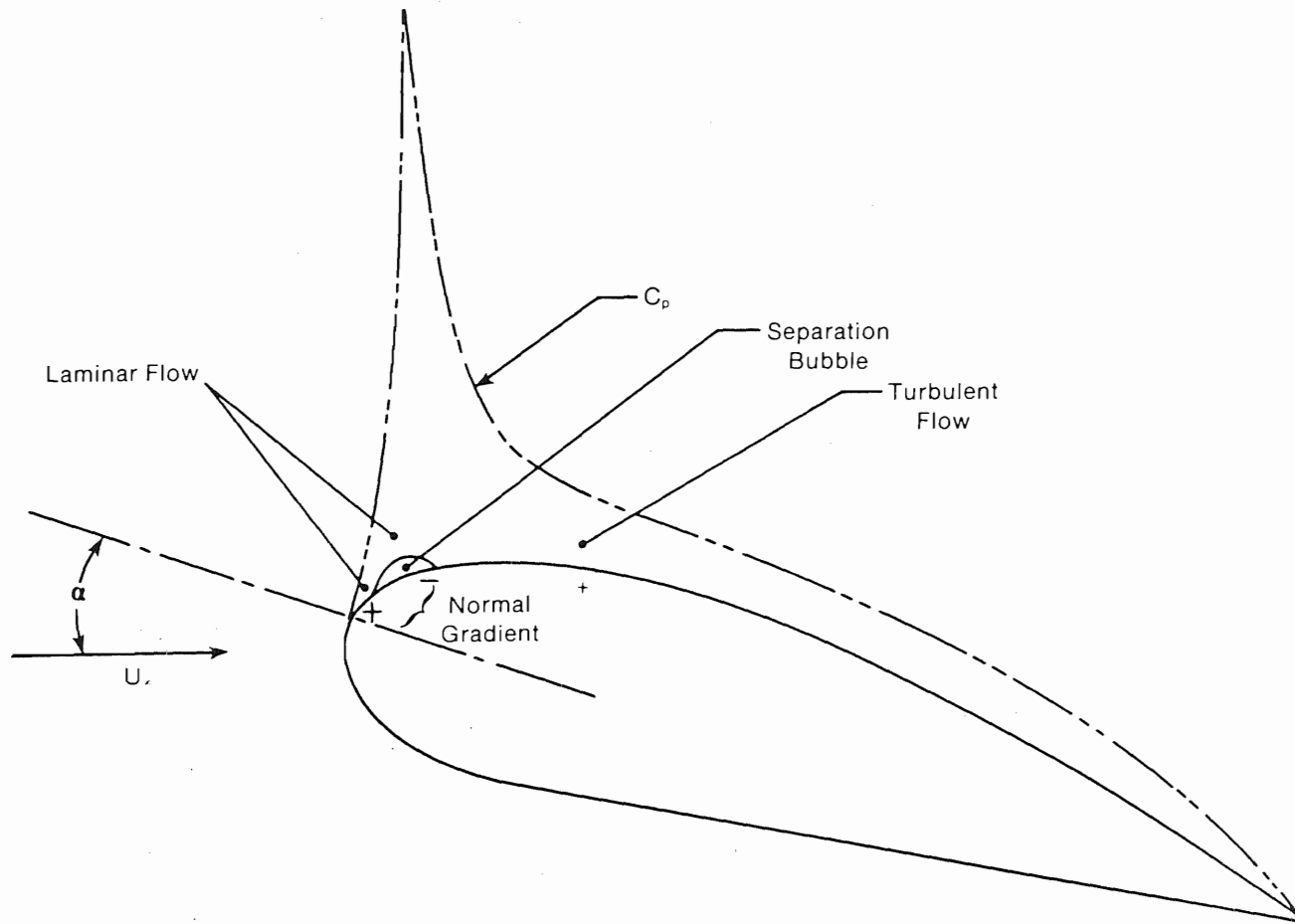


Figure 5-35. Schematic of Airfoil Boundary Layer and Chordwise Pressure Distribution Properties

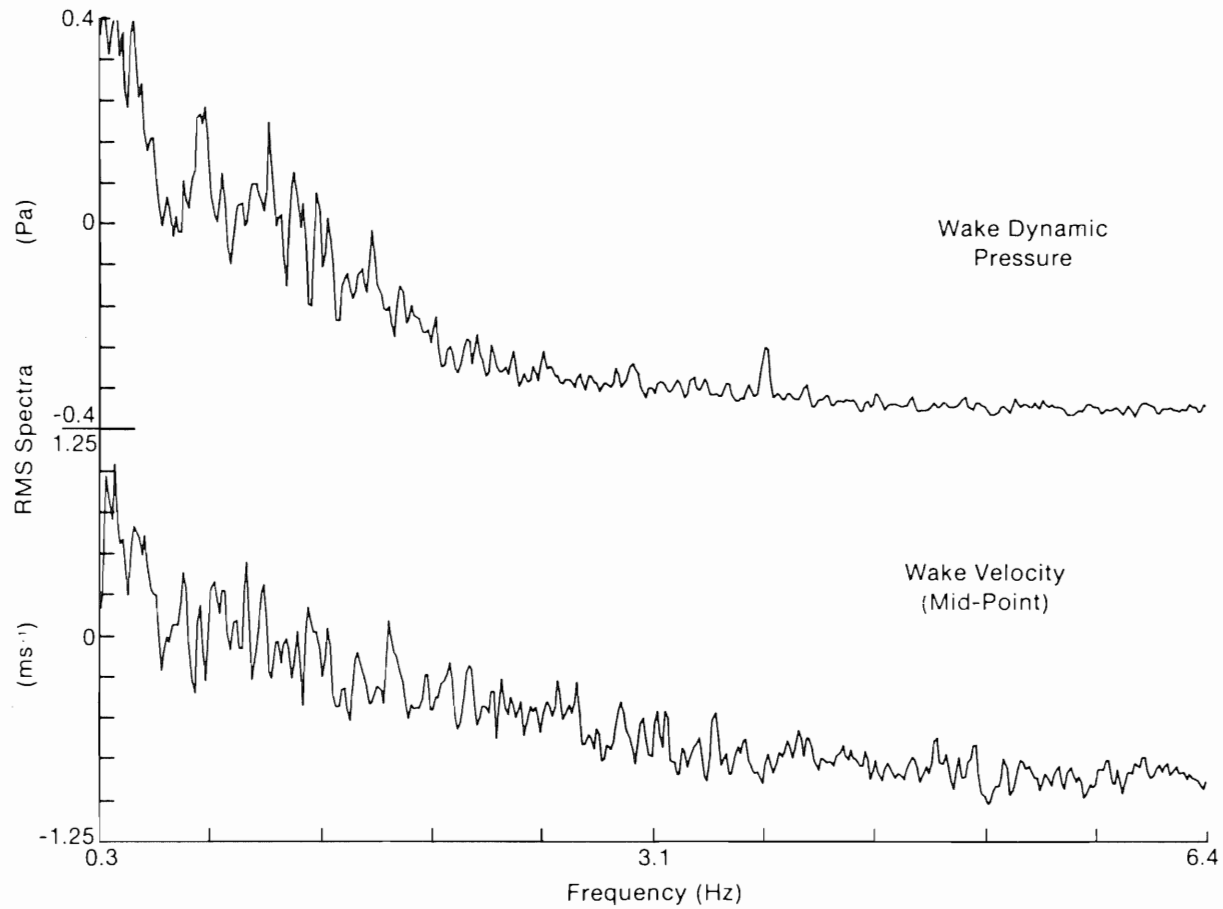
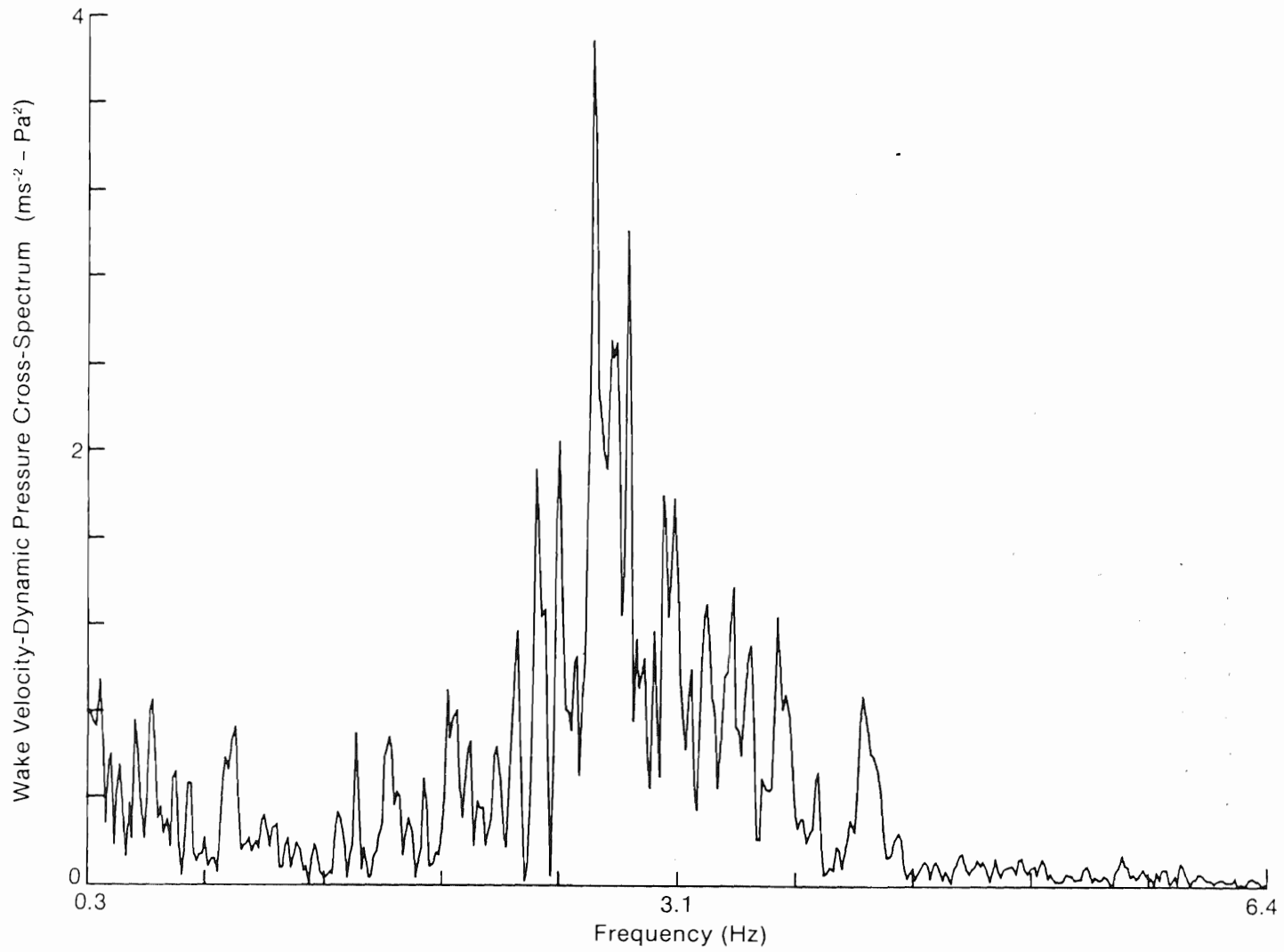


Figure 5-36. Comparison of Wake Velocity and Dynamic Pressure Spectra 1.5D Downstream of a Cylindrical Tower Element



0000015

Figure 5-37. Comparison of Wake Velocity and Dynamic Pressure Spectra Taken 1.5D Downstream of a Perforated Shroud-Covered Cylinder

$$\Gamma = \frac{U_{\infty} D}{St}, \quad (5-12)$$

where he has defined the proportionality constant  $\Lambda$  in terms of the Strouhal shedding frequency or  $f_s = (St \cdot D)/U_{\infty}$ , where  $D$  is the cylinder diameter and  $St$  the Strouhal number. For a freestream velocity of  $10 \text{ ms}^{-1}$ ,  $St = 0.21$ , and a cylinder  $0.5 \text{ m}$  in. diameter, the vortex strength, using Eq. (5-12), would be  $12.1 \text{ s}^{-1}$ . We assume that Eq. (5-12) defines the vortex generation process (i.e., the value of  $\Gamma$ ) and the laws of momentum conservation determine the distribution of the fluid dynamic parameters in the downstream wake. If we further assume that the diameter of the vortex viscous core is equal to or a fraction  $\kappa$  of the mean cylinder wake diameter  $d_w$ , or  $2a = \kappa d_w$ , which is consistent with the findings of Roshko [26] and Fage and Johnson [27], we can write an expression using Eq. (5-10) for the core pressure deficit, or

$$\Delta p_v = \rho \frac{\Gamma^2}{2\pi\kappa d_w} = \rho U_{\infty}^2 \left[ \frac{1}{2\pi\kappa St} \frac{D}{d_w} \right]^2. \quad (5-13)$$

Equations (5-9), (5-12), and (5-13) now give us some insight into the physical parameters influencing the intensity of both the induced velocity and pressure fields in the vortices of cylinder wake flows. The core pressure deficit increases as the square of the freestream velocity and the maximum vortex-induced tangential velocity  $U_a$  (occurring at  $\kappa d_w$ ) is directly proportional to this velocity and inversely proportional to the core width  $\kappa d_w$ . Many of these relationships have already been identified in Section 3.0; i.e., the strong correlation with wind speed and the downstream leg-to-wake distance related to  $d_w$ .

The potential importance of the pressure deficit encountered by the rotor blade can now be demonstrated. The measured chordwise steady pressure distribution along the upper (suction) surface as a function of incidence angle for a NACA 4412 airfoil section, as an example, (approximately that at the 95% span position on a MOD-1 blade) is plotted in Figure 5-38 and summarized in Table 5-5. The forward movement of the peak negative pressure and steepening positive pressure gradient with increasing incidence angle is evident, as is the very small percentage of the chord involved; i.e., less than 2% for  $\alpha > 8^\circ$ . Employing Eq. (5-13) for a freestream velocity  $U_{\infty} = 10 \text{ ms}^{-1}$ , estimated wake widths of 0.8 and 0.46 m at a 7.5D downstream distance for subcritical and supercritical wakes, respectively, based on the data of Eq. [14], and a Strouhal number of 0.21, we computed estimates of the pressure gradient existing across a viscous vortex for core diameters or  $\kappa = 0.10, 0.25, \text{ and } 0.5$  of the wake width  $d_w$ . The results have been plotted as two curves representing sub- and supercritical wake widths as functions of both the estimated vortex core diameters and as a percentage of the MOD-1 blade chord at the 95% span. From the data in Table 5-5, the steady leading edge positive pressure gradients have been indicated in Figure 5-39 for four incidence angles. These curves indicate that the steady, leading edge gradients will become adverse with a superimposed vortex pressure deficit when the core diameter is less than 50% of the wake width (at the 7.5D distance), involving about the leading 35% or less of the blade chord upon encountering a subcritical cylinder wake. In the case of a narrower, more energetic supercritical wake, the figure indicates that adversity is possible with vortex cores covering 75% or less of the wake but again, the first 35% or less of the blade chord would be

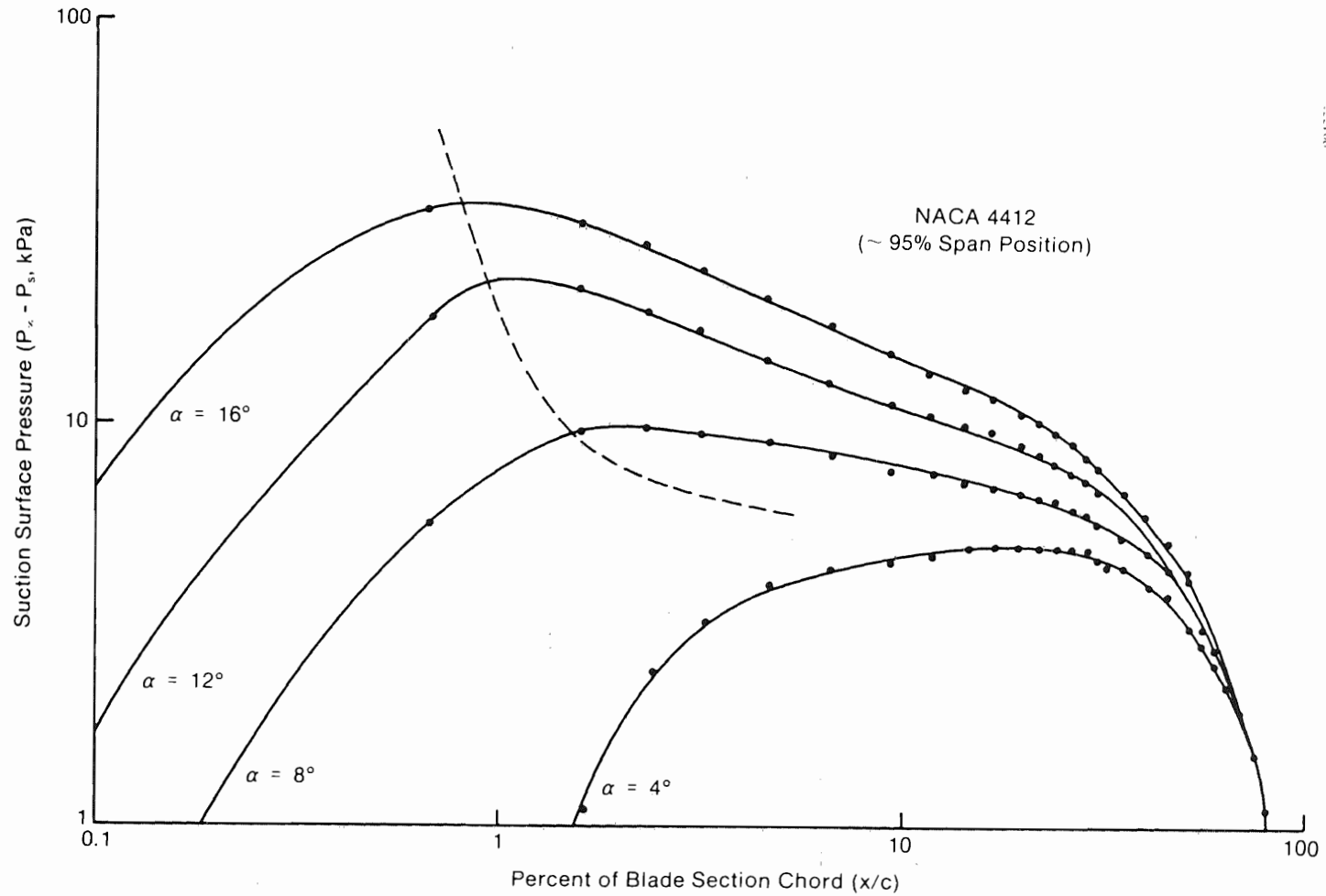
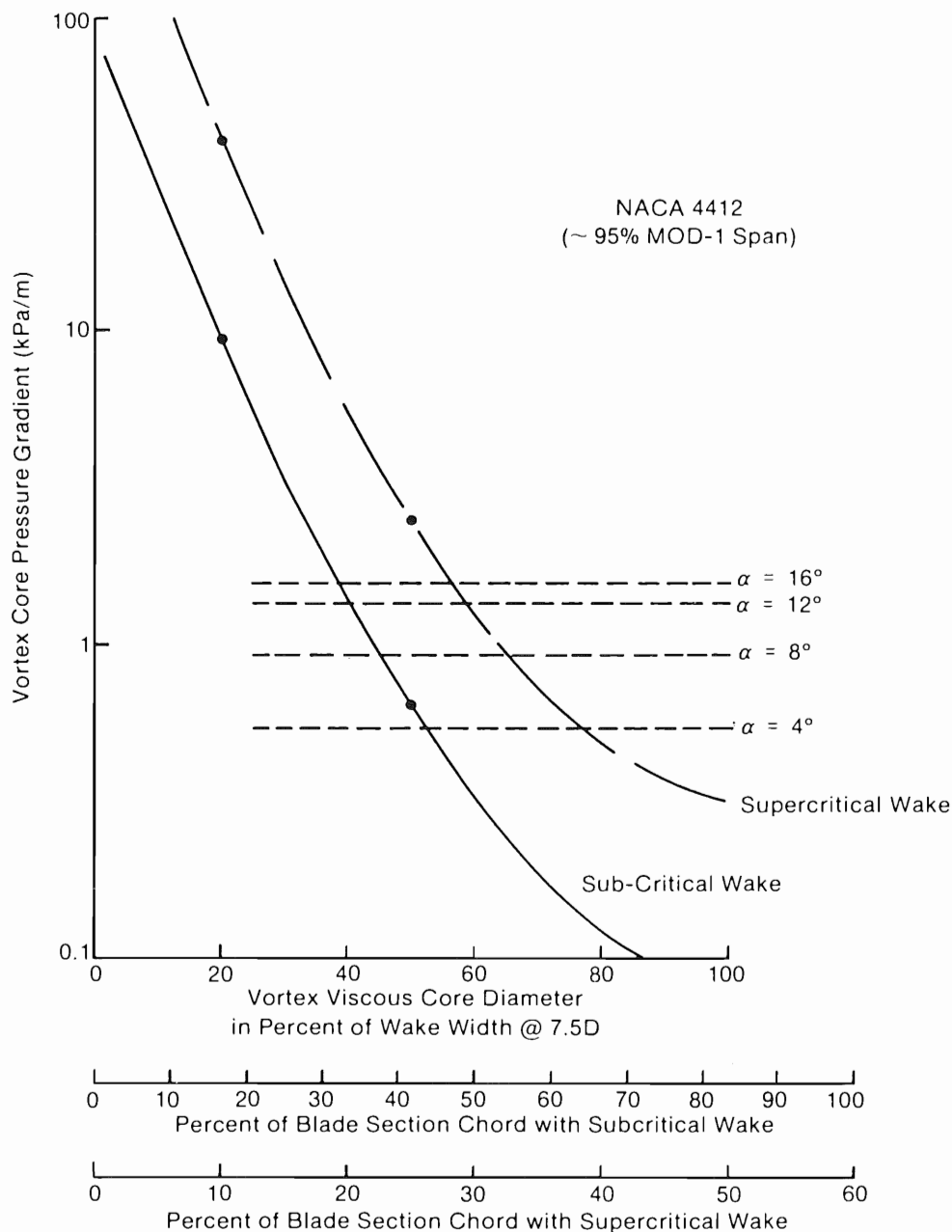


Figure 5-38. Mean Chordwise Pressure Distribution for a NACA 4412 Airfoil Section as a Function of Incidence Angle

Source: Ref. [28].



004776

**Figure 5-39. Vortex Core Pressure Gradient vs. Core Diameter in Percent of Leg Wake Width at 7.5D Downstream for Both Subcritical and Supercritical Regimes (D = tower leg diameter)**



Table 5-5. Steady Leading Edge Chordwise Pressure (Suction) Gradients for a NACA 4412 Airfoil Section (95% MOD-1 Span) at Equivalent 35 rpm Rotational Speed

Incidence Angle (deg)	Normal Mean <sup>a</sup> Gradient			Peak <sup>a</sup> Normal Gradient	
	x/c (%)	Surface Distance (cm)	Gradient (kPa/m)	Gradient (kPa/m)	Location from Leading Edge (cm)
4	16.0	10.6	0.081	0.54	0.68
8	1.3	1.85	0.457	0.93	0.68
12	0.7	1.41	0.928	1.36	0.94
16	0.7	1.41	1.008	1.58	0.94

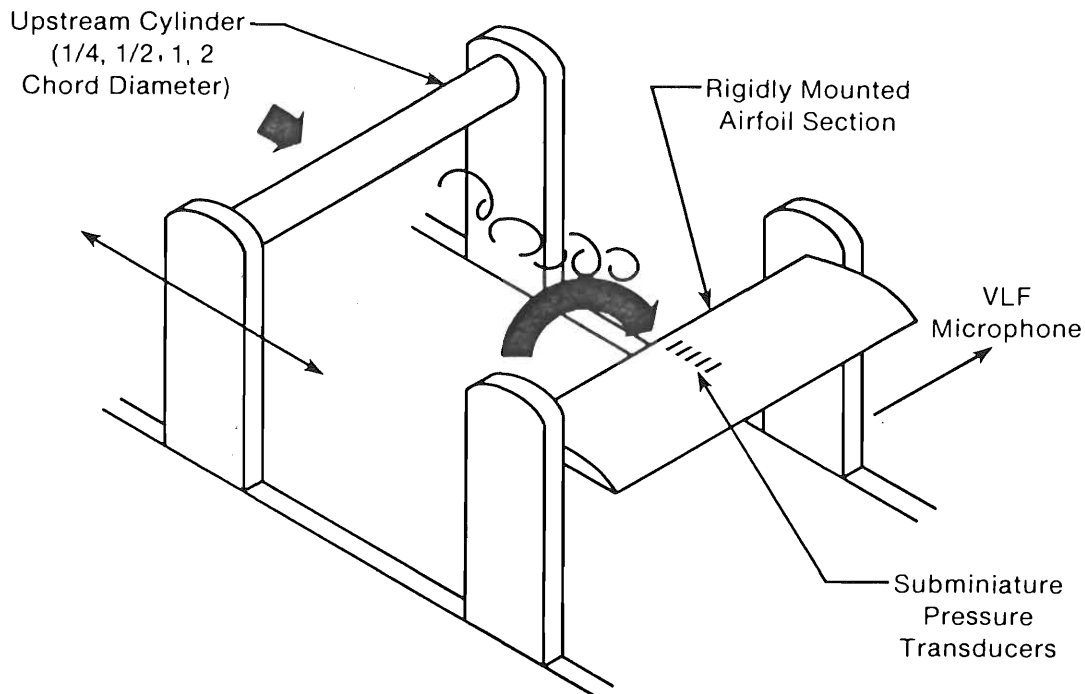
<sup>a</sup>Mean gradients are calculated by normalizing by total surface distance covered by normal gradient, peak value is determined by maximum gradient found between two pressure measurement stations.

involved, as shown by the lower abscissa scale. The data shown in Figure 5-39 demonstrate that the blade-vortex interaction of a 4412 airfoil section and tower leg wakes is a leading edge phenomenon. It is certainly probable that the pressure deficits within the vortex circulations exert a viscous influence, leading to boundary layer separation and an accompanying sudden loss of lift through the imposition of a transient adverse pressure gradient as well as an upwash-induced incidence angle  $\alpha_{\max}$ .

#### 5.2.4.3 Wind Tunnel Verification

The possibility that the pressure deficits contained within the wake vortices is a contributing factor in the suspected leading edge separation has, at least in terms of the existence of adverse pressure gradients, been confirmed by a wind tunnel experiment conducted in the University of Colorado subsonic wind tunnel. Figure 5-40 illustrates the basic tunnel testing configuration. A series of constant chord airfoil sections was constructed with a chord length of 17.8 cm and an aspect ratio of 5 and included the symmetrical NACA 0015, 0018, and 63<sub>2</sub>-015 and cambered 4415, and 23015 shapes. Unfortunately only the three symmetrical sections have been tested and only preliminary analysis results are available at this writing.

The tests were designed to expose a rigidly mounted airfoil section to a reasonably narrowband turbulent flow generated by a series of upstream cylinders (5D cylinder upstream spacing) whose streamwise dimensions (diameter) were an integral or integral fraction of the subject blade chord (i.e., 1/4, 1/2, 1, and 2 chords, similar to the model rotor tests conducted in the MIT anechoic tunnel) and to simultaneously measure the leading surface pressures and radiated acoustic pressure field. This approach allowed us to examine the



004777

**Figure 5-40. Sketch of Experimental Configuration for Unsteady Flow Testing of Rigid Airfoil Sections**

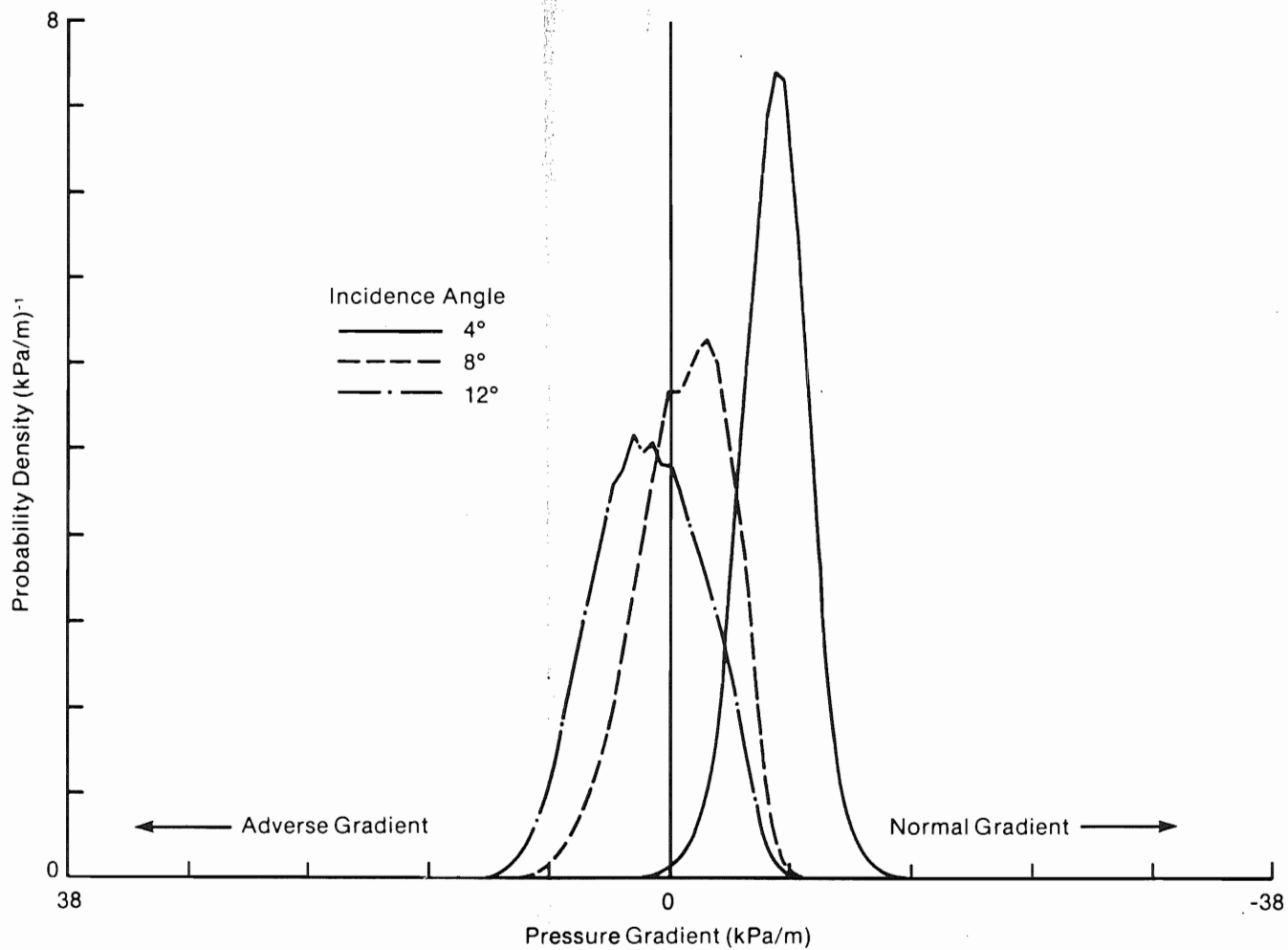
unsteady aerodynamic processes responsible for the radiated acoustic pressure characteristics in terms of many of the fluid dynamics parameters discussed previously while holding others constant. The surface pressures were measured by a series of subminiature pressure transducers with a sensing region 2.4 mm in diameter (or slightly more than 1% of the section chord dimension) placed at the leading edge and the 15%, 25%, and 40% chord positions on the upper (suction) surface and at the 40% chord location on the lower or pressure side. The design frequency response of the experiment was dc-1250 Hz, the upper limit imposed by the tape speed of the FM magnetic recording. The acoustic pressure field was measured by a single VLF microphone equipped with a nose cone and mounted above and slightly downstream of the test airfoil. Measurements of the wake turbulence inflow were taken with two 50- $\mu$ m, constant-temperature, hot-film anemometers mounted parallel to and 2 cm ahead of the airfoil leading edge. A single tunnel speed was used ( $37.5 \text{ ms}^{-1}$ ) which, when coupled with the cylinder wake deficits, translated into a chord Reynolds number of 265,000 at a Mach number of 0.085 compared with about 2,200,000 and 0.26, respectively, for the 80% span position of a MOD-1 blade at 35 rpm.

The objective of these tests was to determine if the properties of wake flows leaving an upstream cylinder could invoke dynamic negative pressure gradients over the leading edge region of the test airfoil sections as a function of incidence angle. The NACA 0015 and 0018 sections, while not used on the MOD-1 or most horizontal axis turbines, are commonly employed on vertical axis machines. All three of these sections, however, exhibit suction-side, chord-wise pressure distributions similar to the NACA 44xx section used on the MOD-1; i.e., the maximum negative pressure very close to the leading edge at incidence angles in excess of about 8 degrees, as indicated in Figure 5-38. While

the conditions for dynamic similarity have again not been met, the relative insensitivity to the Reynolds and Mach number parameters found by other investigators, for at least the deep stall phenomenon, should allow us to at least qualitatively examine the roles of the disturbance-imposed reduced frequency, adverse pressure gradients, and turbulence space scales at three incidence angles in the process leading to the development of transient lift fluctuations and the generation of acoustic impulses.

The NACA 63(2)-015 section was found to be increasingly sensitive to the cylinder wake disturbances with increasing incidence angle, as would be expected. Figures 5-41 and 5-42 present the upper surface leading edge-to-15% and -25% chord pressure gradient probability density functions (PDF) downstream of the two-chord-diameter cylinder at 4-, 8-, and 12-degree incidence angles. A normal gradient exists to the right of the center line (i.e., a pressure decrease between the transitory leading edge and either the 15% or 25% chord position) and an adverse one to the left. As can be seen from both figures, the gradient stays normal for an attack angle of  $4^\circ$  all but a minute fraction of the time. However, as the angle is increased, adverse gradients occur a greater and greater percentage of the time, particularly between the leading edge and the 15% chord position. It is interesting to note the high degree of adversity for an incidence angle at least two degrees below the static stall value. This indicates the effectiveness that turbulence structures containing the right properties have in controlling the boundary layer dynamics of airfoil sections with chordwise pressure distributions peaked near the leading edge. These figures also confirm an increased tendency to transitory leading edge separation with increasing incidence angle.

The role of the turbulent structure being encountered by the airfoil section in Figures 5-41 and 5-42 for a 12-degree angle of attack is shown by the relative transfer function magnitude relating the dynamic response of the radiated acoustic pressure field as excited by the inflow turbulence spectrum in Figure 5-43. The abscissa scales are plotted for both the reduced frequency  $k$  (one for 1/4-chord excitation and one for two-chord excitation, due to the differences in the wake deficits), and a wavelength or space scale normalized by the blade chord dimension. The broad and narrow peaks corresponding to the excitation by the relatively broadband two-chord cylinder wake and narrowband, discrete wake of the 1/4-chord cylinder are quite obvious. The maximum response to the broadband excitation occurs between the  $k$ -values of 0.5 and 2, with a peak at  $k = 1$  and a corresponding disturbance space scale range of 1.5 to 6 chord lengths, peaking at 3.1. The peak response to the narrowband, discrete wake occurs at  $k = 3.5$  (1/4-chord scale) with a perturbation wavelength of 1 chord. The responses to the 1/2- and 1-chord wake excitations, while exhibiting a narrowband peaked response similar to that of the 1/4-chord, occurred at  $k$ -values of 2.0 and 1.4 and wavelengths of 1.6 and 2.1 chords, respectively, but falling coincident with the curve defined by the two-chord wake excitation. In addition, a severe, high-frequency aeroelastic response was visually noted, though not directly instrumented for, during the two-chord broadband forcing including violent pitching (torsional) and translation movements, with the latter exceeding an estimated  $\pm 1$  cm vertical excursion of the rigidly mounted airfoil. In contrast, the 1/4-chord-wake-excited peak exhibited essentially a visually imperceptible elastic response but, as shown, it was reflected only in the radiated acoustic field. The behavior of these two peaks does vary with the smaller incidence angles, the acoustic peak at  $k = 3.5$  becoming predominant at the 4-degree incidence angle.



004776

Figure 5-41. Probability Density of Leading Edge-to-0.15 Chord Pressure Gradient for the 63(2)-015 Airfoil with Two-Chord-Diameter Upstream Cylinder Excitation

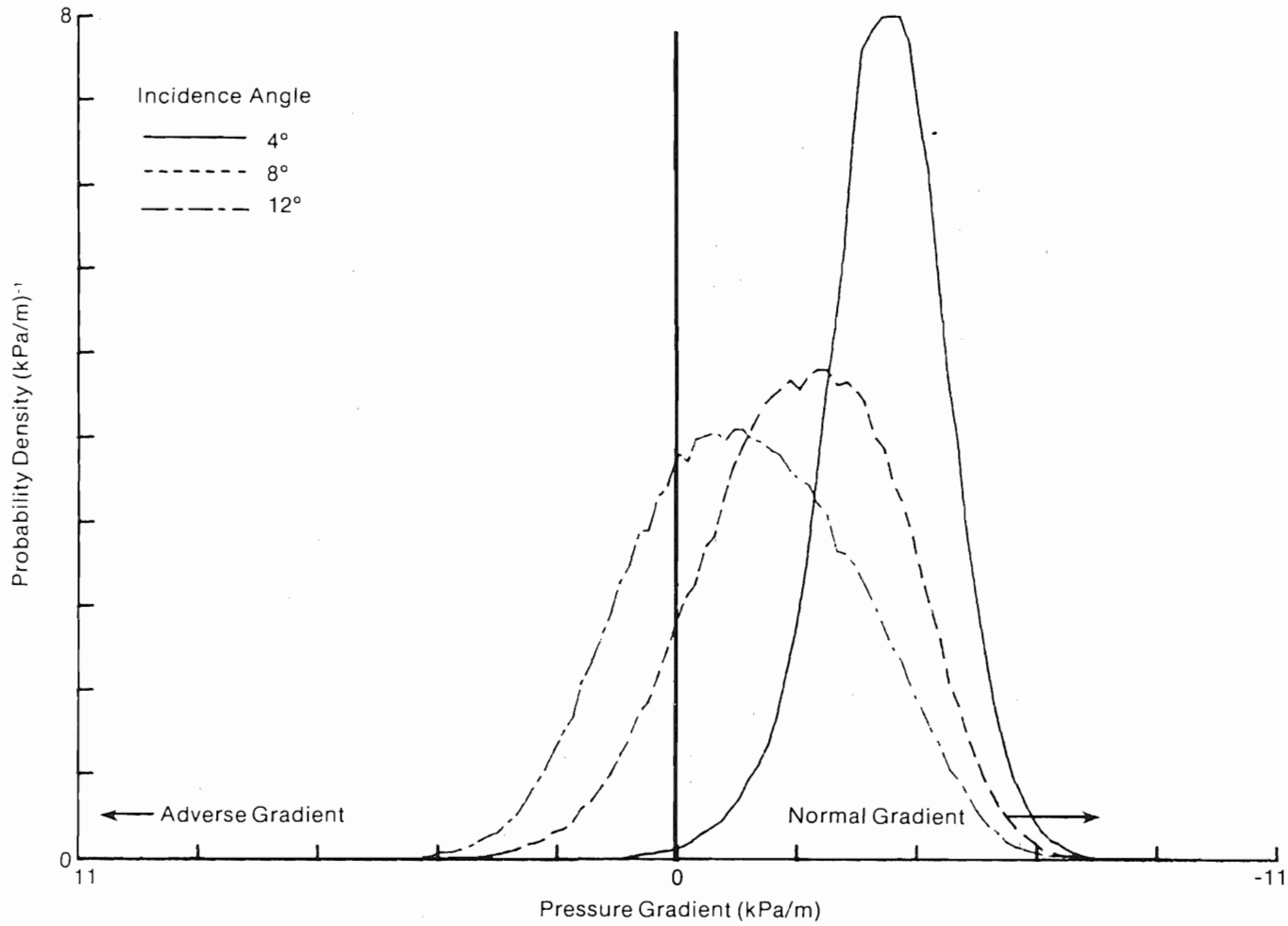
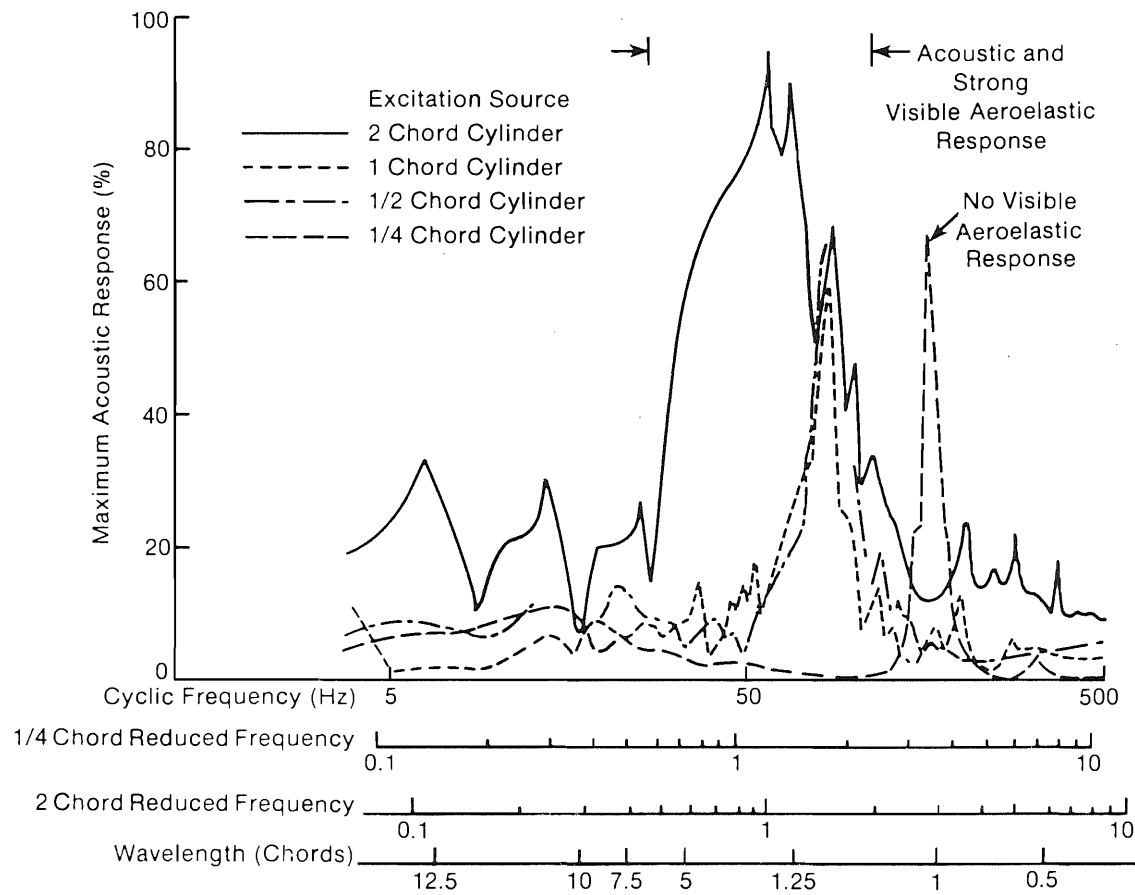


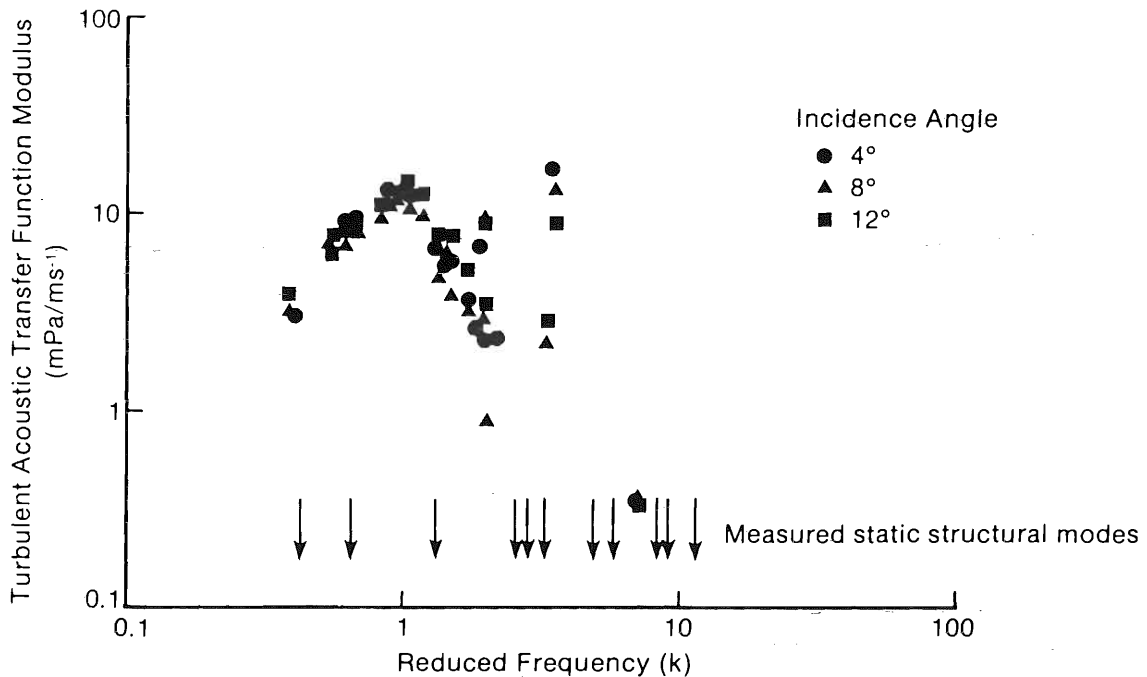
Figure 5-42. Probability Density of Leading Edge-to-0.25 Chord Pressure Gradient for 63(2)-015 Airfoil with Two-Chord-Diameter Upstream Cylinder Excitation



004780

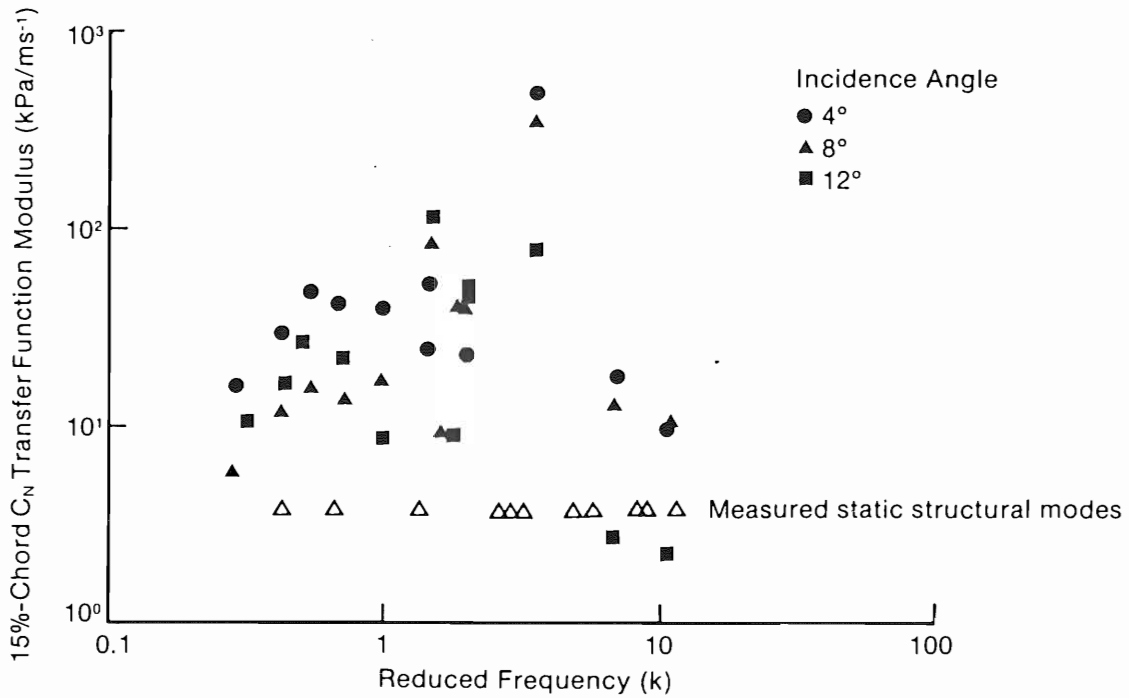
Figure 5-43. Relative Aeroacoustic Transfer Function for the 63(2)-015 Airfoil Section as a Function of Cylinder Wake Perturbations

We conclude from this that perturbations present in a turbulent wake flow can have a significant effect on the unsteady behavior of an airfoil section highly loaded at the leading edge. The relationship between the perturbation-induced unsteady airload (see Figure 5-1) and the resulting acoustic and aeroelastic responses of the NACA 63(2)-015 test section are summarized in Figure 5-44. Figure 5-44a plots the observed acoustic transfer function modulus for three incidence angles: 4-, 8-, and 12-degrees. The measured static structural modes are included in this figure and also summarized in Table 5-6. The transfer function modulus for the 15%-chord position normal force ( $C_n$ ) is presented in Figure 5-44b. Figures 5-44c, d, and e compare the transfer function moduli for the 15%-chord normal force and acoustic radiation at the three incidence angles, respectively. The conclusions one may draw from these graphs (at least as far as the fluctuating surface pressures near the leading edge are concerned) include (a) the acoustic response peak of Figure 5-43 at about  $k = 1$  is essentially independent of incidence angle (and therefore the mean airload) and any structural modes at that particular frequency; and (b) above about  $k = 1.5$ , the acoustic and structural responses are not necessarily tightly coupled, an exception being the mode at 140 Hz or  $k = 3.2$ , where a strong acoustic/aeroelastic coupling exists.



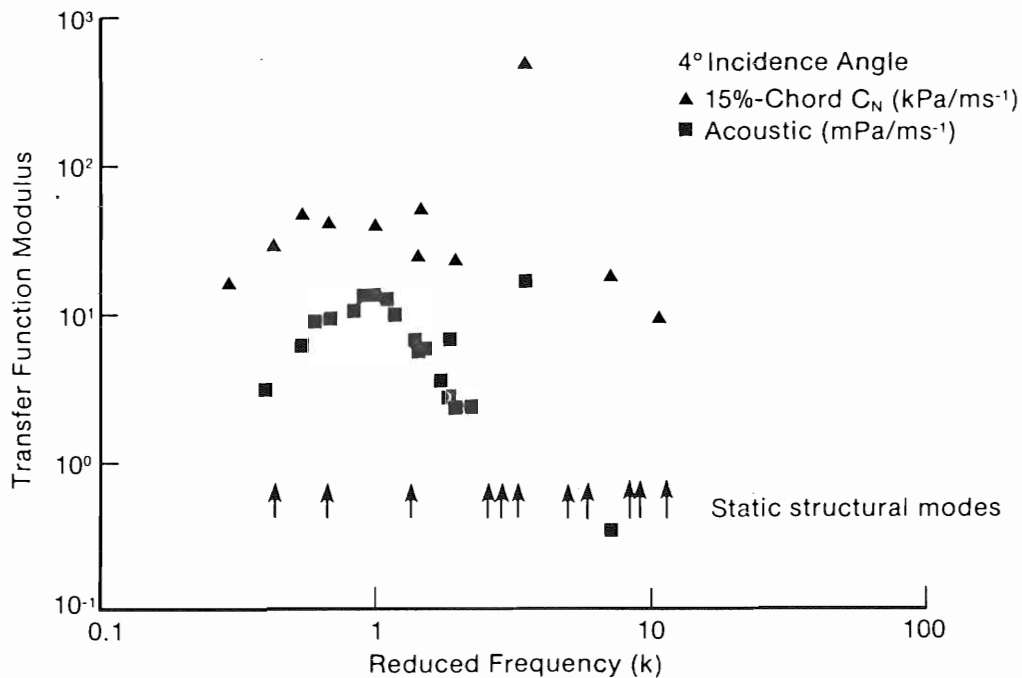
004781

**Figure 5-44a. Measured Turbulent Acoustic Transfer Function Modulus for 63(2)-015 Test Section at Incidence Angles of 4, 8, and 12 Degrees**



004782

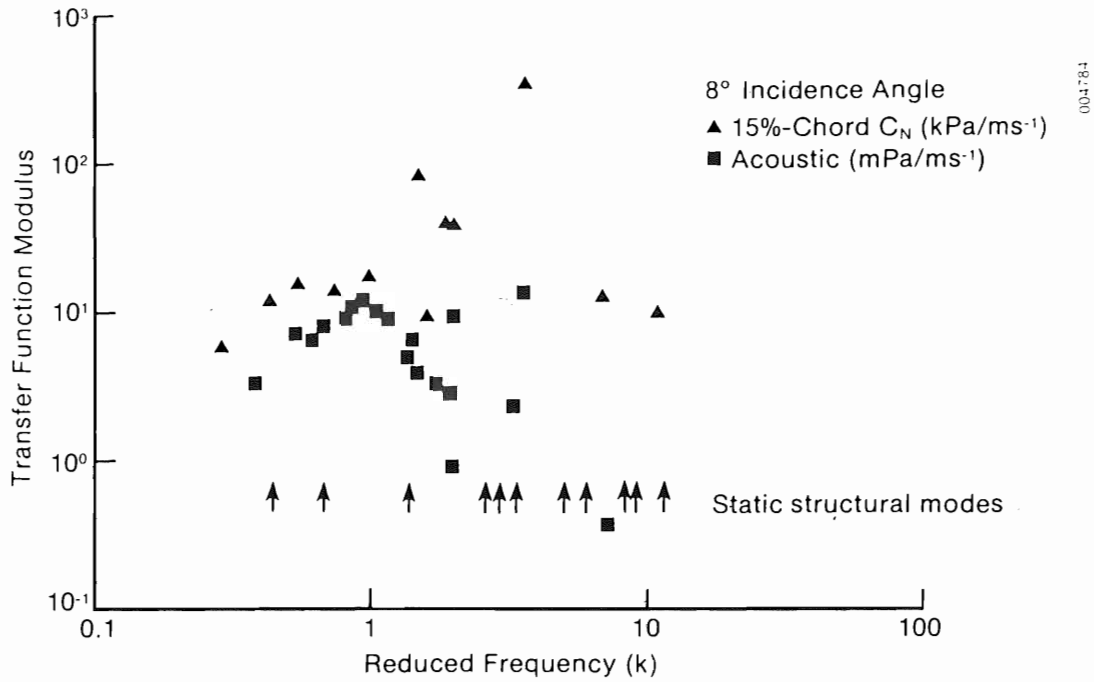
Figure 5-44b. Measured Turbulence Normal Force ( $C_n$ ) Transfer Function Modulus at 15%-Chord for 63(2)-015 Test Section at Incidence Angles of 4, 8, and 12 Degrees



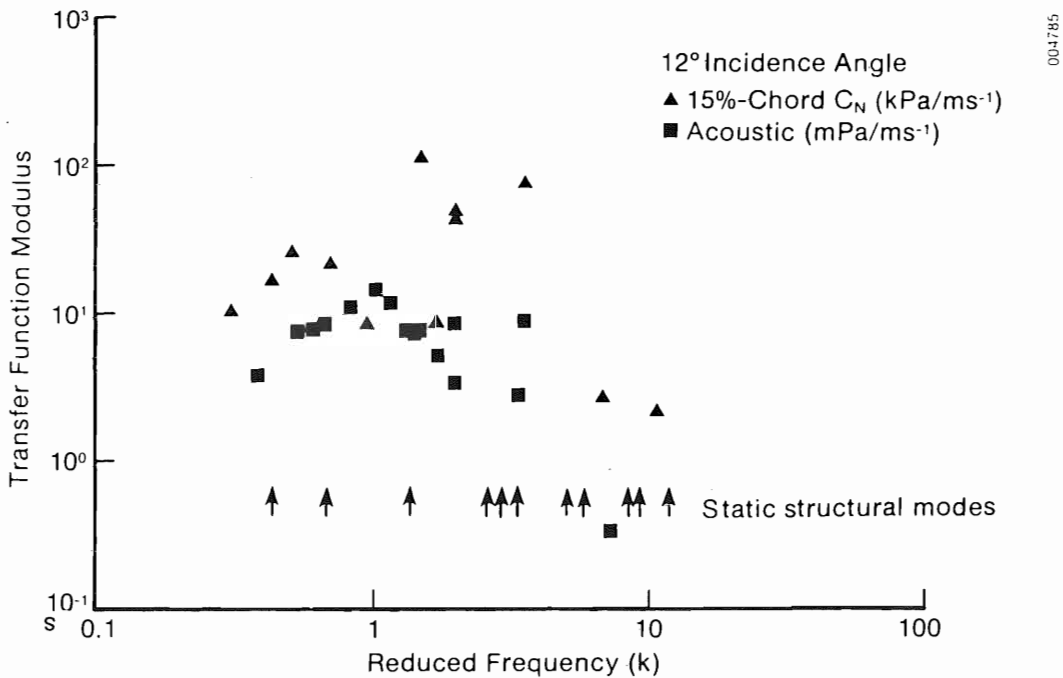
004783

Figure 5-44c. Comparison of Acoustic Emissions and Normal Force ( $C_n$ ) at 15%-Chord Transfer Function Moduli for 63(2)-015 Airfoil Section at an Incidence Angle of 4 Degrees





**Figure 5-44d. Comparison of Acoustic Emissions and Normal Force ( $C_n$ ) at 15%-Chord Transfer Function Moduli for 63(2)-015 Airfoil Section at an Incidence Angle of 8 Degrees**



**Figure 5-44e. Comparison of Acoustic Emissions and Normal Force ( $C_n$ ) at 15%-Chord Transfer Function Moduli for 63(2)-015 Airfoil Section at an Incidence Angle of 12 Degrees**

**Table 5-6. Measured Structural Resonant Modes of 63(2)-015 Airfoil Test Section**

Excitation Frequency		Torsional Mode	Bending Mode	Modal Cross-Coupling Characteristic <sup>c</sup>
Cyclic (Hz)	Reduced <sup>a</sup> (k)	Damping Characteristic <sup>b</sup>	Damping Characteristic <sup>b</sup>	
19.2	0.44	Low	High	Weak
29.6	0.67	Moderate	Moderate	Strong, inphase
58.4	1.33	Low	Moderate	Moderate
112	2.56	Low	Low	Strong
124	2.83	Low	Moderate	Weak
140	3.20	Moderate	High	Weak
228	5.21	Moderate	Moderate	Moderate
255	5.82	Moderate	Moderate	Moderate
364	8.31	Moderate	Moderate	Moderate
385	8.80	High	High	Moderate
480	11.00	High	High	Strong
500	11.42	High	Very High	Weak

<sup>a</sup>Based on 2-chord cylinder excitation tunnel velocity of 32.1 ms<sup>-1</sup>.

<sup>b</sup>Mode damping degree estimate: low =  $\zeta < 0.05$ ; moderate =  $0.05 < \zeta_c$ ; high =  $\zeta > \zeta_c$ .

<sup>c</sup>Cross-coupling mode estimate: weak =  $A_B(f) < 0.1 A_T(f)$ ; moderate =  $0.1 A_T(f) < A_B(f) < 0.9 A_T(f)$ ; and strong =  $A_B(f) \approx A_T(f)$ , where  $A_T(f)$  = torsional response and  $A_B(f)$  = bending response.

### 5.3 SUMMARY AND CONFIRMATION OF CAUSAL FACTORS RESPONSIBLE FOR AERODYNAMIC GENERATION OF MOD-1 ACOUSTIC IMPULSES

In this section, we summarize the physical parameters that contribute to the large transient lift fluctuations and resulting impulsive noise generation by the MOD-1 wind turbine. We also relate, where possible, which of those parameters and their interactions are responsible for the results discussed in Section 4.0.

#### 5.3.1 Summary of Physical Parameters Responsible for MOD-1 Acoustic Impulse Generation

The breadth and depth of the dynamic physical mechanism responsible for the lift transients and impulse noise are substantial and the interactions are complex. The best overall view is found in Figure 5-1, in which the component processes are systematically presented. In order to provide a comprehensive summary of the process, it is both necessary and convenient to subdivide the overall situation into three major components which exert influence over the impulse generation characteristics: operational, cylinder wake, and rotor blade aerodynamic properties. We will identify the major causal factors in each of these categories.

### 5.3.1.1 Operational Parameters

The pertinent physical parameters in this classification can be further subdivided into those that are design related and those that are environmental. The design parameters include the physical shape of the turbine rotor and its support tower consistent with a rated power generation capacity. These constraints have been translated into the rotor diameter and rotational speed and the size of the elements of the pipe-truss tower required to safely support the power train under both operating and survival conditions. The rotor disk size and required rotational speed determine the operating Reynolds and Mach number regimes, which vary as a function of the span distance because of the  $R \Omega$  dependence (where  $R$  is the rotor (span) radius and  $\Omega$  the rotation rate). These two parameters, in conjunction with the airfoil shape, heavily influence blade boundary layer stability and leading edge separation characteristics, thus "locking in" the type of transient, unsteady, lift response that occurs should the outer portions of the rotor encounter the "right" inflow structures. The basic tower design has dictated the cylinder wakes and the blade-to-leg distances that control the downstream blade intersection distances and therefore the wake vortex circulation scales encountered, a major factor in the unsteady processes involved.

Environmental parameters, dominated by the magnitude and turbulence characteristics of the freestream inflow, exert considerable influence over the impulse generation process. Specifically, they are

1. Freestream velocity--controls leg vortex intensity, blade section local Reynolds and Mach numbers, and the quasi-steady value of the blade incidence angle.
2. Vertical wind shear below hub height--controls shedding characteristics of tower legs which in turn determines the range of the reduced frequency parameter  $k$  as well as the level of discreteness found in the wakes. May also exert considerable influence over whether or not the tower leg boundary flows become supercritical, subsequently enhancing the intensity of the vortex elements and setting the wake width.
3. Vertical (hydrodynamic) stability--believed to affect the discreteness of the tower leg wake flows (and therefore the  $k$ -range) through influencing the freestream shear or the leg wakes themselves, or both.
4. Upwind fetch--coupled with the vertical stability, it controls the vertical shear and the turbulence space scales which have a strong influence on the shedding characteristics of the cylindrical tower legs.
5. Wind direction--coupled with the geographic orientation of the tower, it controls the blade-to-leg position in the wakes and the upstream fetch.

As can be seen from the above, the machine designer does have control over many of the factors listed, but an understanding of the complex interaction of these and those following is necessary to minimize impulsive noise generation by design and siting.

### 5.3.1.2 Cylinder Wake Parameters

As the flow diagram in Figure 5-1 indicates, freestream turbulence impinging on a downwind WECS support tower is somehow modified by the incorporated structural elements. We have previously identified the vertical, 0.5-m-diameter, cylindrical legs as the primary source of the MOD-1 impulse noise through the strong wake circulations created in their lee. A number of environmental parameters that exert influence over the dynamic characteristics of these leg wakes were summarized in Section 5.3.1.1.

In Section 5.2, we identified the vortex-dominated wake circulation with its strong, transverse (to the blade plane) velocity fields and viscous core pressure deficits confined to a space scale equivalent to the mean blade chord dimension as the direct cause of the transient lift fluctuations. More comprehensively, the list should include the following:

1. Wake vertical coherency--related to separation along a straight line, these vortices become vortex tubes, which are intersected by the rotor blade simultaneously along a good portion of the span supporting the greatest airload, causing maximum impulsive radiation if involved in a transient leading edge separation and loss of lift.
2. Wake width--bounds the scale of the vortex circulations, thereby effectively bounding the reduced frequency parameter for the transverse direction; has been shown to be the source region for the impulse generation, the peak of which occurs at a disturbance/space scale of the blade chord dimension ( $k \sim \pi$ ).
3. Viscous effects--the strong transverse velocity gradients containing pressure deficit disturbances have been found to be instrumental in causing a transient separation of the blade's leading edge boundary layer.
4. Level of discreteness--broadband wake turbulence has been shown to impart a stabilizing influence on leading edge boundary layer separation, whereas a narrowband, discrete wake exerts a destabilizing effect.
5. Time-varying properties--are far more important in developing an understanding of the unsteady, blade-wake interaction process.

### 5.3.1.3 Blade/Airfoil Properties

The shape of the airfoil section employed in the rotor design, when combined with the local quasi-steady incidence angle, determines the chordwise pressure distribution and separation characteristics; i.e., leading versus trailing edge. The abruptness of leading edge separation, in addition to the blade shape, is influenced by the disturbance reduced frequency  $k$ , inflow pressure deficit  $\Delta p_v$ , and the quasi-steady incidence angle,  $\bar{\alpha}$ .

### 5.3.2 Comparison of Supportive Research Effort Results with Analysis of Physical Parameters Related to MOD-1 Noise Situation

From the results of the full-scale field experiment and the two wind tunnel experiments discussed in this section, we now believe we can offer at least a partial explanation of some of the results of the MOD-1 impulse analysis presented in Section 4.0. First, we must review the significance of the impulse rise-rate and overpressure parameters; the meaning of the energy intensity is not altered. The rise-rate parameter reflects the rate of change in the radiated acoustic pressure field which, through Eq. (4-5) in Section 4.1.1.3, is given by the time rate of change of the lift fluctuations. Thus, the rise-rate parameter can be viewed as a sensitive measure of the lift characteristic related to transiently separating and reattaching boundary layers. The acoustic peak dynamic or overpressure parameter is a measure of (1) the extent of the transient stall observed (i.e., is the lift completely cancelled or does reattachment occur after a delay?); and (2) the magnitude of the instantaneous airload, which is a function of the quasi-steady incidence angle and any hysteresis overshoot present. The statistical distributions of these two parameters, particularly the former, can therefore provide some insight into the unsteady aerodynamic process operating as the MOD-1 rotor blades pass through the tower leg wakes.

### 5.3.3 Interpretation of the MOD-1 Impulsive Noise in Terms of the Unsteady, Fluid Dynamic Parameters

In Section 5.2 we identified several aerodynamic parameters that are responsible in some way for the unsteady, nonlinear phenomena observed. Confirming these with our identification of the spanwise coherency  $\lambda_c$  from Section 4.1.1.2 (which describes a 3-D effect), we can summarize the known or at least suspected unsteady, fluid dynamics parameters that have an influence over the transient, unsteady lift-generated acoustic impulses as the MOD-1 blades pass through the tower leg wakes, including

- the blade airfoil shape
- the reduced frequency  $k$
- the quasi-steady incidence angle  $\bar{\alpha}$
- the section chord Reynolds number  $Re_c$
- the section Mach number  $M_\infty$
- the spanwise lift coherency  $\lambda_c$
- the imbedded vortex core pressure deficits  $\Delta p_v$ .

The principal environmental parameters affecting the unsteady, structural characteristics of the tower leg wakes include

- the freestream velocity  $U_\infty$
- the surface-to-hub height vertical shear  $\partial U_\infty / \partial z$
- the vertical stability of this layer expressed by the gradient Richardson number, or

$$Ri = g(\partial\bar{\theta}/\partial z)/\bar{\theta}(\partial\bar{u}_{\infty}/\partial z)^2, \quad (5-14)$$

where

- $\theta = T(p/P_0)^{0.287} =$  potential temperature
- $p =$  local barometric pressure, kPa
- $P_0 = 100$  kPa = reference barometric pressure
- $g =$  gravity acceleration
- $T =$  absolute air temperature (K)
- $z =$  height (m) ,

plus

- the Strouhal excitation band mean-square velocity  $\bar{u}_{St, \Delta f}^2$
- the wake downstream distance  $d_s$  (in leg diameters)
- the diameter of cylindrical legs  $D$
- the cylinder Reynolds number,  $Re_D$
- the wind direction.

The overall situation (at least from a generation perspective) with at least 14 known variables, not all of which are independent, provides some perspective into the complexity of the process. If we look only at the turbine itself for a moment and concentrate only on 35 rpm operation, the list of blade variables may be reduced to  $k$ ,  $\bar{\alpha}$ ,  $\ell_c$ , and  $\Delta p_v$ , all of which are functions of time. These may be thought of as "receptor" parameters, since they are instrumental in transforming the characteristics of the turbulent wake inflow into an unsteady aerodynamic lift response. At least seven environmental variables influence the structure of the leg wakes, but treating the leg diameter as a constant allows the six remaining to be thought of as "excitor" variables, all of which are tied to local atmospheric conditions. The stochastic nature of these six parameters makes the impulsive acoustic output itself probabilistic.

### 5.3.3.1 Confirmation of Influence of Reduced Frequency Parameter on MOD-1 Impulse Noise Generation

Our wind tunnel experimentation, using a symmetrical airfoil section that exhibits a chordwise pressure distribution similar to the 44xx-series used on the MOD-1, has revealed the reduced frequency sensitivity of the inflow turbulence structure on the radiated acoustic pressure field. Figure 5-43 indicates the most sensitive range of  $k$  from approximately 0.5 to 3.5. The peak sensitivities occurs at  $k \approx 1$  and  $\pi$  signifies a maximum coupling between the wake perturbation excitation and an airfoil. In order to compare the model test results, which admittedly do not achieve the proper dynamic similarity with the operational MOD-1 situation, we have repeated Figure 3-10 as Figure 5-45 of the acoustic frequency spectrum of a single MOD-1 impulse

reaching out of houses 1 km away. In this later figure, we have included the reduced frequency scale. The peaks, as indicated, occur at 13.5, 28, and in the band from 41.8 to 59.1 Hz, which translate to k-values of 0.71, 1.47, and 2.19-3.11 for a blade span position of 80%. It is also reasonably clear from this plot and others that the bulk of the impulse radiation occurred over a k-range of 0.5 to 3.2 during moderate-to-severe generation episodes. The entire range is broader when all cases are considered, varying from 0.33 to 5.1 (6.25-97.3 Hz) at 35 rpm and 0.15 to 2.26 (4.4-6.5 Hz) at 23 rpm. Thus, the moderate-to-severe acoustic impulse radiation occurred over the same reduced frequency range observed in the wind tunnel tests, and this indicates that a similar unsteady physical process is taking place on the MOD-1 blade in the leg wakes.

### 5.3.3.2 Comparison of MOD-1 Results with Other "Receptor" Variables

The remaining "receptor" variables include the quasi-steady incidence angle  $\bar{\alpha}$ , the coherent spanwise lift  $\bar{l}$ , and the imbedded vortex pressure deficits  $\Delta p_v$ . In only  $\bar{\alpha}$  do we have<sup>C</sup> any direct information from the MOD-1, because<sup>V</sup> of the extreme difficulty of obtaining direct measurements of the other quantities. The statistical analysis of the impulses and corresponding operating parameters reported in Section 4.0 found that the impulse severity associated with the south tower leg was positively correlated with the attack angle (as would be expected), but the impulses related to the east leg were weakly negatively correlated (Table 4-8). As mentioned, we attribute some of what was found to the off-design operating conditions under which the data were taken; i.e., the load bank used in the June 1980 testing. We do, however, believe that the marked differences in the attack angle correlation for the two wakes are indicative of substantial turbulent structural variations in the two wakes; this is borne out by other measures, some of which were discussed in Section 4.0.

### 5.3.3.3 Comparison of MOD-1 Results with Available "Excitor" Information

Of the seven "excitor" variables identified in Section 5.3.3, we have quantitative information on only two: the hub-height freestream velocity and the leg-to-blade distance D. We can, however, make some comments regarding the vertical stability and wind shear parameters.

**Attack Angle Correlation.** The results of the statistical analysis reported in Section 4.0 have confirmed that the severity of the generated impulses depends strongly on the magnitude of the wind speed. We indicated earlier, in our discussion of vortex dynamics, that the freestream velocity was a key parameter in determining the embedded vortex radial velocity and core pressure deficit distributions in the tower leg wakes which, when cut transversely by the blade, control the  $C_{Lmax}$  overshoot and leading edge separation.

**Leg-to-Blade Distance Correlation.** This variation, previously discussed, is associated with substantial differences between the radiated impulses as a function of downwind distance from the south and east tower legs. We have attributed this variation to marked differences in the turbulent structural properties of each of these wakes.

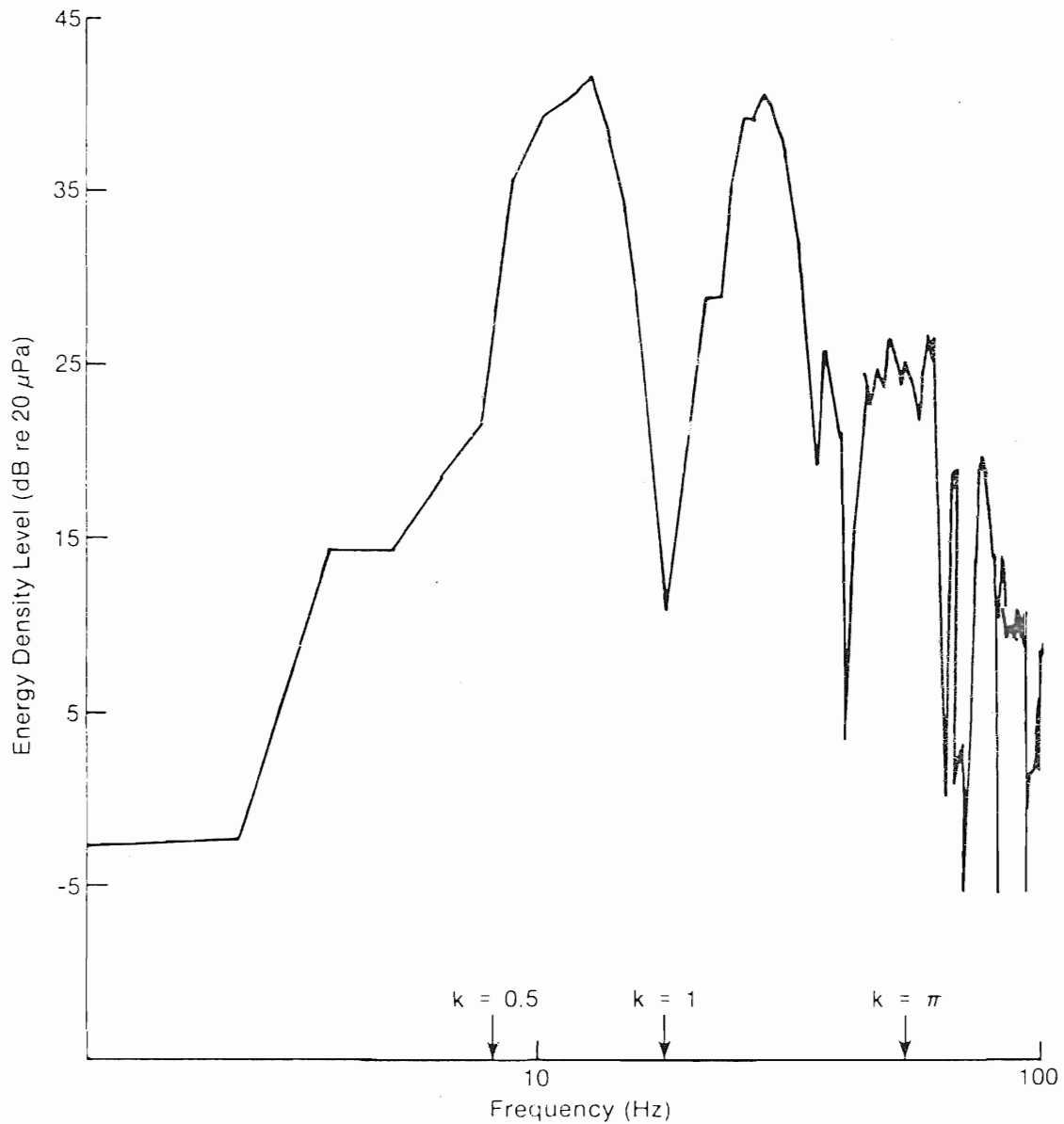


Figure 5-45. Single MOD-1 Impulse Energy Density Level Spectrum Reaching House #8 with Equivalent Critical Reduced Frequency Values Indicated



**Effect of Wind Shear, Stability, and Strouhal Excitation on Observed Impulse Severity.**

While we have no direct information about the vertical shear and stability conditions present during the March and June 1980 testing periods, the results of the Rocky Flats experiments have given us some insight into the importance of these variables. One characteristic of strong shear layers is the tendency for discrete, spatially coherent turbulent flows to develop, particularly if inflectional instabilities also develop. We found, for example, that there is a strong diurnal cycle in the appearance of discrete energy in the tower cylinder Strouhal excitation band. This is tied to the development of the nocturnal boundary layer and is most pronounced an hour or so before to an hour or so after local sunset, with a similar situation at sunrise. The increasing stability of the surface layer in the evening and the opposite in the morning is seen as one of the causes. We observed the worst impulsive situations at the MOD-1 during these periods, particularly during the evening hours, as borne out by the frequency of homeowner complaints.

In Section 4.0 we mentioned the presence of very strong vertical shears upstream of the MOD-1. We believe this has its roots in two sources related to the upstream fetch: the complex terrain upstream of the site and the top of the forest canopy, which reached the height of the lowest elevation of the rotor disk. When compounded by an increased lower layer stability, such turbulence-generating mechanisms could easily produce a flow with considerable discrete energy in the Strouhal excitation band and modify the leg wake turbulent structures in a manner similar to what happened when an augmenting cylinder was placed upwind in the wind tunnel tests. We believe that the more severe impulsive conditions observed during the June 1980 experiments, compared with March (see Figure 4-11), are a direct result of the trees surrounding the turbine being in full leaf. The leaves served to intensify the shear layer existing immediately above the forest canopy and, thus, the Strouhal excitation of the tower legs.

The marked difference in the impulse characteristics between the east and south legs appears to relate to two factors: (1) an upwind fetch influence that affects the Strouhal excitation and therefore the shedding characteristics of the east and south legs, and (2) whether or not the wind direction places these legs in the wakes of their upstream counterparts. All of the June 1980 plots of the impulse characteristics shown in Figures 4-20 through 4-22, particularly the impulse energy intensity plot of Figure 4-20, reflect this upstream influence on the south leg impulses by the peak in the curves when the blade was passing between 7.5 and 8.5 downstream leg diameters. Under this condition, the north and west legs are immediately upstream. That this does not occur for the east leg suggests that different fetch characteristics exist for the flow upstream and parallel to the northeast side of the tower. The open parking area on that side of the tower may have been responsible. The March data, Figures 4-23 through 4-25, show a similar but less intense picture, except for the rise-rate plot of Figure 4-25. This graph indicates a somewhat similar pattern for both legs. Again, the lack of leaves on the upstream forest may have had an influence.

## SECTION 6.0

### THE ROLE OF ATMOSPHERIC PROPAGATION IN THE MOD-1 NOISE SITUATION

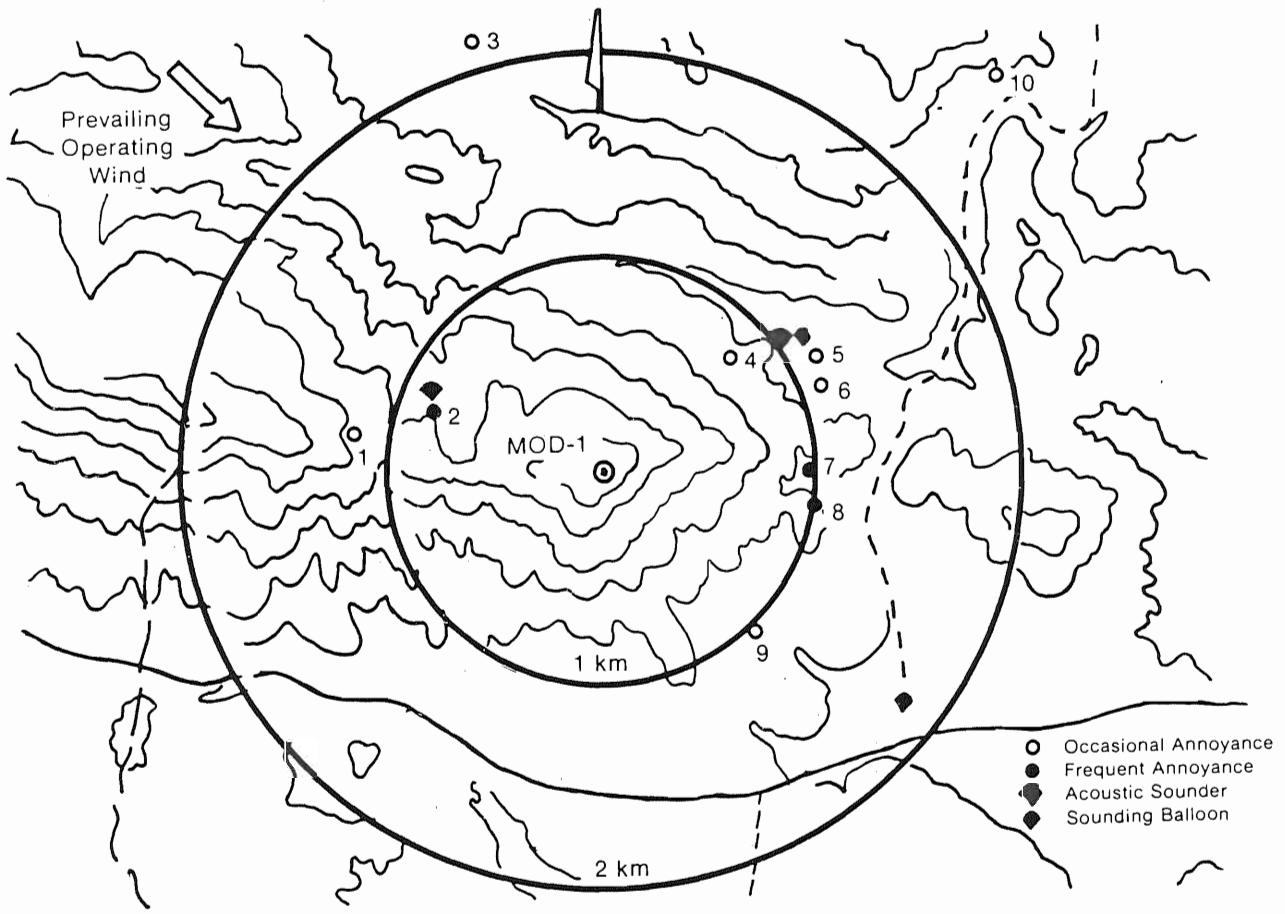
The multidisciplinary group from Penn State was responsible for examining the role of atmospheric and ground propagation of the impulsive noise radiated by the MOD-1 turbine. As mentioned, a more detailed discussion of their initial conclusions appears as SERI Report No. TR-635-1292. In this section, we have included some of the highlights of their investigation.

#### 6.1 ATMOSPHERIC AND TERRAIN STRUCTURAL FEATURES CONTROLLING MOD-1 NOISE PROPAGATION TO AFFECTED HOMES

During our first on-site visit to the MOD-1 late in October 1979, we realized immediately upon viewing the turbine, located atop Howard's Knob (see Figure 6-1) and surrounded by deep valleys in almost every direction, that it presented a complex propagation situation because of terrain features alone. The low-frequency acoustic energy contained in the impulses generated by the MOD-1 is not significantly attenuated by the atmosphere; the only effective extinction mechanism is spherical divergence as the distance from the source increases, or what is usually referred to as "geometric spreading." Furthermore, the acoustical impedance of the surrounding ground and forest in this frequency band (0-100 Hz) is essentially infinite, making reflections from the complex terrain a major factor in the propagation paths.

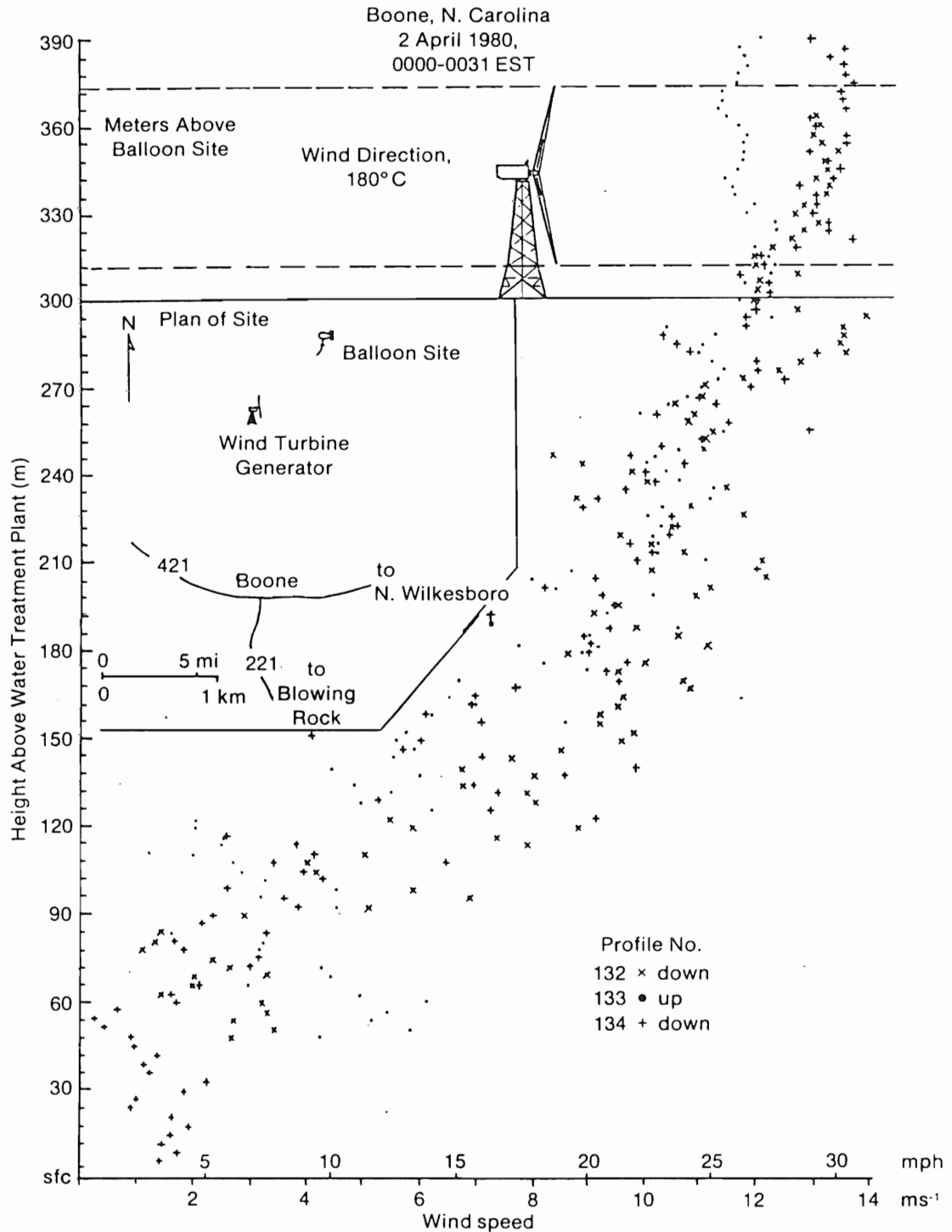
The large elevation differences between the height of the turbine and the houses in the valleys below provide a substantial atmospheric layer in which the vertical distribution of wind velocity and temperature can serve to bend or refract the sound waves away from a radially diverging pattern that would occur in a windless, isothermal atmosphere. Vertical gradients of wind velocity (shear) are about twice as effective in the refraction of sound waves as temperature (density) gradients are. In the deep terrain surrounding the turbine site, it was not initially clear which of these were more important, because strong temperature inversions (stable atmospheric layers in which the temperature increases with height) commonly form in such valleys at night, the time when many of the complaints were received.

Two acoustic sounders or "sodars" were deployed remotely to measure the vertical distributions of thermal disturbances and stratification with height on a continuous basis. One unit was placed in the deep valley immediately to the east of the turbine and the other in a generally upwind location near a home that experienced frequent annoyances (see Figure 6-1). During the major field measurement effort of March-April 1980, two tethered sounding balloon systems supplemented the sodars to obtain direct measurements of vertical profiles of wind velocity and temperature in the valleys to the east and southeast. Figure 6-2 presents three consecutive tethered balloon wind velocity profiles taken from the site at the Appalachian State University (ASU) water treatment plant northeast of the turbine. The marked positive shear (increase in velocity with height) is quite evident up to the height of the turbine. Also significant is the substantial variation in the wind shear at turbine height evidenced by the three profiles, particularly between numbers 133 and



589400

Figure 6-1. Area Surrounding MOD-1 Site Showing Terrain and Locations of Complainants' Homes (Also appears as Figure 1-2)



004786

**Figure 6-2. Three Consecutive Tethered Balloon Profiles of Wind Speed above the ASU Water Treatment Plant**

134, which were taken 10 minutes apart. Figure 6-3 presents representative vertical profiles of wind velocity and temperature, in which a mean has been fitted to the observed points through the use of digital cubic spline filters. Figure 6-4 presents an actual sodar record taken at the ASU water plant on the night of 7 February 1980, when the SERI staff were taking sound measurements at the turbine. The formation of an inversion is evident just below the elevation of Howard's Knob (300 m) and just before 2100 hours local. From 2115-2150 hours the inversion rose from its mean height of 260 m to 420 m, a period when the resident of house #4 complained of being disturbed by the turbine. Again, note the strong shear zone between 175 and 200 m.

## 6.2 RESULTS OF THE PROPAGATION INVESTIGATION

One of the objectives of the Penn State study was to determine whether the turbine-generated disturbance was being propagated through the air, the ground, or both. As we discussed in Section 3.1.2.3, they found that the airborne acoustic impulse was the propagation mechanism responsible for the residents' complaints.

Armed with both the direct and indirect vertical profile measurements acquired from the tethered balloons and sodars, plus information on local terrain contours, Penn State developed a computer program for calculating acoustic ray tracing of the MOD-1 noise propagation along chosen radials. These directions were chosen to pass near or through several of the complainants' homes, to obtain a better appreciation of the acoustic propagation. In particular, the interactions of the terrain, vertical wind and temperature profiles, and occurrences of complaint episodes at these specific locations were of interest.

Figures 6-5 and 6-6 illustrate ray traces made along a  $048^{\circ}$  bearing (with respect to true north) from the turbine, that intersects house #4 (see Figure 6-1) and for which the radial position is shown. These traces represent the modeled acoustic propagation for two vertical profiles taken one hour apart (1930 and 2032 hours, 18 March 1980). Both figures show an enhancement (referred to as a caustic) of the propagated turbine-induced acoustic pressure field over that which would be observed from geometric spreading alone at the base of the ridge at a horizontal radial distance of 1200 m. The trace of Figure 6-6, however, shows this caustic to be more severe, indicating that a higher level of turbine noise would be experienced at this location, while at the same time, turbine sounds are being carried long distances by the acoustic duct present at the elevation of the turbine. Figure 6-6 indicates that the turbine noise levels may be slightly higher at the location of House #4, more than Figure 6-5 does, because of the greater number of rays intersecting the general area.

Figure 6-7 displays an acoustic ray trace analysis for the  $105^{\circ}$  radial from the turbine which passes approximately midway between houses #7 and #8, both of which experienced frequent periods of severe annoyance. This trace shows the existence of an area of enhanced sound levels (caustic) at these homes' position with respect to the turbine. Also, the role of the terrain on the east slope of Howard's Knob in reflecting acoustic energy toward these residential structures is obvious. Figures 6-8 and 6-9 present representative

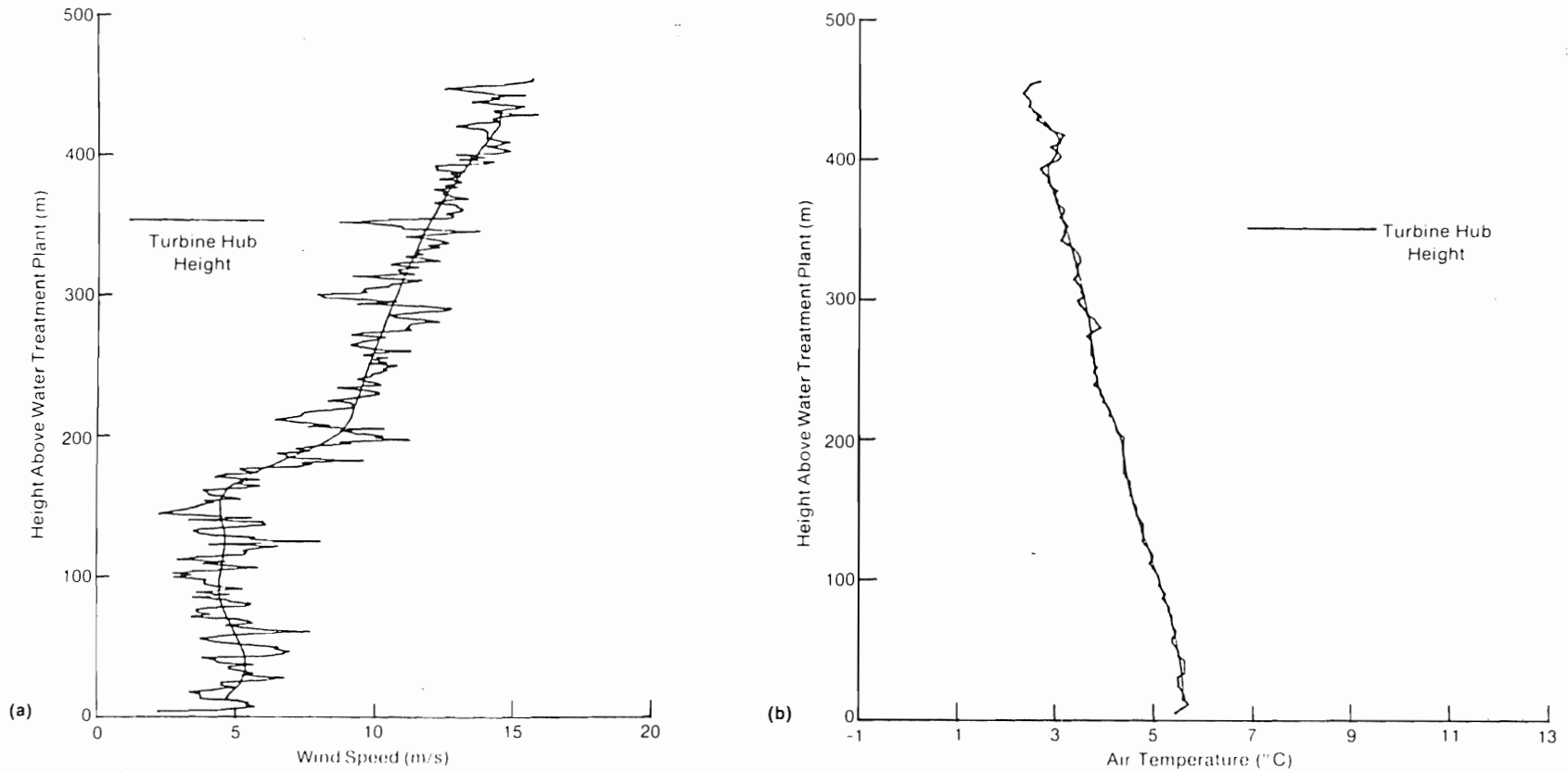


Figure 6-3. Representative Vertical Profiles of (a) Wind Speed and (b) Air Temperature Taken above ASU Water Treatment Plant

Source: Ref. [3].

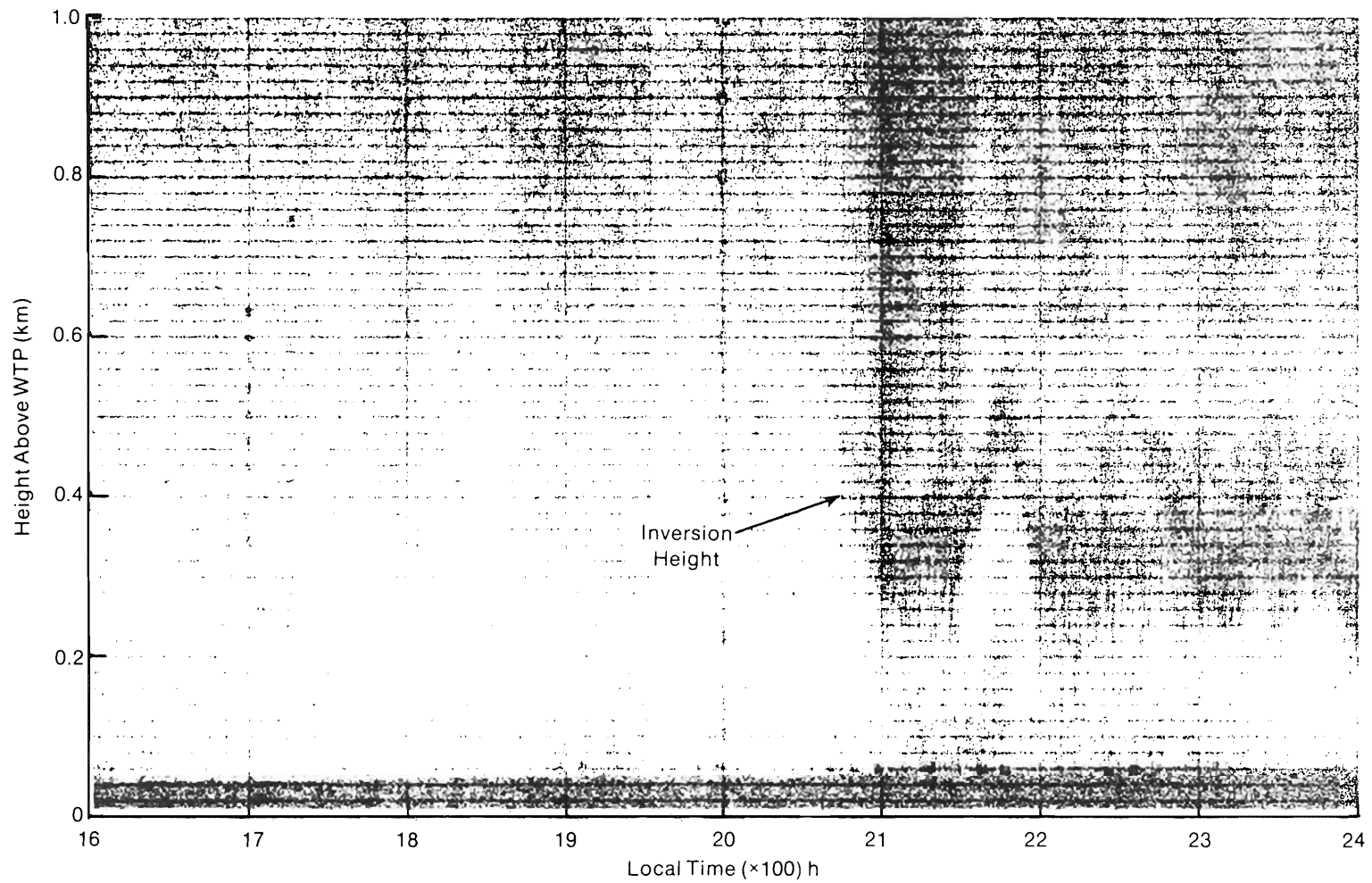
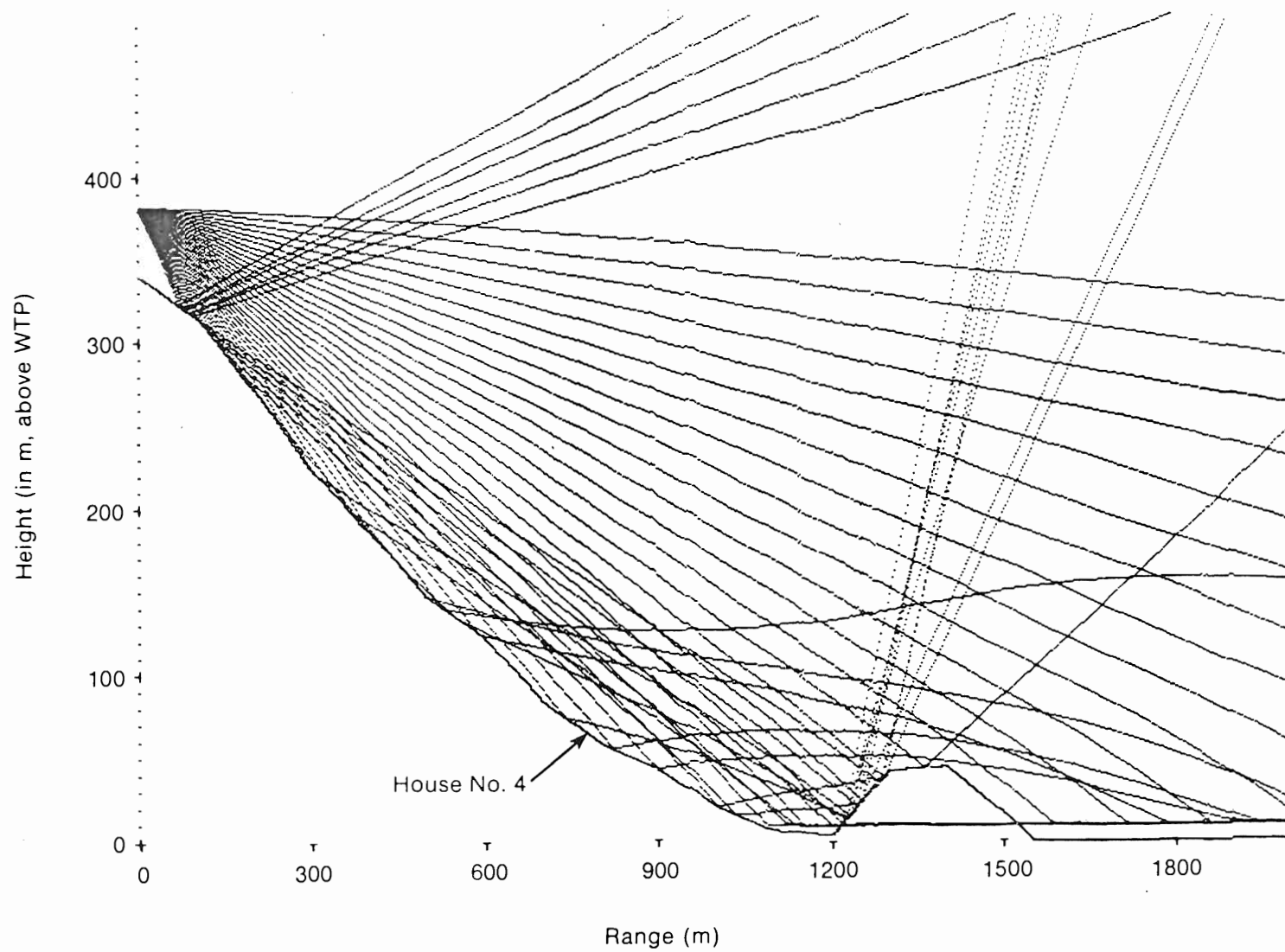


Figure 6-4. SODAR Record of 7 February 1980 above ASU Water Treatment Plant

Source: Ref. [3].



004790

Figure 6-5. Acoustic Ray Tracing for 1930 Hours, 18 March 1980, along 048° Radial from MOD-1 Site (Heights shown above water treatment plant [WTP])

Source: Ref. [3].



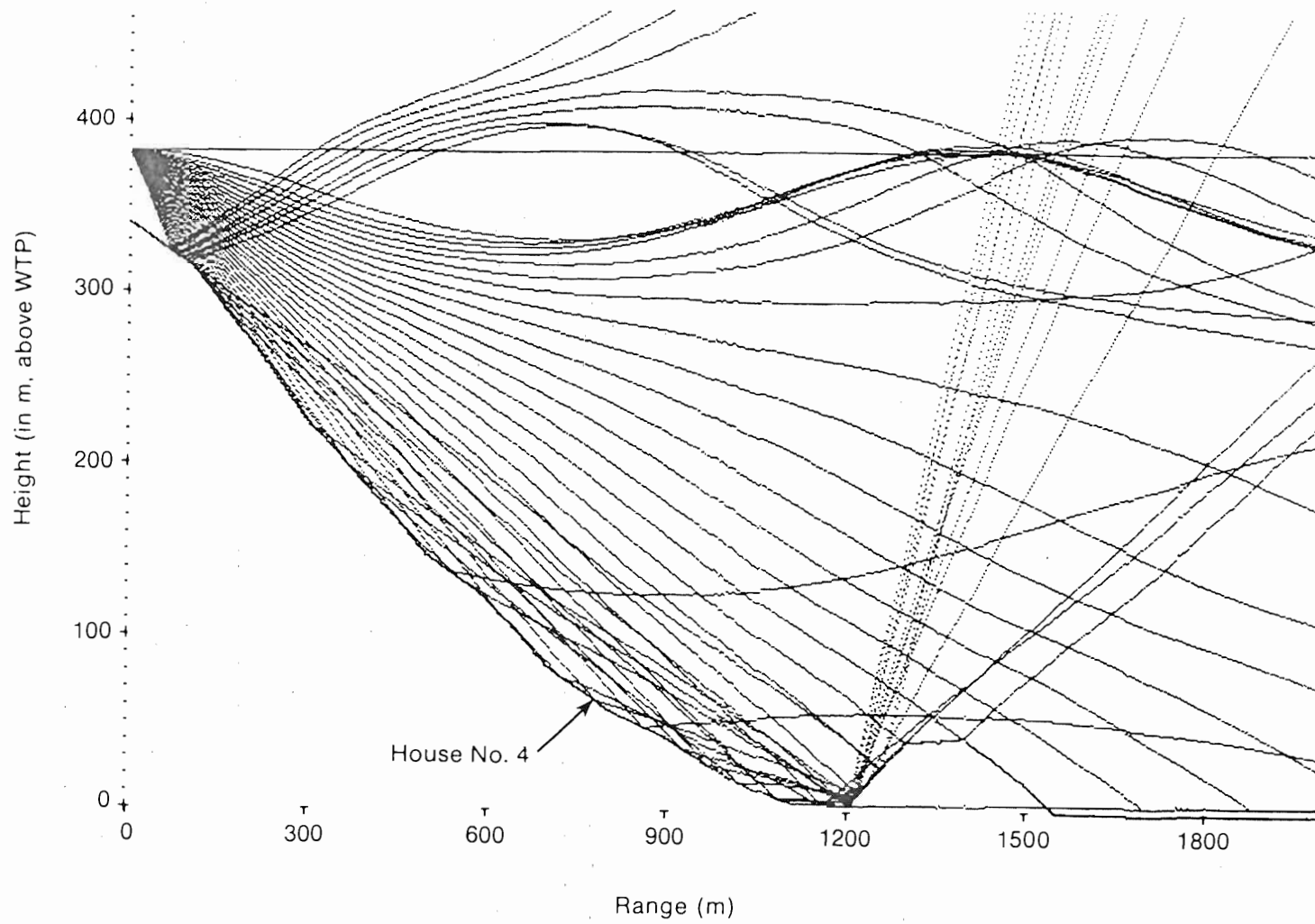
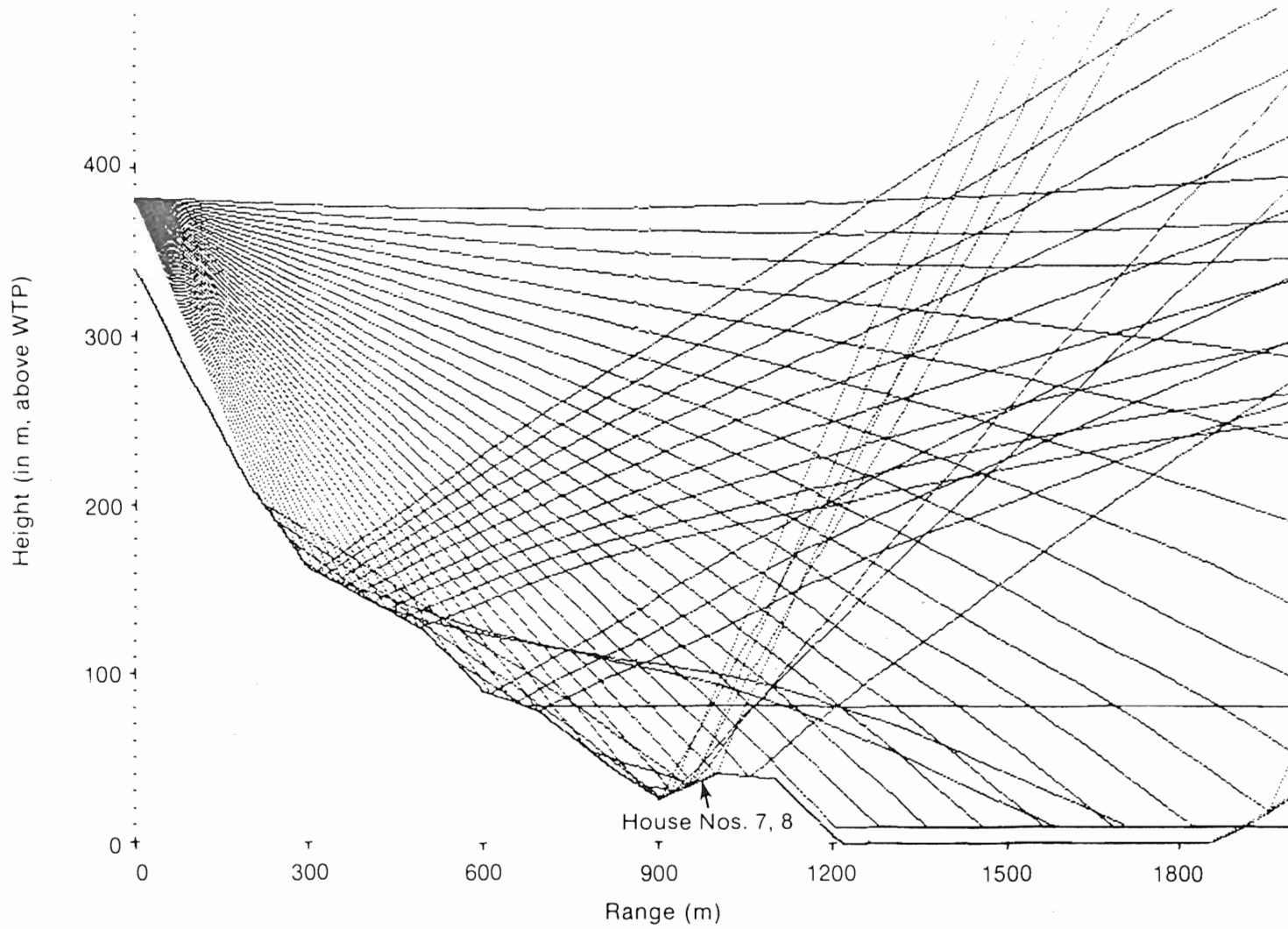


Figure 6-6. Acoustic Ray Tracing along 048° Radial for 2032 Hours, 18 March 1980

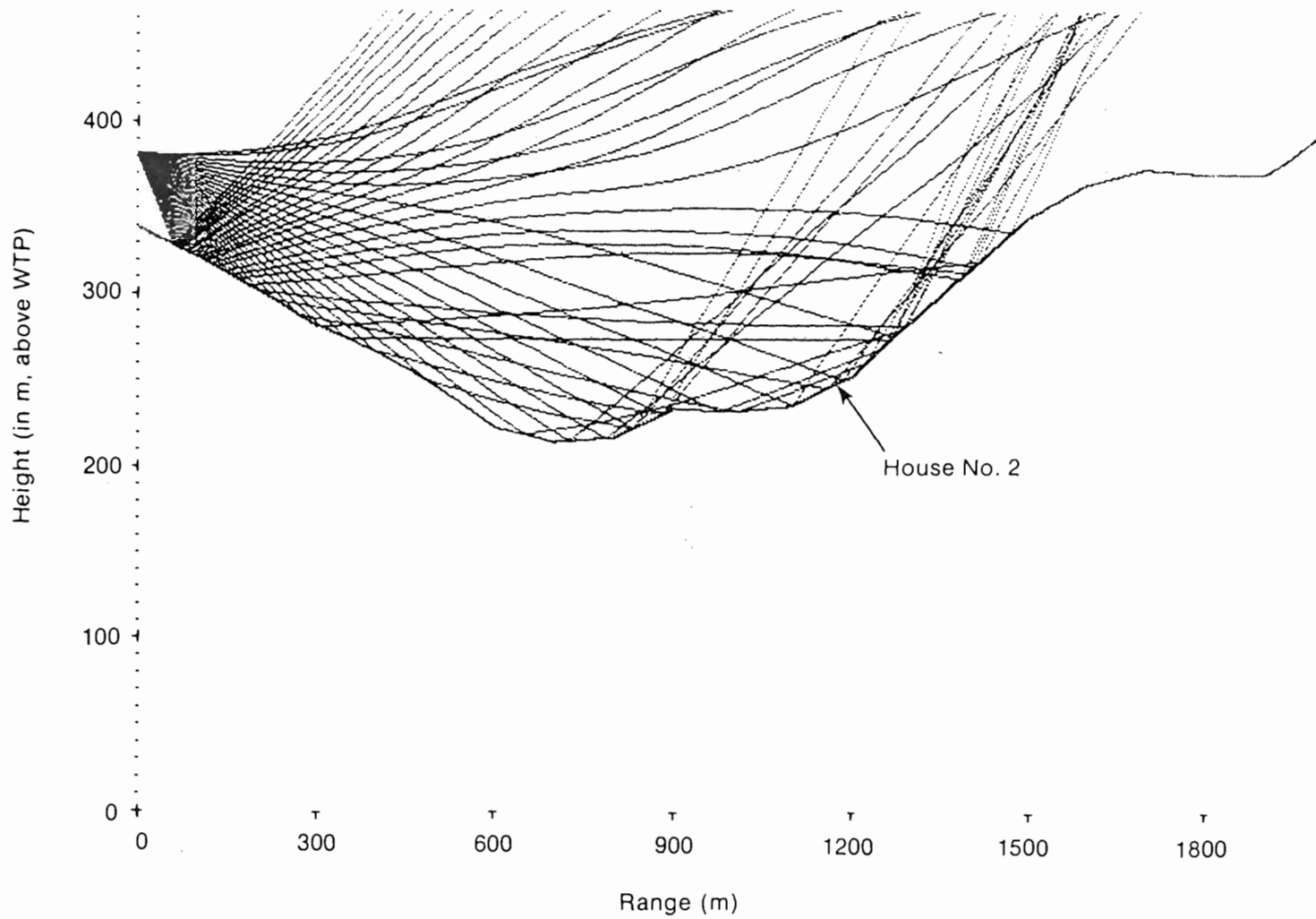
Source: Ref. [3].



004792

Figure 6-7. Representative Acoustic Ray Tracing along  $105^{\circ}$  Radial from MOD-1 Site Passing near Houses #7 and #8

Source: Ref. [3].



00479J

Figure 6-8. Representative Acoustic Ray Tracing along 277° Radial from MOD-1 Site Passing near House #2  
Source: Ref. [3].

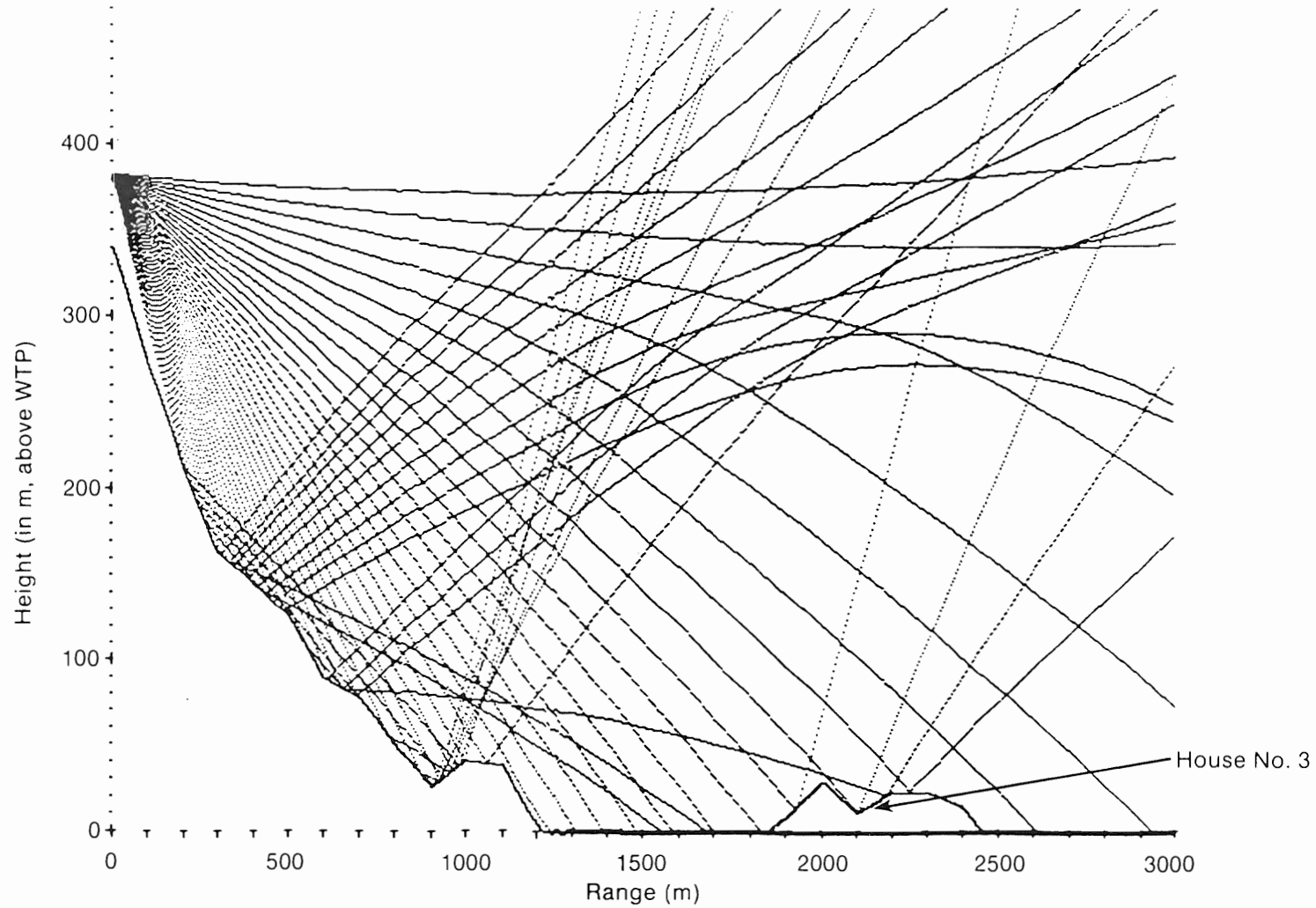


Figure 6-9. Representative Acoustic Ray Tracing for 355° Radial from MOD-1 Site Passing near House #3  
Source: Ref. [3].

traces for bearings of  $277^{\circ}$  and  $355^{\circ}$ , which correspond to radials passing through houses #2 and #3, which experienced annoyance infrequently. The radial positions of the homes with respect to the ray paths indicates, at least in these examples, slightly elevated acoustic levels above a spherically propagated field. Thus, the modeled traces of this series of figures show a strong interaction between the terrain and the sound propagation to produce turbine acoustic radiation patterns that can significantly deviate from the simple spherical divergence model.

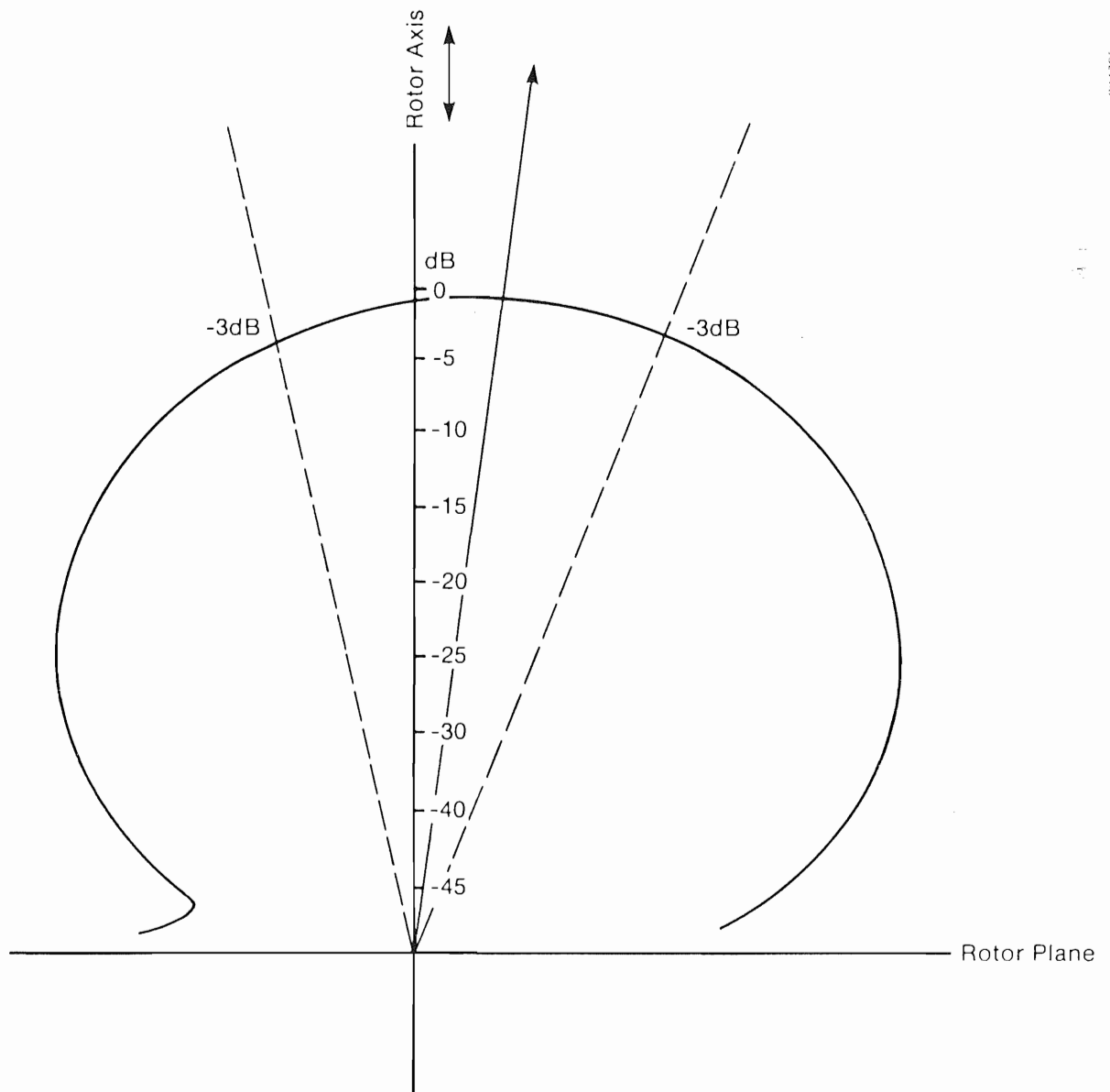
### 6.3 INFLUENCE OF SITE WIND DIRECTION ON PROPAGATION FREQUENCY OF ANNOYANCE

One lobe of the acoustic dipole radiation pattern as a function of azimuth angle for MOD-1 peak emission levels has been calculated in Ref. [2] and resembles the pattern shown in Figure 6-10. The peak occurs approximately  $6^{\circ}$  off the rotor axis (the half-power  $\pm 3\text{dB}$  points are  $+22$  and  $-12$  deg with respect to the same reference). To relate this pattern to the MOD-1 operating true azimuth orientation, Figure 6-11 plots the October 1978 through September 1979 probability distribution or "power wind rose" of hub-height wind speed as a function of azimuth for speeds greater than  $6.5 \text{ ms}^{-1}$ , the approximate cut-in velocity. A comparison of Figures 6-10, 6-11, and 6-1 reveals at least one reason why houses #2, #7, and #8 reported such high frequencies of annoyance. Those homes lay in the most prevalent radiation pattern lobes, dictated by the most prevalent rotor azimuth. House #4, however, tended to be affected only when the wind direction came from the secondary peak in the distribution; i.e., the south-southwest. Thus, in addition to terrain and atmospheric refraction, the wind direction at hub height also influenced the distribution of annoyance by controlling the directivity of the emitted radiation pattern. A compilation of the total wind record taken at the MOD-1 site [29] indicates the overall mean wind direction was  $290.0^{\circ}$  at hub height but became  $286.3^{\circ}$  during the critical 1600-2400 hours, the dusk-to-evening period, when the bulk of the complaints were received. The long-term meteorological record indicates a further reason why residents of houses #2, #7, and #8 complained the most frequently.

### 6.4 CONCLUSIONS REGARDING THE EFFECTS OF PROPAGATION ON THE MOD-1 NOISE SITUATION

Thomson [3,30] has reached the following conclusions, based on the initial Penn State analysis of the MOD-1 situations:

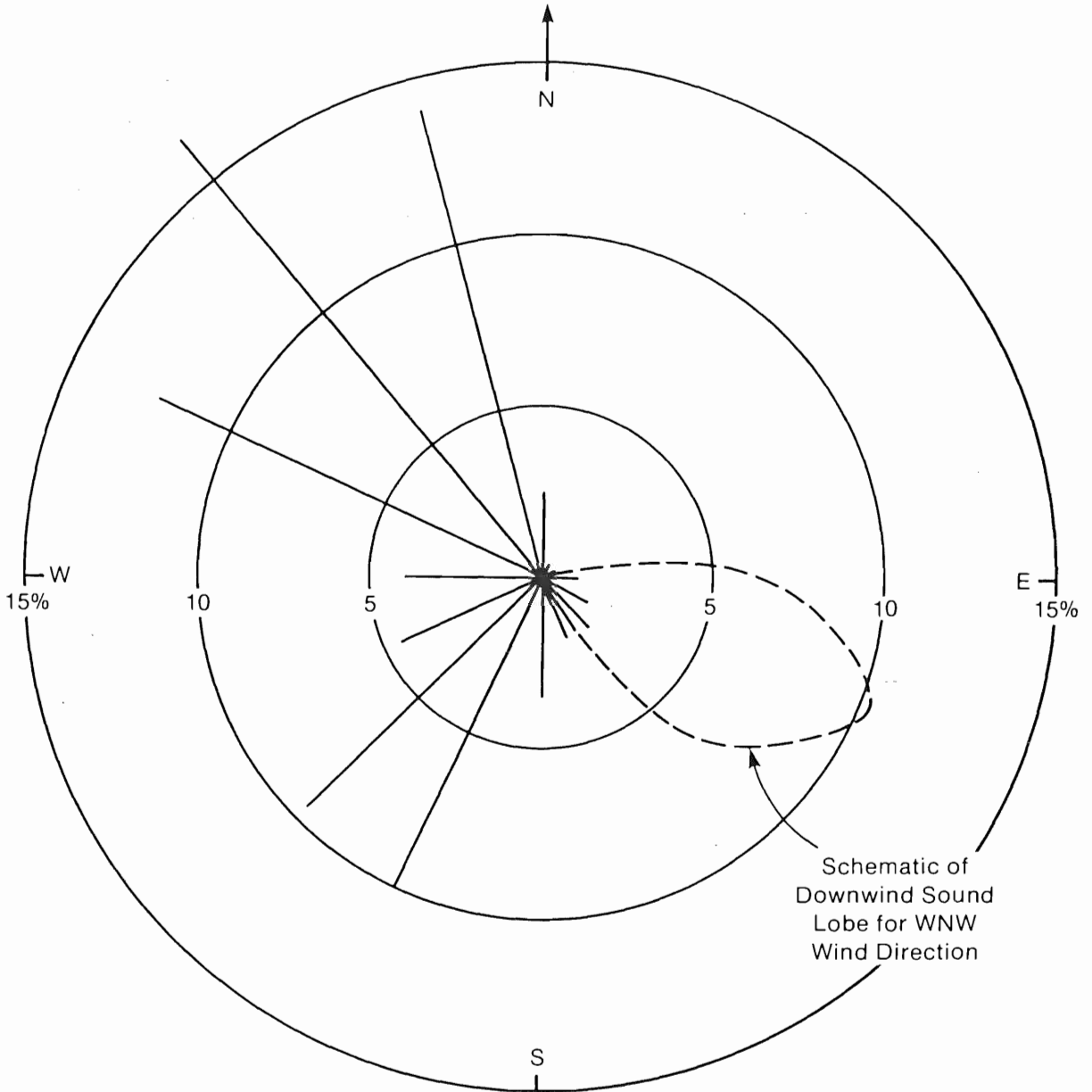
1. The intensity, duration, and location of enhanced, far-field noise levels depend upon the details of the wind- (and bearing) and temperature-dependent sound speed profiles (as well as the orientation of the turbine rotor plane) to such an extent that monitoring is unlikely to yield a satisfactory on-off criteria for a noisy turbine. Controlling the source was the only viable, long-term solution.
2. Conditions appropriate for the most efficient operation of the MOD-1 would most likely produce adverse noise propagation, and such conditions were likely to occur about 30% of the time (based on the limited data sample available).



004795

Figure 6-10. One Lobe of MOD-1 Impulsive Noise Dipole Directivity Pattern

Source: Ref. [2].



014796

Figure 6-11. MOD-1 Site "Power Wind Rose" with  $\pm 3$ db Impulse Noise Directivity Pattern Added for Mean Wind Direction of  $290^\circ$

3. For the low-frequency emitted noise from the MOD-1, adverse noise propagation could occur upwind as well as downwind of the turbine site if "thin" atmospheric layers were present. Amplification at resulting caustics probably did not exceed 6 dB.
4. Surface and ground propagation were negligible in comparison with refractive airborne propagation.
5. The strong terrain-atmospheric refraction has resulted in predictions of far-field enhancements in excess of 25 dB as a result of refractive and terrain focusing. Independent measurements taken near the MOD-1 have experimentally confirmed this [31].



## SECTION 7.0

### A PROPOSED PHYSICAL MECHANISM DEEMED RESPONSIBLE FOR ANNOYANCE FROM MOD-1 IMPULSIVE NOISE

In this section, we discuss our interpretation of the results of the acoustic and seismic monitoring of the two homes discussed in Section 3.1.2 that were undergoing impulsive excitation by the MOD-1. From these measurements and other similar sources, we have derived what we believe to be the physical mechanism primarily responsible for the complaints of the residents of the affected homes. The MOD-1 results are then compared with histories of other cases of low-frequency human annoyance and typical sound levels associated with common events that affect the acoustic environment in residential structures. Finally, we discuss our development of an assessment method to subjectively evaluate the annoyance potential of low-frequency acoustic emissions from a specific wind turbine.

#### 7.1 CHARACTERISTICS OF LARGE WIND TURBINE NOISE

Figure 7-1 schematically summarizes an averaged, large wind turbine acoustic frequency spectrum and indicates the dominant noise sources as a function of the radiated frequency. Not all of the features shown will be present at any one period of time, as we discussed in Section 3.0. The ultimate cause of most of the aerodynamically generated noise is the unsteady loading of the blades, which, when substantial, is responsible for the temporal distribution of the radiated acoustic energy across the frequency range defined by Figure 7-1.

Conventional classifications of rotor noise include rotational, broadband or vortex, and impulse noise. Rotational noise is characterized by the large number of discrete frequency bands or tones, harmonically related to the frequency of blade passage, in a spectrum in which a large number of rotor revolutions have been averaged. The amplitude of these tones is determined by the sum of the steady and unsteady air loads, the latter arising from many of the mechanisms discussed in Section 5.0. Broadband or vortex noise is the result of an interaction of the unsteady lift and the blade boundary layer and is related to such mechanisms as trailing edge separation and vortex shedding. Broadband noise, which can be described as the "swishing" sounds associated with a wind turbine operation, are distinguished as being largely incoherent, and they cover a wide frequency range with a "spectral hump" sometimes found at relatively high frequencies, as indicated in Figure 7-1. Impulsive noise, such that observed with the MOD-1, is identified with short, transient pulses that can contain considerable acoustic energy. Tonal acoustic energy, in the areas of Figure 7-1 indicated by the vertical dashed lines, which transcends the rotational and broadband regions, is an indication that a rotor is undergoing periodic, transient lift fluctuations. Impulsive noise generally tends to be the most annoying because it dominates all other sources because of its high degree of phase coherency and radiation efficiency. From Figure 7-1, we see that the peak levels of acoustic energy reside in the low audible and what is normally thought of as subaudible (<20 Hz) frequency ranges. The presence of short-period, transient blade loads will increase the levels of discrete or tonal radiation in the higher rotational harmonics, usually peaking in the 10-30 Hz range.

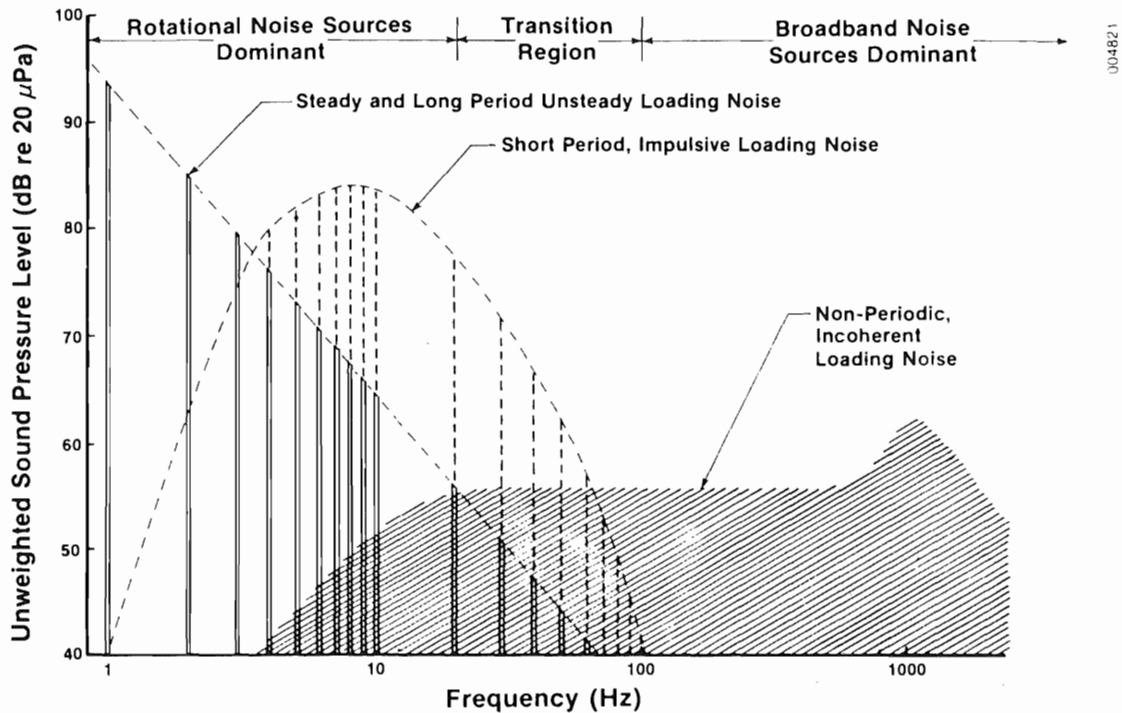


Figure 7-1. Schematic Representation of an Averaged Radiation Sound Pressure Spectrum from a Large Wind Turbine

The low-frequency-dominated spectrum of Figure 7-1 is a result of the low rotational speed of a large wind turbine (such as the MOD-1), compared with other forms of turbo machinery. At present, no adequate standard exists for evaluating the potential for human annoyance from impulsive noise, particularly when the acoustic energy tends to be concentrated below 100 Hz, as in this case. This deficiency is a result of our meager knowledge of human psychophysical response and of the important physical factors involved in the perception of transient sounds as annoyance. The psychoacoustics group at the NASA Langley Research Center has made progress in determining a typical human perception threshold to low-frequency impulse sounds which have their roots at frequencies similar to the MOD-1 ( $\sim 1$  Hz) [32]. This work, however, is only applicable in a non-reverberant environment, such as outdoors, because an "anechoic" room was purposely used to collect the subjective response data.

## 7.2 A PROPOSED PHYSICAL MECHANISM RESPONSIBLE FOR MOD-1 ANNOYANCE

### 7.2.1 Factors Controlling the Internal Dynamic Pressure Fields of Subject Rooms

A close examination of the acoustic and structural vibration information collected in the two Boone, North Carolina, homes affected by excitation from the MOD-1 impulses has revealed a repeated tendency for both the indoor dynamic pressure field and the vibration frequency spectra to show discrete peaks at the same frequencies, as well as higher dynamic peak overpressures inside the homes than outside. This strong harmonic behavior of the indoor pressure

field when excited by the periodic transient loadings of the MOD-1 impulses, points to a complex resonant coupling between a room's air volumes and the vibration deformation of the walls and floors surrounding the room. NASA studied the dynamics of residential structures under acoustic loading [33] as part of their sonic boom noise investigation. Using sinusoidal mechanical excitation, aircraft flyovers, and actual sonic booms, they determined that the characteristic dynamic response of typical frame houses was largely independent of their geographical location and age and more dependent on standardization of building codes, that specify such design details as stud and beam spacing. This study also found, due to the construction similarities called for by the codes, that resonant frequencies associated with the structural elements of most residential construction fall within the same range but also depend on the individual construction details of each house.

The dynamic (acoustic) pressure field within a residential room is controlled by (1) changes in the shape of the room caused by a diaphragm action from internal and external pressure changes (loadings); (2) higher mode resonances in the walls and floors; (3) cavity oscillations (Helmholtz-type resonances) from an air volume moving in and out of the room through an opening such as a door or window; and (4) the resonant modes of the air volume itself. The ranges of these various resonances are plotted in Figure 7-1, and the factors controlling structural mode damping are added in Figure 7-2. Table 7-1 lists the various modes measured and calculated from the dimensions of the two rooms in the Boone homes surveyed.

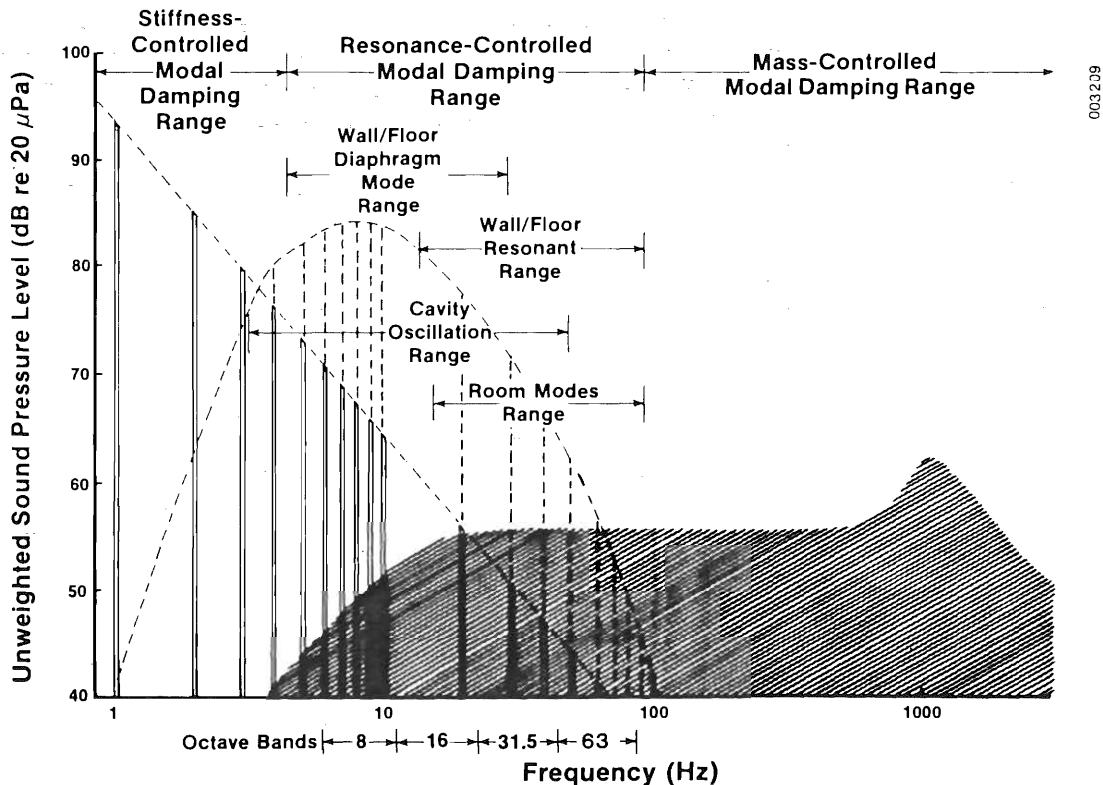


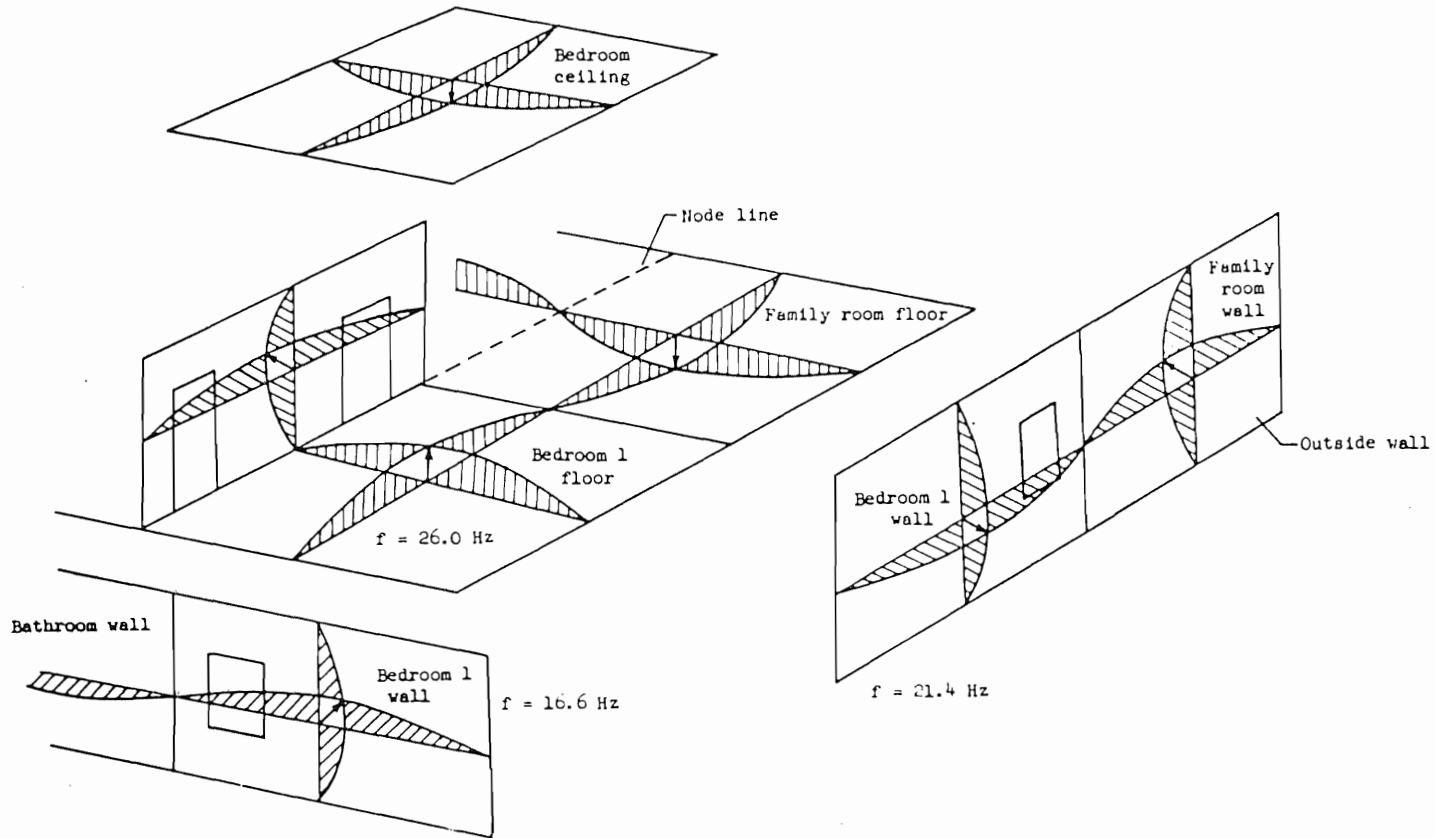
Figure 7-2. Schematic Sound Spectrum of Figure 7-1 with Structural Modes and Applicative Damping Mechanisms Added

Table 7-1. Resonant Modes of Rooms in Houses #7 and #8

	House #7	House #8
Dimensions (m)	3 x 3 x 2.1	3.6 x 3.5 x 2.4
Wall/floor resonances (measured) (Hz)	9,14,20,30,59,79	9,14,21,26,50,60,65
Cavity oscillation (calculated) Frequency (door open) (Hz)	≈ 44	≈ 35
Room mode frequencies (Hz) (calculated)	56[100,010] <sup>a</sup> 79[110] 80[001] 98[101,011]	47[100,010] 68[110] 70[001] 85[101,011] 98[111]

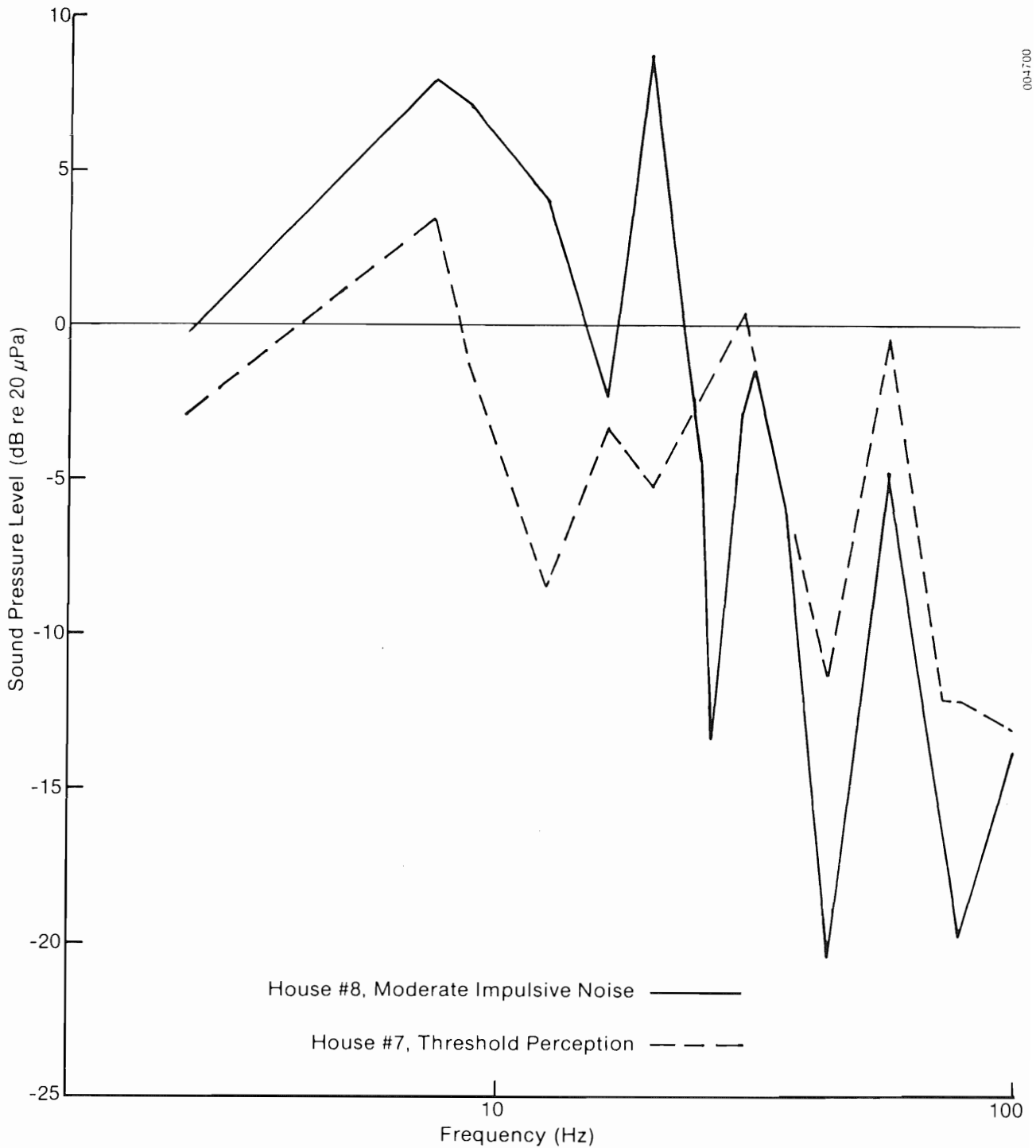
<sup>a</sup>The x,y,z normal modes are in brackets.

Many of the frequencies listed in Table 7-1 can be found in Figures 3-19, 3-20, and 3-21 (observed structural response) as well as in the acoustic spectra of Section 3.1.2, particularly at the 9 and 14 Hz diaphragm modes. Figure 7-3 presents an illustration from Ref. [33] showing the relationship of these modes to the structural features. From the available data, we concluded that the internal pressure field in these rooms is being driven dynamically through the diaphragm action of the outside walls facing the turbine's periodic impulsive loads. This conclusion is supported by the degree of dynamic coupling existing between the horizontal floor vibration deformation and the internal pressure field, as indicated by Figure 3-21. The overshoot of the internal pressure levels, evident in Figure 3-15 and repeated as Figure 7-4, indicates that a dynamic amplification is taking place under the impulsive excitation, intensifying the low-frequency pressure fluctuations in the rooms. Therefore, the impulsive acoustic loads associated with the MOD-1 operation are transiently exciting the lightly damped structural modes of the two houses, resulting in a complex resonance condition occurring between the walls and air volumes of these rooms. Table 7-2 lists the measured major normal and cross-coupled modes for these rooms with estimates of their modal damping characteristics. If we compare the preferred spectral peaks in typical MOD-1 impulses, as summarized in Table 7-3, the close match is obvious. The relationship of the critical reduced frequency  $k$ , in a range of  $0.5 \leq k \leq \pi$ , can also be noted in this figure. Thus, the houses are being elastically driven by a coupling of the spectral energy in the impulsive acoustic loads through lightly damped structural modes of the walls and windows which subsequently excite higher modes in the walls, floors, air volume, and room cavity resonances, and which set up strong harmonic oscillations between the room deformation and pressure field that last 150-200 times longer than a MOD-1 impulse.



0004797

Figure 7-3. Diagram Showing Relationship of Fundamental Structural Resonances to Construction Details of Typical Homes



004700

Figure 7-4. Peak Internal-External Sound Pressure Level Differences for Moderate Annoyance and Threshold Perception in Houses #7 and #8 ( $B_e = 1.25$  Hz)

Table 7-2. Major Normal and Coupled Structural Modes of Houses #7 and #8

Frequency (Hz)	Floor Mode Damping Characteristics			Window Mode Damping Characteristics	
	Vertical <sup>a</sup>	Horizontal <sup>a</sup>	Cross <sup>b</sup>	(Perpendicular Mode)	Cross w/Floor Modes <sup>c</sup>
<b>House #7</b>					
8.6 <sup>d</sup>	L	M	M	M	M
20	M	L	S	L	S+
30	M	VL	S+	L	S+
59	L	M	M	L	M
79	L	M	M	L	M
89	VL	M	S	L	S
96	VL	M	M	M	M
<b>House #8</b>					
8.9 <sup>d</sup>	L	L	S	VL	S+
14	L	L	S		
21	M	L	S		
26	L	L	S		
32				L	W
50	VL	VL	S+	L	M
60	VL	VL	S+	L	S+
65	L	VL	S+		

<sup>a</sup>Modal damping degree estimate: VL = light ( $\zeta < 0.05$ ); L = light ( $0.05 \leq \zeta \leq 0.1$ ); M = moderate ( $\zeta > 0.1$ ).

<sup>b</sup>Estimated degree of cross-coupling between vertical and horizontal modes: M = moderate; S = strong; S+ = very strong.

<sup>c</sup>Estimated degree of cross-coupling between floor and window modes: W = weak; M = moderate; S = strong.

<sup>d</sup>Estimated to be the house's fundamental resonant frequency.

### 7.2.2 Human Perception of Internal Pressure Field

Not surprisingly, the perceptions of the residents of the rooms in which these strong harmonic pressure fields existed under MOD-1 excitation included both audible and other sensations, including vibration and sensed pressure changes. Figure 3-16, repeated as Figure 7-5, compares both the observed internal peak dynamic pressure spectra for moderate ("thumping") annoyance and minimal perception, as well as that observed outdoors, all referenced above existing background levels. This figure also shows the NASA impulse noise audibility criteria [32] devised for an anechoic environment. A study of the figures of Sections 3.1.2.1 and 3.1.2.2 plus Figures 7-4 and 7-5 indicates that major differences existed in the internal pressure distributions between what was reported as moderate annoyance (thumping sounds and vibration) and threshold stimuli (a barely discernible thumping sound but no sensation of vibration), the peak level of subaudible acoustic energy being most noticeable.

**Table 7-3. Preferred Acoustic Pressure Spectral Peaks for Typical MOD-1 Impulses**

Rotor rpm	Frequency (Hz)	$k_{80}^a$	Relative Level (dB)
35	6.25	0.33	0
	16.25	0.86	-9
	26.25	1.39	-23
	45.0	2.38	-39
	62.5	3.31	-47
	81.3	4.3	-51
	97.3	5.1	-56
23	4.4	0.15	0
	10.6	0.37	-9
	17.5	0.61	-15
	25.6	0.89	-29
	30.6	1.07	-38
	38.8	1.35	-44
	51.9	1.80	-47
	65.0	2.26	-55

<sup>a</sup>Reduced frequency as referenced to the chord dimension at the 80% span position.

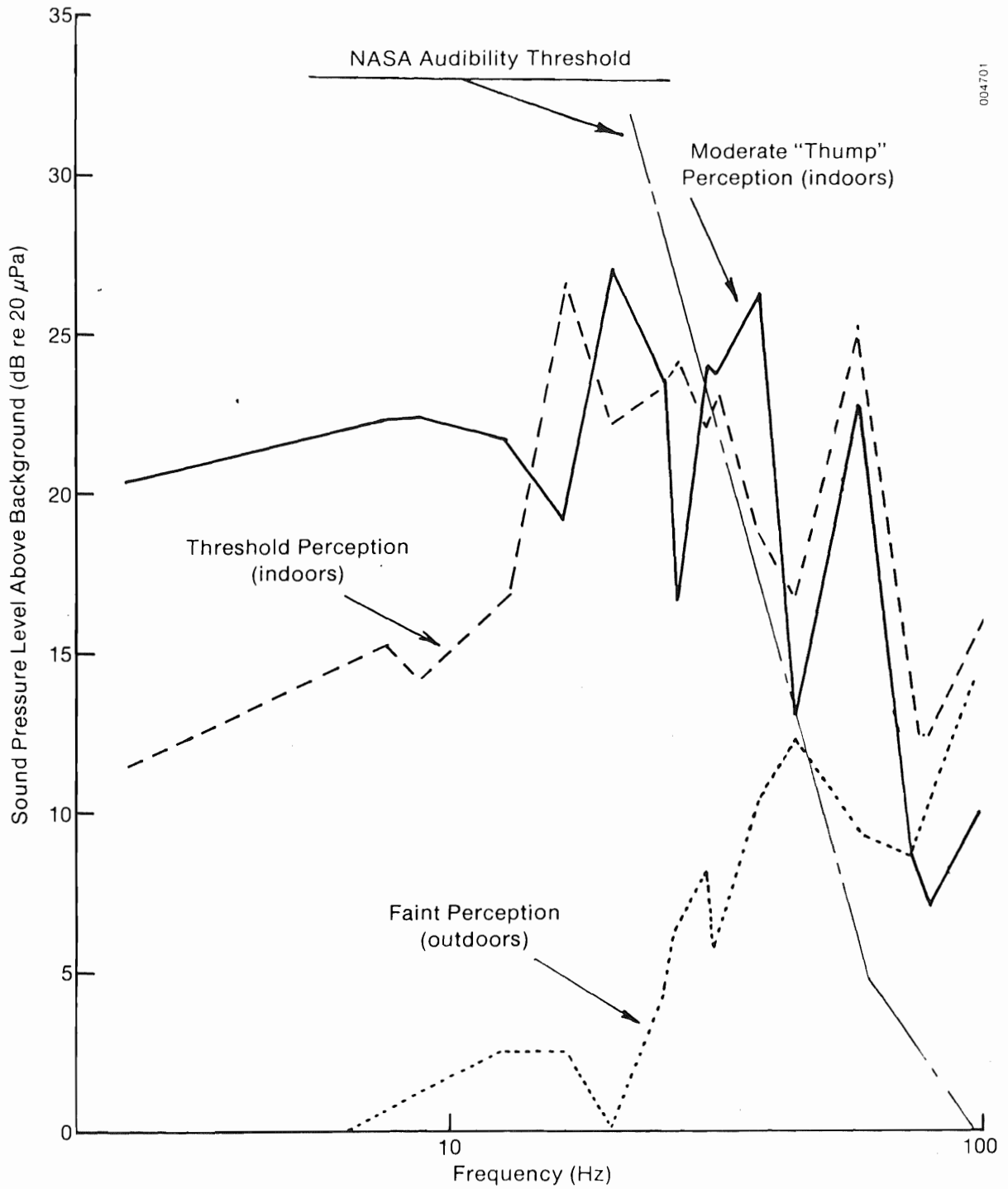
### 7.3 COMPARISON OF ANNOYANCE RELATED TO MOD-1 WITH SIMILAR SITUATIONS

In this section, we discuss the results of our research and that of NASA Langley [32] in locating cases of human annoyance where low or subaudible frequency noise was involved. We also review the structural resonance situation, particularly in the frequency region where the peak wind turbine noise output is known to occur; i.e., the 8-30 Hz band. We examine a situation involving non-impulsive excitation of several residential structures by a 100 MW gas turbine peaking station and compared that with the MOD-1 results. Finally, we compare the severity of the MOD-1 annoyance with other known low-frequency noise sources such as airplanes, road traffic, trains, and normal household noises as well as nearby industrial sources.

#### 7.3.1 Low-Frequency Resonant Properties of Residential Structures

The importance of the resonant properties of typical residential structures in the propagation and interior amplification of the MOD-1 noise has been demonstrated particularly by Figure 7-2, which relates wind turbine impulsive emissions to these dynamic characteristics. In order to assess how serious a problem coherent, low-frequency acoustic radiation would be from large wind turbines such as the MOD-1 in various parts of the country, we searched for sources of data in addition to the NASA report to confirm the potential universality of these sensitivities. A study by Medearis [36] to identify





004701

Figure 7-5. Peak Sound Pressure Levels Existing above Background for Moderate Impulsive Excitation (Outdoors and Indoors, House #8) and Threshold Perception (Indoors, House #7) ( $B_e = 1.25$  Hz)

structural damage criteria for low-rise buildings from blasting vibrations gives us some additional house sensitivity data as a function of geographic location. Table 7-4 lists statistics regarding the fundamental natural frequency and damping characteristics of 61 residences in four states as a function of the number of stories. The data in the table clearly indicate that (1) these fundamental resonances lie in the same frequency range as the maximum short period blade load noise from large wind turbines (Figures 7-1 and 7-2); (2) the fundamental tends to decrease with the vertical height of the structure; and (3) very little damping is present at the fundamental mode, averaging 5%-6% of critical, which means it can be easily excited.

**Table 7-4. Average Residence Properties By Geographic Location**

Structure Stories	Number	Age (Years)	Fundamental Natural Frequency (Hz)	Percent of Critical Damping (%)
<u>Colorado</u>				
1	16	18	12.0	5.0
1-1/2	6	4	10.3	7.4
2	16	50	7.2	6.1
All	38	29	9.7	5.9
<u>New Mexico</u>				
1	4	15	12.0	5.2
1-1/2	1	20	11.7	5.1
2	0	--	--	--
All	5	16	12.0	5.2
<u>Illinois</u>				
1	3	45	10.4	7.9
1-1/2	1	17	10.4	6.0
2	7	68	5.7	4.0
All	11	57	7.4	5.2
<u>California</u>				
1	4	10	12.3	5.7
1-1/2	0	--	--	--
2	3	11	7.5	5.2
All	7	16	10.2	5.5
<u>Total</u>				
1	27	21	11.9	5.5
1-1/2	8	8	10.5	6.9
2	26	50	6.9	5.4
All	61	32	9.6	5.6

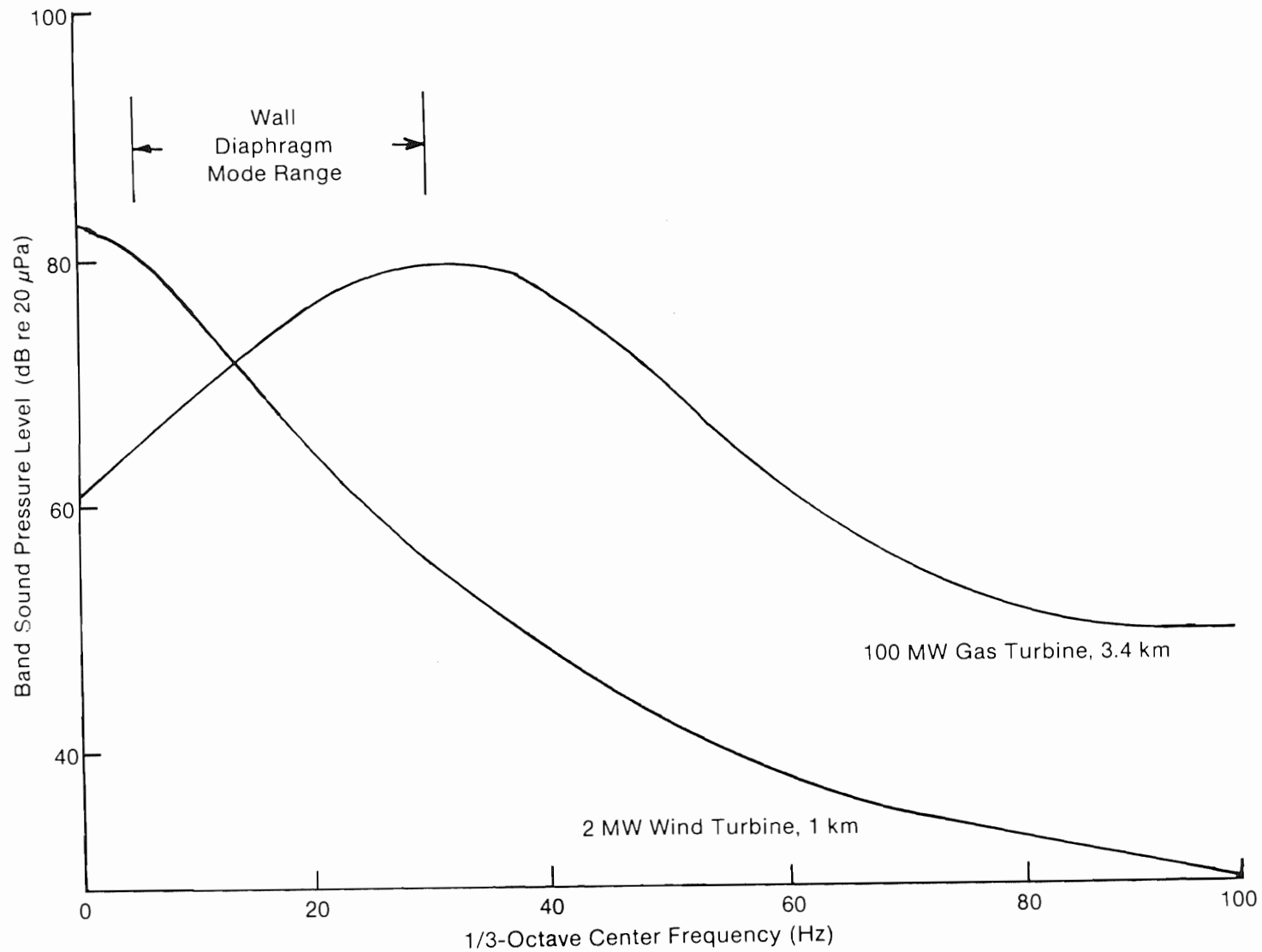
Source: Ref. [36].

Medearis found the taller structures "tended to respond exclusively in the fundamental mode and displayed very consistent frequency and damping characteristics." Ford, in his studies of noise and vibration propagation in residential structures [37], found that the fundamental mode is likely to be excited at low frequencies because the acoustic wavelength exceeds the structural bending wavelength, with the higher modes progressively excited, though less efficiently, through cancellation effects. Our measurements of the Boone homes support the NASA, Medearis, and Ford conclusions, particularly in reference to excitation near the fundamental. However, what is unique in the MOD-1 acoustic loading is that energy is not only coupling to the structure at or near the fundamental but simultaneously in several of the higher resonant modes, because of the coherent radiation characteristic of the impulses, as indicated in Tables 7-2 and 7-3. Apparently, this situation increases the audibility of the transient loads inside a house, making the perception of annoyance more severe.

We conclude that the low-frequency coherent aspects of the turbine acoustic radiation must be controlled at the source, because even if such emissions are effectively held to below-normal audibility ( $<20$  Hz), they may be of sufficient magnitude and persistence, when coupled with an unfavorable propagation situation, to excite a nearby residence at the fundamental. Under such excitation, the higher modes may also be excited and become detectable, perhaps reaching annoyance levels. From the NASA studies and the Medearis data in Table 7-4, we see that such structural sensitivities are essentially independent of geography and, in planning for large wind turbine installations, we must consider the possibilities discussed here.

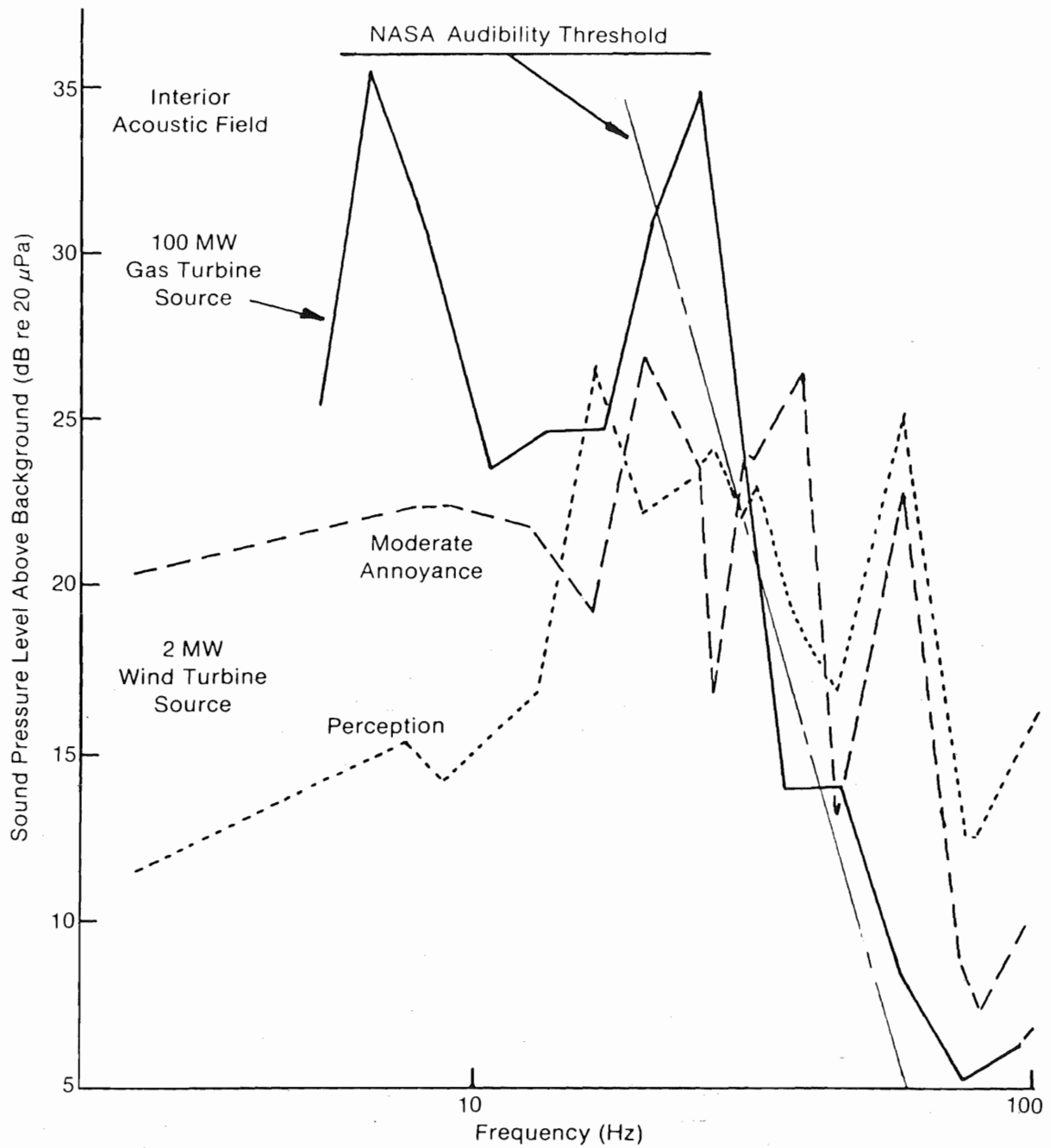
### **7.3.2 Low-Frequency Excitation by a Nonimpulsive Source**

Because the strong impulses associated with the MOD-1 may be unique and the evidence from our measurements seems to indicate that partially coherent radiation is far more likely, we needed to find a well-documented source of low-frequency sound and structural response with which to compare our results in Boone. We were fortunate to obtain data related to the noise emitted from a 100-MW gas turbine peaking station in southwest Oregon [38]. The complaints of the homeowners living near the station were the same as those of the Boone residents in almost all ways except for a lack of distinct interior audibility; i.e., they that reported nonauditory sensations were dominant. Figure 7-6 compares the features of typical averaged outdoor sound pressure spectra for the two types of turbines taken near affected homes. The characteristic sound of the gas turbine, a result of resonances caused by the gases passing through the exhaust stacks (which has since been corrected), was not impulsive, but a slow modulation was reported. While the peak frequencies of the two spectra in Figure 7-6 are different, the levels are almost equivalent in the region near 12 Hz, or the structural fundamental mode range. Figure 7-7 replots the data of Figure 7-4 to which the interior data from one of the homes near the peaking station has been added. These particular occupants reported sensations similar to those of the Boone residents, but very little audible sound; i.e., the feeling of pressure, uneasiness, vibrations, etc.



004798

Figure 7-6. Comparison of the External Averaged, Radiated Acoustic Spectral Characteristics of a 100-MW Gas Turbine Peaking Station and the 2-MW MOD-1 Wind Turbine



00-799

Figure 7-7. Same as Figure 7-5, but Adding the Response of Oregon Home to 100-MW Gas Turbine

Figure 7-8 plots the details of the outdoor, indoor, and indoor-background 1/3-octave band pressure levels for 100-MW operation of the turbine. It is important to note that while the peak of the external excitation is in the 31.5 Hz band, the indoor peak occurs between the 12.5 and 20 Hz bands and is about 30 dB, on the average, and is higher when the turbine is operating than when it is shut down. The quasi-steady dynamic overpressure for this home is compared with those measured in the two Boone homes in Figure 7-9. Here, the gas turbine and moderate MOD-1 impulse excitation are roughly equivalent up to about 20 Hz, but the former spectrum exhibits a very sharp resonant peak, more than 15 dB greater than the wind turbine, at 25 Hz, followed by a very rapid fall-off--which agrees well with Figure 7-8.

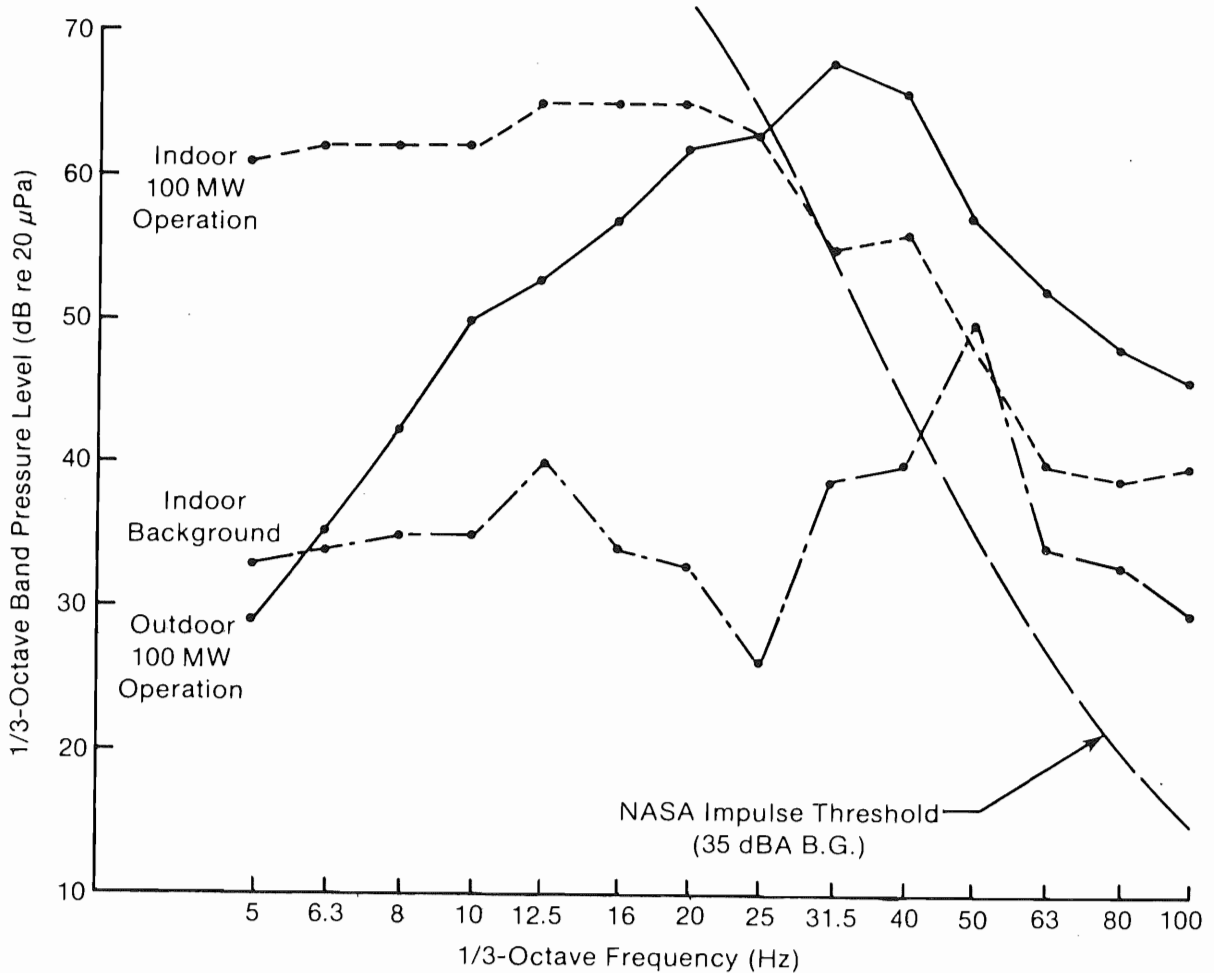


Figure 7-8. Comparison of Averaged External and Internal Acoustic Pressure Fields Associated with Low-Frequency Annoyance from 100-MW Gas Turbine at a Distance of 1 km (B.G. = background)

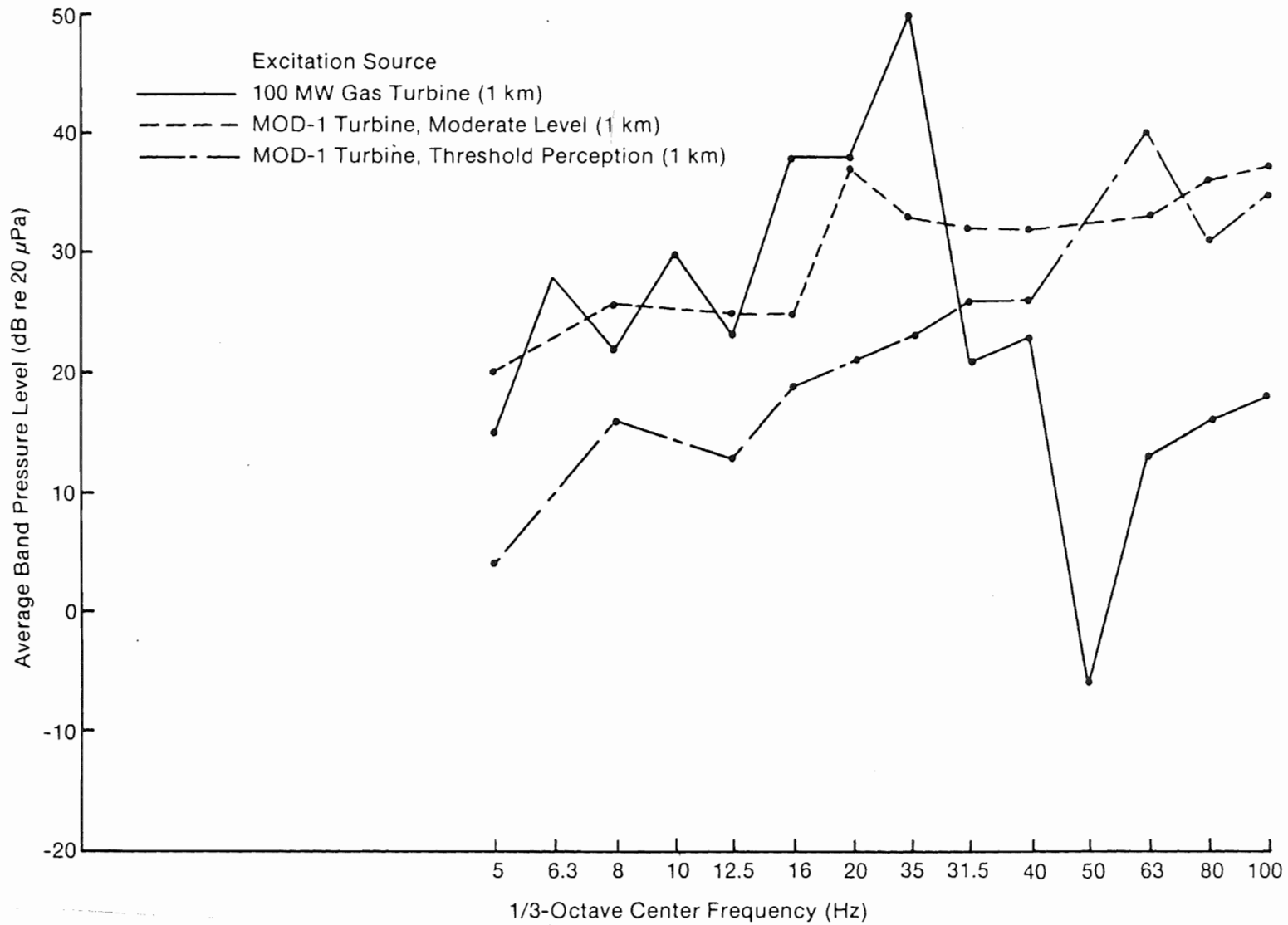


Figure 7-9. Comparison of Averaged, Interior 1/3-Octave Band Pressure Levels for Excitations by 100-MW Gas Turbine and Moderate Annoyance and Threshold Perception from MOD-1 Wind Turbine

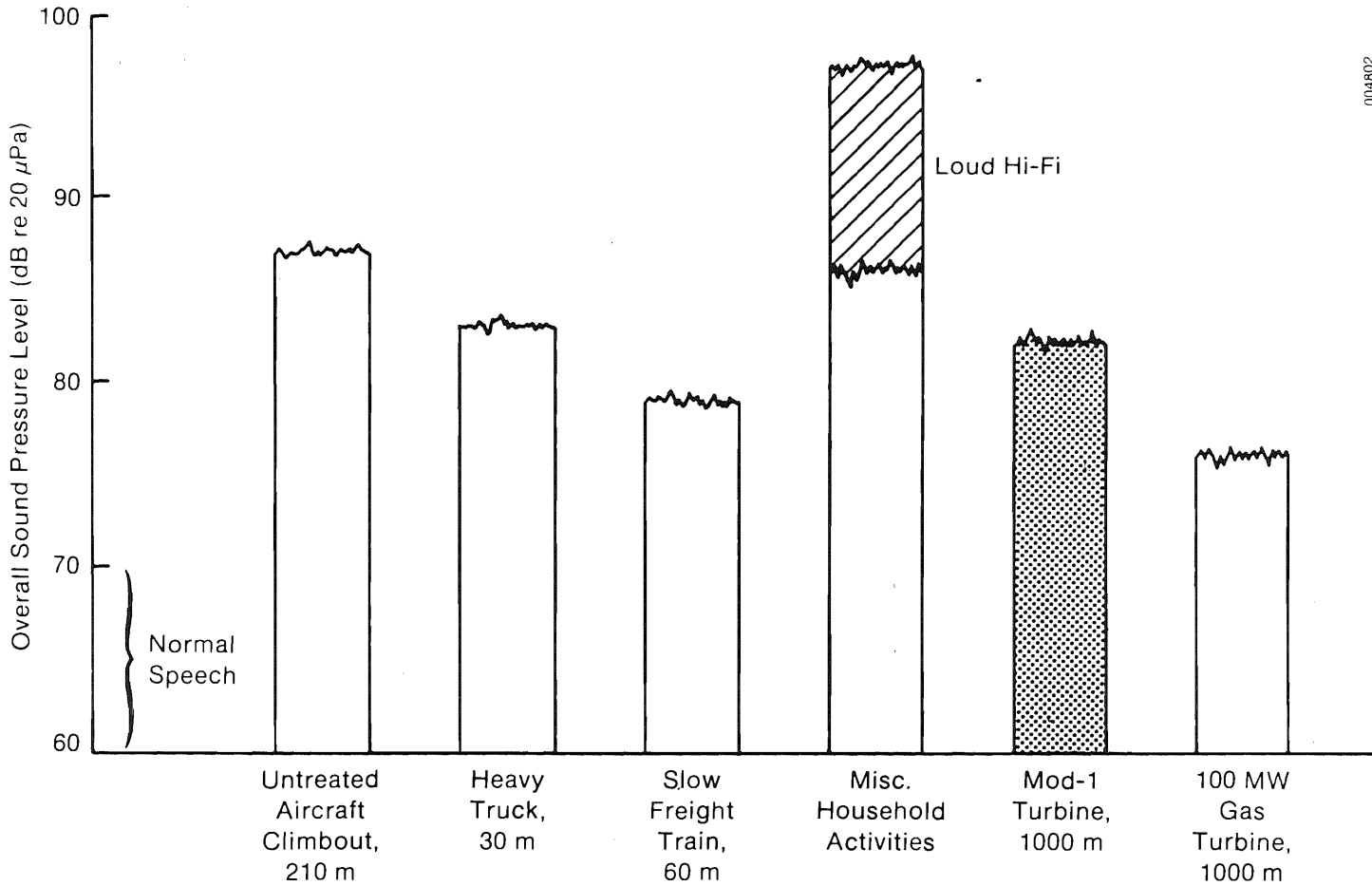
We concluded, then, that the annoyance in the Oregon house was being driven primarily through the diaphragm action of the walls facing the turbine, the location of the room in which the acoustic measurements were taken. The strong harmonic peak at 31.5 Hz in Figure 7-7 is to be expected, due to the accompanying external excitation peak at that frequency; but the peak at 6.3 Hz was not expected, and therefore must be a consequence of excitation of the structure fundamental mode. It is also not difficult to see why little audible sound was reported in the Oregon home, in light of the rapid fall-off above 30 Hz in all of the figures. The Boone homes, in comparison, indicate significant harmonic content above the NASA impulsive threshold curve. Also, the instantaneous impulses striking the two Boone houses contained considerable energy in these higher frequency modes which is not evident in the averaged spectra of Figure 7-6. We believe that the energy in these higher modes drives the corresponding structural and air volume resonances and adds to the audibility perception.

We also conclude that while the MOD-1 impulsive excitation contained more energy at higher frequencies, the energy near the structure fundamental mode alone, particularly facing the source, could raise the harmonic pressure levels within the homes to sufficiently high levels to be responsible for an annoyance perception in some people. Thus, comparing these two situations shows that it is not necessary to have a strong, low-frequency impulsive component exciting a residence to produce annoyance. Only similar levels of sub-audible acoustic energy near the home fundamental mode and above existing background may be all that is necessary. This process also explains the reported annoyance within homes when no perceptible sounds could be detected outdoors, a situation that occurred in Boone on several occasions. Again, given this evidence, we must stress the need for control of the noise at the source, since little can apparently be done in terms of damping affected structures once the condition exists.

### 7.3.3 Comparison of the Severity of the MOD-1 Situation with Other Low-Frequency Noise Situations

The MOD-1 noise situation, while it had several unique characteristics such as periodicity and sharp impulsiveness, does fall into a larger category of noise complaints in which low-frequency sound has been documented as playing a role. As part of their sonic boom studies in the early 1970s, NASA collected sound and vibration data of structures being acoustically loaded by a wide range of sources rich in low-frequency components, such as aircraft climbout, heavy truck traffic, slow freight trains, and the noise levels found inside homes themselves from such sources as high-fidelity sound systems, tools, appliances, etc. [39]. Figure 7-10 compares the overall sound pressure levels (OASPL) for these sources with the level measured in house #8 under moderate impulsive excitation and with the Oregon home described earlier near the gas turbine operating at its 100-MW capacity. The OASPL criteria of Figure 7-10, while giving a qualitative comparison, does not fully reflect the differences in the spectral content of both the source and the room interiors, which we have shown may be important.





208400

Figure 7-10. Comparison of Interior Overall Sound Pressure Levels (OASPL) for Common Low-Frequency Sources and Moderate Annoyance from the MOD-1 Wind and 100 MW Gas Turbines

Source: Ref. [39].

Hubbard [32] has summarized the available data on industrial operations that have been the source of complaints in nearby residential areas and for which low-frequency sounds are believed to be responsible. Hubbard's cross-hatched area, which encompasses the frequencies and levels thought to have caused the complaints, is shown in Figure 7-11, in which the region of octave band levels measured in house #8 under moderate impulsive excitation by the MOD-1 have been added. The observed points corresponding to octave band levels in the home in Oregon also have to be plotted, as well as the NASA impulse threshold and tone minimal-audible-field (MAF) [40] for comparison. Figure 7-12 presents a similar plot in which the threshold perception measured in house #7 is plotted. These figures indicate that the Boone complaints fall into the same category as similar ones for equivalent frequencies and octave band pressure levels. The observed perception threshold of Figure 7-12 appears reasonable in comparison with the NASA and MAF curves as well. The measurements of moderate annoyance used to develop Figure 7-11 were derived from our March 1980 field investigation, but our analysis of the June 1980 data has uncovered a far more severe impulsive situation, indicating that the annoyance area shown should be expanded upward. We conclude therefore that the conditions causing the Boone residents to complain have in fact been identified previously in documented low-frequency annoyance situations and in that respect are consistent with findings in the limited available literature.

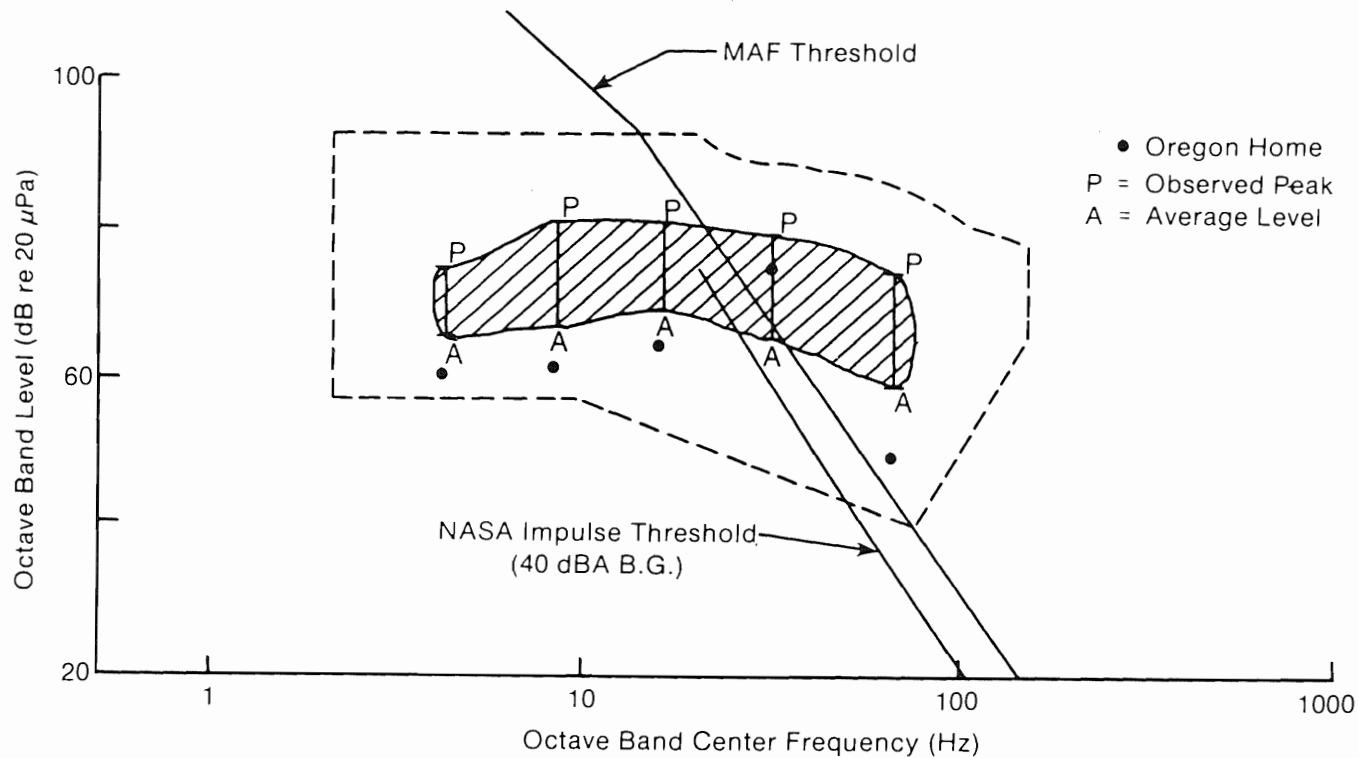
#### **7.4 AN ANNOYANCE POTENTIAL ASSESSMENT METHOD**

In order to be able to assess the effectiveness of various noise amelioration techniques and procedures on the MOD-1, as well as compare other turbine designs to the MOD-1, we have developed an acoustic data processing technique that allows us to statistically determine the degree of low-frequency coherence in the radiated turbine acoustic spectrum. Recall that it is the degree of coherency between discrete frequency bands or impulsiveness in the acoustic output of wind turbines that is a factor in the level of annoyance perceived by humans in both interior and exterior environments.

##### **7.4.1 A Synopsis of the Technique**

The coherence between discrete energy bands in the structurally sensitive frequency range of 5-100 Hz is determined by computing the joint probability density distributions of the band spectrum levels in a series of four contiguous ISO octave frequency bands. These bands, which are indicated in Figure 7-2, account for more than 90% of the resonance-controlled frequency range and consist of the standard 8, 16, 31.5, and 63 Hz octaves. The 8 and 16 Hz bands cover most of the fundamental and wall/diaphragm modes, and the 31.5 and 63 Hz bands cover the wall/floor cavity and air volume resonances. In order to take into account the nonstationarity of the MOD-1 noise, the time for one complete blade revolution is used as the nominal sampling period for computing the density distributions.

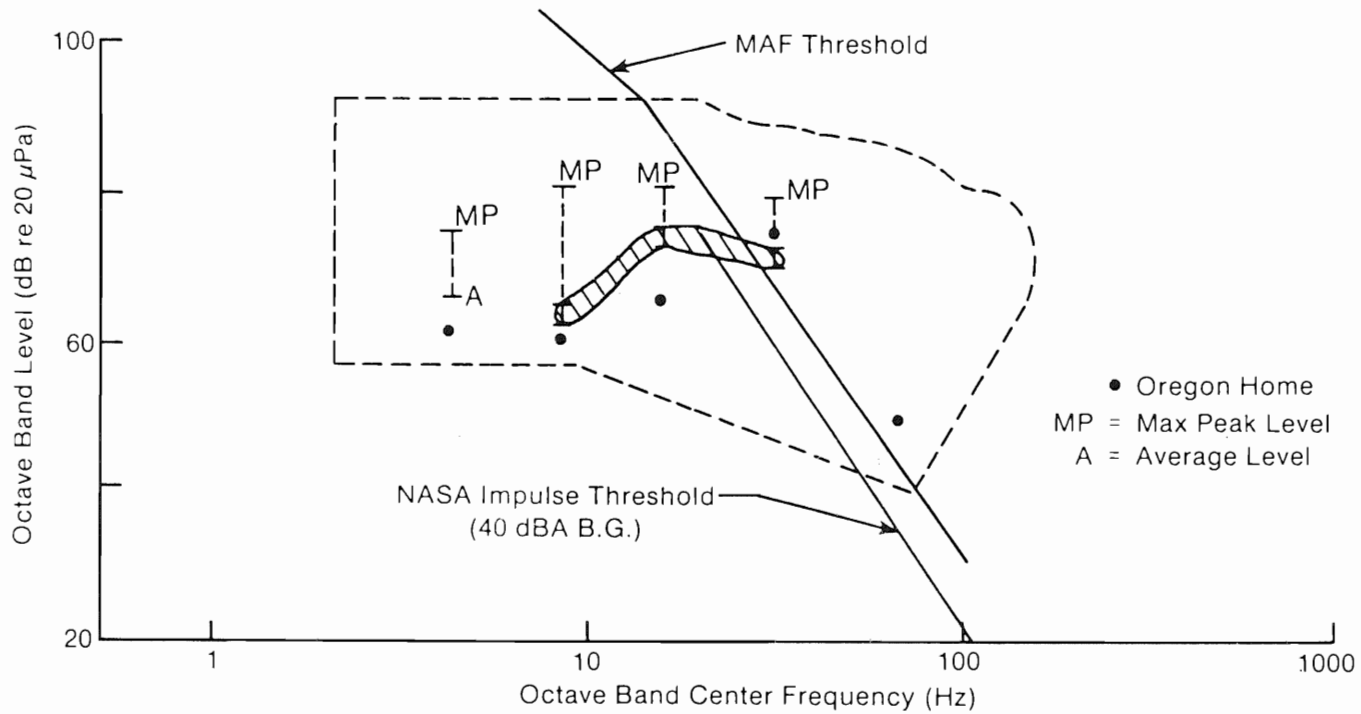
The actual technique involves the use of an 800-line resolution spectrum analyzer under the control of an external computer. The analyzer acquires a sample acoustic time series corresponding to the closest standard sampling period available to a single blade rotation period, transforms it into a nar-



004803

Figure 7-11. Comparison of Summary of Documented Low-Frequency Annoyance Cases with Observed Octave-Band Acoustic Levels Associated with Moderate Annoyance from MOD-1 Turbine in House #8

Source: Ref. [32].



00-4804

Figure 7-12. Comparison of Documented Low-Frequency Annoyance Cases with Threshold Perception of MOD-1 Impulsive Noise at House #7

Source: Ref. [32.].

rowband frequency spectrum, and finally transfers it to the computer where the four octave band levels are calculated. The computer, using the method of bins, develops the joint probability density functions (PDFs) using a 5 dB pressure level increment for the joint band combinations 8/16, 16/31.5, and 31.5/63 Hz, and a triple combination of 8/16/31.5 Hz. The results are then plotted as a series of surfaces containing isopleths of equal joint probability.

#### 7.4.2 Analysis Results

Figures 7-13, 7-14, and 7-15 display the observed joint PDFs for the 8/16, 16/31.5, and 31.5/63 Hz octave band spectrum levels for the maximum dynamic range of impulse activity we have recorded from the MOD-1. The surfaces at the lower left of each figure represent the local background and the threshold perception case measured outside house #7 in March 1980. The tight surfaces depicted at the upper right reflect the observed distributions for the most severe MOD-1 impulse radiation recorded 1.5 rotor diameters upwind of the turbine late in the evening of 9 June 1980. Figure 7-16 plots the 8/16/31.5 HZ BPL joint probability surfaces for this case in which the conditional probability of an 8 Hz band spectrum level (BSL) of 70 dB/Hz or more was used. The distributions of the night of 9 June also correspond to reports of severe annoyance by the residents of house #8 and their neighbors. Unfortunately, we had no measurements in or outside the affected homes themselves during this period. The surfaces of these figures now allow us to correlate the acoustic radiation characteristics of the MOD-1 over a wide emissions range, particularly in relation to the degree of phase coherency present; i.e., a high joint probability between two or more bands is equivalent to a high degree of phase coherency in the radiated acoustic energy.

The closely packed isopleths to the right and upper right of Figures 7-13, 7-14 and 7-15 indicate coherent radiations of 75, 75, 70, and 58 dB levels as much as 50% of the time (each contour represents a 10% increase in probability) in the 8, 16, 31.5, and 63 Hz bands, respectively. However, according to the threshold values in the lower left, perception (not annoyance) will just occur at 50, 45, 35, and 35 dB in the same respective bands, 20% or more of the time. Figures 7-13 and 7-14 show that interior perception occurs at only 5 dB above background levels in the 8 and 16 Hz bands (which correspond to the fundamental and first harmonic of the wall/floor diaphragm modes), but Figure 7-15 indicates no difference between the turbine radiation and background in the 31.5 and 63 Hz bands, indicating they were probably not contributing to indoor perception.

The results of this joint probability analysis have given us a crude measure of the threshold sensitivity of humans in a structure undergoing low-level, impulsive acoustic loading. In terms of the MOD-1 situation (and for other wind turbines installed near human populations, particularly residential communities), these figures give us a target below which we must limit turbine coherent, low-frequency emissions in the acoustic far-field. Allowing for the effects of terrain and atmospheric refraction on the propagation in which the effects of focusing can reduce the fall-off with distance, as discussed in Section 6.0, we must at least assume that the impulse levels measured at the 1.5 rotor diameter reference point near the turbine should not exceed these

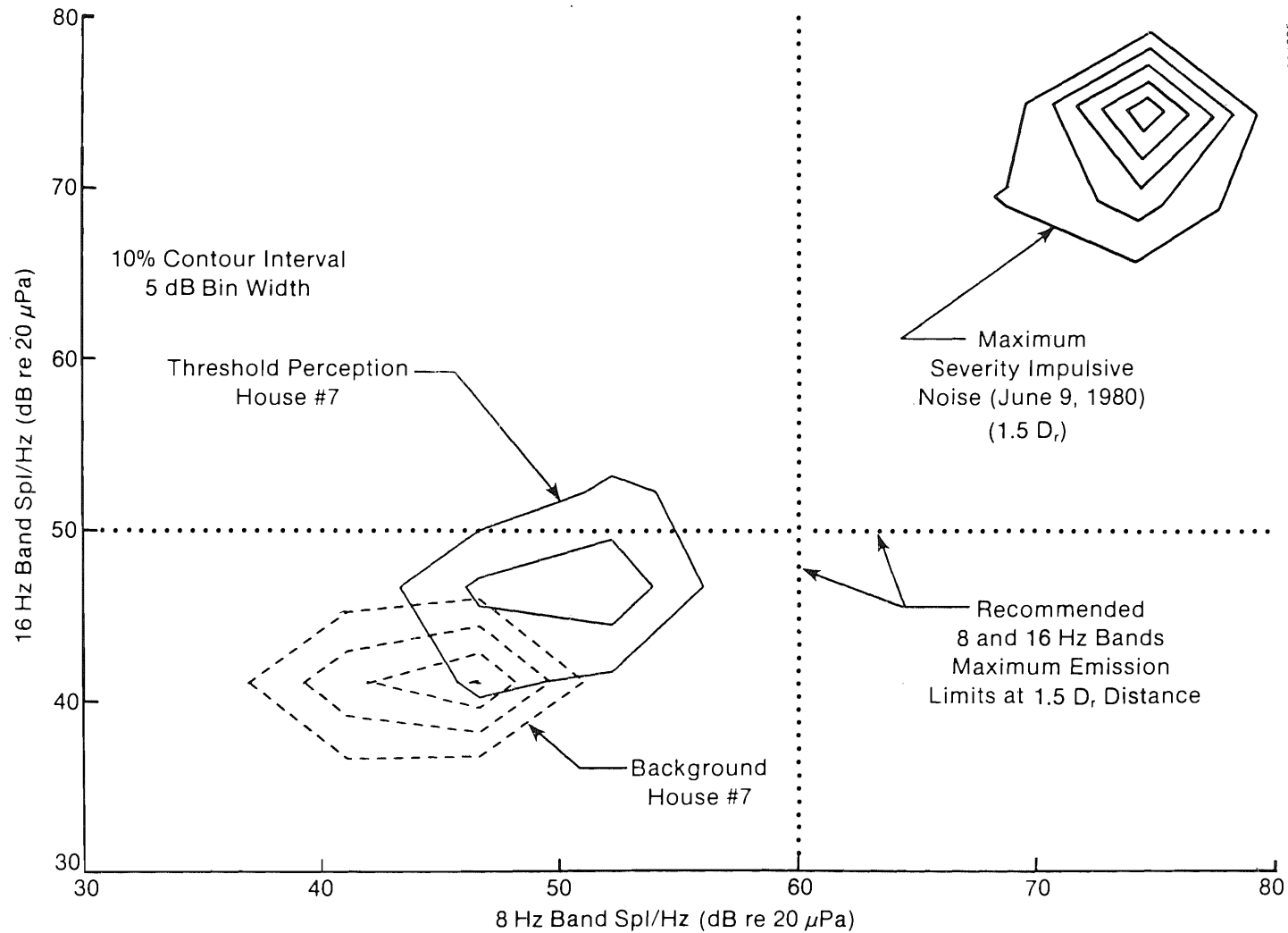
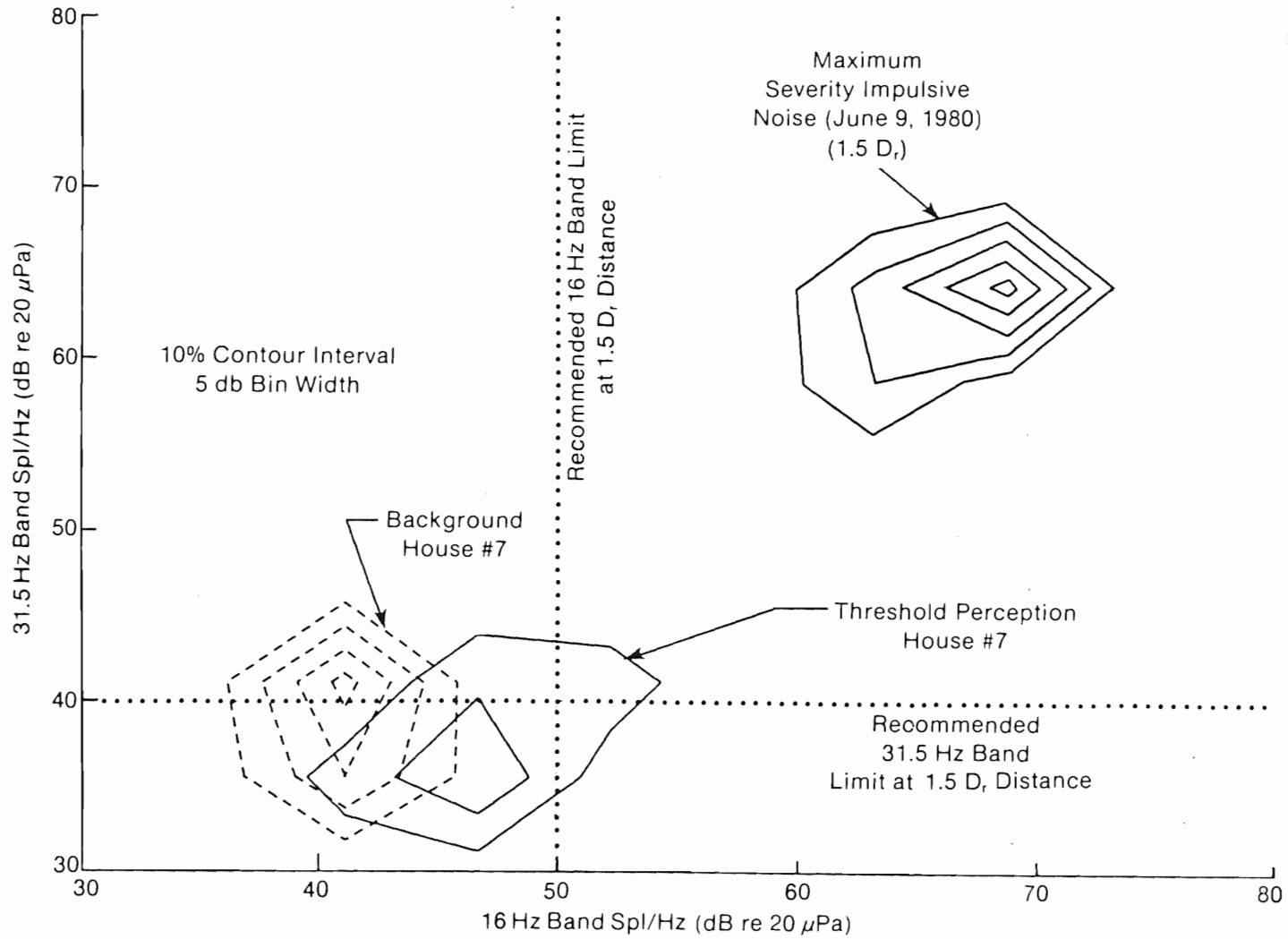
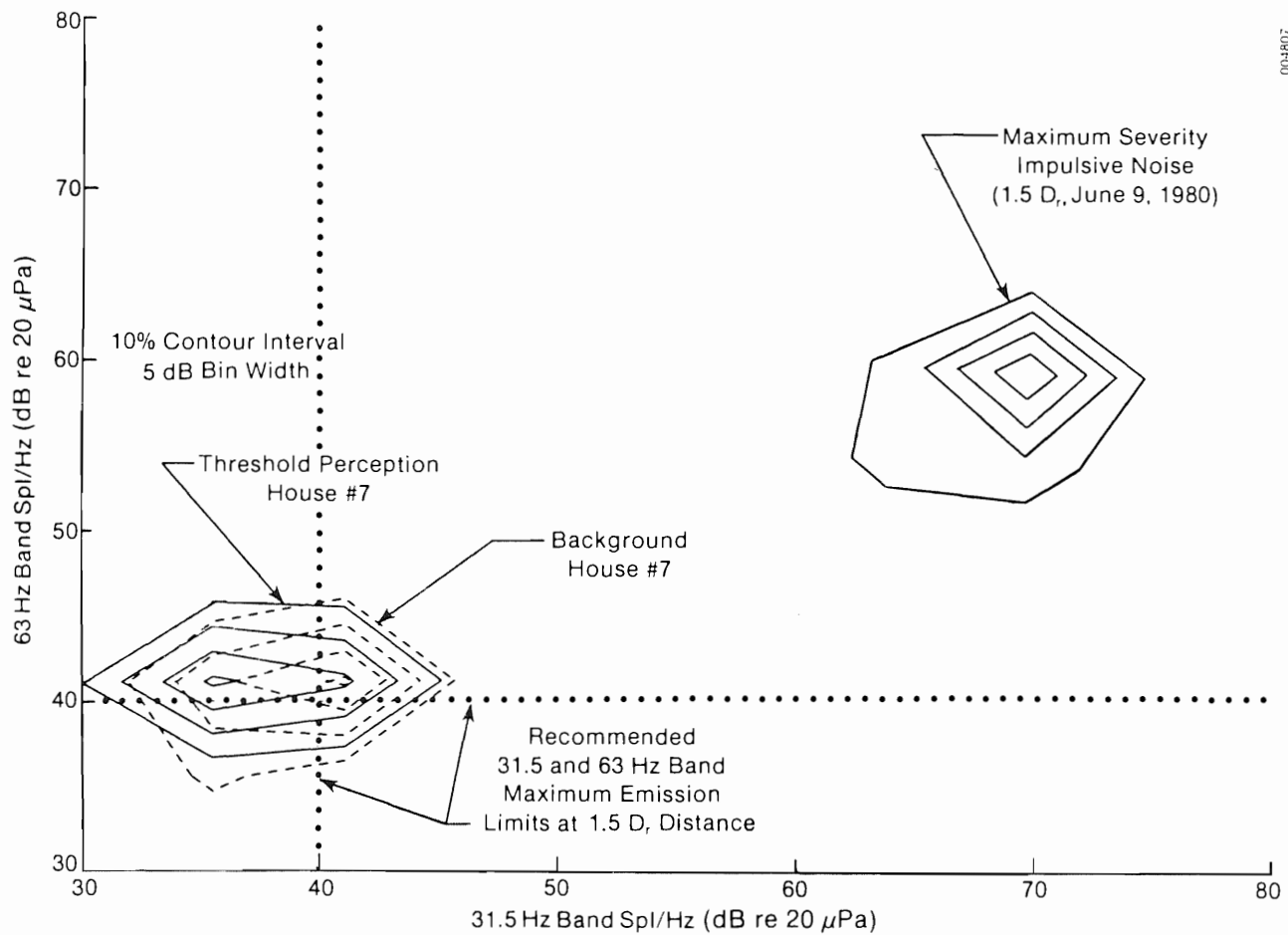


Figure 7-13. Joint Probability Distributions of 8/16 Hz Octave Band Spectrum Levels for House #7 Background and Threshold Perception and Maximum Impulse Severity at 1.5D from MOD-1 Turbine ( $D_r$  = rotor diameter)



00-4806

Figure 7-14. Same as Figure 7-13, but for 16/31.5 Hz Octave Band Spectrum Level



00-1807

Figure 7-15. Same as Figure 7-14, but for 31.5/63 Hz Octave Band Spectrum Level



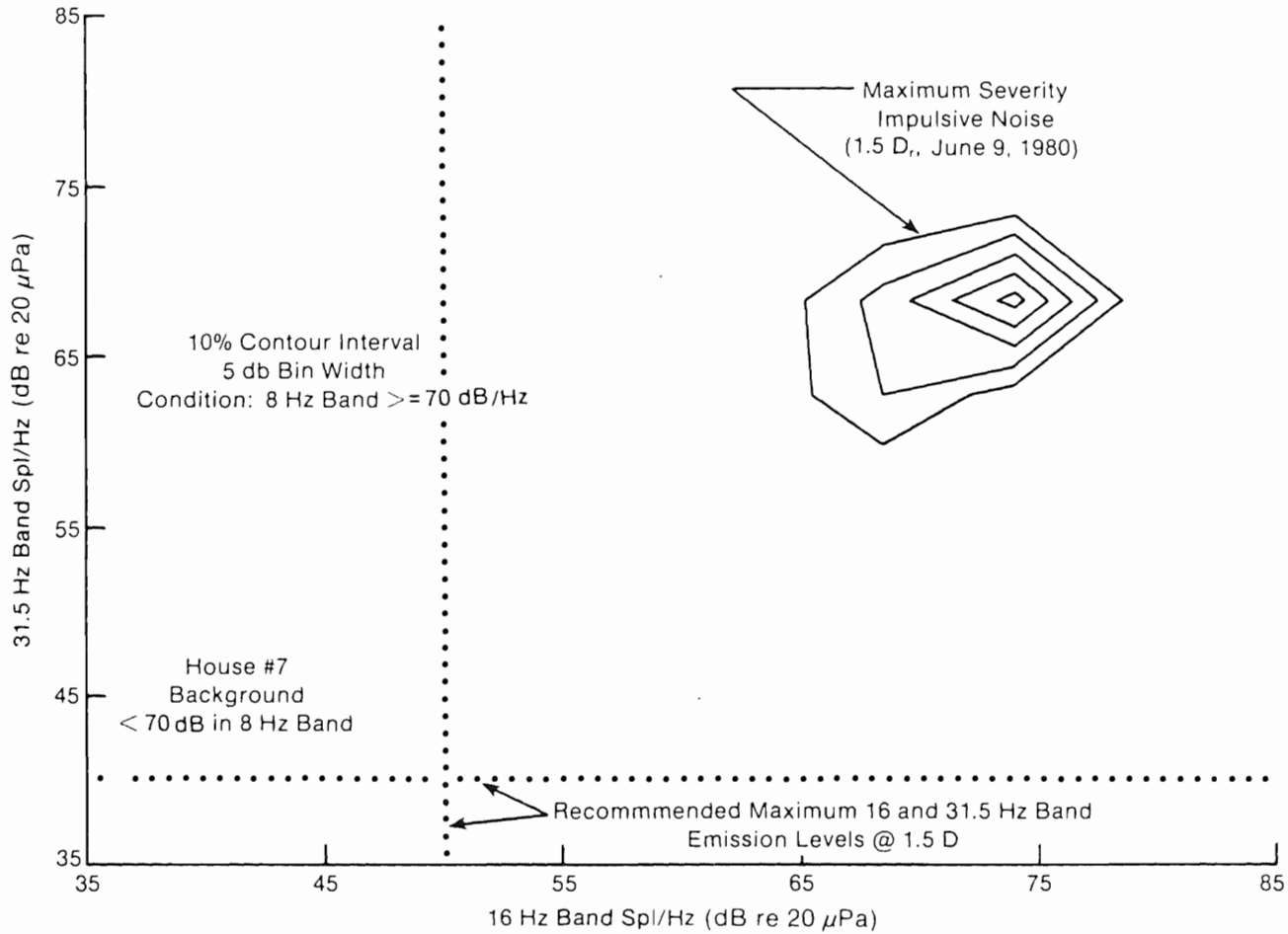


Figure 7-16. Triple Joint Probability of 8/16/31.5 Hz Octave Band Spectrum Levels with Conditional Probability of an 8 Hz Band Spectrum Level  $>$  70 dB (House #7 background and threshold levels are  $<$  70 dB BSL and do not appear)

threshold limits as a design guide. In particular, joint radiation in the 8, 16, 31.5, and 63 Hz octave bands should not exceed 60, 50, 40, and 40 dB (re  $1 \text{ pWm}^{-2}$ ) intensity levels more than 20% of the time the turbine is in operation.

#### **7.4.3 Comparison of Proposed Low-Frequency Coherent Emission Guidelines with Available Data**

Obviously, these guideline figures are a rough measure because they are based on the reaction of only four people in a single situation. Unfortunately, that is all we have to go on in the Boone situation. We can, however, compare these figures with Hubbard's data summary [32], discussed in Section 7.3.3 and shown in Figures 7-11 and 7-12. Figure 7-17 presents Hubbard's low-frequency annoyance area, but with the threshold octave band levels measured at house #7 shown as rectangles  $\pm 5$  dB (allowing for systematic errors) about the design guideline levels. As shown, these levels essentially coincide with the lower limit of Hubbard's band pressure level data and agree quite well in frequency, ending within 5 Hz of his upper frequency limit. We believe therefore that our measurements of threshold sensitivities are consistent with the documented low-frequency annoyance literature and can be used as design-goal criteria to reduce noise levels, in the MOD-1, in particular, and in wind turbines, in general.

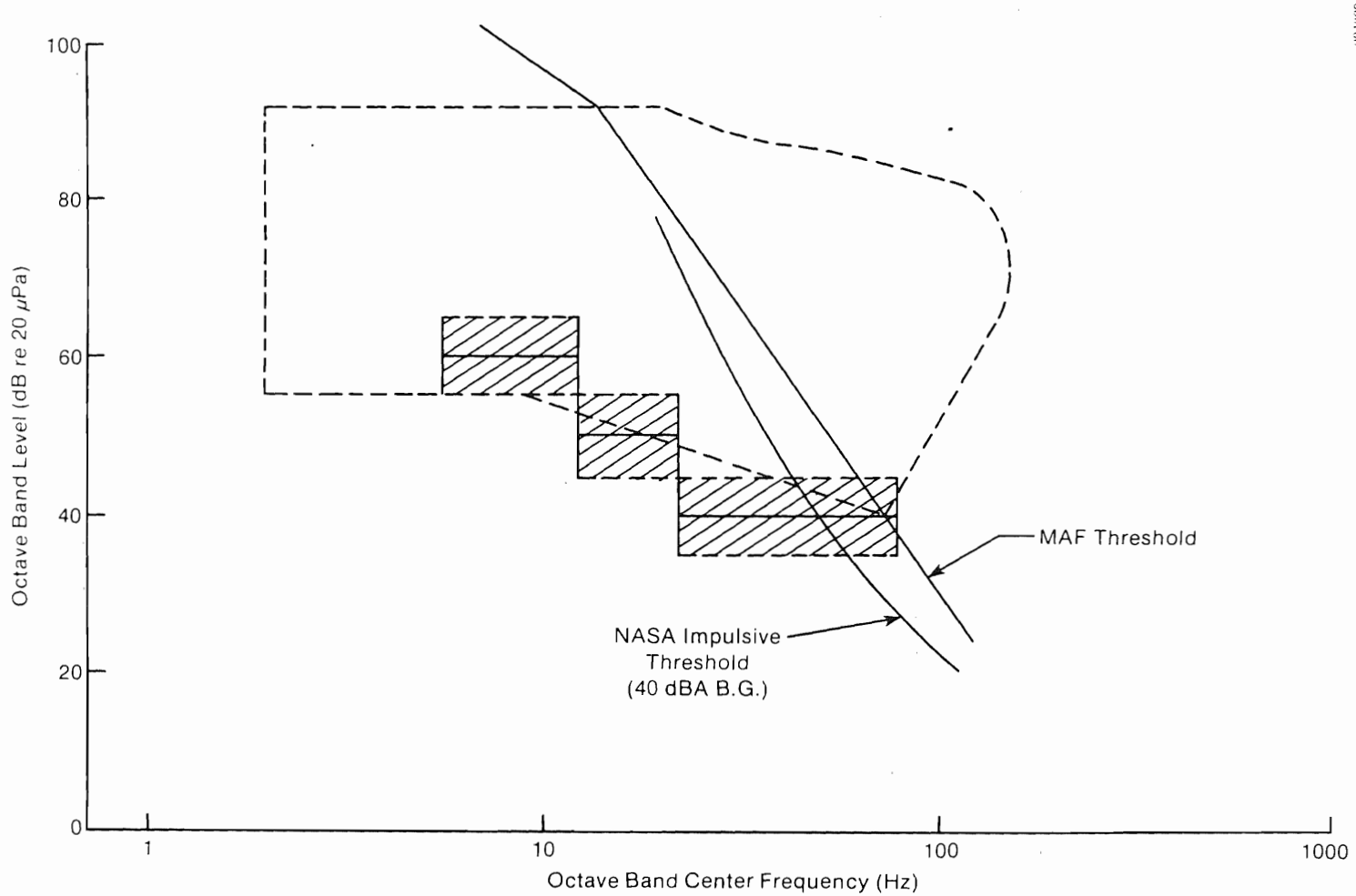


Figure 7-17. Comparison of Suggested Minimum Wind Turbine Radiated Joint Octave Band Pressure Levels at 1.5D with Low-Frequency Annoyance Summary

Source: Ref. [32].

6084700

## SECTION 8.0

### PROCEDURES FOR MITIGATING MOD-1 IMPULSIVE NOISE RADIATION

It is clear from our discussion in the previous sections that the only acceptable method of curtailing complaints from residents in the vicinity of an operating MOD-1 turbine is to eliminate, or at least reduce, the impulsive character of the disturbing acoustic radiation to below perceptible levels. The task was made more difficult by the level of conditioning and resulting sensitivity of a few of the families involved, particularly the residents of houses #2, #7, and #8 (and their immediate neighbors). In this section, we review the options available, some of which have been evaluated in actual practice, and discuss what we believe to be the most effective amelioration approaches, given the constraints of a fixed turbine design (i.e., rotor shape and support tower) but some operational flexibility.

#### 8.1 POSSIBLE WAYS TO AMELIORATE THE MOD-1 IMPULSIVE NOISE

As a result of the intensive investigation by a number of organizations, several possible procedures have been suggested to reduce the intensity of the impulsive acoustic radiation from the MOD-1. The suggestions fall into essentially three categories: (1) convert the turbine to an upwind configuration; (2) reduce the rotor's rotational speed; and/or (3) somehow treat the offending cylindrical tower legs aerodynamically to modify their downstream wakes to reduce the transient lift fluctuations responsible for the impulsive noise. Converting to an upwind configuration, while feasible for limited testing, has been deemed impractical (at least for the current turbine configuration) for several reasons, including tower-rotor clearance and a derated overall efficiency should the blades operate in an inverted position. Thus, reducing the rotor rotational speed and the aerodynamically modifying of the tower legs have been the options considered most. We treat each of these approaches in the following sections.

#### 8.2 DECREASING IMPULSIVE NOISE INTENSITY BY REDUCING ROTOR ROTATIONAL SPEED

Abating impulsive noise by reducing the rotor blade speed was based on the theory that the wake deficits existing in the lee of the large, vertical tower legs are responsible for rapid lift fluctuations and impulsive noise generation. By reducing the blade's relative translational velocity through these deficits, the rapid change in lift experienced at the original design speed will be sharply diminished through the increased residence time of the blade in the wake. This action will then prevent the associated acoustic impulses from reaching annoying levels.

The reasoning behind this approach has been founded on what we believe to be an incorrect assumption that the wake deficit is the primary cause of the impulse generation, as discussed in our analysis presented in Sections 4.0 and 5.0. The resulting reduction in impulse levels is related to the decrease in the magnitude of the steady lift attainable at the lowered relative blade velocity. Strong impulses could still be observed at this slower speed, the

result of the transient unsteady lift fluctuations encountered as the blade passes through coherent vortex structures that, as shown in Section 5.0, are independent of the rotor rotational (translational) speed. Thus, while the overall impulsiveness is reduced by this approach, the chief result is the derating of the turbine operating capacity from a 2-MW peak to something less than 1.5 MW under optimum operating conditions.

The reason why all impulses are not reduced below perceptible levels at the slower blade speed under all conditions, as stated above, continues to be the turbulent, discrete characteristics of the tower leg wakes. This can be seen more clearly if we describe these wakes at the point of blade intersection in terms of the time-dependent vortex circulations contained within, in terms of a spectrum of the reduced frequency  $k$ . In Section 5.2.4, we described the role of several unsteady aerodynamic parameters in which the reduced frequency  $k$  was shown to be of major significance. We confirmed this dependence in the wind tunnel testing described in Section 5.2.4.3 particularly in reference to the result that a reduced frequency range of approximately  $0.5 \leq k \leq \pi$  was responsible for maximum unsteady excitation of the airfoil boundary layer and for the observed strong acoustic radiation and aeroelastic responses. Keeping this in mind, we examine the width of the leg wakes as a function of the tower leg-to-blade distance. Typically, the wake width ranges from about 0.6 m at a downwind distance of four leg diameters to about 0.8 m at 12 diameters [14]. From our vortex analysis in Section 5.2.4.2, we estimated the width of the viscous core vortices to be typically half the wake width. Using the expression  $k = \pi c / \lambda$ , where  $\lambda$  is the disturbance wavelength (assumed half the wake width), the corresponding critical reduced frequencies for downstream distances of 4, 8, and 12 leg diameters are 3.8, 3.6, and 2.8, respectively, at the 80% span position. All are either within or near the critical  $k$ -range ( $0.5 \leq k \leq \pi$ ) and independent of the rotor speed. Thus, the chief benefit of lowering the rotational speed is derived from a reduction in the upper limit of the static lift, which in turn influences the peak levels of the transient, unsteady component toward lower values. The price of this improvement, of course, is less generating capacity than before, at every wind speed.

### 8.3 AERODYNAMIC MODIFICATION OF TOWER LEGS TO CONTROL IMPULSIVE NOISE GENERATION

We have identified four important fluid dynamic parameters that control the severity of acoustic impulses generated as the MOD-1 blades pass through the tower leg wakes, including the freestream velocity, vortex core central pressure deficits, vertical or spanwise coherence (vortex tube), and a wake disturbance scale expressed by the reduced frequency parameter  $k$ . Wake disturbances, whose spatial scale corresponds to a critical reduced frequency range of approximately  $0.5 \leq k \leq \pi$ , are the most important and therefore should be minimized, by aerodynamic modification of the tower legs, as well as the destruction of any vertical coherency. The latter is important because it controls the spanwise lift coherency  $\ell_c$  and therefore the fraction of the blade leading edge radiating impulsively.

The objective of aerodynamically modifying the turbine legs is to prevent the shedding of discrete vortex tubes which, when coupled with the lee disturbance space scale determined by the wake width, produce the optimum conditions for

impulse generation; i.e., discrete vortices within the critical reduced frequency range and spanwise coherency. Since little can be done to significantly increase the lateral dimensions of the wake, the primary objective of an aerodynamic device or spoiler attached to the tower leg is to destroy the vertical coherence by converting a flow containing discrete, organized 2-D elements to a much more broadband, 3-D one. In Section 5.1.2 we discussed the role of the separation line which is parallel to the major axis of a cylindrical bluff body and responsible for the roll-up of vortex tubes being shed downstream (see Figure 5-4). We also saw that if this line was distorted from its parallel orientation, circulation differences would develop in the downstream flow causing the 2-D discrete narrowband organization to become 3-D wideband chaotic. A device (or devices) which could be attached to the existing tower legs that would spoil the normal boundary layer to distort the parallel separation has been sought as a potential solution to the situation. Three types of spoiling devices, plus a roughening of two of the actual tower legs with wire mesh, have been investigated in this regard. The purpose of the wire mesh was to force the cylinder boundary layer into the supercritical regime which, it was thought, would produce the 3-D wideband structure. From our acoustic impulse analysis results presented in Section 4.2.3.2 and from measurements taken at the Rocky Flats Research Center using the 0.5 cylinder and small wind turbine, we now know that this approach does not provide the degree of vertical separation line distortion necessary to achieve the desired result. In fact, though the periodic component may disappear in a turbulent supercritical wake, strong vortex circulations are often still present. Below we present preliminary results from our investigation of three potential spoiling devices tested at the Rocky Flats Research Center: the perforated shroud, the vortex generator, and the helical strake.

### **8.3.1 The Perforated Shroud Spoiler**

Practical objectives in evaluating spoiler designs were compatibility and ease of attachment to the legs of the MOD-1, both necessary in view of the difficulties of working on such a large structure. We have reviewed the work of several investigators at the National Physical Laboratory in Great Britain [41] who were responsible for the development of a number of aerodynamic spoiling devices which have been successfully used to prevent catastrophic oscillatory forces from developing in tall cylindrical structures (such as smokestacks) from periodic vortex shedding. In a joint effort with NASA, we initially chose the perforated shroud device developed by Walshe and Wootton [41], a section of which is shown in Figure 8-1. This device had been shown to be effective in reducing oscillatory vortex excitation of cylindrical structures and also was relatively simple to manufacture and attach to the MOD-1 legs. While the devices constructed by NASA have never been actually installed and evaluated on the MOD-1 turbine itself, we were lent a single 1.8-m section to evaluate on the small turbine at Rocky Flats.

As shown in Figure 8-1, the shroud section was attached to the 0.5-m-diameter cylindrical test section mounted on the normal turbine support tower. Acoustic and turbulence measurements of the wake were conducted in a manner similar to those of the bare cylinder reported in Section 5.1.4.

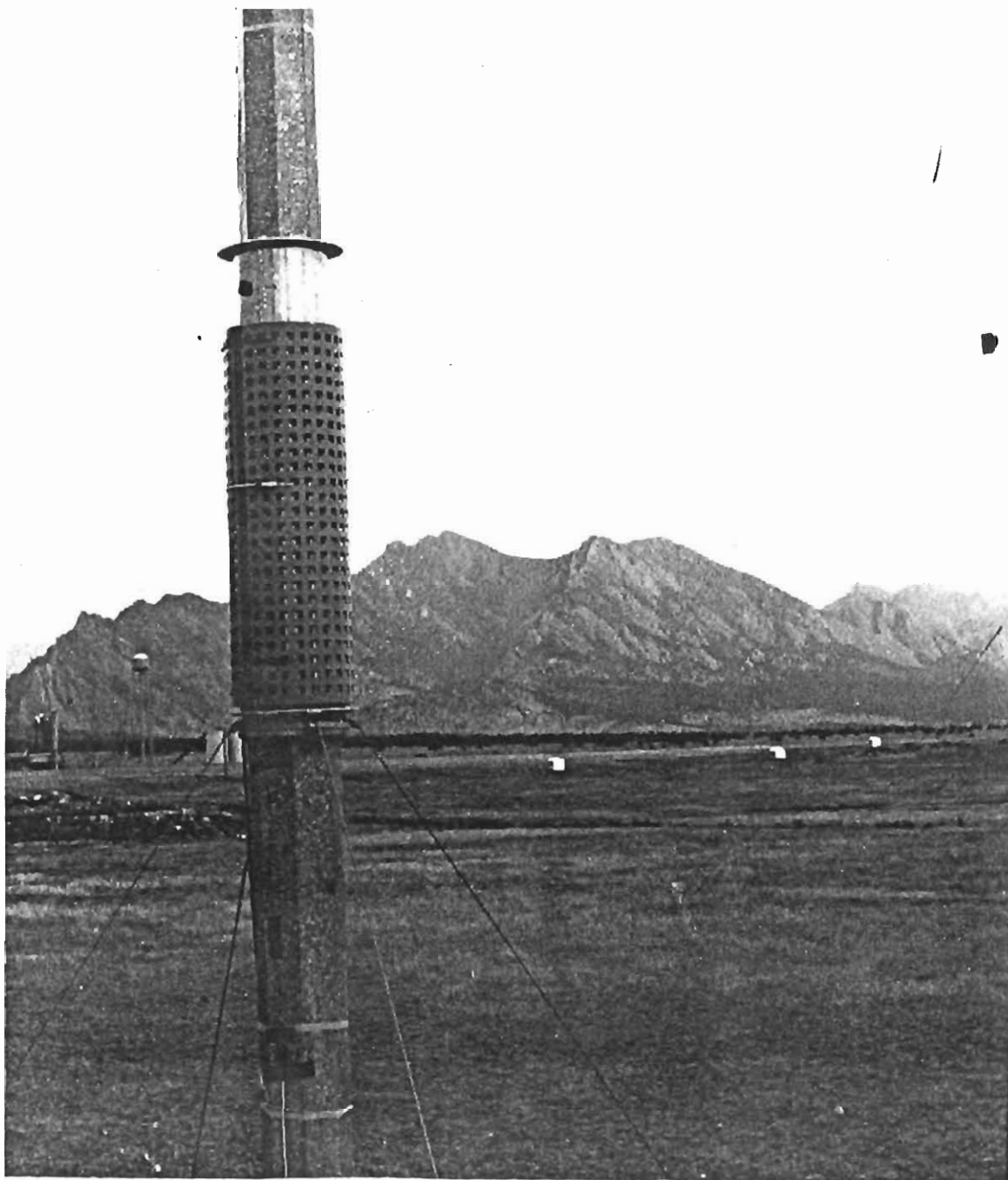


Figure 8-1. View of a Section of the Perforated Shroud Spoiler Installed on the 0.5-m Cylindrical Test Section at the Rocky Flats Wind Energy Research Center

### 8.3.1.1 Acoustic Results

Surprisingly, we found that the perforated shroud enhanced the impulse intensity, in comparison to the bare cylinder. A deep, transient stall is evident in the acoustic-pressure time signature of Figure 8-2, taken from the tower-mounted microphone on the high-pressure (inflow) side of the rotor as the blade passes through the wake 1.5 tower diameters ( $D$ ) downstream.

### 8.3.1.2 Wake Characteristics

The discrete, vertically coherent nature of the wake at 1.5D downstream (the rotor plane) is shown in Figures 8-3 and 8-4 by the velocity and cross-spectra of the upper and lower hot-film anemometer probes (positioned near the center and the shrouded cylinder base, respectively). The strong relationship between the velocity and dynamic pressure fields in the tower wake are illustrated in the spectra and cross-spectrum of the upper hot-film anemometer and boom-mounted microphone of Figures 8-5 and 8-6, respectively.

### 8.3.1.3 Interpretation

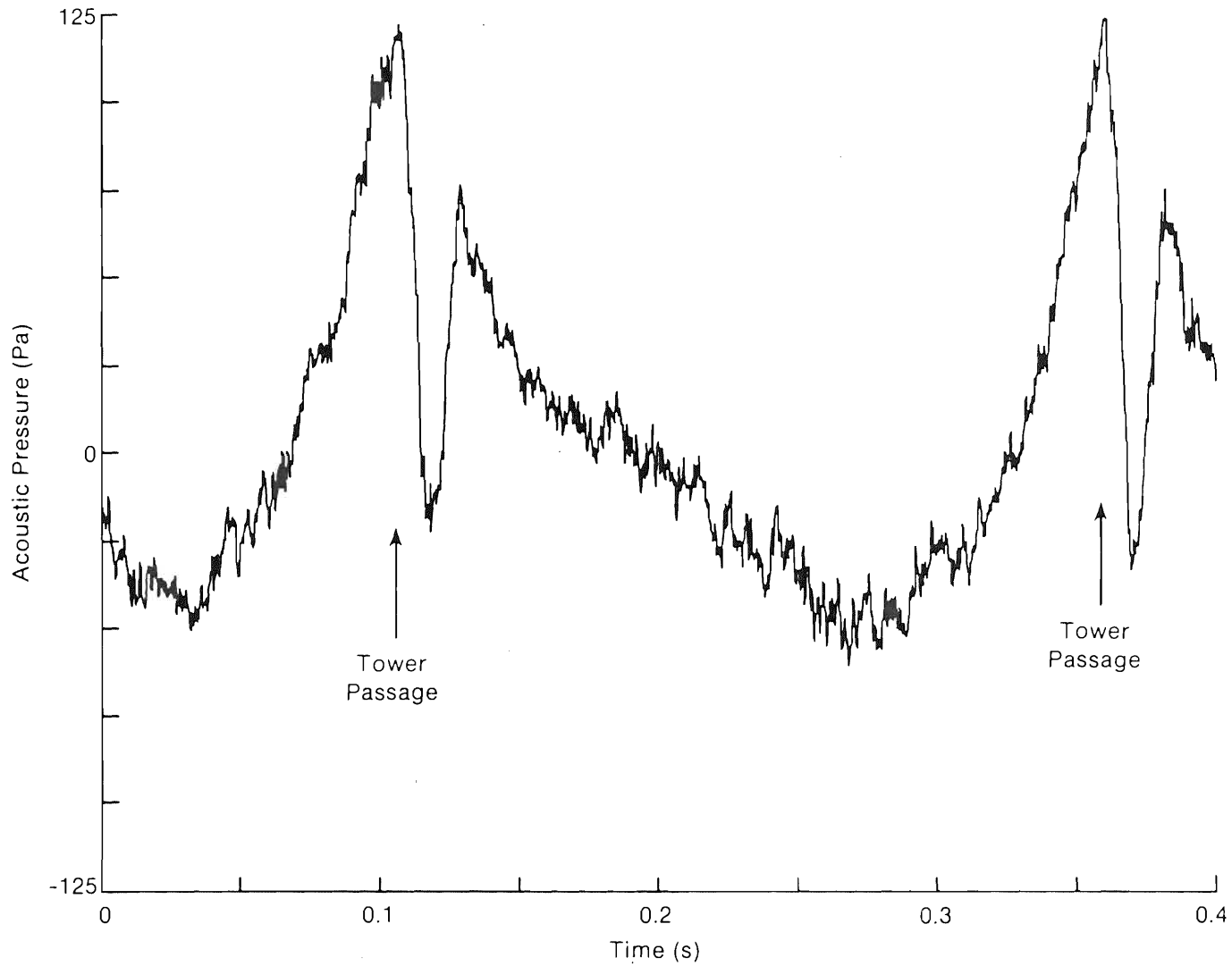
It is obvious that the vigorous impulse activity described in Section 8.3.1.1 is being brought about by strong, vertically coherent vortices present in the shrouded cylinder wake at the 1.5D downstream position. A similar situation occurred during testing at the MIT anechoic wind tunnel, described in Section 5.2.1. In addition to the solid cylinders used in the experiments, NASA furnished a 5.1-cm-diameter cylinder in which elongated perforations had been machined. The resulting on-axis, peak sound pressure level with the cylinder  $3D_r$  upstream of the rotor was the highest of all the diameters tested at that position but fell off rapidly as the upstream distance increased, as shown in Figure 8-7.

We have interpreted this behavior to possibly mean that the shroud wake in the downstream region closest to the cylinder (near-wake) maintains a strong discrete nature but is unstable and may eventually become wideband chaotic by the time the far-wake region is reached ( $3-5D_r$ ). After reducing our available aerodynamic data, taken in full-scale and wind-tunnel testing, we may be in a position to support or deny this delayed wake transition theory. In the meantime, we do not recommend the use of this device for this purpose unless a full-scale, operating Reynolds and Mach number wind tunnel test is conducted (similar to those of Snyder and Wentz [14]) and the dynamic characteristics of the wake are documented at downstream spacings out to  $16D_r$ .

### 8.3.2 The Vortex Generator Spoiler

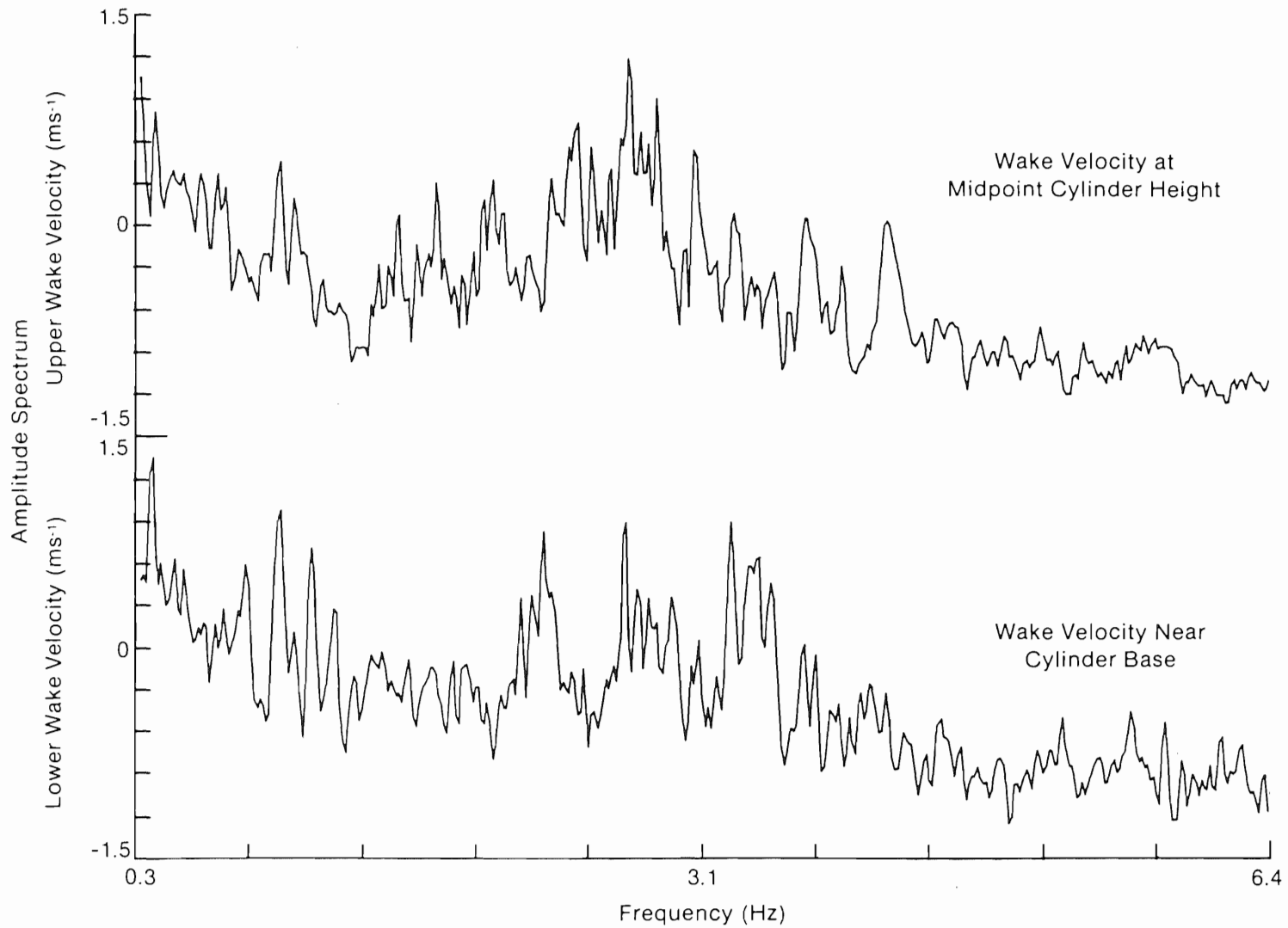
Another way we know to destroy or "trip" a smooth boundary layer is by using a series of vanes placed at acute angles to the flow. These are often referred to as "vortex generators" since they produce a broadband, turbulent wake due to their sharp edges. We employed this technique as shown in Figure 8-8 on our 0.5-m cylindrical test section. Each vane was 0.78 cm (2 in.) square or 10% of the cylinder diameter. The purpose of testing this type of spoiling





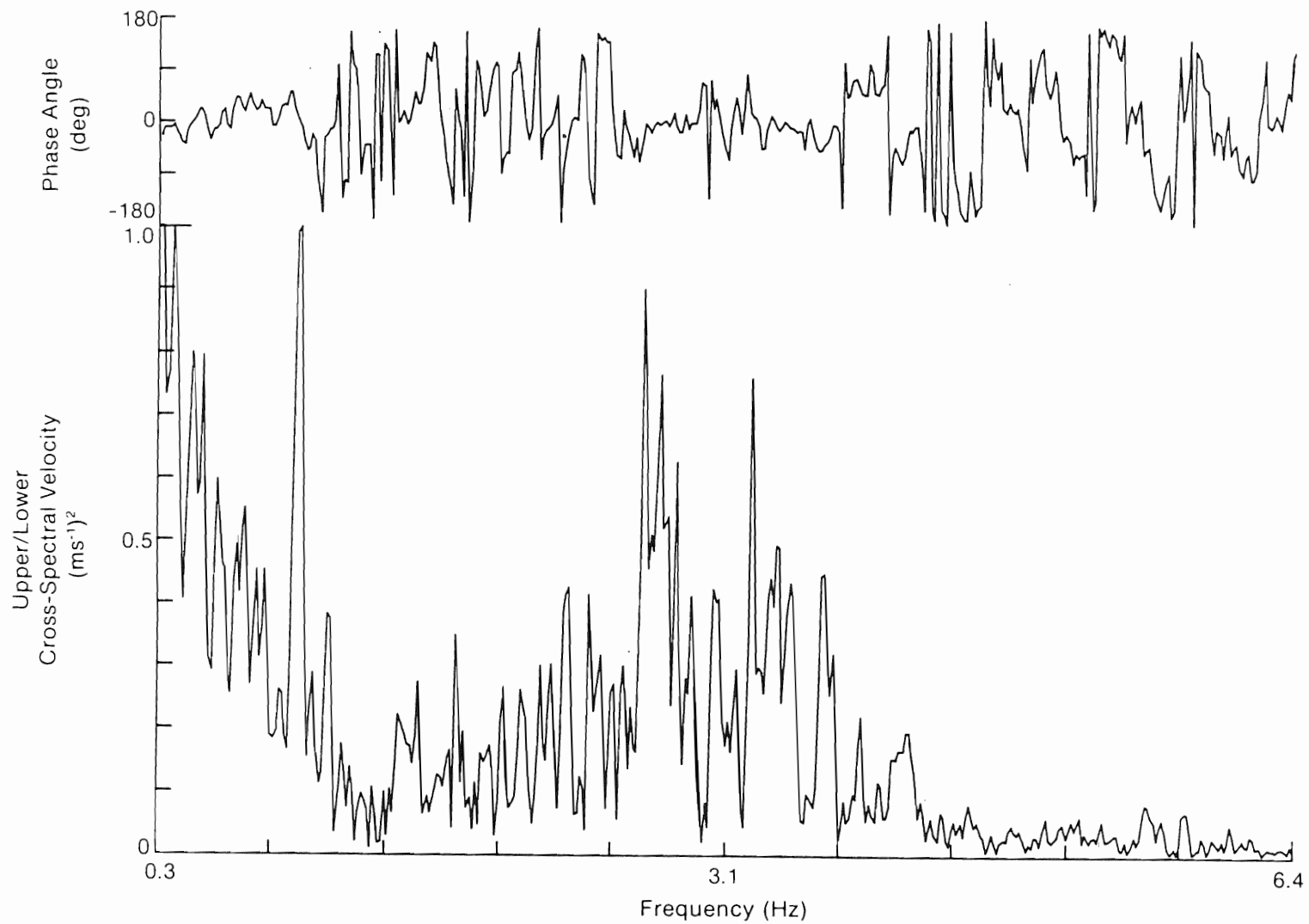
004810

Figure 8-2. Cylinder Base Acoustic Pressure Time Signature for Two Blade Passages by the Tower with the Perforated Shroud Installed



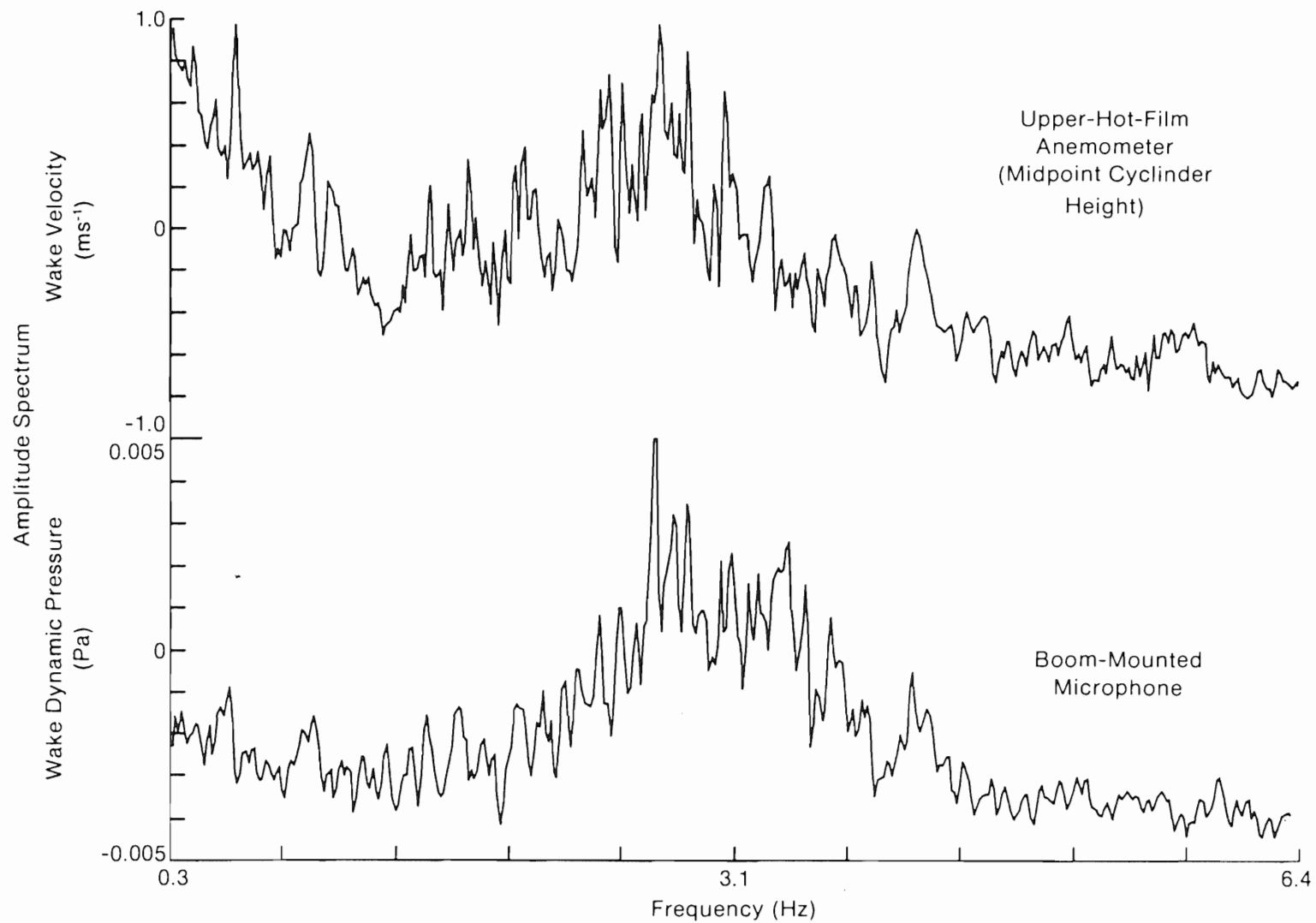
004812

Figure 8-3. Upper (Cylinder Midpoint Height) and Lower (Cylinder Base) RMS Wake Velocity Spectra Measured 1.5D Downstream of Shrouded Test Section on Tower. (D = cylinder diameter or 0.5 m)



004813

Figure 8-4. Same as Figure 8-3, but Cross-Spectrum and Phase of Upper and Lower Wake Velocities



004814

Figure 8-5. RMS Spectra of Wake Velocity (Measured at Cylinder Midpoint) and Dynamic Pressure for Shrouded Cylinder at 1.5D Downstream

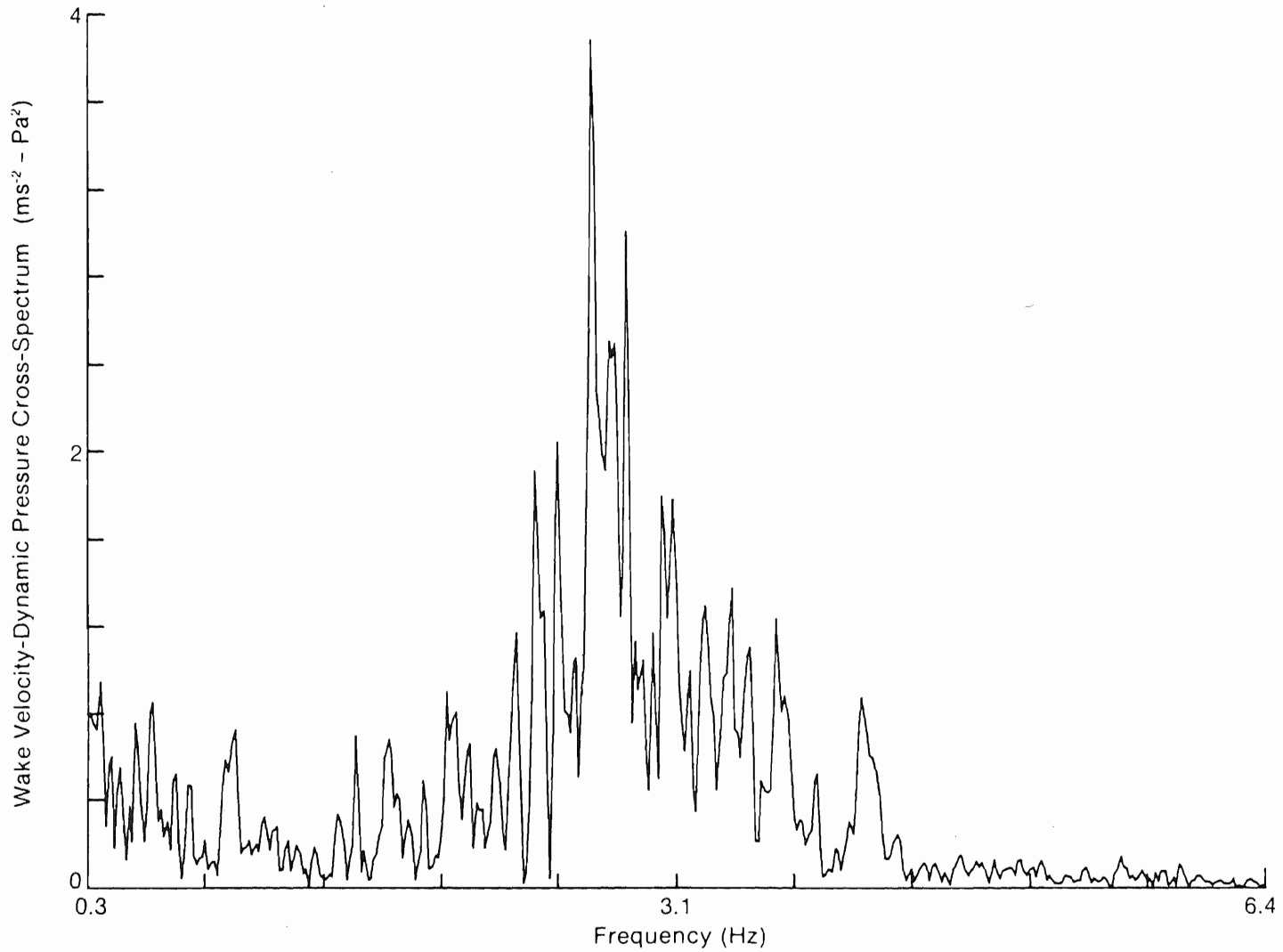
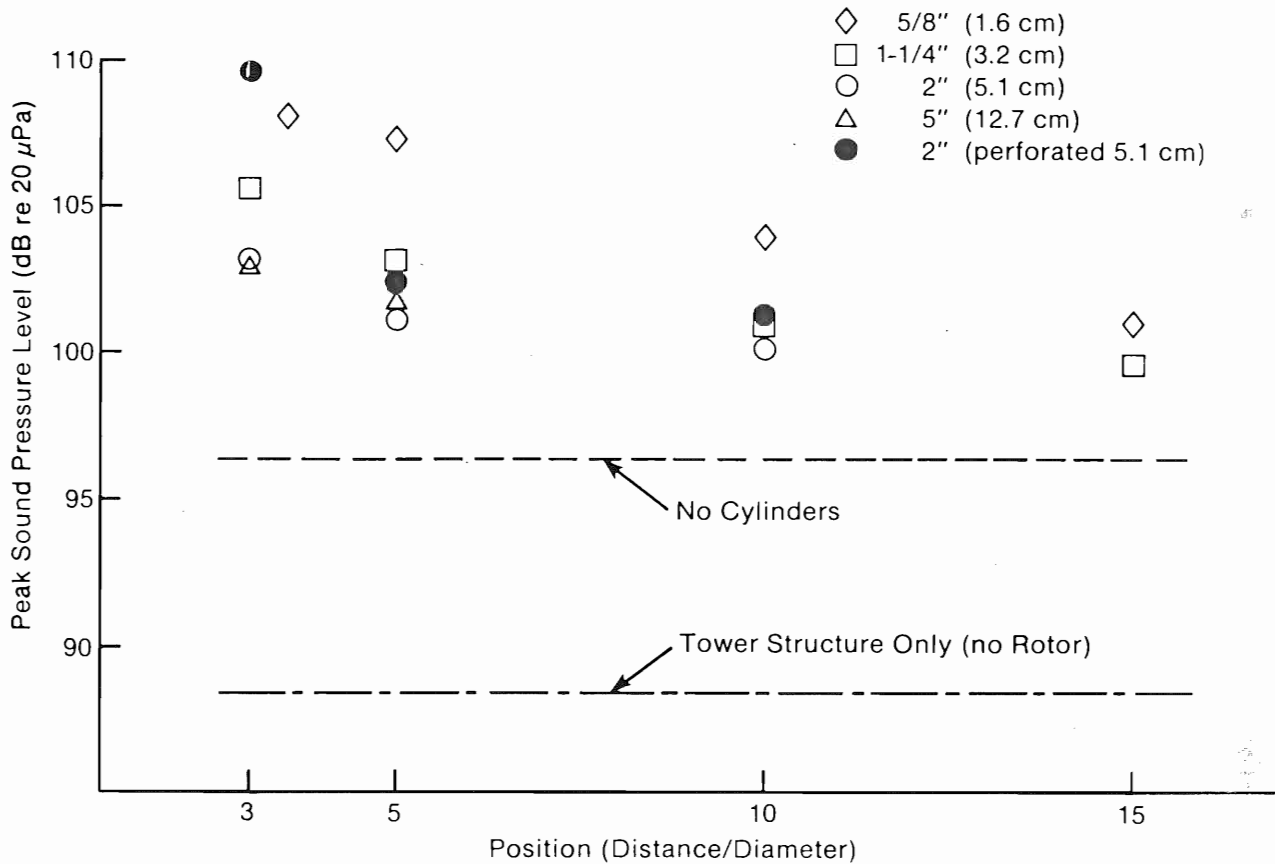


Figure 8-6. Cross-Spectral Magnitude of Wake Velocity and Dynamic Pressure of Figure 8-5  
(Also appears as Figure 5-37)



**Figure 8-7. Peak Sound Level of On-Axis Microphone**

Source: Ref. [15].

device was to evaluate its ability to destroy the strong 2-D shedding of a bluff body (cylinder) by direct mechanical means. Because of the complexity of this type of device (i.e., the making and mounting of so many "turbulator" vanes) it may be not practical to employ it on large tower members such as those of the MOD-1.

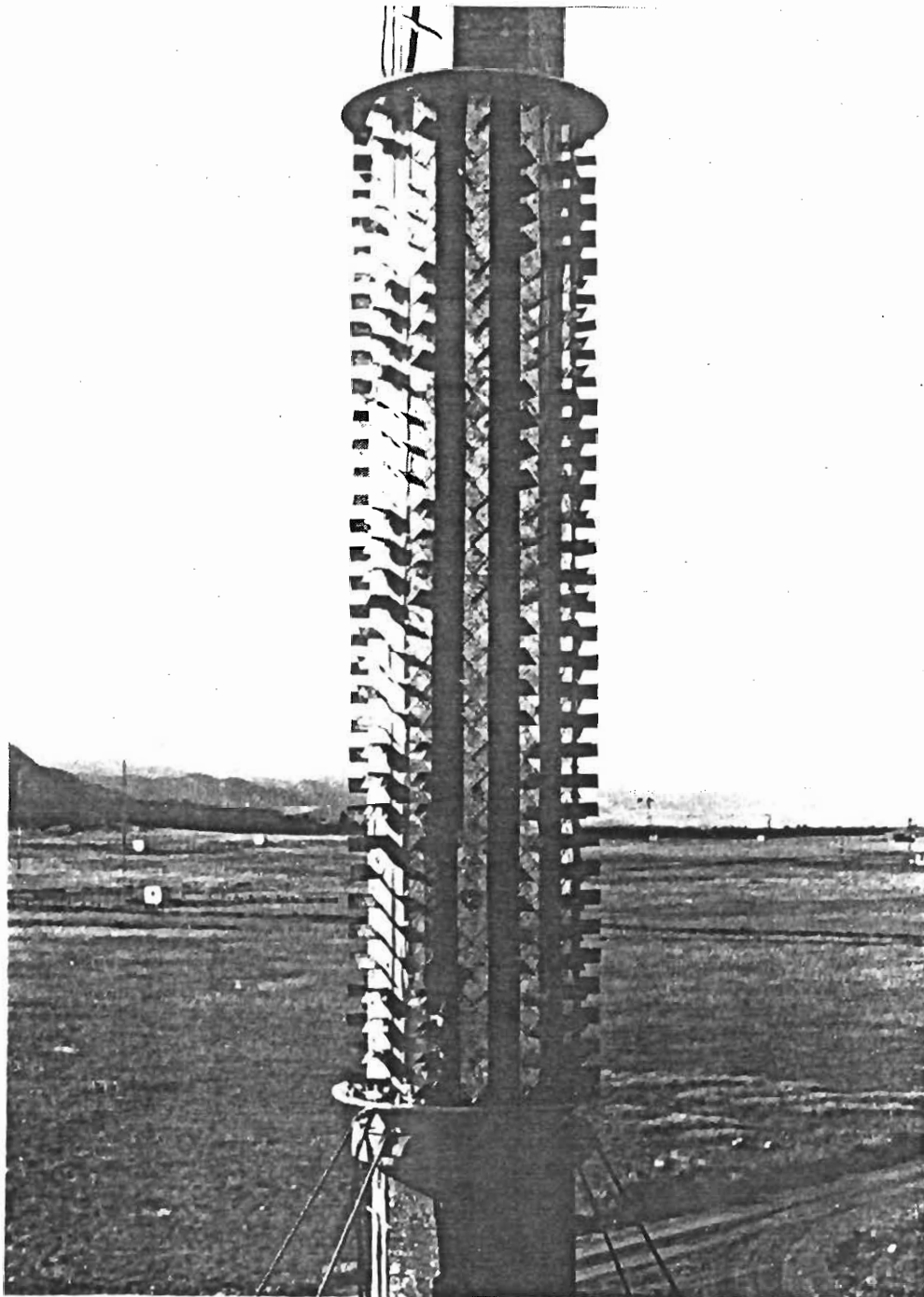


**Figure 8-8.** View of Vortex Generator or Turbulator Spoiler Installed on 0.5-m Cylindrical Test Section. (Note microphone installed at cylinder base.)

### 8.3.2.1 Acoustic Results

In cylinder-height winds averaging  $7-9 \text{ ms}^{-1}$ , no strong impulsive behavior was aurally detected similar to that observed with the perforated shroud and, to a lesser extent, to the bare cylinder in the same wind-speed range. A coherent power analysis of the tower-mounted microphone and freestream turbulence signals in Figure 8-9 shows that the tower shedding is locked into a Strouhal-type excitation in the inflow with a peak at 1.51 Hz. A detailed acoustic analysis of these data, however, remains to be done.

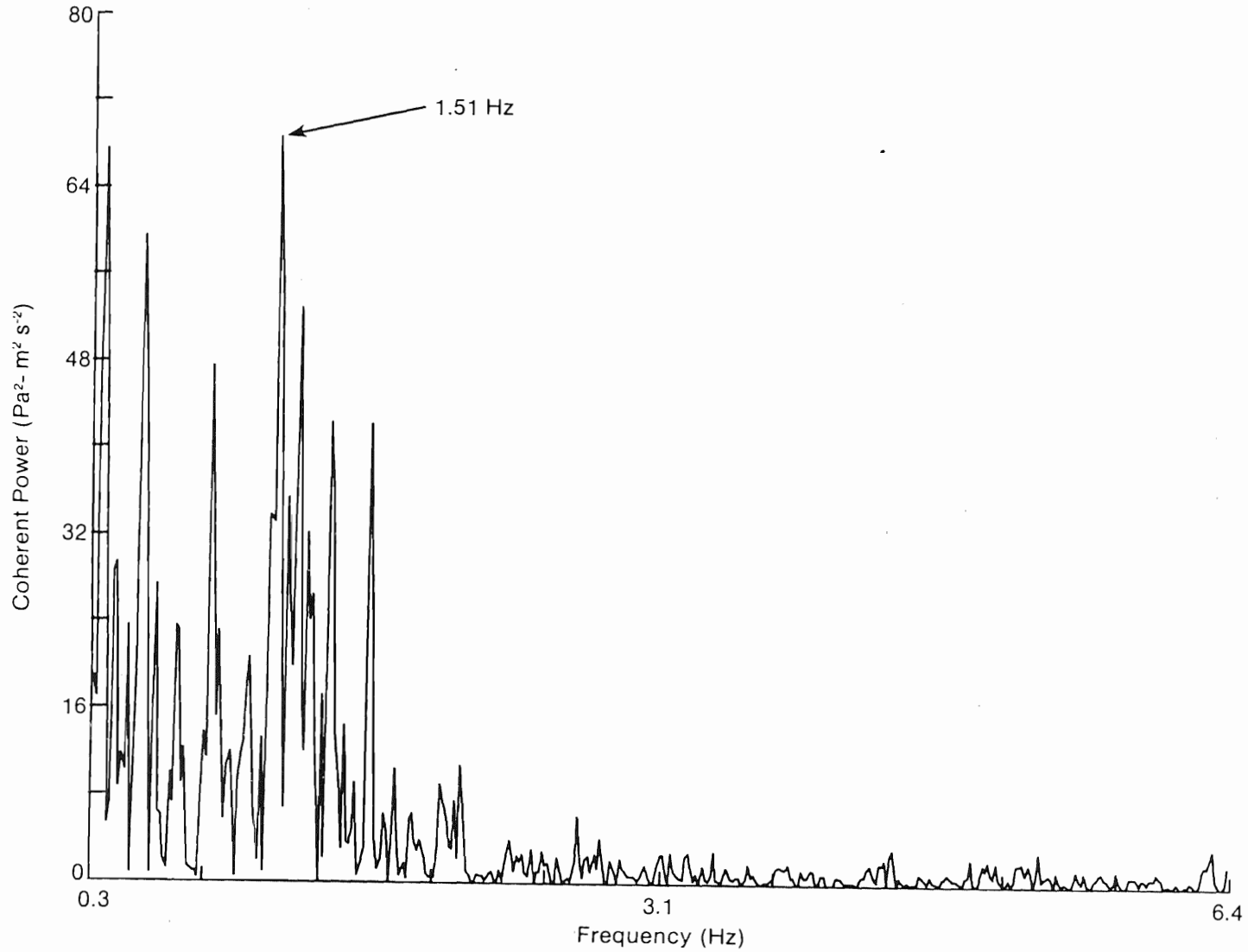
### 8.3.2.2 Wake Characteristics

This test revealed a very important characteristic of WECS tower wake flows. The photograph of the test configuration shown in Figure 8-8 indicates that our spoiler section occupied only that portion of the support tower immediately upwind of the rotor disk with no treatment above or, more importantly, below the tip of the blade. The consequences of treating only a portion of a bluff body with a spoiling device are evident in Figure 8-10, in which averaged wake velocity spectra are presented from the upper hot-film anemometer (positioned about half-way up the cylinder) and its lower counterpart (near the cylinder base). The upper velocity spectrum indicates, as expected, a generally incoherent, broadband turbulent flow demonstrating that the spoiler was operating in a desirable mode. However, when we examine the lower spectrum, we find that discrete shedding is evident. The coherent power analysis of Figure 8-11 for these two velocity signals indicates that some vertical structure does exist from the cylinder base to the midpoint at a discrete frequency of 1.58 Hz, which is close to the coherent Strouhal shedding frequency indicated in Figure 8-9 at 1.51 Hz. This vertical coherence also appears in the correlation between the wake dynamic pressure and the velocity field as indicated in the coherent power analyses with the upper and lower hot-film signals in Figures 8-12a and 8-12b.

### 8.3.2.3 Interpretation

The acoustic and wake characteristic analysis has indicated that the vortex generator spoiler was at least partially functioning. The general broadband nature of the wake turbulence spectrum as measured at the cylinder midpoint indicates an effective destruction of the vertical separation line found on the base cylinder. The presence, however, of relatively strong, discrete components near the cylinder base, along with weak vertical coherence extending up to the midpoint, demonstrates the substantial influence of the unaffected shedding process above and below the treated portion of the cylinder. We attribute this phenomenon to the cogency of the pressure forces present and to their influence extending vertically, most likely through the strong central pressure gradients present in the shed vortices. Snyder and Wentz [14] found a wake shed from a polygonal shaped bluff body (an eight-sided body in our case) tended to be more periodic or discrete than a comparably true cylindrical shape. This indicates that the vortex elements are probably much stronger due to the well-defined vertical separation lines afforded by the edges on the body itself.

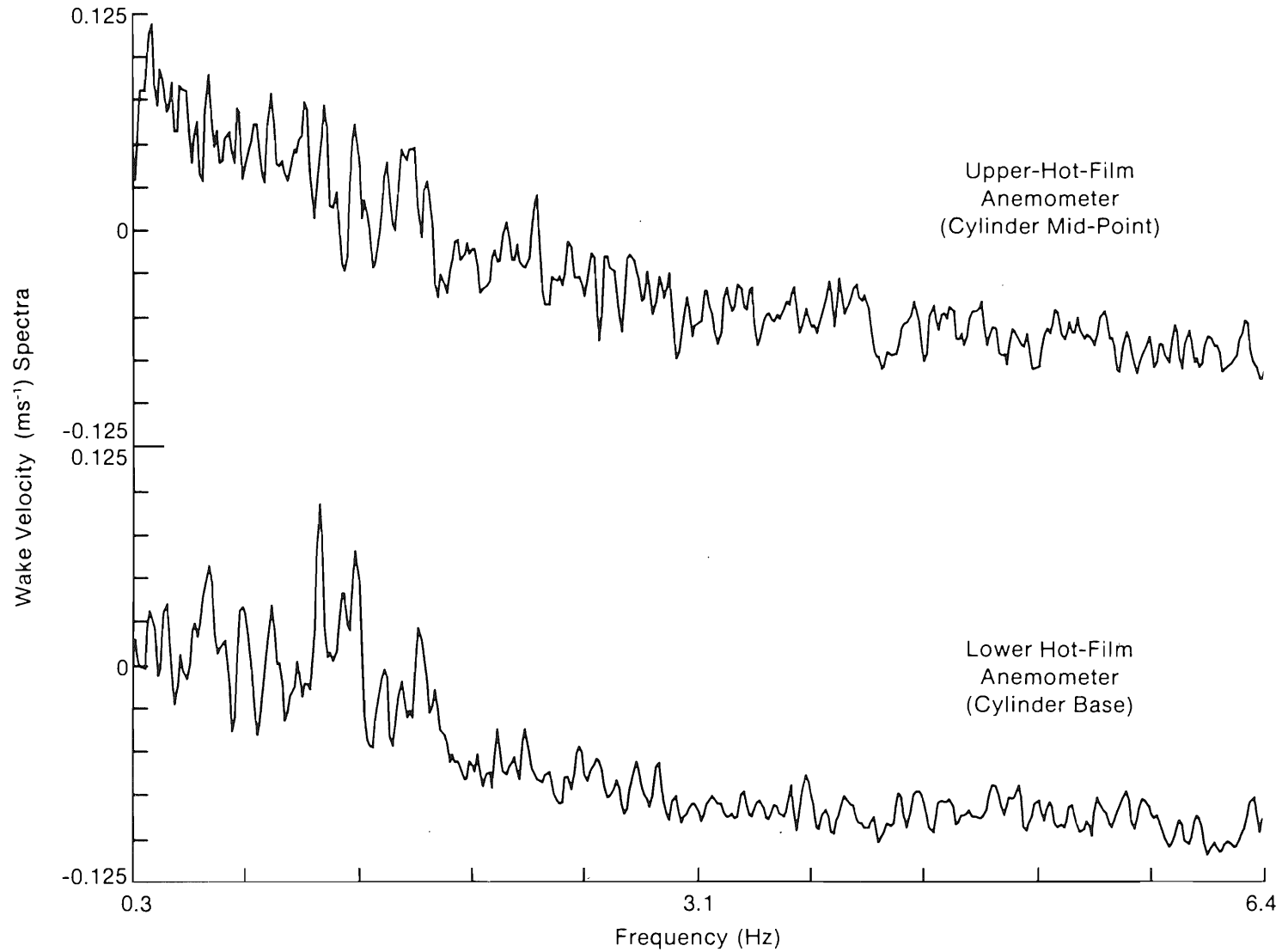




818700

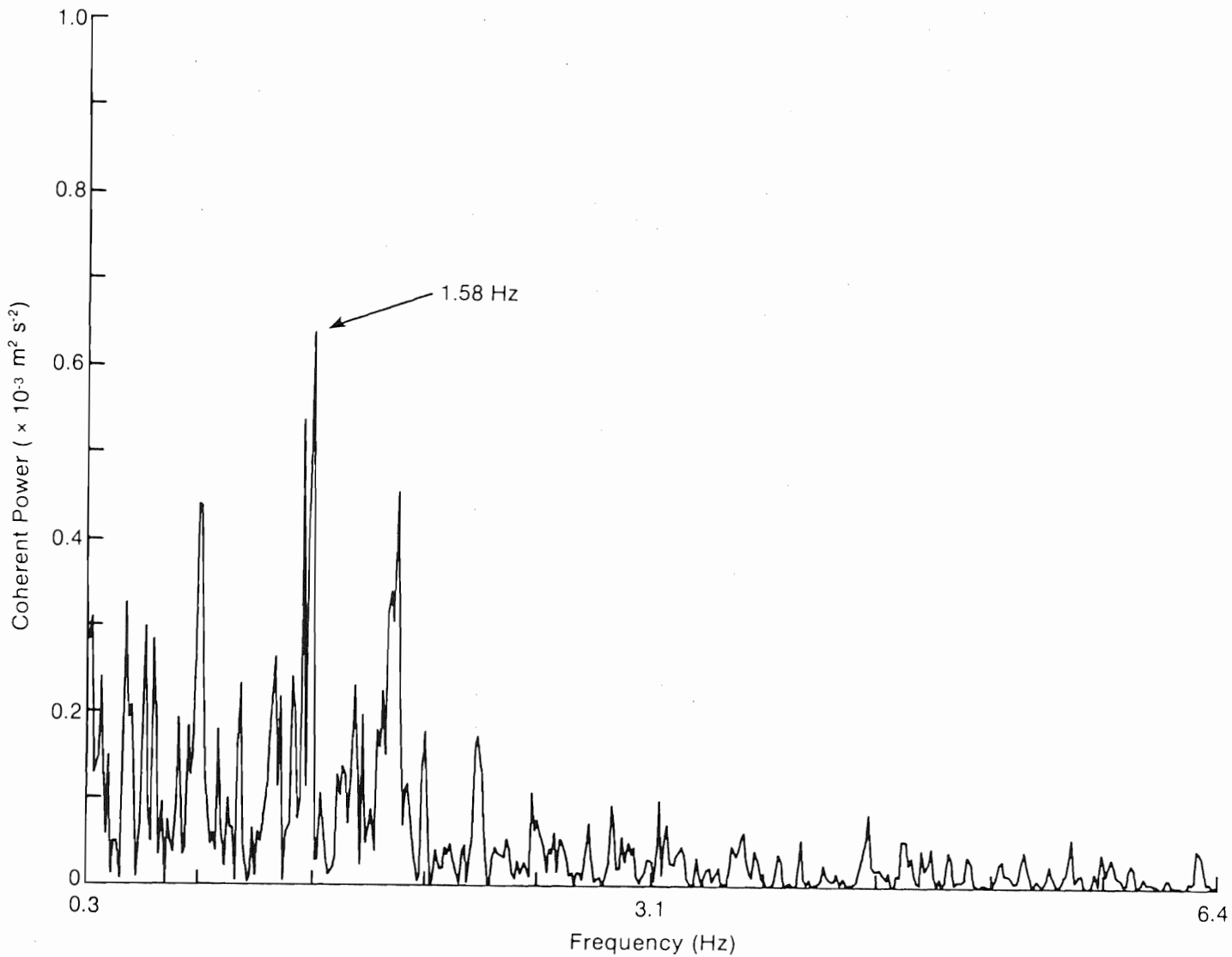


Figure 8-9. Coherent Power Analysis of Freestream Turbulence and Tower Base Dynamic Pressure



6184819

Figure 8-10. Upper (Cylinder Midpoint) and Lower (Cylinder Base) RMS Velocity Spectra at 1.5D Downstream of Vortex Generator-Modified Cylinder



004847

Figure 8-11. Coherent Power Analysis of Upper and Lower Wake Velocities of Figure 8-10

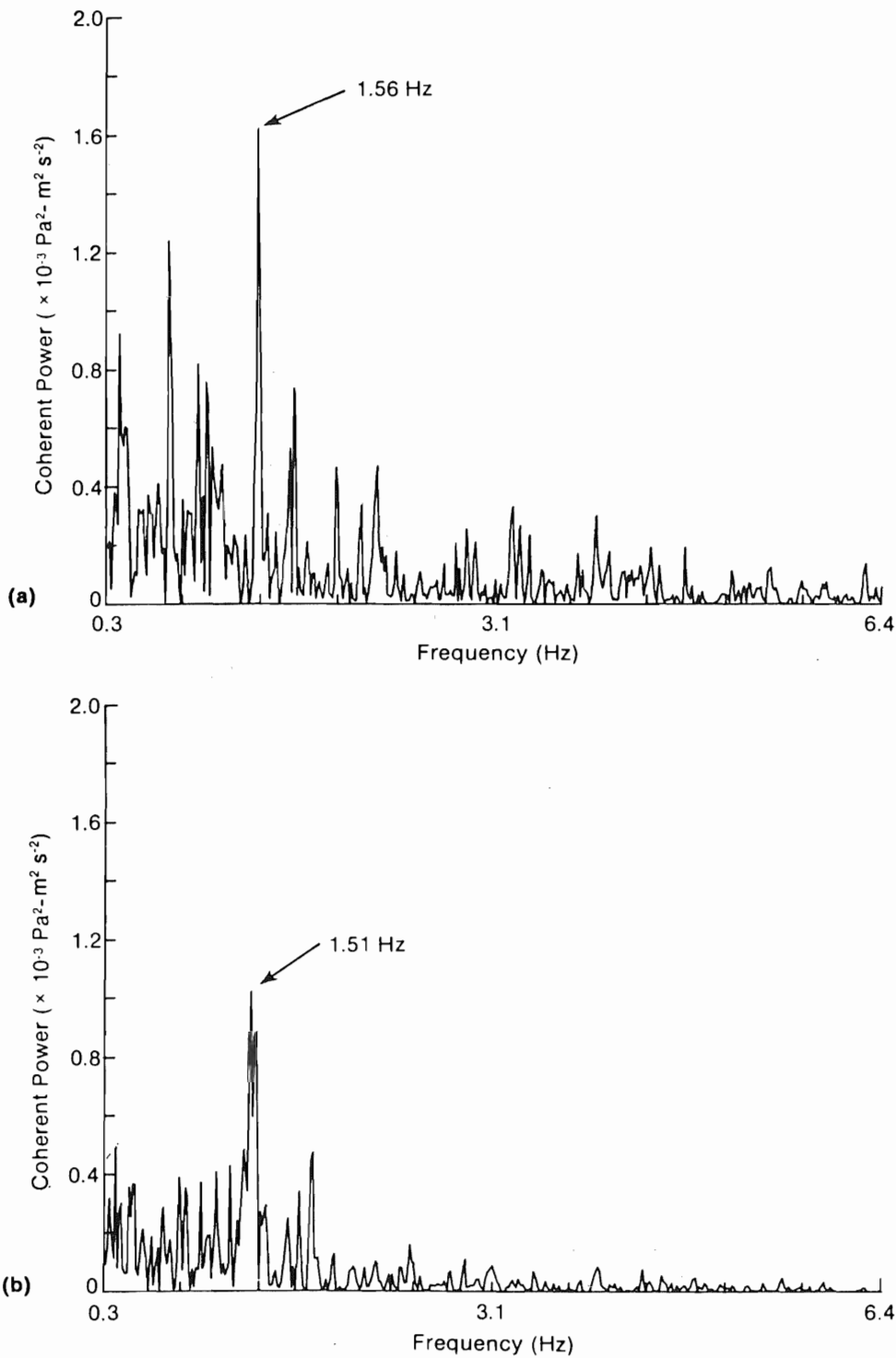


Figure 8-12. Coherent Power Analysis of Upper (a) and Lower (b) Wake Velocities and Dynamic Pressure at 1.5D Downstream of Vortex Generator-Treated Cylinder

We conclude that the vortex generator or turbulator type of spoiler will provide the separation line distortion required to prevent strong 2-D wakes from developing in the lee of cylindrically shaped support tower elements. This particular experiment, however, has shown the need to treat not only the portion of the tower element immediately upstream of the rotor plane, but also at least the length of the rotor below the blade tip in order to minimize effects of untreated areas and thus reenergize the spoiler-derived portion of the wake with discrete structures.

### **8.3.3 The Helical Strake Spoiler**

The third type of aerodynamic spoiler investigated has been the helical strake (or spiral fence). This device was first proposed by Scruton and Walshe [42] as a means of preventing aeolian instabilities which, if coupled to lightly damped modes, could be responsible for failures of cylindrically shaped structures such as tall, smokestacks. The advantage of the strake, and the two previous devices discussed, is that they are omnidirectional in their effectiveness. We have considered other devices that have been suggested (such as airfoil sections, upstream fences, etc.), but all suffer from the disadvantage of needing to be moved with the wind azimuth to be effective. This ability to follow the wind necessitates additional mechanical devices such as low-friction bearings and complicated mounting devices, which, if they fail to function properly, may make the noise problem more severe than if the problem were left untreated.

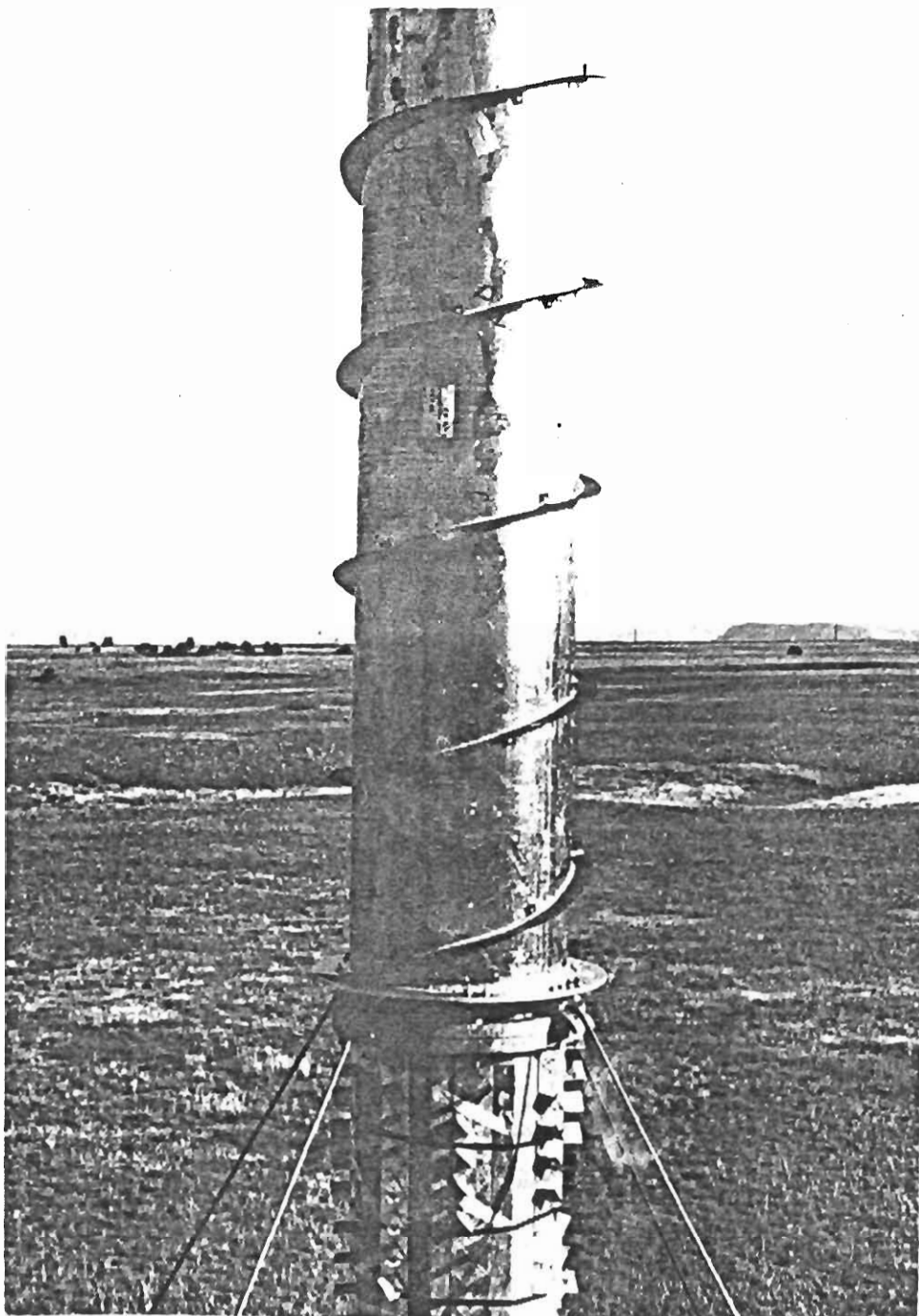
The theory behind the helical strake, as shown in Figure 8-13 installed on our cylindrical test section, is that it continuously distorts the parallel or vertical separation line from which the 2-D wake is generated. Woodgate and Maybrey [43] performed extensive testing to determine the most effective strake configuration (in terms of minimizing aeolian instabilities) and found the optimum to be three strakes (fences), a screw pitch angle equivalent to about 5 cylinder diameters (D) ( $30^{\circ}$ - $40^{\circ}$ ), and a height of about  $0.1D$ . Our test item, which was manufactured by a special machine designed to make auger elements, was constructed of  $5 \times 0.1$  cm ( $2 \times 0.25$  in.) steel bar stock formed into a spiral with a 10 pitch (the shape most readily available). We also reinstalled short sections of the vortex generators below the base of the test cylinder in an effort to minimize "crosstalk" between the treated and untreated portions of the support tower, as pictured in Figure 8-13.

#### **8.3.3.1 Acoustic Results**

In winds averaging  $7-8 \text{ ms}^{-1}$  and with a good indication of the Strouhal excitation of the tower wake, no impulsive-type noise could be audibly detected. A more quantitative analysis of the available data remains to be done, however.

#### **8.3.3.2 Wake Characteristics**

The wake characteristics, as measured in the rotor plane  $1.5D$  downstream, are exemplified in the velocity spectra derived from hot-film anemometers placed at the cylinder midpoint height and near the base of the test cylinder as



004823

Figure 8-13. View of Helical Strake (Spiral Fence) Spoiler with Vortex Generator Sections Installed Below on 0.5-m Test Cylinder

shown in Figure 8-14. The upper probe spectrum is essentially broadband with a mean-square value of  $0.868 \text{ m}^2\text{s}^{-2}$ . The flow at the cylinder base is more energetic (probably influenced by the vortex generators immediately below), with a mean-square value of  $4.16 \text{ m}^2\text{s}^{-2}$  but with what appears to be a discrete component at 2.31 Hz. The coherent power analysis of Figure 8-15 does, however, indicate some vertical coherency between the base and midpoint of the straked cylinder, which we believe to be the result of influences from either below or above the treated area, or both. The coherent power analysis between the wake velocity and dynamic pressure fields strengthens the argument that the wake at midpoint height is broadband chaotic, as evidenced by Figure 8-16a and with some discrete elements in the wake near the base, as indicated by Figure 8-16b.

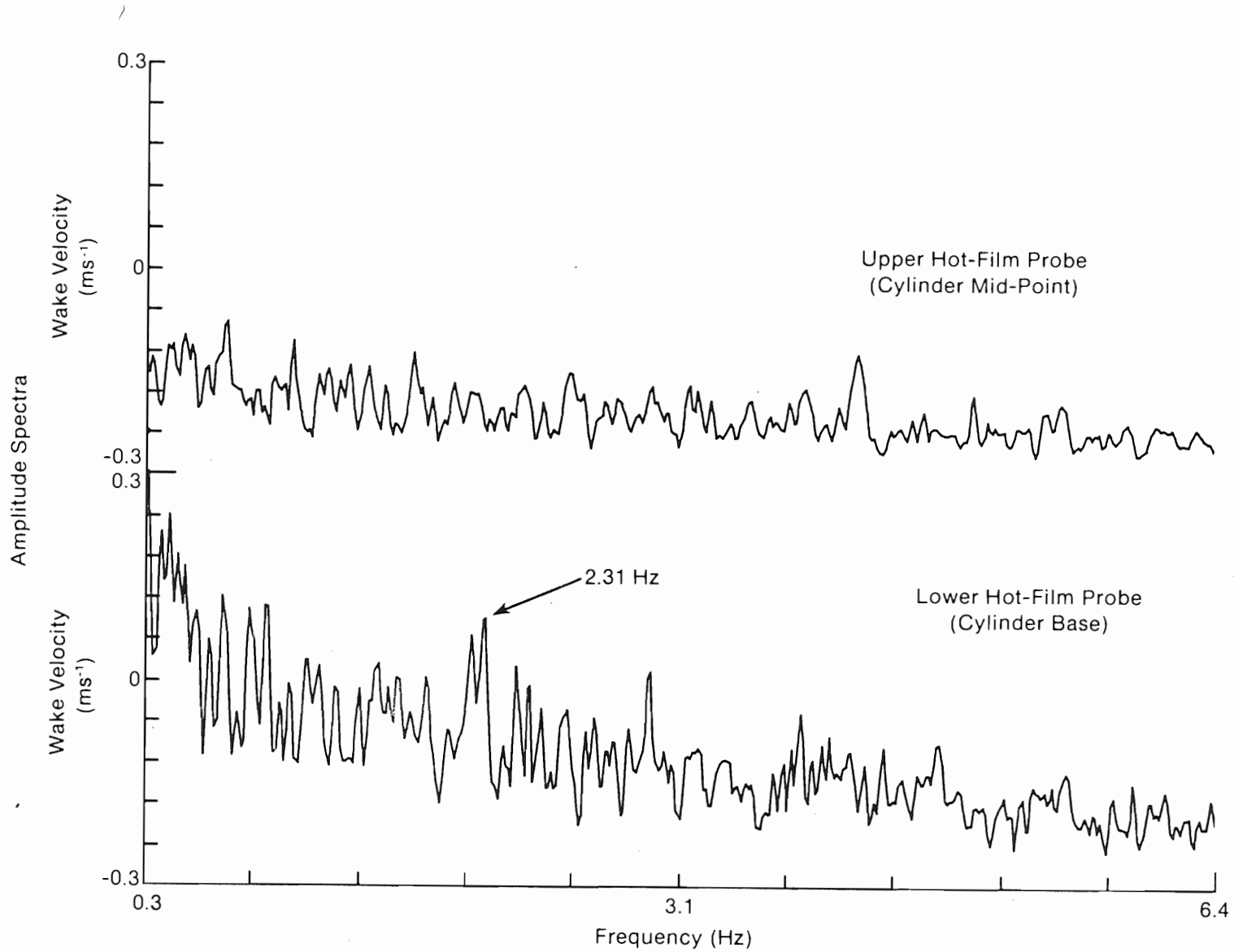
### 8.3.3.3 Interpretation

The wake measurements at the cylinder midpoint height, where the influence of the untreated tower sections appears to be minimal, confirms the effectiveness of the helical strake in converting a discrete 2-D flow into a chaotic 3-D circulation--the desired goal. These results are in agreement with those of Snyder and Wentz [14] who found a similar wake structure downstream of a straked 0.5 cylinder in their full-scale Reynolds number wind tunnel test.

There has been some criticism of using spoiling devices such as the strake because of the potential for an increased wake deficit caused by the high drag coefficient in the supercritical Reynolds number ( $Re > \sim 300,000$ ), as plotted in the data of Figure 8-17 from Ref. [44]. We believe this may only be a consideration for turbines whose rotors pass in the near-wake region or closer than about  $3D$  because the strong 3-D circulation prevalent in the far-wake region tends to diminish the mean deficit rapidly by being re-energized by freestream turbulence entrainment. Further, the space-scale spectrum of the wake turbulence created by strake action appears not only to be broadband but also dominated by a scale that removes much of the remaining perturbations from the critical unsteady excitation range discussed in Section 8.2. It is also known that a predominance of small-scale turbulence can be beneficial, because it has a stabilizing influence on the airfoil boundary layer and delays separation, something we found to be true in our analysis of the MIT anechoic wind tunnel tests reported in Section 5.2.1.

## 8.4 CONCLUDING REMARKS

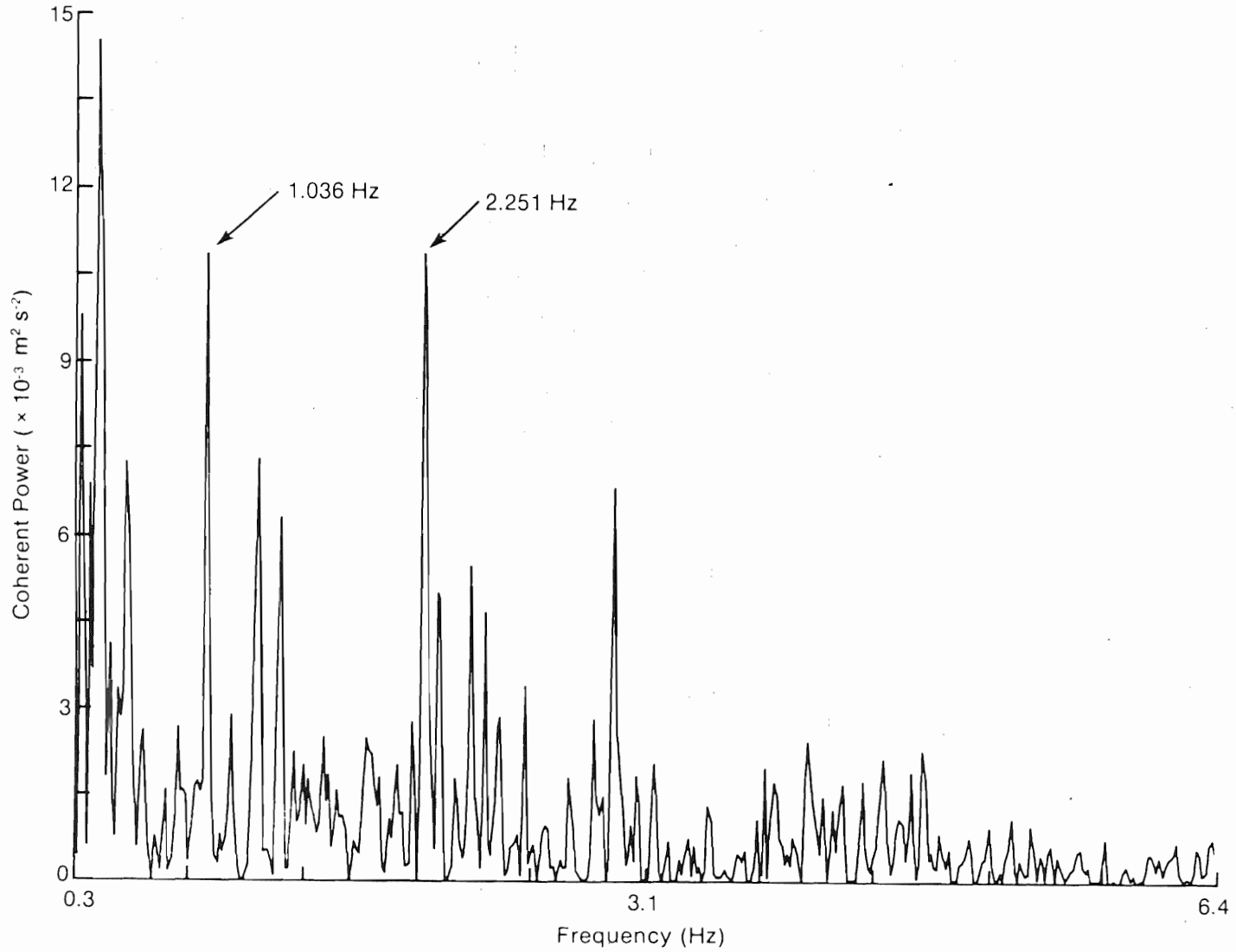
In this section, we have reviewed our results in evaluating the effectiveness of various aerodynamic spoiler designs whose purpose is to (1) destroy the parallel or vertical separation line of a cylinder wake responsible for vertically coherent, 2-D vortex wakes in the lee of the MOD-1 tower legs, and (2) convert the wake turbulence from narrowband discrete to a broadband characteristic with a chaotic 3-D circulation. While we cannot yet be sure about the perforated shroud (which needs more study), the vortex generator or turbulator and the helical strake spoilers (if installed properly) do perform the required functions. The strake, however, appears to be the most desirable, based on construction and installation simplicity. We suggest, therefore, the installation of appropriately configured strakes to almost the entire height



004824

Figure 8-14. Upper and Lower RMS Wake Velocity Spectra Measured  $1.5D_r$  Downstream of Cylinder Treated with Helical Strake





004825

Figure 8-15. Coherent Power Analysis of Upper and Lower Wake Velocities of Figure 8-14

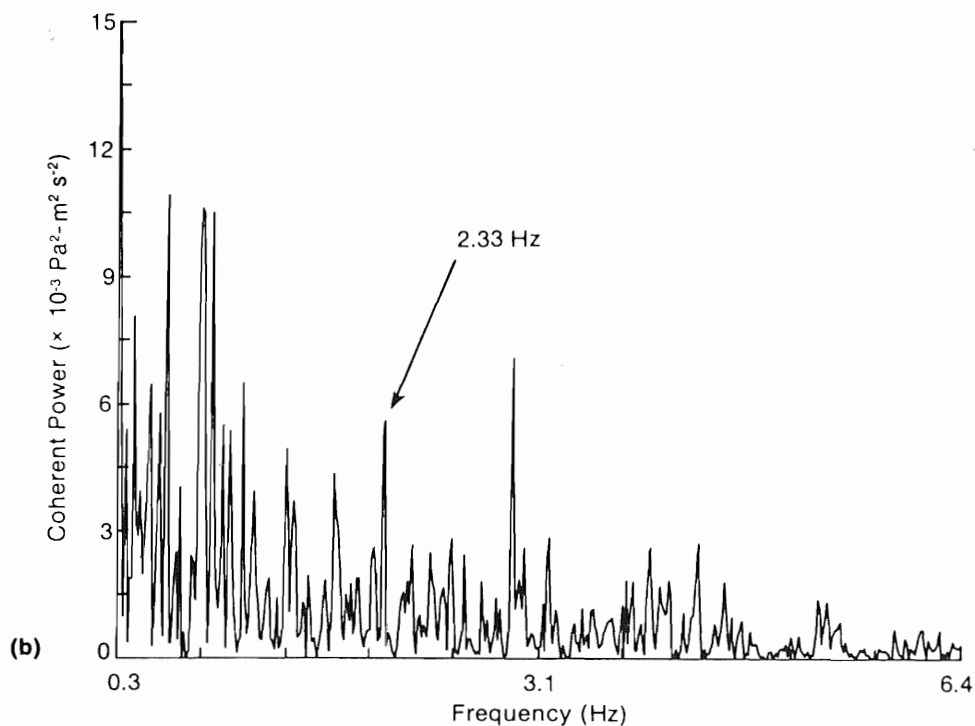
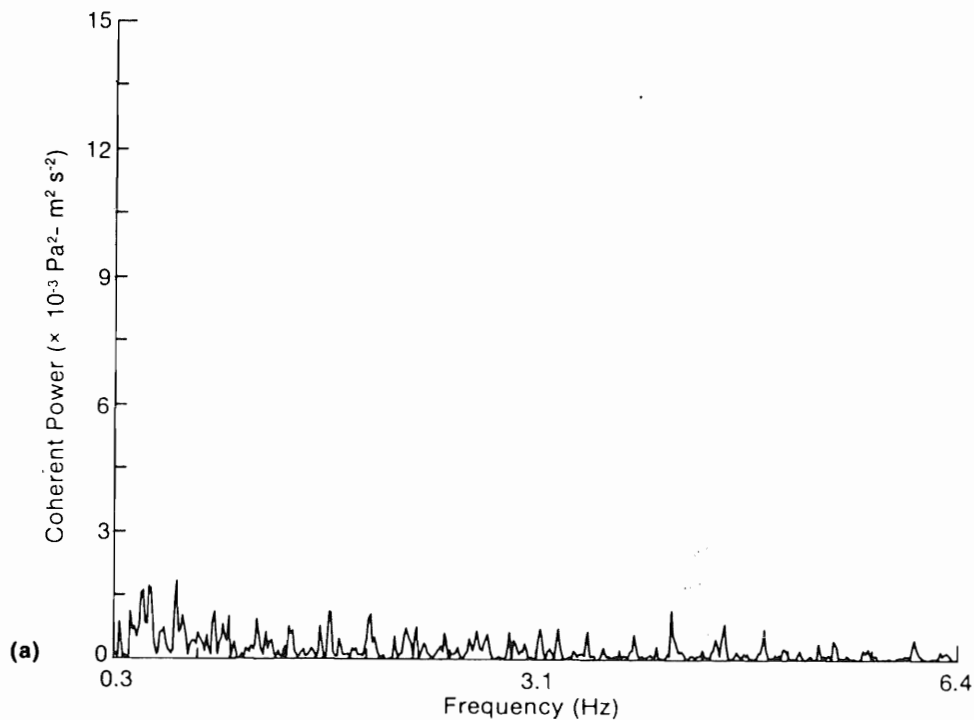
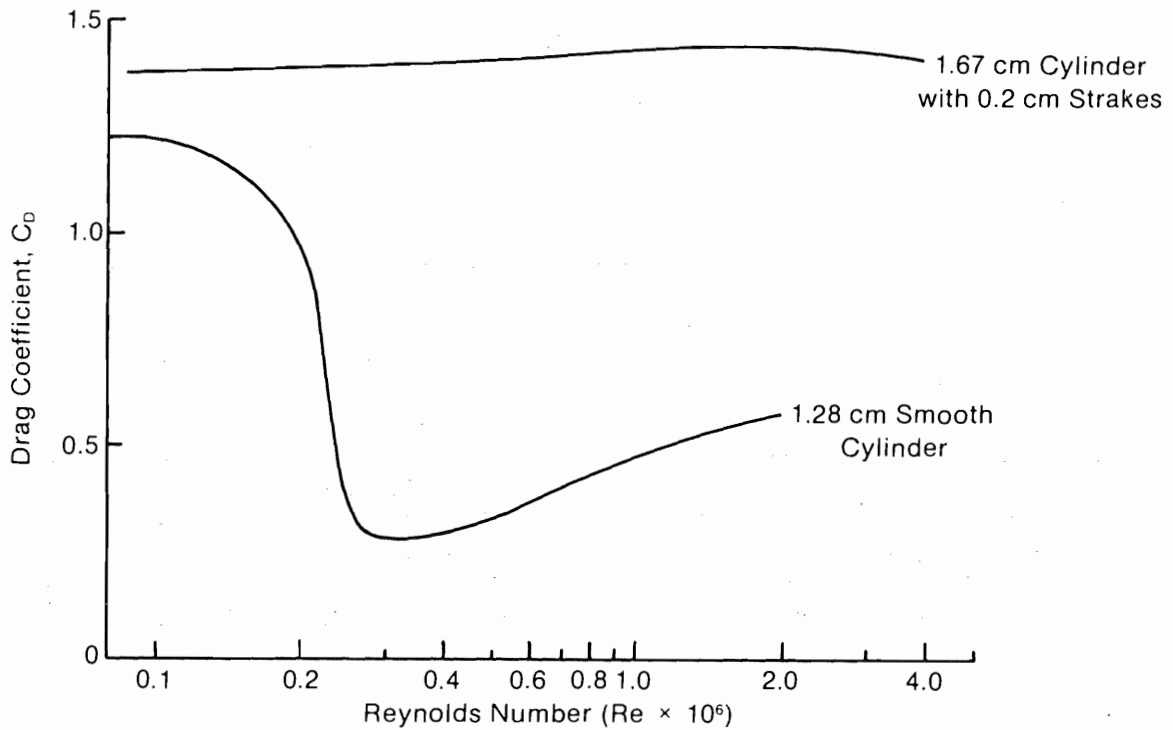


Figure 8-16. Coherent Power Analysis of (a) Midpoint Wake Velocity and Dynamic Pressure and (b) Base Velocity and Wake Dynamic Pressure

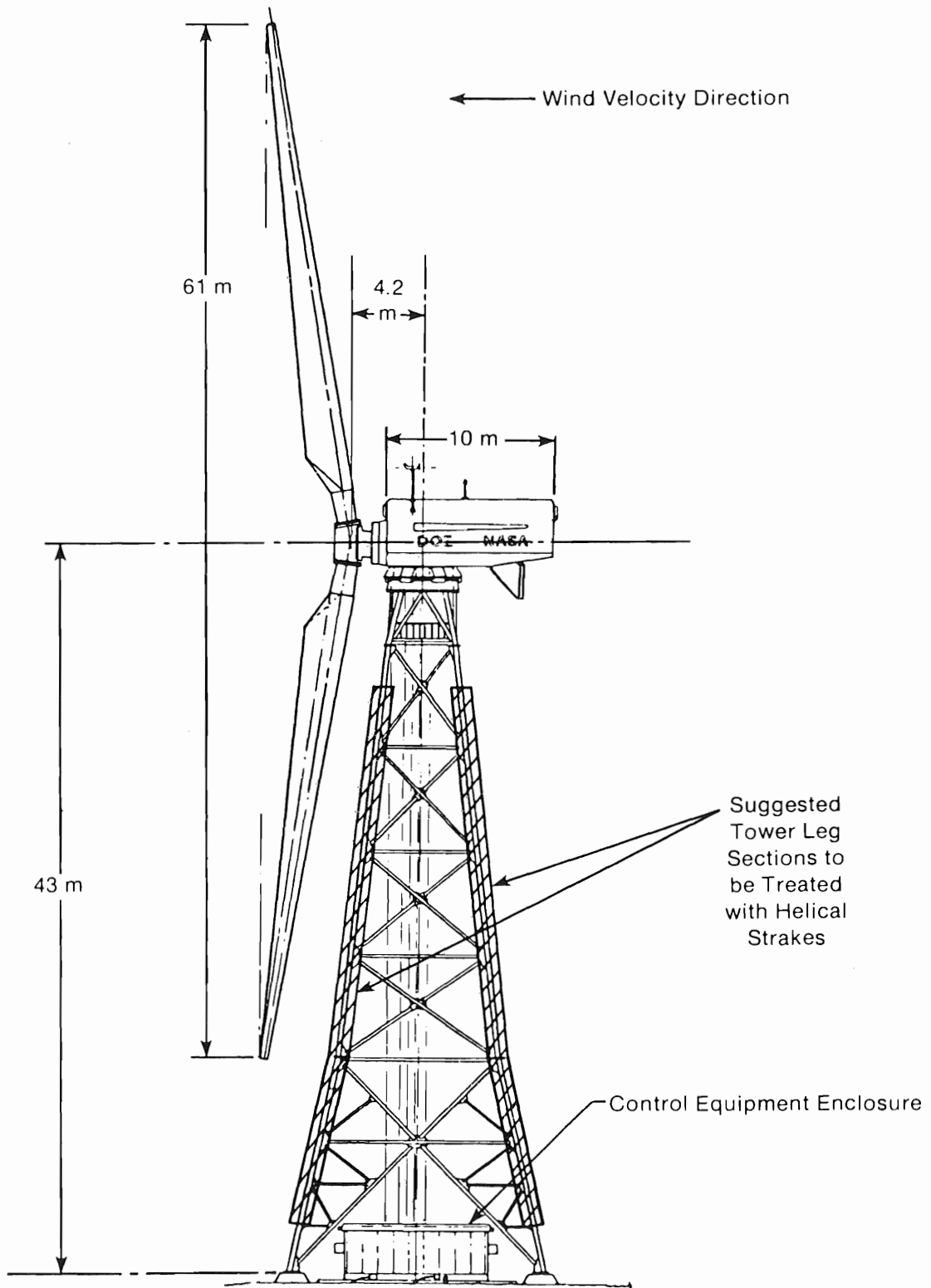
of the large 0.5-m-diameter vertical MOD-1 tower members. We suggest that these devices be installed over the large cylindrical members shown in Figure 8-18 before a turbine of this design is operated in the future.



004827

**Figure 8-17. Drag Coefficients vs. Reynolds Number for Smooth and Straked Cylinders**

Source: Ref. [44].



828400  
004828

Figure 8-18. Suggested Helical Strake Treatment of MOD-1 Tower Legs

## SECTION 9.0

### CONCLUSIONS

The objectives of this study have been to investigate the physical mechanisms responsible for the generation, propagation, and impact of the annoyance associated with the operation of the MOD-1 wind turbine near Boone, North Carolina. It was necessary to develop a definitive knowledge of each of these areas in order to (1) best decide on the most effective abatement procedure to employ on the MOD-1 itself, and (2) apply this knowledge to noise control in other wind turbine designs, both large and small.

#### 9.1 A PROPOSED PHYSICAL MECHANISM RESPONSIBLE FOR HUMAN ANNOYANCE

In this section we summarize our conclusions in defining proposed physical mechanisms responsible for the annoyance (impact) of the dozen families involved in the study and the process involved in the generation and propagation of the noise to the affected homes.

Our detailed field investigation of the effect of the MOD-1 noise on two of the affected houses during March 1980 corroborated and confirmed the nature of the annoyance. We have found strong evidence that the major causal agent responsible for the annoyance of the complaining residents was the excitation of highly resonant structural and interior air volume modes by the acoustic impulses generated by the operation of the MOD-1 turbine. The coherent, low-frequency acoustic radiation indicative of these impulses coincides almost perfectly with the fundamental and higher resonant structural modes of the homes. Comparison with a nonimpulsive, low-frequency source affecting residential structures has supported the existence of the annoyance situation perceived by the Boone residents and has shown the same strong acoustic-structural dynamic interaction.

The audible-range sounds perceived indoors by the Boone residents appear to have had at least two sources: (1) secondary emissions from the vibrating of loose objects or very lightly damped structural elements, and (2) direct radiation from the turbine impulses transmitted through the structure. We believe that source (1) was dominant at Boone. The general lack of audible-range sounds present in the homes undergoing nonimpulsive acoustical loading appears to be a consequence of the low emission levels at these higher frequencies and the nontransient, temporal characteristic (low coherence) of the radiation source.

The coherence (impulsiveness) of the emitted low-frequency acoustic radiation has been identified as a major factor in determining not only the level of potential annoyance to residents within a structure, but perception as well. We developed a joint probability technique to assess the level of impulsiveness in wind turbine acoustic radiation using four contiguous octave-frequency bands covering the structurally sensitive range of 5-100 Hz. Using this technique, we were able to make a rough estimate of external joint band intensity levels which can cause perception (not annoyance) within a typical residential

structure. The joint radiation levels (expressed in terms of acoustic intensity and measured external to a structure) in the 8, 16, 31.5, and 63 Hz standard (ISO) octaves should not exceed band intensity threshold limits of 60, 50, 40, and 40 dB (re  $1 \text{ pWm}^{-2}$ ) more than 20% of the time. These figures compare favorably with a summary of low-frequency annoyance situations by Hubbard [32]. Thus, these figures provide the basis for an acoustic figure of merit of the annoyance potential of a particular wind turbine design when compared with actual measurements of joint band levels made at an on-axis reference distance of 1.5 rotor diameters up or downwind of the machine.

## 9.2 AERODYNAMICS GENERATING MECHANISM RESPONSIBLE FOR MOD-1 IMPULSIVE NOISE

The intersection of the MOD-1 rotor blades and the vortex tubes contained in the downstream wakes of the large, 0.5-m-diameter cylindrical tower legs have been shown to be the most likely source of the intense acoustic impulses responsible for the annoyance of the nearby residents. The scale of these disturbances (which is controlled by the tower's major support leg diameter), their vertically coherent structure, and the vortex strength (a function of the freestream velocity) when coupled with the 44xx-series airfoil shape create a strong, transient lift change possibly related boundary to layer separation on the turbine blades, which radiates as a dynamic pressure wave or impulse. We have also shown that the character of the leg wakes is strongly influenced by such environmental factors as the freestream velocity, vertical wind shear and stability, and upwind fetch properties. For these reasons, the severity of the impulses is not simply related to the mean wake deficit, and they exhibit a probabilistic distribution in their physical properties. As a consequence, we have determined that the impulse generation is a result of two narrowband stochastic processes: one is related to boundary layer instabilities in the airflow around the tower legs which controls the downstream wake embedded vortex characteristics and the other, a somewhat similar situation, involves the stability of the boundary layer of the rotor leading edge as it cuts through these wakes.

We have shown that a reduction in impulse intensity below nominally perceptible limits is only possible by (1) making the rotor blade loads insensitive to the 2-D wake disturbances (which would require, in all probability, a different shape and therefore a new rotor), or (2) converting, by some suitable means, the strong, 2-D narrowband wake characteristics into 3-D broadband chaotic throughout the critical perturbation reduced frequency range of  $0.5 < k < \pi$ . Slowing the rotation rate, which has been tried, has been shown to be only partially successful, since no modification of the wake characteristics takes place and the improvement is strictly related to the decrease in the magnitude of the quasi-steady lift. In this regard, we suggest installing an appropriate aerodynamic spoiling device such as the helical strake or fence on each of the four major legs.

## 9.3 ROLE OF ATMOSPHERIC PROPAGATION IN THE SEVERITY OF THE MOD-1 ANNOYANCE

As a result of an analytical and field measurement effort, the Penn State Group [3,30] has found that a combination of terrain reflection and atmospheric refraction is responsible for focusing the turbine impulses into

locations occupied by several of the affected homes. They have estimated, and it has been experimentally verified, that this focusing is capable of raising local incident levels to more than 25 dB above the figure expected from the spherical spreading of the source alone. They also found that ground propagation was insignificant in comparison with reflection and refractive airborne propagation. These results underscore the need to control the noise at the source, not only in the case of the MOD-1, but where any large wind turbines are installed near human populations.

#### 9.4 ANSWERS TO QUESTIONS POSED IN SECTION 1.5

Three specific questions were posed in Section 1.5 of this report, and our answers are presented here.

1. Why did the noise not reach annoying levels each time the turbine was operating? We have shown that the characteristics of the tower leg wakes were very important in whether or not strong impulses were produced. These characteristics (vortex strength, in particular) are functions of the freestream velocity, turbulent energy levels in the critical Strouhal shedding frequency range, vertical shear and stability, and upwind fetch. Further, certain wind directions tended to orient the turbine and its radiating lobes away from the most frequently affected homes at times, or a combination of terrain and atmospheric refraction failed to focus the sound sufficiently to be heard.
2. Why were some families annoyed more often than others and why did the situation confine itself to such a small fraction of the overall population living within 3 km of the machine? Again, the reason why certain homes were affected more frequently was because of three factors: (a) the orientation of the turbine (which positions the lobes of the acoustic dipole in their general direction) (a function of the site climatology); (b) the terrain along the centerline of these dipoles; and (c) the vertical variation of wind speed and temperature. By far, factors (a) and (b) appear to be the most influential, since they both subsequently have an influence over (c). Figures 6-5 through 6-9 show sound ray paths for various radial directions from the turbine, and the importance of the terrain is clear. The small population fraction bothered by the turbine happened to live in locations where a combination of terrain and refractive focusing reached maximums, or caustics, a good portion of the time.
3. Why did the noise appear more noticeable inside the affected homes and why did it become more persistent and perhaps louder during the evening hours? The noise was more noticeable within the homes because of the dynamic amplification and resonances created in the internal acoustic pressure field because of the interaction between the external transient acoustic loading and the lightly damped elastic response of the residential structure. This dynamic interaction serves to extend the impulse time period from a few milliseconds outside to more than a second indoors. There were two reasons why the sounds became more persistent and perhaps more severe at night. The first reason again relates to the site's climatology, in which the diurnal variation in wind speed tends

to reach a maximum during the period slightly before local sunset and continues up to the early hours of the next morning, with a secondary peak occurring just after local sunrise and continuing for one or two hours thereafter. A coupling of this evening wind-speed maximum with the second reason, the transition from a daytime to nocturnal atmospheric surface layer, in which the surface to hub-height stability increases and encourages the development of turbulent shear layers, resulted in a greater degree of Strouhal excitation of the tower leg wakes. This combination of higher wind speeds and Strouhal excitation increased the intensity and 2-D structure of the embedded wake vortices and, subsequently, the severity of the impulse generated by the turbine rotor blades. These conditions may have persisted for up to four or five hours, depending on conditions, and therefore appeared more severe and persistent to the affected residents during those periods of the day. Furthermore, generally lower ambient noise levels occur during the early evening hours, which perhaps also contributed to the increased sensitivity of the affected residents.



## SECTION 10.0

## REFERENCES

1. Balombin, J. R. 1980. An Exploratory Survey of Noise Levels Associated with a 100 kW Wind Turbine. NASA TM-81486. Cleveland, OH: NASA Lewis Research Center.
2. Martinez, R.; Widnall, S. E.; Harris, W. L. 1982. Prediction of Low-Frequency Sound from the MOD-1 Wind Turbine. SERI TR-635-1247. Cambridge, MA: MIT Fluid Dynamics Research Laboratory.
3. Thomson, D. W. 1982. Analytical Studies and Field Measurements of Infrasound Propagation at Howard's Knob, North Carolina. SERI/TR-635-1292. University Park, PA: The Pennsylvania State University, Department of Meteorology.
4. Savino, J. M.; Wagner, L. H.; Nash, M. 1978 (Apr.). Wake Characteristics of a Tower for the DOE/NASA MOD-1 Wind Turbine. NASA TM-78853. Cleveland, OH: NASA Lewis Research Center.
5. Wright, S. E. 1969. "Sound Radiation from a Lifting Rotor Generated by Asymmetric Disk Loading." J. Sound & Vibration. Vol. 9 (No. 2): pp. 223-240.
6. Wright, S. E. 1971. "Discrete Radiation from Rotating Periodic Sources." J. Sound & Vibration. Vol. 17 (No. 4): pp. 437-498.
7. George, A. R. 1978. "Helicopter Noise: State of the Art." J. Aircraft. Vol. 15, (No. 11): pp. 707-711.
8. Lighthill, M. J. 1952. "On Sound Generated Aerodynamically--I: General Theory." Proc. Royal Society (London). Vol. A264: pp. 564-587.
9. Leverton, J. W.; Amor, C. B. 1973. "An Investigation of Impulsive Rotor Noise of a Model Rotor." J. Sound & Vibration. Vol. 28 (No. 1): pp. 55-71.
10. Garstang, M.; Snow, J. W.; Emmitt, G. D. 1981. "Measurement of Wind Shear at the NASA MOD-1 Site." J. Energy. Vol. 5 (No. 3): pp. 146-151.
11. Roshko, A. 1961. "Experiments on the Flow Past a Cylinder at Very High Reynolds Numbers." J. Fluid Mechanics. Vol. 10: pp. 345-356.
12. McCroskey, W. J. 1977. "Some Current Research in Unsteady Fluid Dynamics--The 1976 Freeman Scholar Lecture." Trans. ASME--J. Fluids Engineering. Vol. 99: pp. 8-38.
13. Naumann, A.; Quadflieg, H. 1968. "Aerodynamic Aspects of Wind Effects on Cylindrical Buildings." Proc. Symp. Wind Effects on Buildings and Structures; Loughborough Univ. of Tech. 2-4 April 1968; pp. 9.1-9.13.

14. Snyder, M. H.; Wentz, W. H. 1981 (Jan.). Characteristics of Wakes Downstream of Circular Cylinders and 12-Sided Cylinders as Determined by Wind Tunnel Test. Wind Energy Report No. 13. Wichita, KS: Wind Energy Laboratory, Wichita State University.
15. Park, C. C.; Harris, W. L. 1981 (Aug.). Laboratory Measurements of Noise from a Downwind Rotor Horizontal Axis Wind Turbine. FDRL Report No. 81-4. Cambridge, MA: Massachusetts Institute of Technology, Department of Aeronautics and Astronautics; 94 pp.
16. Marcus, E. N.; Harris, W. L. 1982 (Aug.). Experimental Results of Acoustic Tests on a 1/53 Scale Model of the MOD-1 Wind Turbine. FDRL Report No. 82-2. Cambridge, MA: Massachusetts Institute of Technology, Department of Aeronautics and Astronautics; 180 pp.
17. McCroskey, W. J. 1982. "Unsteady Airfoils." Ann. Review Fluid Mech. Vol. 14: pp. 286-311.
18. McCroskey, W. J. 1981. The Phenomenon of Dynamic Stall. NASA TM-8124. Moffett Field, CA: NASA Ames Research Center; 38 pp.
19. Schlichting, H. 1979. 7th Edition. Boundary Layer Theory. New York, NY: McGraw-Hill; pp. 452-453.
20. Liiva, J. 1969. "Unsteady Aerodynamics and Stall Effects on Helicopter Rotor Blade Sections." J. Aircraft. Vol. 6 (No. 1): pp. 46-51.
21. Ericsson, L. E.; Reding, J. P. 1970. Proc. AIAA 8th Aerospace Sciences Meeting. AIAA Paper No. 70-77, New York, NY: 10 pp.
22. Birkoff, G.; Zaronello, E. H. 1957. "Jets, Wakes and Cavities." Appl. Math. Mech. Vol. 2. New York, NY: Academic Press.
23. Berger, H.; Wille, R. 1972. "Periodic Flow Phenomena." Ann. Review of Fluid Mech. Vol. 4: pp. 313-340.
24. Loth, J. L. 1978. "Wind Power Limitations Associated with Vortices." J. Energy. Vol. 2 (No. 4): pp. 216-222.
25. Lamb, H. 1945. Hydrodynamics. 6th Edition. New York, NY: Dover Press.
26. Roshko, A. 1953 (Mar.). On the Development of Turbulent Wakes from Vortex Streets. NASA TN-2913. Pasadena, CA: Calif. Inst. of Tech.; 77 pp.
27. Fage, A.; Johansen, F. C. 1928 (Feb.). "The Structure of Vortex Sheets." Proc. Roy. Soc. (London), Series A 116: pp. 170-200.
28. Pinkerton, R. M. 1936. Calculated and Measured Pressure Distributions over the Midspan Section of the NACA 4412 Airfoil. NACA Report No. 563. Langley Field, VA: NACA Langley Memorial Aeronautic Laboratory.

29. Sandusky, W. F.; Renne, D. S.; Hadley, D. L. 1982 (Sept.). Candidate Wind Turbine Generator Site Summarized Meteorological Data for the Period December 1976 through December 1981. PNL-4407. Richland, WA: Pacific Northwest Laboratory.
30. Thomson, D. W. 1982 (May). "Noise Propagation in the Atmosphere's Surface and Planetary Boundary Layers." Proc. 1982 International Conf. on Noise Control Engineering. Edited by J. G. Seebold. San Francisco, CA: 17-19 May 1982. Poughkeepsie, NY: Noise Control Foundation; pp. 351-354.
31. Wells, R. J. 1981. "GE MOD-1 Noise Study." Proc. Wind Turbine Dynamics Conf. Edited by R. W. Thresher. Cleveland, OH; 24-26 February 1981. NASA Conf. Publication 2185; SERI/CP-635-1238; NASA Lewis Research Center; pp. 389-395.
32. Stephens, D. G.; Shepherd, K. P.; Hubbard, H. H.; Grosveld, F. W. 1982 (Mar.). Guide to the Evaluation of Human Exposure to Noise from Large Wind Turbines. NASA TM-83288. Hampton, VA: NASA Langley Research Center; 70 pp.
33. Carden, H. D.; Mayes, W. H. 1970. Measured Vibration Response Characteristics of Four Residential Structures Excited by Mechanical and Acoustical Loadings. NASA TN D-5776. Hampton, VA: NASA Langley Research Center; 59 pp.
34. Tempest, W. (Ed.) 1976. Infrasound and Low Frequency Vibration. London: Academic Press; pp. 211-212.
35. Bruel & Kjaer, Inc. 1973. Technical Review, Vol. 3: pp. 14-25.
36. Medearis, K. 1976 (Aug.). The Development of Rational Damage Criteria for Low-Rise Structures Subjected to Blasting Vibrations. A Report to the National Crushed Stone Assoc., Washington D.C. Fort Collins, CO: Kenneth Medearis Associates; 93 pp.
37. Ford, R. D. 1970 (July). "The Propagation of Noise and Vibration in Houses." Environmental Engineering; pp. 13-18.
38. Robin Towne Assoc. 1974. Environmental Study of Low Frequency Noise & Vibration. A Report to the Portland General Electric Co., Portland, OR. Portland, OR: Robin Towne Assoc., 144 pp.
39. Mayes, W. H.; Edge, P. M.; Connor, A. B. 1970. "Research Approaches to the Alleviation of Aircraft Noise." Presented at the 16th Annual Meeting of the Institute of Environmental Sciences. Boston, MA: 17-20 April 1970. NASA Langley Research Center; 24 pp.
40. International Standards Organization. "Normal Equal Loudness Contours for Pure Tones and Normal Threshold of Hearing under Free Field Listening Conditions." ISO Recommendation R226, 1961.

41. Walshe, D. E.; Wootton, L. R. 1970. "Preventing Wind-Induced Oscillations of Structures of Circular Section." Proc. Inst. of Civil Engineers. Vol. 47: pp. 1-24.
42. Scruton, C.; Walshe, D. E. 1957 (Oct.). A Means for Avoiding Wind-Excited Oscillations of Structures with Circular or Nearly Circular Cross-Section. NPL/Aero/335. Great Britain: National Physical Laboratory; 13 pp.
43. Woodgate, L.; Maybrey, J.F.M. 1959 (June). Further Experiments on the Use of Helical Strakes for Avoiding Wind Excited Oscillations of Structures with Circular or Near Circular Cross-sections. NPL/Aero/381. Great Britain: National Physical Laboratory; 31 pp.
44. Cowdrey, C. F.; Lawes, J. A. 1959 (July). Drag Measurements at High Reynolds Numbers of a Circular Cylinder Fitted with Three Helical Strakes. NPL/Aero/384 Great Britain: National Physical Laboratory; 5 pp.
45. Greene, G. C. 1981. "Measured and Calculated Characteristics of Wind Turbine Noise." Proc. Wind Turbine Dynamics Conf. Edited by R. W. Thresher. Cleveland, OH; 24-26 February 1981. NASA Conf. Publication 2185; SERI/CP-635-1238; NASA Lewis Research Center; pp. 355-361.
46. Viterna, L. A. 1981. "The NASA-LeRC Wind Turbine Sound Prediction Code." Proc. Wind Turbine Dynamics Conf. Edited by R. W. Thresher. Cleveland, OH; 24-26 February 1981. NASA Conf. Publication 2185; SERI/CP-635-1238; NASA Lewis Research Center; pp. 411-417.
47. Wells, R. J. 1980 (Oct.). MOD-1 Wind Turbine Generator Noise Studies, Vols I & II. A Report to the NASA Lewis Research Center, Cleveland, OH. Schenectady, NY: General Electric Company, Corporate Research and Development.
48. Spencer, R. H. 1981. "Noise Generation of Upwind Rotor Wind Turbine Generators." Proc. Wind Turbine Dynamics Conf. Edited by R. W. Thresher. Cleveland, OH; 24-26 February 1981. NASA Conf. Publication 2185; SERI/CP-635-1238; NASA Lewis Research Center; pp. 419-423.
49. Metzger, F. B.; Klatte, R. J. 1981. "Status Report on Downwind Rotor Horizontal Axis Wind Turbine Noise Prediction." Proc. Wind Turbine Dynamics Conf. Edited by R. W. Thresher. Cleveland, OH; 24-26 February 1981. NASA Conf. Publication 2185; SERI/CP-635-1238; NASA Lewis Research Center; pp. 425-430.
50. National Research Council, Comm. on Hearing, Bioacoustics, and Biomechanics of Assembly of Behavioral and Social Sciences, 1977 (June). Guidelines for Preparing Environmental Impact Statements on Noise. National Research Council, CHABA WG 69 on Evaluation of Environmental Impact of Noise. 144 pp. Available from: U. S. Department of Commerce, NTIS, Springfield, VA, Stock NO. AD/A-044-384.

51. Greene, G. C.; Hubbard, H. H. 1980. Some Calculated Effects of Non-Uniform Inflow on the Radiated Noise of a Large Wind Turbine. Hampton, VA: NASA Langley Research Center. NASA TM 81813.
52. Gutin, L. 1947. On the Sound Field of a Rotating Propellor (Translation). NACA Technical Memo No. 1195.

<b>Document Control Page</b>	1. SERI Report No. SERI/TR-635-1166	2. NTIS Accession No.	3. Recipient's Accession No.
4. Title and Subtitle Acoustic Noise Associated with the MOD-1 Wind Turbine: Its Source, Impact, and Control		5. Publication Date February 1985	
7. Author(s) N. D. Kelley, H. E. McKenna, R. R. Hemphill, C. L. Etter, R. L. Garrelts, N. C. Linn		8. Performing Organization Rept. No.	
9. Performing Organization Name and Address Solar Energy Research Institute 1617 Cole Boulevard Golden, Colorado 80401		10. Project/Task/Work Unit No. 1066.70/4803.10	
		11. Contract (C) or Grant (G) No. (C) (G)	
12. Sponsoring Organization Name and Address		13. Type of Report & Period Covered Technical Report	
		14.	
15. Supplementary Notes			
16. Abstract (Limit: 200 words) This report summarizes extensive research by staff of the Solar Energy Research Institute and its subcontractors conducted to establish the origin and possible amelioration of acoustic disturbances associated with the operation of the DOE/NASA MOD-1 wind turbine installed in 1979 near Boone, North Carolina. Results have shown that the source of this acoustic annoyance was the transient, unsteady aerodynamic lift imparted to the turbine blades as they passed through the lee wakes of the large, cylindrical tower supports. Nearby residents were annoyed by the low-frequency, acoustic impulses propagated into the structures in which the complainants lived. The situation was aggravated further by a complex sound propagation process controlled by terrain and atmospheric focusing. Several techniques for reducing the abrupt, unsteady blade load transients were researched and are discussed in the report.			
17. Document Analysis a. Descriptors Acoustic Measurements ; Aerodynamics ; Noise ; Noise Pollution ; Turbine Blades ; Vortex Flow ; Wind Turbines b. Identifiers/Open-Ended Terms c. UC Categories 60			
18. Availability Statement National Technical Information Service U.S. Department of Commerce 5285 Port Royal Road Springfield, Virginia 22161		19. No. of Pages 262	
		20. Price A12	